AD NUMBER

AD484260

NEW LIMITATION CHANGE

TO

Approved for public release, distribution unlimited

FROM

Distribution authorized to U.S. Gov't. agencies and their contractors; Administrative/Operational use; May 1966. Other requests shall be referred to Air Force Aero Propulsion Laboratory, Wright-Patterson Air Force Base, Ohio 45433.

AUTHORITY

AFAPL ltr, 12 Apr 1972

AFAPL-TR-66-30

NORTH AMERICAN AVIATION, INC. / LOS ANGELES DIVISION

EXPERIMENTAL REVIEW OF TRANSONIC SPILLAGE DRAG OF RECTANGULAR INLETS

Martine W. Petersen
Gordon C. Tamplin

FOREWORD

This report was prepared by North American Aviation, Inc., Los Angeles Division, under Air Force Contract AF 33(615)-2496, "Experimental Study of Additive Drag of Supersonic Propulsion Systems". The report was previously issued as contractor's report NA-66-10 prior to Air Force approval.

The program was sponsored by the Components Branch, Research and Technology Division, Wright-Patterson Air Force Base, Ohio. Program monitor was Mr. H. J. Gratz, APTC. The USAF Project and Task numbers were, respectively, 3066 and 306603.

The program was initiated on 1 April 1965 and completed on 1 April 1966, and the report was submitted by the authors on 19 May 1966 for approval. Experimental work was carried out during 21 July thru 13 August in the NASA Ames 6' x 6' Supersonic Wind Tunnel with the assistance of NASA personnel R. A. Taylor, Project Coordinator, and C. E. Hedstrom, Project Engineer. Principal contractor personnel were G. C. Tamplin, M. W. Petersen and L. C. Young.

The Aero Propulsion Laboratory, Turbine Engine Components Branch (APTC) is maintaining a copy of the full test program data tape. Information concerning tape availability can be requested thru that office.

Publication of this report does not constitute Air Force approval of the report findings or conclusions. It is published only for the exchange and stimulation of ideas.

Ernest C. Simpson
Chief, Turbine Engine Division

ABSTRACT

Inlets sized for supersonic aircraft operation are oversized at transonic speeds. Spilling excess air around the inlet creates spillage drag which can seriously penalize the low altitude penetration range of mixed mission aircraft. Spilling, also creates inlet cowl lip suction forces which can cancel a portion of this drag, but available data on spillage drag and its partial recovery on the cowl lip were not sufficient for necessary design and performance studies. Generalized wind tunnel studies of inlet spillage were required to supply the needed information.

In 1964, NAA/LAD designed and built a "workhorse" model for in-house tests of pitot inlet spillage drag. Under contract AF 33(615)-2496, the "workhorse" portion of this model was fitted with rectangular supersonic inlets. Wind tunnel tests were conducted and are reported herein. Testing was done in the NASA Ames Research Center's 6' x 6' Supersonic Wind Tunnel, primarily in the 0.7 to 1.4 Mach number range. The model had four interchangeable ramps, four sets of side plates and ten interchangeable cowls. The primary test configurations were shock-on-cowl Mach 2.2 and Mach 3.0 design point inlets.

Low drag flow spillage requires decreasing the inlet flow area by (a) increasing the external ramp angle or (b) rotating the cowl inward. Test data show that ramp spillage creates lower total drag. The minimum spillage drag configuration would use minor deflections of both ramp and cowl. However, the cowl actuation weight penalty must be considered.

Experimental transonic ramp pressure drags were normalized and compared with transonic similarity work on wedge airfoils. These ramp drag data, together with cowl drag and spillage drag correction (K_{ADD}) factors developed in this report, are valuable tools for inlet design and performance studies.

TABLE OF CONTENTS

LIST OF ILLUSTRATIONS

LIST OF TABLES

LIST OF ABBREVIATIONS AND SYMBOLS

ITEM	DEFINITIONS
a	Most aft external station of force model exposed to flow.
A	Area.
A*	Sonic flow area.
A_c	Inlet capture area. The frontal projected area of an inlet, in the freestream velocity vector direction, bounded by the cowl leading edge, side plate leading edges and initial ramp leading edge.
A_e	Exit area.
A_{LIP}	Cowl lip station inlet area.
A_o	Airflow streamtube area in the freestream.
A_o/A_c	Inlet mass flow ratio; mass flow entering the inlet ratioed to capture area of the inlet.
$(A_o/A_c)_{MAX\ COMPUTED}$	The inlet maximum mass flow ratio computed from the Supersonic Mathematical Model of Appendix II.
$(A_o/A_c)_{REF}$	Reference mass flow ratio of the inlet.
∂A	Infinitesimal area.
c	Ramp or wedge chord length.
$C_{C_{ADD}}$	Cnord direction additive drag coefficient.
$\left[C_{C_C} + C_{C_S}\right]$	Cowl plus side plate pressure drag integration coefficient in D/q_oA_c form.
C_{C_e}	N/q_oA_c.
D	Drag.

D_{ADD}	Additive Drag.
ΔD_{ADD}	The change in additive drag between inlet operation at (A_O/A_C) and $(A_O/A_C)_{REF}$.
$D_{ADD\ THEORY}$	Theoretical additive drag.
$\Delta D_{ADD\ THEORY}$	The change in theoretical additive drag between inlet operation at (A_O/A_C) and $(A_O/A_C)_{REF}$.
$(D_{ADD\ THEORY})_{REF}$	Theoretical additive drag at $(A_O/A_C)_{REF}$.
$(D_{ADD})_{REF}$	Additive drag at $(A_O/A_C)_{REF}$.
D_f	Friction drag.
$(D)_{REF}$	Drag at $(A_O/A_C)_{REF}$.
D_R	Ramp drag.
$(D_R)_{REF}$	Ramp drag at $(A_O/A_C)_{REF}$.
D_{TOTAL}	Total inlet drag.
f, f'	General mathematical functions.
F_{BAL}	Balance force.
F_{INT}	See equation 1.
F_N	Net thrust.
$(F_{INT})_{COR}$	See equations 2 and 3.
g	Gravitational constant.
H	Total pressure.
K_{ADD}	Additive drag correction factor (see equation 4).
L.E.	Leading Edge.

M	See equations 8 and 9.
M	Mach number, always used with subscript.
M_e	Exit station Mach number.
M_o	Freestream Mach number.
M_{LIP}	Mach number at the cowl lip station.
N	A drag as defined by equation 6.
N_{REF}	Value of N at $(A_o/A_c)_{REF}$.
ΔN	Change in value of N between (A_o/A_c) and $(A_o/A_c)_{REF}$.
P	Pressure.
P_e	Pressure at an exit station.
P_{LIP}	Cowl lip station pressure.
P_o	Freestream pressure.
P_R	Pressure on inlet ramp.
dP/dx	Rate of change of pressure with axial distance.
q_o	Freestream dynamic pressure.
s	Stagnation.
t	Ramp or wedge thickness.
V_o, V_e	Freestream and exit velocities, respectively.
W_o, W_e	Weight rate of airflow entering and exiting from a control volume at freestream and exit stations.
α	Angle of the initial inlet ramp relative to the freestream velocity vector.

β	Angle of the second external inlet ramp relative to the freestream velocity vector.
Δ	Change in a quantity.
γ	Ratio of specific heats.

SUBSCRIPTS

ITEM	DEFINITION
e	Exit station conditions.
∞	Freestream station conditions.
B1, B2	Denotes base areas 1 and 2.
LIP	Denotes a quantity at the cowl lip station of an inlet.
NS	Denotes conditions behind a normal shock wave.
R	Denotes conditions on inlet ramp.
REF	Denotes quantity at $(A_0/A_c)_{REF}$.

Special nomenclature used in Appendixes I, II and III have not been included. All important nomenclature is either fully explained in the text of the Appendixes or a special nomenclature listing is given.

I

INTRODUCTION

The objectives of this work were (1) the experimental study of inlet geometric factors affecting spillage drag of rectangular supersonic inlets and (2) the conversion of measured data to correction factors which may be applied to calculated theoretical additive drag values to realistically estimate spillage drag and improve the accuracy of inlet-engine performance predictions.

Previous experimental work, references 1 thru 10, has generally been restricted to drag studies of complete airplane configurations. This means that a wide variation of inlet geometric factors were not considered, and, more importantly, that a relatively small error in measurement of complete configuration drag creates a large spillage drag inaccuracy. If spillage drag is ten percent of the total vehicle drag, an error of only one percent in total drag measurement precludes meaningful spillage drag studies of many inlet geometric variations.

The wind tunnel test model used in this investigation was an inlet model only, not a full configuration model. The model was constructed so that a number of inlet cowls, side plates and external initial ramps could be interchanged and tested.

The test Mach number range was primarily limited to Mach 0.7 to Mach 1.4. At lower Mach numbers, spillage drag is seldom of importance, and at higher Mach numbers it is generally felt that theoretical predictions of spillage drag are reasonably accurate.

The wind tunnel test phase is briefly summarized in Section II. Sections III thru VII are background information for the experimental results given in the later portion of this report.

II

WIND TUNNEL TEST PHASE SUMMARY

1. Model. A comprehensive description of the wind tunnel force model used in the investigation is given in Appendix I. It was a rectangular, supersonic inlet model having two external ramps. The second external ramp was variable from 5° to 12° relative to the freestream vector. The inlet was constructed so that several cowls, side plates and fixed initial ramps could be interchanged. Ten cowls, C1 thru C10, four fixed initial ramps, R1 thru R4, and four side plate sets, SP1 thru SP4, were tested.

2. Wind Tunnel. Testing was conducted in the continuous flow NASA Ames 6' x 6' Supersonic Wind Tunnel. Nominal test conditions were

M_0	Total Press.
0.7	1960 psf
0.85	1960
1.1	1400
1.3	1400
1.4	1475
1.7	1335
2.2	2190

3. Configurations Tested. The following listing summarizes the configurations and Mach numbers at which data were obtained. The ramp, side plate, and cowl configurations listed are illustrated in Appendix I. Angles of the initial and second ramps are α and β, respectively, with respect to the freestream vector.

Test Mach Numbers

Config.	Design M_0	α	β	.70	.85	1.1	1.3	1.4	1.7	2.2
R1SP1C1	3.0	5°	5°	x	x	x	x	x	x	x
↓	↓	↓	9°	x	x	x	x	x		
			12°	x	x	x	x	x		
R1SP1C2			5°	x	x	x	x	x		
R1SP1C3			↓	x	x	x	x	x		
R1SP1C4				x	x	x	x	x		
R1SP1C5				x	x	x	x	x	x	
R1SP1C6				x	x	x	x	x		
R1SP1C7				x	x	x	x		x	
R1SP1C8				x	x	x	x	x	x	
R1SP1C9				x	x	x	x	x		
R1SP1C10				x	x	x	x	x		
R1SP2C1				x	x	x	x	x		
↓			12°	x	x	x	x			
R1SP3C1			5°	x	x	x	x	x		
R1SP1SP3C1	↓	↓	↓				x	x	x	

Test Mach Numbers

Config.	Design M_o	α	β	.70	.85	1.1	1.3	1.5	1.7	2.2
R2SP1C1	2.2	7°	7°	x	x		x			
R3SP1C1	—	12°	12°	x	x	x	x	x		
R4SP4C1	—	5°	5°	x	x	x	x	x		
↓	↓	↓	12°		x	x	x			
R4SP4C4	—	↓	5°	x	x	x	x	x		
↓	↓	↓	9°				x	x		
R4SP4C6	—	↓	5°	x	x	x	x	x		
↓	↓	↓	9°		x	x	x	x		
↓	↓	↓	12°		x	x	x			

As indicated in the second column, inlets having R1 were shock-on-cowl design point inlets for Mach 3.0. Inlets having R2 were shock-on-cowl at Mach 2.2. R3 and R4 first ramps had their leading edges at the same station as R1 as shown on figure 16. The R3 and R4 ramp configurations were included to show the effects of first ramp angle.

Since the model did not have boundary layer control features, subcritical stability at Mach 2.2 was limited. No analysis of these data was worthwhile. Analysis of the four sets of Mach 1.7 data was limited because of tunnel flow problems as explained later.

III

ADDITIVE DRAG CONCEPT

The additive drag concept is fully accepted in calculating airplane performance although no real counterpart of the concept exists in nature. It is a thrust-drag bookkeeping tool which conveniently bridges the gap between the engine manufacturer's definition of net thrust, F_N, and the airframe manufacturer's requirement for internal thrust, F_{INT}, for airplane performance prediction.

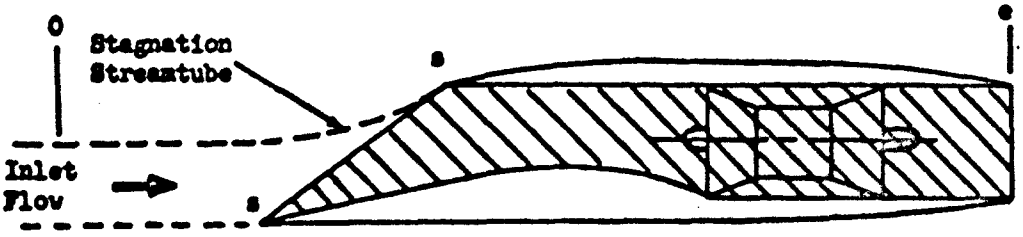

Figure 1 . Propulsion Nacelle in Freestream

The airframe manufacturer requires evaluation of F_{INT}

$$F_{INT} = \int_s^e (P - P_0)dA$$

P ⟵ local static pressure
dA ⟵ incremental frontal area

where the integral is taken around <u>all</u> of the internal surfaces of the propulsion system. The integral region is shown on figure 1 as the cross-hatched area extending from streamtube stagnation, s, on inlet leading edges to the exit from the nacelle. F_{INT} is the internally generated thrust which provides the propelling force for the airplane, but it is not evaluated by performing the complex internal integration. Instead, the starting point is the engine manufacturer's net thrust

$$F_N = \left[(P_e - P_0)A_e + W_eV_e/g\right] - \left[(P_0 - P_0)A_0 + W_0V_0/g\right]$$

A force-momentum balance on the cross-hatched free body of figure 2 illustrates that F_{INT} is evaluated by subtracting "drag" of the unbounded streamtube from F_N:

$$F_{INT} = F_N - \int_0^s (P - P_0)dA = F_N - D_{ADD} \qquad \text{Eq. (1)}$$

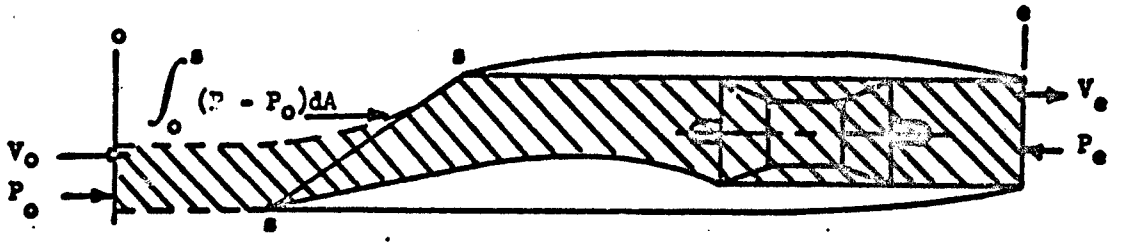

Figure 2 . Propulsion Nacelle in Freestream

This unbounded streamtube "drag" is termed additive drag, D_{ADD},

$$D_{ADD} = \int_o^s (P - P_o)dA$$

D_{ADD} is not felt on an aircraft surface , but it must be subtracted from F_N to obtain the required F_{INT} force-momentum balance.

Detailed examination of the D_{ADD} integral shows additive drag to be caused by airflow spillage around the inlet. Figure 3 illustrates that for the no spillage case, $A_o/A_c = 1.0$, D_{ADD} is zero because the streamtube has no frontal area for drag to occur. As mass flow is reduced, drag area of the streamtube increases, static pressure within the streamtube increases, and D_{ADD} can become large. Spillage causes additive drag at supersonic speeds as well as at the subsonic speeds used in the illustration.

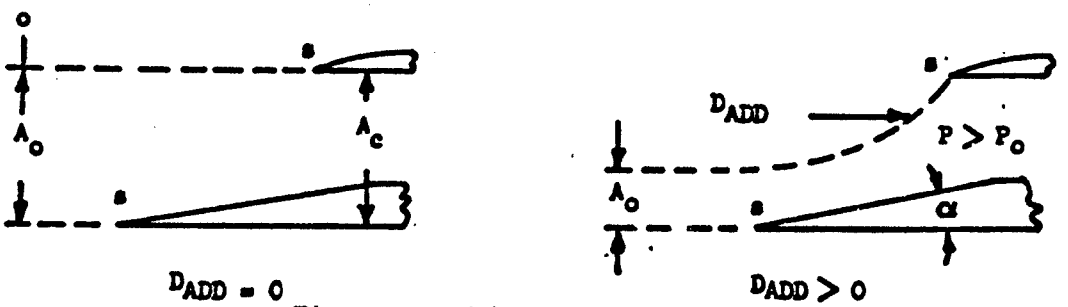

Figure 3 . Subsonic Additive Drag

External geometry of the inlet affects the magnitude of the D_{ADD} integral over the streamtube. A given spillage can be obtained with various external ramp and inlet side plate geometries. Ramp angle may be raised or lowered; side plates may be cut-back, allowing side spillage, or extended. Each external inlet geometry creates a particular stagnation streamtube shape and particular flow conditions within the streamtube. In magnitude, D_{ADD} is a function of both the amount of spillage and the way it is spilled (external inlet geometry).

IV

ADDITIVE DRAG RECOVERY

The full value of D_{ADD} should rarely be charged as a penalty to the airplane at subsonic and low supersonic speeds. Air spilling around the inlet increases velocity and decreases pressure on the leading portions of cowl and side plates. At reduced mass flow ratios surface pressures drop below ambient, and these surfaces produce thrust rather than drag. This is illustrated in figure 4 by a typical subsonic data sample from this research program. Part of the D_{ADD} spillage drag penalty is offset by spillage thrust created by suction on cowl and side plate lips.

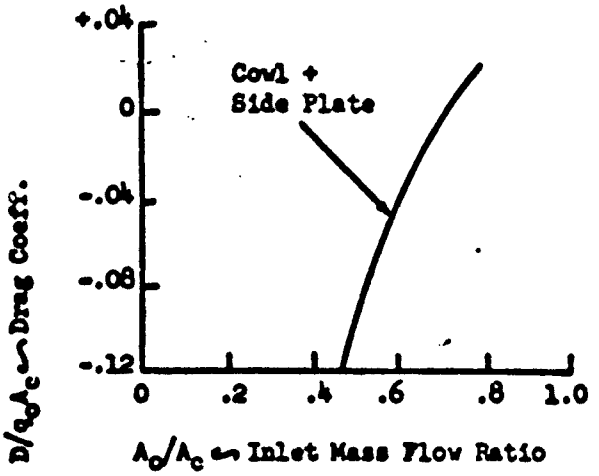

Figure 4 . Additive Drag Recovery

In airplane thrust-drag bookkeeping, it is usual practice to consider external airplane drag as invariant with inlet mass flow ratio. Thrust-drag items which do vary with mass flow ratio are included within the scope of the propulsion system performance. Thus, for a given flight condition a fixed airplane external drag is assigned, corresponding to operation at a given inlet reference mass flow ratio. Then, rather than equation 1, a new equation of the form

$$(F_{INT})_{COR} = F_N - f\left[D_{ADD} - (D_{ADD})_{REF}\right] = F_N - f(\Delta D_{ADD}) \qquad \text{Eq. (2)}$$

is used to represent the propulsion system.

Equation 2 is an idealized situation because $f(\Delta D_{ADD})$ of the particular airplane is presumed to be known. This requires the construction and testing of a ducted aerodynamic force model of the given configuration over the required range of inlet mass flow ratio. Much more frequent is performance prediction for "drawing board" airplanes, and such data is unavailable.

In practice then, equation 2, is modified to become

$$(F_{INT})_{COR} = F_N - f' \left[D_{ADD\ THEORY} - (D_{ADD\ THEORY})_{REF} \right] \quad \text{Eq. (3)}$$
$$= F_N - f' \left(\Delta D_{ADD\ THEORY} \right)$$

A theoretical computed additive drag is substituted for actual additive drag. The f' factor is selected from previous test data of inlets as nearly like the one in question as obtainable. Obviously, if $(D_{ADD\ THEORY})$ duplicates D_{ADD}, the desired f' and f factors are identical. In the remainder of this report, the f' factor will be called the <u>additive drag correction factor</u> and will be symbolized as K_{ADD}, conforming to the usage in published literature:

$$(F_{INT})_{COR} = F_N - K_{ADD} \left(\Delta D_{ADD\ THEORY} \right) \quad \text{Eq. (4)}$$

It is desirable that the theoretical and actual additive drags be in reasonable agreement. Only then will K_{ADD} retain the physical significance of the f function of equation 2. A later section deals with the theoretical additive drag calculations used for this project and compares theoretical and "measured" additive drags.

V

METHOD OF DETERMINING EXPERIMENTAL VALUES OF K_{ADD} AND ΔD_{ADD}

Figure 5 shows a schematic of the test phase wind tunnel force model and a free body diagram of the force-momentum balance which was solved to determine K_{ADD} and ΔD_{ADD}. In addition to instrumentation for determination of station o and station e conditions, base pressures and balance force, static pressure instrumentation was required on the cowl and side plate lip regions so that numerical integrations of cowl and side plate pressure drag could be made. This latter instrumentation is described in Appendix I .

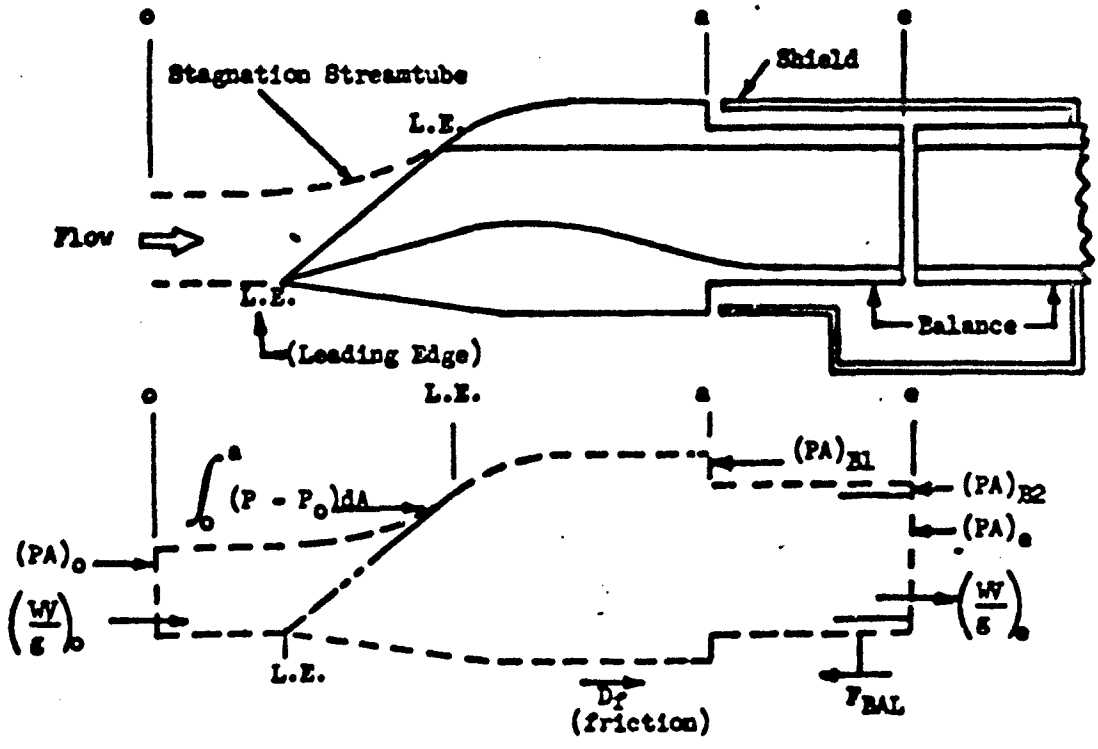

Figure 5 . Inlet Schematic and Free Body Diagram

From figure 5 , the chord direction force-momentum balance, the quantity

$$\int_o^a (P - P_o)dA + D_f$$

can be evaluated as

$$\int_0^a (P - P_o)dA + D_f = F_{BAL} - (W/g)_o + (P_e - P_o)A_e + (W/g)_e + \sum_{BASES} (P_{BASE} - P_o)A_{BASE} = N \qquad \text{Eq. (5)}$$

By separating the integral into three components, streamtube drag, cowl and side plate drag, and drag of the under-body of the model

$$\int_0^{L.E.} (P - P_o)dA + \left[\int (P - P_o)dA\right]_{\substack{\text{Cowl +} \\ \text{Side Plate}}} + \left[\int (P - P_o)dA\right]_{\substack{\text{under-} \\ \text{body}}} + D_f = N$$

Then, considering both the change in friction with mass flow ratio and the change in pressure drag of the under-body with mass flow ratio to be negligible

$$D_{ADD} + \left[\int (P - P_o)dA\right]_{\substack{\text{Cowl +} \\ \text{Side Plate}}} + (\text{CONST.}) = N \qquad \text{Eq. (6)}$$

From equation 6, it is clear that the change in N with mass flow is identical with the change in unrecovered additive drag with mass flow, and

$$K_{ADD} = \frac{N - N_{REF}}{\Delta D_{ADD\ THEORY}} = \frac{\Delta N}{\Delta D_{ADD\ THEORY}} \qquad \text{Eq. (7)}$$

where

N_{REF} ⟵ value of N at the reference inlet mass flow ratio, $(A_o/A_c)_{REF}$

The quantity ΔD_{ADD} was found by substituting into equation 6 the numerically integrated values of cowl and side plate pressure drag

$$D_{ADD} + (\text{CONST.}) = N - \left[\begin{matrix}\text{Cowl + Side Plate} \\ \text{Numerical Pressure} \\ \text{Drag Integration}\end{matrix}\right] = M \qquad \text{Eq. (8)}$$

Then,

$$\Delta D_{ADD} = M - M_{REF} = \Delta M \qquad \text{Eq. (9)}$$

Figures 6 and 7 illustrate a typical relation between ΔD_{ADD}, $\Delta D_{ADD\ THEORY}$, $K_{ADD}(\Delta D_{ADD\ THEORY})$, and K_{ADD} found for subsonic flow situations. The short (dotted) extrapolations of measured data shown in figure 6 were normally required to reach the selected inlet reference mass flow ratio.

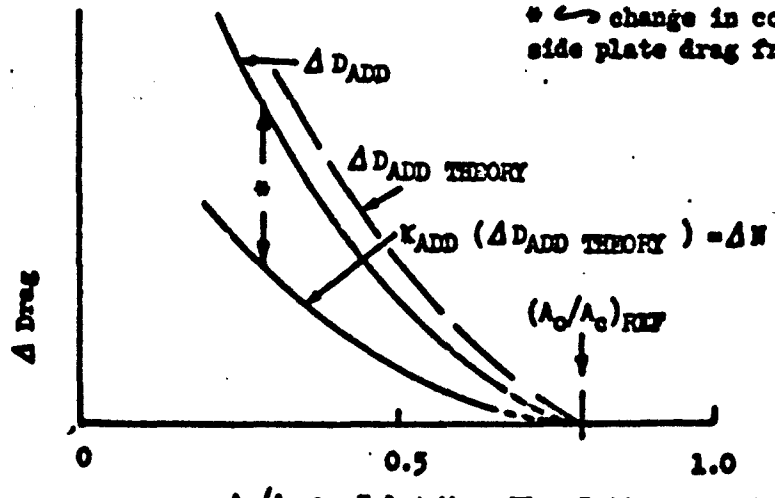

Figure 6 . Typical Subsonic Flow Results

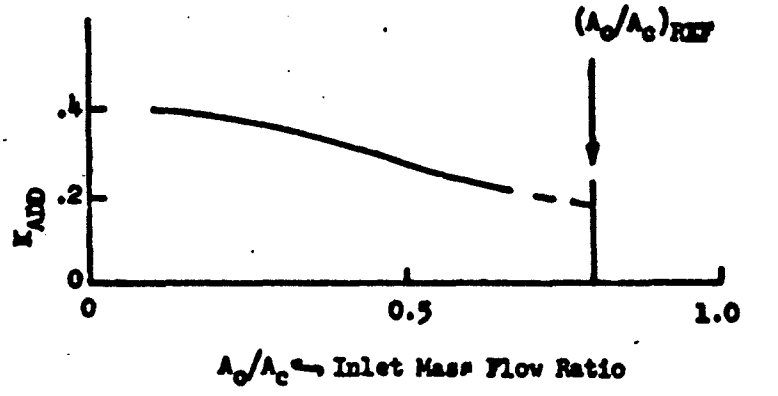

Figure 7 . Typical Subsonic K_{ADD}

Comparisons of ΔD_{ADD} data and $\Delta D_{ADD\ THEORY}$ are examined in Section VIII. A detailed discussion of the mathematical models and computer program for $\Delta D_{ADD\ THEORY}$ is given in Appendix II. The mathematical models for $\Delta D_{ADD\ THEORY}$ were deliberately simplified to allow hand calculations.

VI

CALCULATION OF $\Delta D_{ADD\ THEORY}$

Mathematical models were devised for the calculation of $D_{ADD\ THEORY}$. The models were kept reasonably simple to allow hand computations by the user. However, because of the large number of calculations involved in data analyses, a Fortran IV computer program was written and used. Both mathematical models and computer program are described in detail in Appendix II.

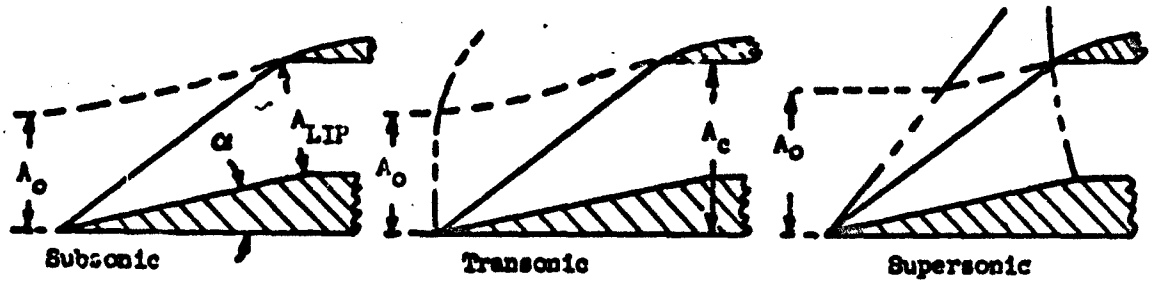

Figure 8 . Three Flow Regimes

Three mathematical models were constructed: a subsonic, a transonic (detached shock wave), and a supersonic model. Figure 8 illustrates the three flow regimes.

The subsonic model considers that flow rotates α degrees from freestream to ramp direction without increasing ramp pressure. Ramp pressure is a lumped parameter defined as

$$P_R = (P_o + P_{LIP})/2$$

where P_{LIP} is a function of mass flow ratio only. All flow enters the inlet in direction α, and the subsonic flow field is considered isentropic and one-dimensional.

In reality, a force is required to rotate the flow from the freestream to the ramp direction. Ramp pressures even at maximum mass flow ratio, $M_{LIP} = 1.0$, will rise above P_o locally. Side spillage of airflow from the higher pressure ramp to the freestream will occur, but side spillage does not affect the maximum inlet mass flow ratio in a subsonic flow field. Therefore, the simplifying assumption of one-dimensional flow is used in the mathematical model, and side spillage is neglected.

For the transonic model a (non-isentropic) normal shock wave is added forward of the inlet, and ramp pressure is defined as $(P_{NS} + P_{LIP})/2$.

The supersonic case treats additive drag from three spillages:

1) supersonic spillage over the cowl,
2) subsonic spillage over the cowl and
3) supersonic spillage around the side plate from the supersonic region forward of the terminal shock wave.

The maximum mass flow ratio and associated drag are computed considering the side spillage.

For data analysis, $D_{ADD\ THEORY}$ and $(D_{ADD\ THEORY})_{REF}$ were individually computed using the spillage models. Then $\Delta D_{ADD\ THEORY}$ was determined by

$$\Delta D_{ADD\ THEORY} = D_{ADD\ THEORY} - (D_{ADD\ THEORY})_{REF} \qquad \text{Eq. (10)}$$

VII

SELECTION OF THE INLET REFERENCE MASS FLOW RATIO

Several factors were considered in the selection of $(A_o/A_c)_{REF}$. A listing of the desirable characteristics of the reference value should include:

1) The reference A_o/A_c should be a uniquely definable flow condition, not some arbitrary fraction of A_c;
2) The reference should not be restrictive of side plate geometry, ramp angle or ramp length;
3) The reference should be a computed rather than a measured value since, in most cases, the user will not have a measured reference value;
4) The reference mass flow ratio should not be smaller than the normal operating mass flow ratio of the inlet since K_{ADD} is not defined above $(A_o/A_c)_{REF}$;
5) The reference mass flow ratio should not be so large that extrapolated data are physically unrealistic.

These factors suggest one of two maximums, the first being a computed value of maximum inlet flow, the second being the largest mass flow ratio at which the inlet may be expected to operate.

For the subsonic regime the selected reference mass flow ratio is

$$(A_o/A_c)_{REF} = A_{LIP}/A_c \qquad \text{Eq. (11)}$$

This represents $M_{LIP} = M_o$ and $P_{RAMP} = P_o$. The measured maximum mass flow ratio at $M_o = 0.69$ for the basepoint configuration, R1SP1C1 and $\alpha = \beta = 5^o$, was one-half percent larger than the reference value. Normally, boundary layer, internal contraction in the inlet, and "sharp lip losses" dictate inlet operation below the reference.

For the transonic regime, the same reference is used

$$(A_o/A_c)_{REF} = A_{LIP}/A_c$$

The supersonic regime requires a different reference. Maximum mass flow ratio computed from the Supersonic Mathematical Model of Appendix II was selected:

$$(A_o/A_c)_{REF} = (A_o/A_c)_{MAX\ COMPUTED} \qquad \text{Eq. (12)}$$

Although supersonic side spillage was considered in computing the maximums, boundary layer and inlet internal contraction caused measured maximums to be several percent lower than the computed reference values for the basepoint inlet at Mach 1.3 and 1.4.

The difference between the reference value and the measured maximums for the basepoint inlet can be seen on figures 45 thru 50 of Appendix III.

VIII

MEASURED vs. THEORETICAL ADDITIVE DRAG INCREMENT

Equation 8 shows how the D_{ADD} curve shape can be obtained from experimental data. Written in terms of drag coefficient, the equation becomes

$$(D_{ADD})/q_o A_c + (\text{CONST.}) = N/q_o A_c - \begin{bmatrix} \text{Cowl + Side Plate} \\ \text{Numerical Pressure} \\ \text{Drag Integration} \end{bmatrix} = C_{C_e} - \left[C_{C_C} + C_{C_S}\right]$$

Plots of this equation as a function of mass flow ratio for configurations NLSP1C1 thru C6 where $\alpha = \beta = 5^o$ are shown on figures 45 thru 50 for the six test Mach numbers between 0.69 and 1.69. The change in

$$\left\{C_{C_e} - \left[C_{C_C} + C_{C_S}\right]\right\}$$

with mass flow ratio is identical with the change in $(D_{ADD})/q_o A_c$ or $(\Delta D_{ADD})/q_o A_c$ with mass flow ratio. Since additive drag is relatively independent of cowl shape, conglomerate plots of data for all six cowls can be made at each Mach number.

Plots of $D_{ADD\ THEORY}$ (or $\Delta D_{ADD\ THEORY}$) adjusted in absolute value to correspond with the measured data at $(A_o/A_c)_{REF}$ are also given on the figures so that a direct comparison between ΔD_{ADD} and $\Delta D_{ADD\ THEORY}$ can be made. Except for Mach 1.69, the figures show the measured and theoretical curve shapes and slopes to be very similar. This means that K_{ADD} curves maintain much physical significance even though they are obtained from $\Delta D_{ADD\ THEORY}$, not ΔD_{ADD}.

For the subsonic cases where $\Delta D_{ADD\ THEORY}$ lies above ΔD_{ADD},

$$\frac{\Delta D_{ADD}}{\Delta D_{ADD\ THEORY}} < 1$$

and K_{ADD} values should be less than 1.0.

For the supersonic cases ΔD_{ADD} lies above $\Delta D_{ADD\ THEORY}$. Therefore

$$\frac{\Delta D_{ADD}}{\Delta D_{ADD\ THEORY}} > 1$$

and K_{ADD} values may be greater than 1.0.

In view of realistic flow situations, agreement between measured values and theoretical values is remarkably good.

The few cases of Mach 1.69 test data included in this report have questionable validity. Tunnel flow problems were encountered at this Mach number. Shadowgraph pictures taken during the testing show that a shock wave from the tunnel wall struck the model several inches forward of the cowl lip during two of the data runs. During the other two Mach 1.69 data runs there was a change in flow angularity relative to the model as a function of time. For these reasons, the remaining test cases scheduled for Mach 1.69 were replaced by other testing at lower Mach numbers.

IX

COWL AND SIDE PLATE PRESSURE DRAG

Cowl plus side plate pressure drags are shown on figures 51 thru 55 of Appendix III for configurations R1SP1C1 thru C6 at the five test Mach numbers between 0.69 and 1.39. On the figures, each drag curve has a different zero drag reference. This spreads and separates the data for clarity. The basic drag scale on each figure is applicable to configuration R1SP1C1 only.

At both subsonic and supersonic speeds cowl plus side plate pressure drag is decreased as inlet mass flow ratio is reduced. Additive drag is partially recovered on cowl and side plate lips. At lower mass flow ratios, the drag is negative. These surfaces actually produce thrust. Subsonically and supersonically (0.84 and 1.29 M_0), the drag drops to zero at mass flow ratios as little as 5 or 6 percent below $(A_0/A_c)_{REF}$.

As expected at subsonic speeds the rate of change of cowl plus side plate drag with mass flow ratio is not maximum at maximum mass flow ratio. The drag recovery curves are much like the mathematical reciprocal of the ΔD_{ADD} or $\Delta D_{ADD\ THEORY}$ curve shapes shown on figures 45 thru 46. At Mach 1.29 and 1.39 the reciprocal similarity does not hold between $\Delta D_{ADD\ THEORY}$ and cowl plus side plate drag. Figures 54 and 55 show the rate of change of drag with mass flow ratio to be, generally, maximum at maximum mass flow ratio. Figures 48 and 49 show the $\Delta D_{ADD\ THEORY}$ slope to be minimum at maximum mass flow ratio and show the ΔD_{ADD} slopes to be nearly constant for a wide range of mass flow.

At Mach 0.84, the curved (circular arc) cowl configurations have low drag at high mass flow ratios and low drag with 0.20 A_0/A_c spillage. The straight cowls are definitely second best.

At Mach 1.3, the 10° curved cowl inlet configuration, R1SP1C1, still gives the best performance, but the 6° straight cowl inlet configuration is not too far behind. Of course, at high supersonic speeds, low cowl angles are best.

Cowl selection should be made on the basis of the over-all airplane mission and the relative importance of the critical design points.

X

ADDITIVE DRAG COEFFICIENT, K_{ADD}

Plots of the additive drag coefficient, K_{ADD}, are given in figures 56 thru 94. Coefficients for the following data are presented in order of the indicated nominal Mach number listings[1]:

CONFIG.	α°	β°	Mach Number 0.7	0.85	1.1	1.3	1.4	1.69
R1SP1C1	5	5	x	x	x	x	x	x
R1SP1C2	5	5	x	x	x	x	x	
R1SP1C3	5	5	x	x	x	x	x	
R1SP1C4	5	5	x	x	x	x	x	
R1SP1C5	5	5	x	x	x	x	x	x
R1SP1C6	5	5	x	x	x	x	x	
R1SP1C1	5	9	x	x	x			
R1SP1C1	5	12	x	x	x			
R1SP2C1	5	5	x	x	x	x	x	
R1SP3C1	5	5	x	x	x	x	x	
R1SP1SP3C1	5	5						
R2SP1C1	7	7	x	x		x		
R3SP1C1	12	12	x	x	x	x	x	
R4SP1C1	5	5	x	x	x	x	x	
R4SP4C4	5	5			x	x	x	
R4SP4C6	5	5	x	x	x	x	x	
R4SP4C6	5	9		x	x			
R4SP4C1	5	12		x	x			
R4SP4C6	5	12		x	x			

All curves are faired to the reference mass flow ratio. Because of the large and questionable fairing required for R1SP1C1, $\alpha = 5^\circ$, $\beta = 12^\circ$, $M_o = 1.09$, the fairing is shown as a dotted extension of the data. For other cases, extensions were shorter and were simply extrapolations of better defined curve shapes. As discussed and illustrated earlier (figures 45 thru 50), fairing to $(A_o/A_c)_{REF}$ generally means a small extrapolation only.

It was pointed out in Section VIII that the ratio $(\Delta D_{ADD})/(\Delta D_{ADD\ THEORY})$ would

1) cause K_{ADD} values to be less than 1.0 at subsonic and transonic speed, and
2) cause maximum values of K_{ADD} to often be greater than 1.0 at Mach 1.3 and 1.4.

The K_{ADD} curves show these effects.

---

1. The configuration R1SP1SP3C1 has two different side plates, an SP1 and an SP3 side plate.

At Mach 1.09 and to a degree at 0.84, the K_{ADD} curves for R1SP1C4 have an unusual relationship with data of other configurations. Examination of the data substantiates this trend. First, the cowl plus side plate drag curve shown on figure 53 for R1SP1C4 at $M_o = 1.09$ does show a reverse of the usual curvature. These data are independent of the K_{ADD} development, yet they agree. Second, examination of the cowl pressure profiles clearly show a departure from the usual trend. On figure 95, centerline cowl pressure are plotted for both the C3 (10° straight) and C4 (15° straight) cowls. Considering the C3 data to represent the usual pressure profile trend, a clear substantiation for the C4 K_{ADD} data is apparent. The C4 data show that a very large decrease in pressure-area integrated drag occurs between mass flow ratios of 0.68 and 0.58.

At low mass flows both cowls have pressure distributions typical of separation near the leading edge of the cowl. Cowl C3 shows separation even at high mass flow ratios. Cowl C4, at $A_o/A_c = 0.68$, shows minor separation then re-attachment of the flow. No separation is indicated at $A_o/A_c = 0.73$ for cowl C4.

The K_{ADD} coefficients for R1SP1C1 thru C6 were conceptually computed as indicated in Section V. However, because only the cowl was changed from configuration to configuration it was possible to eliminate data scatter seen in figures 45 thru 50. ΔN of equation 7 was found by adding the change in integrated cowl plus side plate drag to the ΔD_{ADD} values found from the faired curves of figures 45 thru 50.

$$\Delta N = \Delta D_{ADD} + \left[\begin{array}{l}\text{Cowl + Side Plate}\\ \text{Numerical Pressure}\\ \text{Drag Integration}\end{array}\right] - \left[\begin{array}{l}\text{Cowl + Side Plate}\\ \text{Numerical Pressure}\\ \text{Drag Integration}\end{array}\right]_{REF}$$

There was very little scatter in the integrated cowl plus side plate drags as shown on figures 51 thru 55, and almost all K_{ADD} errors due to data scatter (inaccuracy) could be eliminated for the six cowl comparisons.

XI

EFFECT OF SIDE PLATE GEOMETRY ON K_{ADD}

Side plate geometry effects on K_{ADD} are shown for five nominal test Mach numbers between 0.7 and 1.4 in figures 96 thru 100. K_{ADD} is shown for configurations R1SP1C1, R1SP2C1, R1SP3C1, $\alpha = \beta = 5^{\circ}$.

At Mach 0.7, side plate geometry has very little effect on inlet drag except for large flow spillages. There, the drag of the extended side plate configuration is larger.

The same general trends are shown at Mach 0.85. The cut-back side plates look best for high spillages, and the extended side plates are considerably worse.

Transonically at Mach 1.1, side spillage becomes very important. High drag will result from spillage with extended side plates. The cut-back side plates are obviously the best if large spillages are necessary.

At the supersonic speeds K_{ADD} comparisons do not give spillage drag comparisons directly since a different $(A_0/A_c)_{REF}$ is used. Over-all propulsion system performance should be evaluated.

XII

RAMP PRESSURE DISTRIBUTIONS

Ramp drag is pertinent to data presented in the following sections of this report. As shown in Appendix I, the initial fixed ramp was instrumented with four static pressure taps, and the variable external ramp was instrumented with twenty-one static pressure taps. Ramp drag coefficients used in data analysis were obtained by mathematical pressure-area integrations based upon these twenty-five measured pressures.

Figures 101 thru 108 show typical subsonic ($M_0 \approx 0.85$) and supersonic ($M_0 \approx 1.3$) ramp centerline pressure distributions for a range of inlet mass flow ratios. Pressure distributions for the following configurations are given at each Mach number:

R1SP1C1, $\alpha = \beta = 5^\circ$
R1SP1C1, $\alpha = 5^\circ, \beta = 12^\circ$
R1SP2C1, $\alpha = \beta = 5^\circ$
R1SP3C1, $\alpha = \beta = 5^\circ$

These configurations illustrate each major flow situation since ramp angle and side plate geometry are the primary geometric variables affecting ramp pressure distribution.

All four subsonic cases show that force is exerted by the ramp in turning the flow from the freestream direction. The R1SP1 and SP2 cases show pressures at the leading edge to be about 1.14 P_0. The extended side plates, R1SP3, create ramp leading edge pressures in the 1.2 P_0 to 1.3 P_0 range, and mass flow changes were clearly felt over the entire ramp length. The R1SP1C1, $\alpha = 5^\circ$, $\beta = 12^\circ$, configuration shows the pressure rise on the second ramp due to the additional turning. All cases show the expected ramp pressure decay after flow turning is accomplished.

Supersonically R1SP1C1, $\alpha = \beta = 5^\circ$, shows the effect of supersonic side spillage in the pressure decay on the ramp aft of the leading edge (figure 105). The change of terminal shock wave position with mass flow ratio can also be seen. Due to boundary layer build-up on the inlet surfaces and slight internal contraction, a true maximum mass flow ratio case with shock-on-cowl was not obtained. The measured maximum was 0.76. Extrapolations of data to $(A_0/A_c)_{REF} = .780$ were used in the analysis.

Figure 106 shows the situation of a detached shock wave caused by the second external ramp of configuration R1SP1C1, $\alpha = 5^\circ$, $\beta = 12^\circ$. Figure 107 shows the ramp pressure distribution with the SP2 cut-back side plates.

Supersonically, configuration R1SP3C1, $\alpha = \beta = 5^\circ$, with the extended side plates produced an unexpected ramp pressure distribution at maximum mass flow ratio. No ramp pressure decay is expected forward of the point where an expansion fan originating at the intersection of initial oblique shock wave and upper limit of the side plate would strike the ramp. No ramp pressure decay is seen in this region, but the pressure decay aft of

this point is extremely rapid. The dP/dx in this region is approximately twice as great as the maximum dP/dx for the SP1 triangular side plates and approximately equal to the maximum dP/dx of the SP2 cut-back side plates. Further, the minimum pressure after decay is only 1.03 P_0, even lower than the minimum pressure recorded with the cut-back side plates. As can be seen, the terminal shock wave did reach the cowl lip. This did not happen with the other configurations.

The terminal shock travel distance per unit change in mass flow ratio was largest for the SP3 side plates and smallest for the SP2 side plates as would be expected. The larger the possible subsonic side spillage, the smaller the necessary terminal shock travel for that spillage. From this data it is apparent that a rigorous mathematical model of the inlet flow situation must relate shock travel to side plate geometry.

At $M_0 \approx 1.3$, the R1SP2C1 configuration captured the greatest mass flow, and R1SP3C1 captured the least. In general, as seen from the terminal shock wave position, maximum mass flow ratio was determined by inlet choking. The apparent trend is: the more extensive the side plates, the more the boundary layer build-up and the smaller the maximum mass flow ratio.

XIII

SYNTHESIZING TOTAL INLET DRAG

To select the proper inlet configuration for an airplane, the evaluation of

$$(F_{INT})_{COR} = F_N - K_{ADD}(\Delta D_{ADD\ THEORY}) \qquad \text{Eq. (13)}$$

is not enough. The <u>total</u> drag chargeable to the inlet must be evaluated and compared. This is

$$D_{TOTAL} = K_{ADD}(\Delta D_{ADD\ THEORY}) + (D_{ADD})_{REF} + \left(\begin{array}{l}\text{Cowl + Side Plate}\\ \text{Pressure Drag}\end{array}\right)_{REF} \qquad \text{Eq. (14)}$$

It is proposed that the user obtain D_{TOTAL} from a synthesis of measured data and theoretical calculations. The quantity $K_{ADD}(\Delta D_{ADD\ THEORY})$ can be estimated from information already presented. The quantity

$$\left(\begin{array}{l}\text{Cowl + Side Plate}\\ \text{Pressure Drag}\end{array}\right)_{REF}$$

can be estimated from figures 51 thru 55 for the user's calculated value of $(A_o/A_c)_{REF}$.

It is proposed that the final quantity for equation 14, $(D_{ADD})_{REF}$, be evaluated by using the methods of the mathematical flow models of Appendix II -- with one exception. The exception is that ramp drag at the reference mass flow ratio, $(D_R)_{REF}$, be evaluated on an empirical rather than a theoretical basis. Section XIV presents the empirical basis for $(D_R)_{REF}$.

XIV

RAMP DRAG AT $(A_o/A_c)_{REF}$

Reference 11 presents a compilation of theory and experimental data on transonic flow over two-dimensional wedges from the work of J. D. Cole, H. S. Tsien, J. Baron, W. G. Vincenti and G. Gunderly. The compilation, illustrated in figure 9 , is presented in the form of "reduced drag coefficient" and "reduced Mach number", both of which are functions of wedge thickness to chord ratio (t/c). In the "reduced" form, data from many wedges can be coalesced or normalized into the single curve of figure 9 . A great deal of original test data from reference 11 supports the validity of this single wedge drag curve.

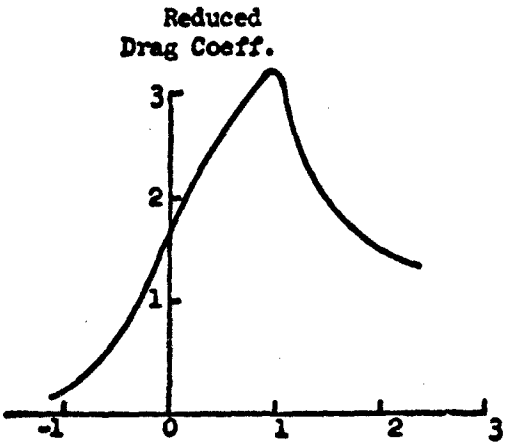

Figure 9 . Wedge Drag

A similar normalization of reference ramp drag, $(D_R)_{REF}$, has been attempted. It is understood that complete data coalescence can not be expected because of inlet side spillage effects, particularly above $M_o = 1.0$. Ramp drags for both single ramp ($\alpha = \beta$) and double ramp ($\alpha \neq \beta$) inlets are included by defining thickness and chord as shown in figure 10.

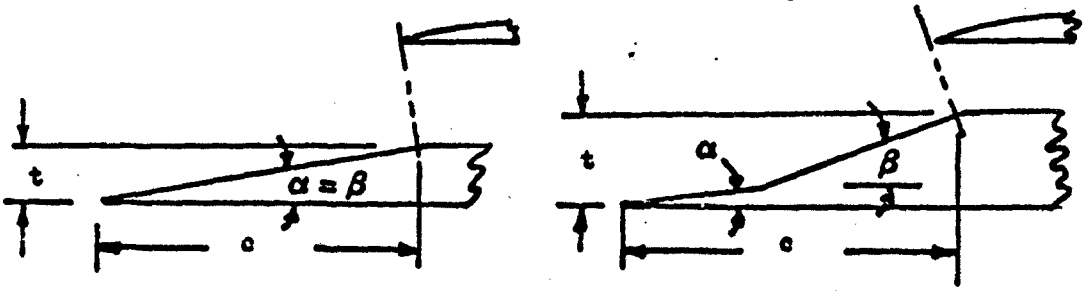

Figure 10. Inlet Ramp Thickness and Chord

For the tested configurations, if measured maximum mass flow ratio exceeded $(A_o/A_c)_{REF}$, $(D_R)_{REF}$ was obtained by the straightforward process illustrated in figure 11. However, inlet choking caused by internal contraction and boundary layer build-up normally limited the maximum $(A_o/A_c) > (A_o/A_c)_{REF}$ situation to the Mach 0.7 test data. Thus, at higher Mach numbers, extrapolations of the ramp drag data were required, also, as illustrated in figure 12.

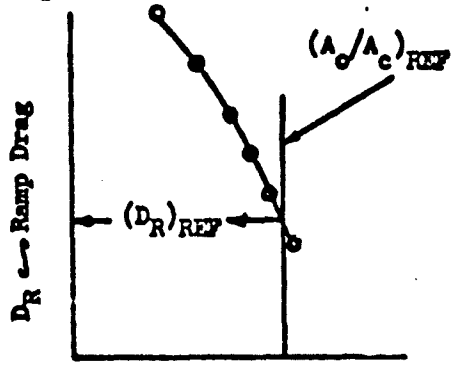

Figure 11. Ramp Drag where Max. $A_o/A_c > (A_o/A_c)_{REF}$

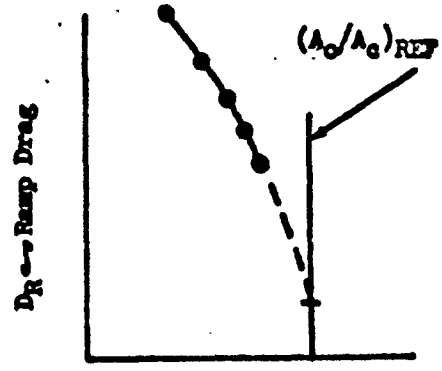

Figure 12. Ramp Drag where Max $A_o/A_c < (A_o/A_c)_{REF}$

A_o/A_c ↔ Inlet Mass Flow Ratio

Several restrictions were placed upon the allowable extent of extrapolation to insure against extrapolating to drag levels below the physically obtainable minimum. Two restrictions were imposed:

Restriction 1) For the subsonic and supersonic detached shock wave cases, D_R was not extrapolated beyond the value at which corresponding ramp pressure extrapolations showed sonic flow on the ramp at the cowl lip station.

Restriction 2) For attached shock supersonic cases, D_R was not extrapolated below the value corresponding to the terminal shock wave at the cowl lip as determined by ramp pressure profile analysis.

Both restrictions are given more detailed treatment below. Restriction 2) requires the least discussion and is covered first.

Restriction 2) was applied to only two cases used in the $(D_R)_{REF}$ summary, R1SP3C1 at $M_o = 1.3$ and at $M_o = 1.4$. Figure108 illustrates the ramp pressure profile for the Mach 1.3 case. The terminal shock wave was obviously at the cowl lip at the maximum measured mass flow ratio. The Supersonic Mathematical Model of Appendix II accounted for no side spillage and gave an $(A_o/A_c)_{REF}$ larger than the measured maximum. For these two cases the integrated ramp pressure drag at the maximum measured mass flow ratio was used for $(D_R)_{REF}$. For the remaining attached shock cases, $(D_R)_{REF}$ was taken as the extrapolated value of D_R at $(A_o/A_c)_{REF}$.

Restriction 1) is based upon a hypothesis of the effect on ramp drag of the presence or absence of boundary layer. Certainly there is no question of the validity of ramp drag extrapolation to account for internal contraction in the inlet, but what of extrapolation beyond the point where local Mach number would become sonic on the ramp at the cowl lip station as illustrated in figure 13?

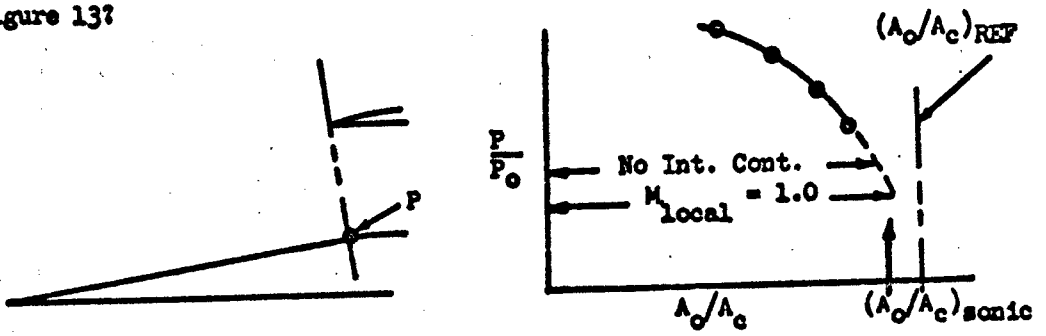

Figure 13. Sonic Flow at Inlet Lip

The figure shows a typical variation of measured pressure at the lip station vs. (A_o/A_c) found during testing at $M_o \approx 0.85$ and supersonically for detached shock wave cases. Before the extrapolation reaches $(A_o/A_c)_{REF}$, pressures which would cause local sonic flow on the ramp are encountered. Elimination of boundary layer would not allow extrapolation to $(A_o/A_c)_{REF}$, but it would allow the (P/P_o) vs. (A_o/A_c) curve to shift to the right until it intersects the $(A_o/A_c)_{REF}$ line properly at or above the sonic pressure ratio.

It is hypothesized that the ramp pressure distribution, hence minimum ramp drag, will be essentially the same when sonic flow is encountered at the lip station regardless of the presence or absence of small amounts of boundary layer.

Using this hypothesis, then, for all subsonic and supersonic detached shock cases, $(D_R)_{REF}$ was taken as the higher of the two following values:

1) the ramp drag at $(A_o/A_c)_{REF}$,
2) the ramp drag at which local sonic flow would occur on the ramp at the cowl lip station.

A summary of $(D_R)_{REF}$ values obtained is given on figure 109 along with the two-dimensional wedge drag curve of reference 11. As noted on the figure, planform ramp area is used as the ramp reference area rather than projected frontal area in order to allow direct comparison to the wedge drag curve of reference 11. In all other portions of this report, A_R refers to ramp projected frontal area.

In figure 109 the subsonic $(D_R)_{REF}$ points are the symbols in the negative region of reduced Mach number. Regardless of side plate or ramp geometry or test Mach number, these data coalesced excellently. These subsonic reference drags, particularly those at Mach 0.7, lie above the wedge drag curve as should be expected. Wedge flow corresponds to higher values of $(A_o/A_c)_{REF}$ than have been assigned to the inlets.

It can be seen that $(D_R)_{REF}$ is not zero subsonically as is predicted by the mathematical models of Appendix II. For this reason an empirical rather than a theoretical value of ramp drag has been suggested for calculating D_{TOTAL} of equation 14.

The solid symbols on figure 109 represent inlet operation at supersonic speeds with a shock wave detached from the initial inlet ramp. All data except the Mach 1.3 and 1.4 cases of R3SP1C1 show reasonable coalesence, especially since data separation due to side spillage is to be expected supersonically. It is apparent that side spillage causes the reference ramp drag values to fall well below the two-dimensional wedge drags.

The five flagged symbols represent two-ramp inlet operation ($\alpha \neq \beta$) where an oblique shock wave is attached at the initial ramp and a detached shock wave stands just forward of the second ramp. The mathematical models of Appendix II were not designed to compute a reference mass flow ratio for these cases. Therefore, these five points are shown for the maximum measured mass flow ratio. Because tunnel flow was slightly misaligned at Mach 1.3 and 1.4 and because on a comparable $(A_o/A_c)_{REF}$ basis these drags should be somewhat lower, it is suggested that $(D_R)_{REF}$ values for similar inlet operation be selected at the lower limit of the "primary range of data" shown on the figure.

The open symbols (unflagged) at the right of figure 109 denote $(D_R)_{REF}$ values for the supersonic flow case where an oblique shock wave is attached at the initial inlet wedge and $\alpha = \beta$. Except for the R1SP3C1 cases, ramp drags were extrapolated to $(A_o/A_c)_{REF}$ to find $(D_R)_{REF}$. Analysis of the ramp pressure profiles for these cases showed that the computed $(A_o/A_c)_{REF}$ values were too small to correspond to shock-on-cowl operation.

It is proposed that reference ramp drags, $(D_R)_{REF}$, be selected from the "primary range of data" of figure 109.

As a first attempt, ramp drag normalization has been very successful subsonically and reasonably successful supersonically. A means of unification of ramp drag data for performance prediction seems to be almost a necessity considering the geometric variations from inlet to inlet. The reduced drag vs. reduced Mach number presentation of figure 109 appears to offer a reasonable approach. More sophisticated mathematical flow models for $(A_o/A_c)_{REF}$ predictions, especially at the higher supersonic speeds, are a desirable refinement of this approach.

XV

SPILLAGE DRAG COMPARISON - R1SP1C1 THRU R1SP1C6

The chargeable inlet spillage drag, D_{TOTAL}, is given in coefficient form for configurations R1SP1C1 thru C6 at Mach 0.84 and 1.29 in figures 110 and 111 of Appendix III. D_{TOTAL} in equation 14 was defined as

$$D_{TOTAL} = K_{ADD}\left(\Delta D_{ADD\ THEORY}\right) + \left(D_{ADD}\right)_{REF} + \left(\begin{matrix}\text{Cowl + Side Plate}\\ \text{Pressure Drag}\end{matrix}\right)_{REF} = D_{ADD} + \left[\int (P-P_o)dA\right]_{\text{Cowl + Side Plate}}$$

and its evaluation was explained. Evaluation of D_{TOTAL} from actual experimental data, as in this case, is more direct. Consideration of equations and 14 shows that

$$D_{TOTAL} = \left[D_{ADD} - (D_{ADD})_{REF}\right] + \left[\int (P-P_o)dA\right]_{\substack{\text{Cowl +}\\ \text{Side plate}}} + (D_{ADD})_{REF} \quad \text{Eq. (15)}$$

The first term was obtained directly from figures 45 thru 50, the second term from figures 51 thru 55. The term $(D_{ADD})_{REF}$ was evaluated as discussed in Sections XIII and XIV.

As can be seen from the figures, the circular arc cowls are best subsonically. The three straight cowls are definitely second best. Supersonically at Mach 1.29, the C1 10° circular arc cowl and the 6° straight cowl, C2, were best and quite comparable. At high supersonic speeds low angle cowls are, of course, best.

The thick cowl, C6, had low drag both subsonically and supersonically at Mach 1.3 for very large spillages. However, at high supersonic Mach numbers the drag of C6 is expected to be large.

CVI

SPILLAGE DRAG OF VARYING RAMP OR COWL

Measured external model drag coefficients vs. mass flow ratio are given for configurations

R1SP1C1; $\alpha = 5^\circ$, $\beta = 5^\circ$
R1SP1C1; $\alpha = 5^\circ$, $\beta = 9^\circ$
R1SP1C1; $\alpha = 5^\circ$, $\beta = 12^\circ$

R1SP1C1, $\alpha = \beta = 5^\circ$
R1SP1C9, $\alpha = \beta = 5^\circ$
R1SP1C10, $\alpha = \beta = 5^\circ$

for Mach 0.85, 1.1 and 1.3 in figures 112 thru 114 of Appendix III. The upper parts of these figures illustrate the effect of increasing the variable ramp angle. The lower curves show the effect of varying the cowl.

On the abscissa axis of the figures, the captured airflow, A_o, is ratioed to the capture area of the R1SP1C1 configuration. This was done because of the changing inlet capture area involved in varying the cowl. Using a fixed A_o in the A_o/A_c ratio allows direct comparison of spillage drag by varying the ramp angle and by varying the cowl.

The ordinate axis show measured model drag as defined by equation Thus, the ordinate axis drags are

$$D_{ADD} + \left[\int (P-P_o)dA\right]_{\substack{\text{Cowl +} \\ \text{Side Plate}}} + (\text{CONST.}) = N$$

and contain a constant drag value pertaining only to the model, not to an aircraft propulsion system.

The chargeable inlet drag at $(A_o/A_c)_{REF}$ for R1SP1C1, $\alpha = \beta = 5^\circ$,

$$(D_{ADD})_{REF} + \left(\begin{matrix}\text{Cowl + Side Plate} \\ \text{Pressure Drag}\end{matrix}\right)_{REF} = (D)_{\substack{REF \\ R1SP1C1,\ \alpha = \beta = 5^\circ}}$$

as defined in equation 14 is indicated on each figure. Then, the chargeable drag for any configurations becomes

$$D_{TOTAL} = D_{ADD} + \left[\int (P-P_o)dA\right]_{\substack{\text{Cowl +} \\ \text{Side Plate}}} \qquad \text{Eq. (16)}$$

$$= N - \left[N_{REF} - (D)_{REF}\right]_{\substack{R1SP1C1 \\ \alpha = \beta = 5^\circ}}$$

For example on figure 112 D_{TOTAL} of R1SP1C10 at Mach 0.85 becomes

$$\frac{D_{TOTAL}}{q_o A_c} = \frac{N}{q_o A_c} - (.2060 - .0254)$$

$$= \frac{N}{q_o A_c} - (.1806)$$

where A_c, again, is the capture area of R1SP1C1.

As can be seen from the data of figures 112 thru 114 both increasing the ramp angle and varying the cowl reduce spillage drag. For the particular model geometries tested and for anticipated spillages, ramp variation showed lower spillage drags than cowl variations. A minimum drag configuration could be obtained by using the combination of ramp and cowl variation. Most supersonic aircraft must have a variable ramp. A variable cowl would be an addition. The variable cowl weight penalty must be traded against lower spillage drag before a variable cowl can be justified.

XVII

SPILLAGE DRAG, SHARP vs. BLUNT COWL LIPS

Several blunted lip cowls were tested for possible application in hypersonic inlets. Figure 115 shows a comparison of the external drags of configurations R1SP1C1, C7 and C8 at Mach 0.85 and 1.29. The abscissa and ordinate axes of the figure and the "zero drag reference" of a similar presentation were explained in detail in the preceeding section. Again, drag is shown ratioed to the capture area, A_c, of configuration R1SP1C1.

Cowl C1 had a sharp lip. Cowls C7 and C8 had lip radii of 0.04" and 0.1", respectively. At 0.85 Mach the drags of R1SP1C1 and C7 are very comparable. The small drag difference at the high mass flow end of the plot may, in part, be due to data scatter. The larger lip radius on R1SP1C8 did cause a drag penalty.

At Mach 1.29, configuration drag was very definitely a function of lip bluntness. The smaller the lip radius, the smaller the drag.

XVIII

CONCLUSIONS AND RECOMMENDATIONS

1. When transonic inlet performance is considered in inlet selection, the total chargeable drag of the various inlet configurations should be evaluated. Though a given inlet may achieve a high degree of additive drag cancellation, the total drag of that inlet may eliminate it from consideration.

2. Lower spillage drags were obtained by using rotation of the variable external ramp of the inlet to deflect excess airflow than by using inward rotation of a variable cowl to spill air. Since a variable second external ramp is normally required on supersonic rectangular inlets, there is no additional weight penalty involved in using the variable ramp to obtain lower transonic spillage drags.

3. The combination of variable cowl and variable ramp should achieve lower spillage drag than the ramp alone. However, the transonic spillage drag decrease must be traded-off against variable cowl weight penalties.

4. Blunting the leading edge of the 10° circular arc cowl had little effect upon additive drag cancellation, and edge blunting did increase total chargeable inlet drag. If lip blunting is required for take-off performance increases, for anti-icing or for heat-transfer or structural reasons, the blunting penalties at transonic speeds can be estimated from data included in this report.

5. Circular arc cowls with 10° and 15° initial angle showed lower drag than the 6°, 10° and 15° straight cowls at Mach 0.85, both at the reference mass flow ratio and 0.20 A_o/A_c lower. Supersonically at Mach 1.3, the 10° circular arc cowl was still best, but the 6° straight cowl was a very close second. Of course, at high supersonic speeds low cowl angles are desirable.

6. Mathematical models for the computation of theoretical additive drag have been devised. The models were deliberately simplified to make hand calculations practical. Because of the large number of such calculations involved in test data analysis a computer program was written and is included. In addition, additive drag correction factors, K_{ADD}, were determined for a number of inlet configurations from experimental data. By using K_{ADD} and $\Delta D_{ADD\ THEORY}$ which is obtainable from the mathematical models, the drag for airflow spillage below the reference mass flow ratio can be determined.

7. Ramp pressure drags at the reference mass flow ratio for transonic speeds have been normalized and compared with wedge drag theory developed in reference 11. These data provide useful empirical information. Cowl plus side plate drags for a number of configurations have also been determined. The empirical ramp drag and cowl plus side plate drag (at the reference mass flow ratio) can be used to compute total inlet drag at the reference mass flow ratio.

8. Total chargeable inlet drag at any mass flow can be found by summing K_{ADD} ($\Delta D_{ADD\ THEORY}$) from item (6) and total drag at the reference mass flow ratio as discussed in item (7). It is recommended that care be taken in selecting K_{ADD} and the cowl plus side plate drag. Cowl shape was found to be very important in spillage drag.

APPENDIX I

WIND TUNNEL MODEL DESCRIPTION

1. General. The model description within this appendix includes all information needed for comprehension of the reported data. A detailed description of the model, model construction drawings and a description of the on-test-site data reduction equations are available in references 12 or 13 .

2. Over-all Arrangement. Figure 14 illustrates the force model assembly. In general, only components of aerodynamic interest are shown. Basically, the inlet is categorized as

a) supersonic,
b) rectangular,
c) external ramp type.

Interchangeable cowls, side plates and fixed initial ramps were constructed for the model and tested. Variable ramps were attached to the aft end of the fixed initial ramp. The ramp train consisted of the fixed initial ramp (interchangeable), a second external ramp, an internal throat panel and an aft panel. The three variable panels were remotely actuatable from the wind tunnel control room, allowing the second external ramp to be adjusted thru an angular range of 5° to 12° with respect to the free stream vector.

The ramp train was connected together by rotating "piano" hinges. For each interchangeable ramp installation, the forward hinge axis of the variable external ramp was fixed. Power linkage of the parallelogram type was attached to the throat panel only. Thus, all throat panel locations could be described by a series of translations of the panel along and perpendicular to the fixed longitudinal axis of the model. A sliding hinge at the aft end of the last panel in the ramp train allowed the end of that panel to slide back and forth along the subsonic diffuser wall.

To simplify drag measurements neither the ramp train nor any other surface of the model had boundary layer removal provisions. Since boundary layer was not bled off, care was taken to eliminate the possibility of flow separations in the forward portion of the inlet caused by jets of high pressure air fed into the duct from beneath the ramp train. "Teflon" strips were inserted into the edges of the external ramp and the throat panel. This created a tight, though sliding, seal between ramps and duct walls. The "piano" hinges at the juncture of the external ramps and at both ends of the throat panel were entirely encased in hardened liquid rubber. The rubber, though filling all joints of the hinges, was sufficiently elastic to allow the necessary minor rotations of the ramps.

At the juncture of the "live" and "dead" portions of the force model a labyrinth seal was installed which virtually eliminated flow leakage,

Though small, the leakage flow was calculated from measured pressures across the seal using seal calibration curves. All data were corrected for seal leakage. "Live" section exit conditions (total and static pressures) were measured by total head rakes, static rakes and wall static taps. Flow straigtening screens were installed forward of the "live" section exit to improve the exit velocity profile.

The "live" and "dead" portions of the model were attached thru a 2 1/2 inch diameter Task Mark III-40037 six component force balance (280 lb. rated chord force) supplied by NASA Ames. All pressure taps located on the "live" section of the model were read out thru NASA Ames supplied "Scannivalves" located on the "live" section. This eliminated the need for jumpering flexible pressure tubes between "live" and "dead" model portions, which could have caused force measurement errors.

A large aerodynamic shield was fixed to the forward end of the "dead" section of the model. The shield projected forward over a considerable portion of the "live" section. Not only did the shield surround the balance and "Scannivalves", but it surrounded all portions of the "live" section of the model where unwanted changes in pressure drag (as a function of inlet mass flow ratio) might occur from flow spillage over the cowl and around the side plates.

The initial portion of the "dead" section consisted of a diffusing pipe and a long section of flow straightening pipe ahead of the flow metering nozzle. Four different metering nozzles had been constructed to assure proper meter size for various test conditions. Most "dead" section pressures were read out thru "Scannivalves" located on the "dead" section. The metering nozzle pressure instrumentation, however, was routed outside the tunnel and read on high accuracy equipment to assure valid mass flow data.

A remotely actuatable throttling plug located at the end of the model was used for inlet mass flow control.

The entire model assembly was cantilevered from the vertical tunnel strut, and the model longitudinal axis was fixed at 0° angle of attack, 0° angle of yaw for the entire wind tunnel test.

3. Interchangeable Components. Several different initial ramps, sets of side plates and inlet cowls were constructed. The model was such that many ramp, side plate and cowl combinations could be assembled and tested. Figure 15 illustrates the assembly R1SP1C1, combining initial ramp R1, side plate set SP1 and cowl C1.

In all, four initial ramps, four sets of side plates and ten cowls were constructed. Ramps R1 thru R4 are described in figure 16, side plates SP1 thru SP4 in figure 17, and cowls C1 thru C10 in figures 18 thru 20. The following combinations were tested:

R1SP1C1	[illegible]	[illegible]
R1SP1C2	[illegible]	[illegible]
R1SP1C3	[illegible]	[illegible]
R1SP1C4	[illegible]	[illegible]
R1SP1C5	[illegible]	[illegible]
R1SP1C6	[illegible]	[illegible]

The R1SP1 ramp-side plate combination represents a shock-on-cowl Mach 3.0 inlet. R1SP1C1 thru C6, then, emphasize cowl shape variation. The R1SP1C7 and C8 assemblies were blunted leading edge (hypersonic) configurations. The R1SP1C9 and C10 configurations, together with the basic R1SP1C1, simulated hinged cowl operation.

Combinations R1SP1C1, R1SP2C1, [illegible] and [illegible] have side plate (side spillage) area differences. Initial ramp angle changes are brought out by the R1SP1C1, R2SP1C1 and [illegible] assemblies.

The R4SP4C1, C4 and C6 series is a Mach 2.2 shock-on-cowl inlet with three cowl shape variations.

4. Pressure Instrumentation. Ramps R1 thru R4 were each instrumented with four static pressure taps (Figure 21). Twenty-one static pressures were recorded on the external variable ramp (Figure 22). Cowls C4 thru C10 were each instrumented with two pressure taps (Figure 23). Only side plates SP1 and SP3 were instrumented (Figure 24).

Ramp, side plate and cowl pressures have the predominant part in reported data. Although many other model pressures were recorded and used in data reduction, they are not illustrated or listed. References 12 or 13 give complete instrumentation details.

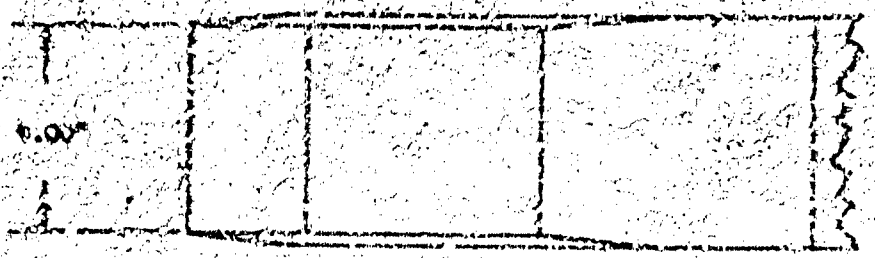

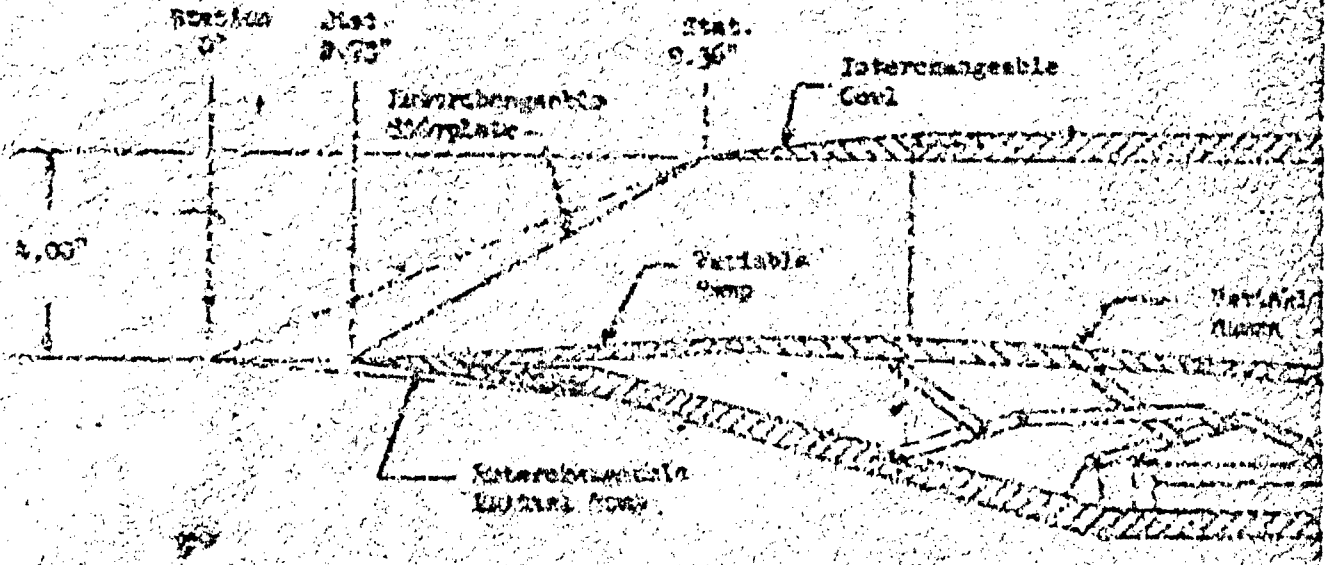

Station 0" - Model loading edge with initial radius
R1, R2 or R3 installed.

Station 2.73" - Model leading edge with ramp
R4 installed.

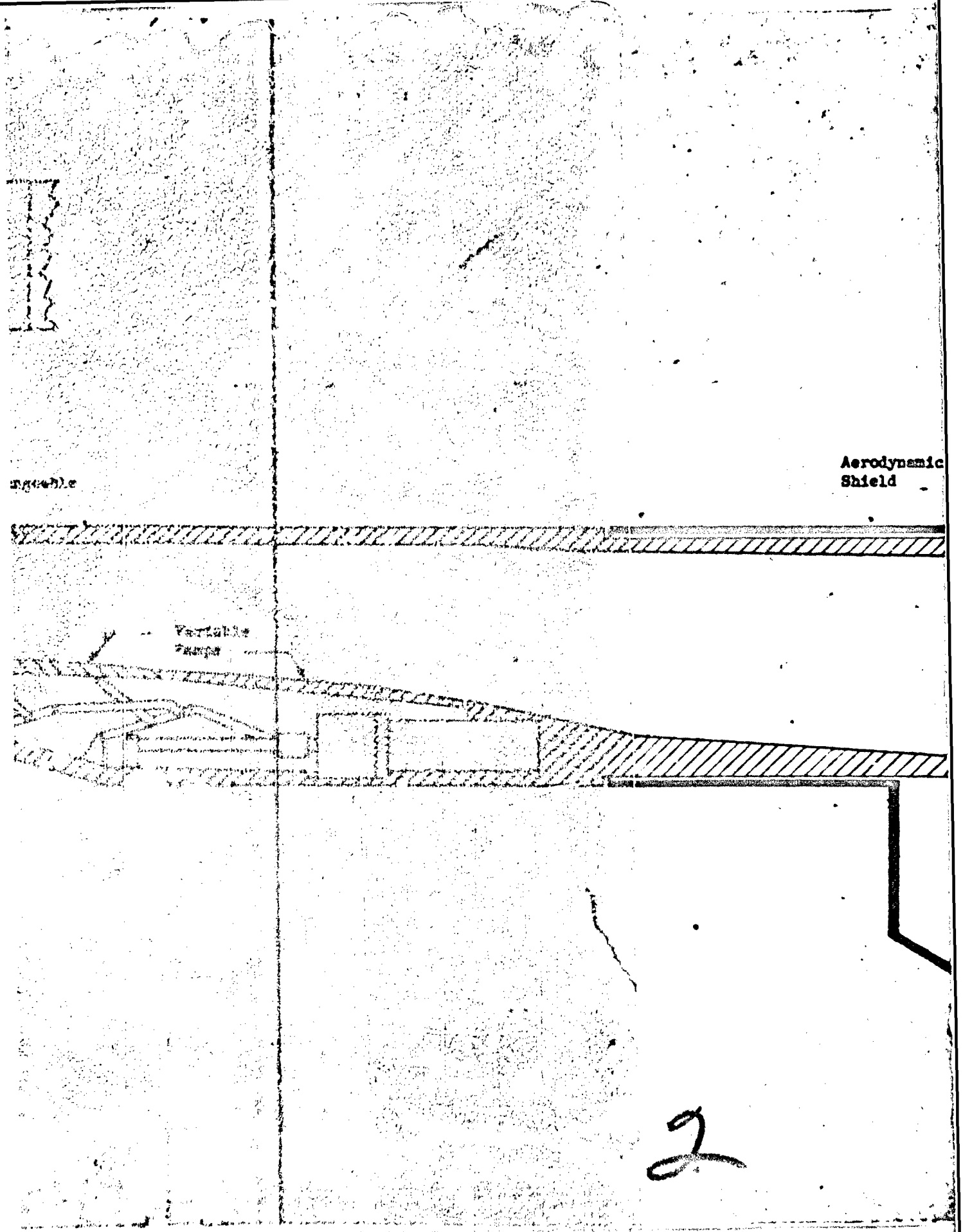

2

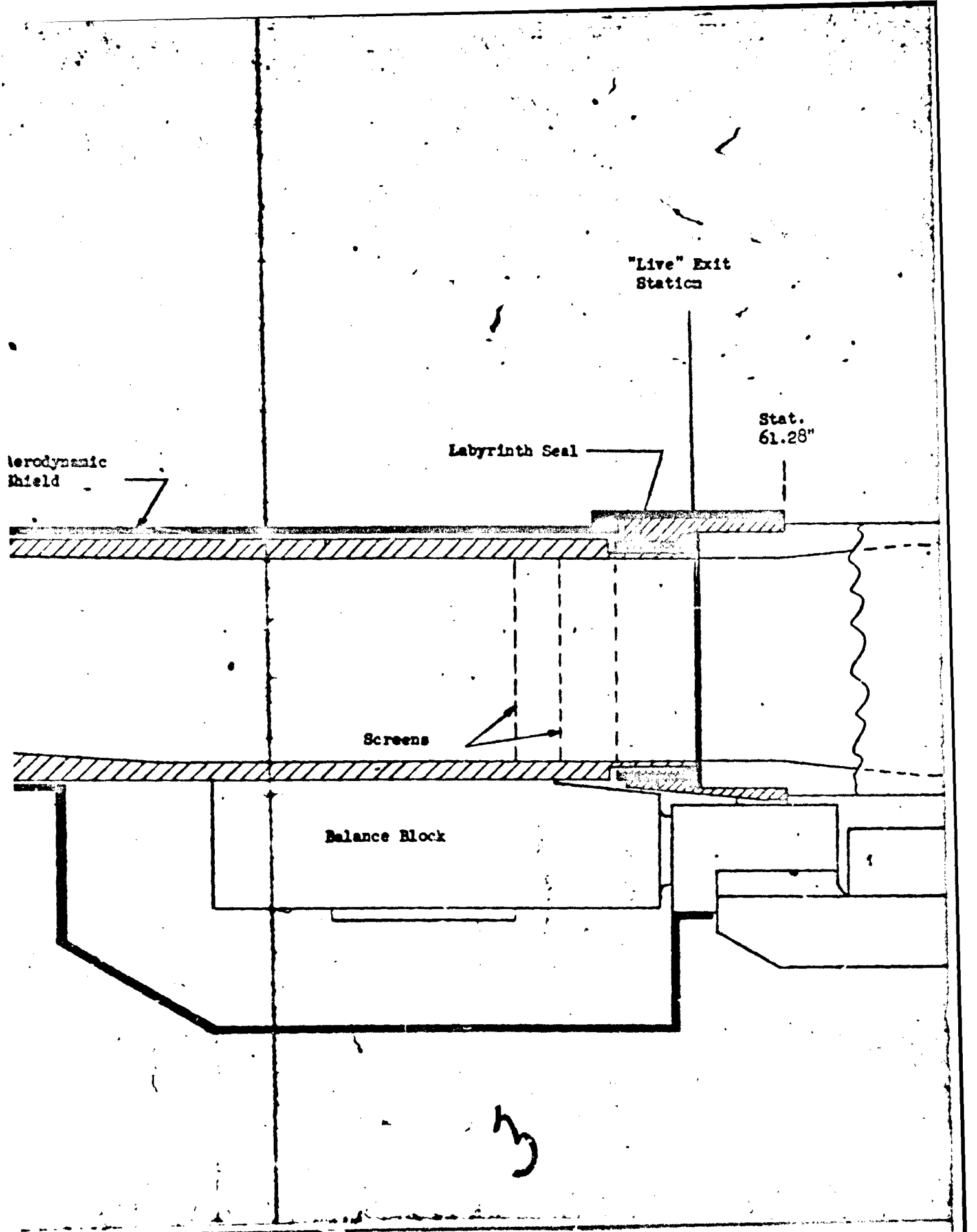

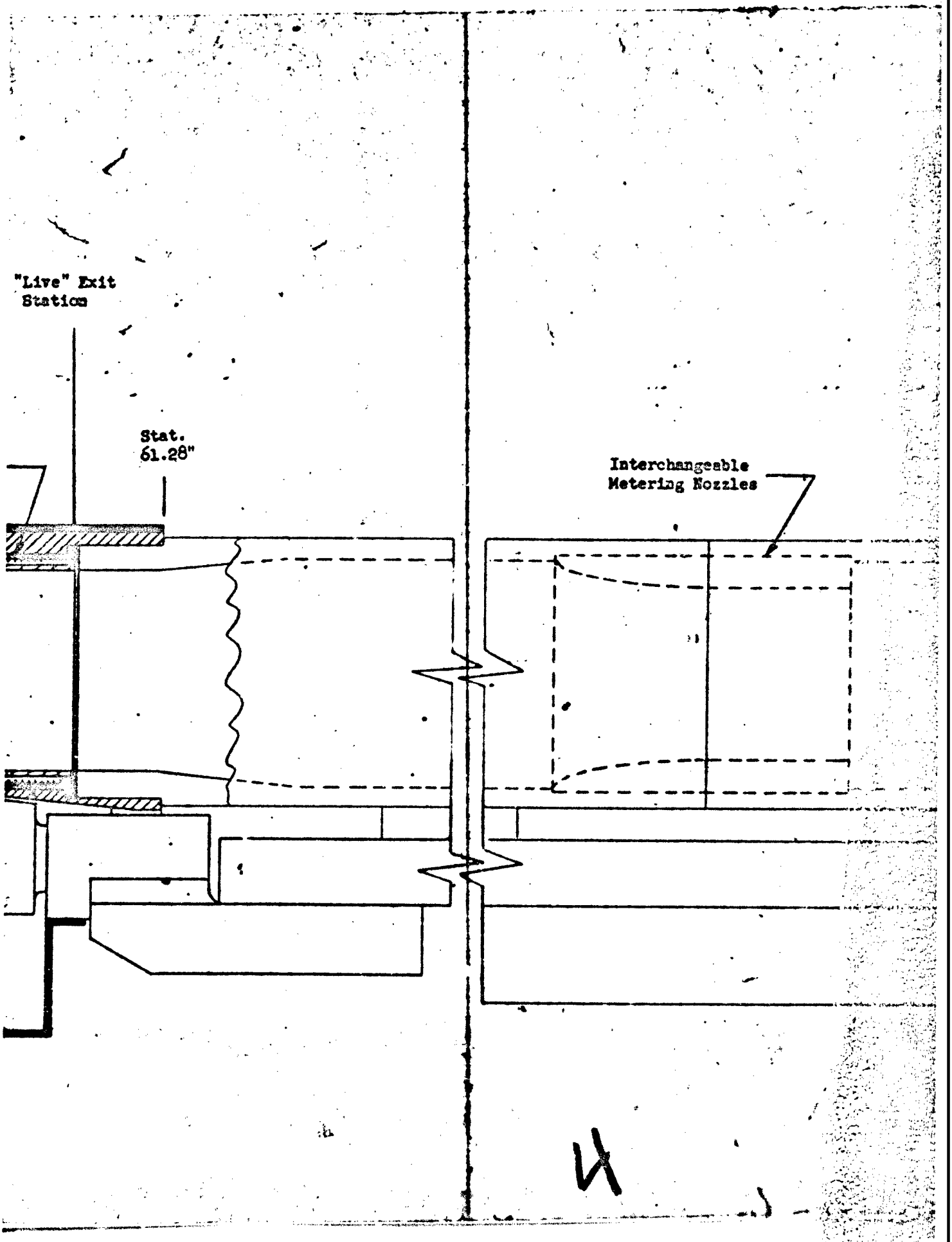

4

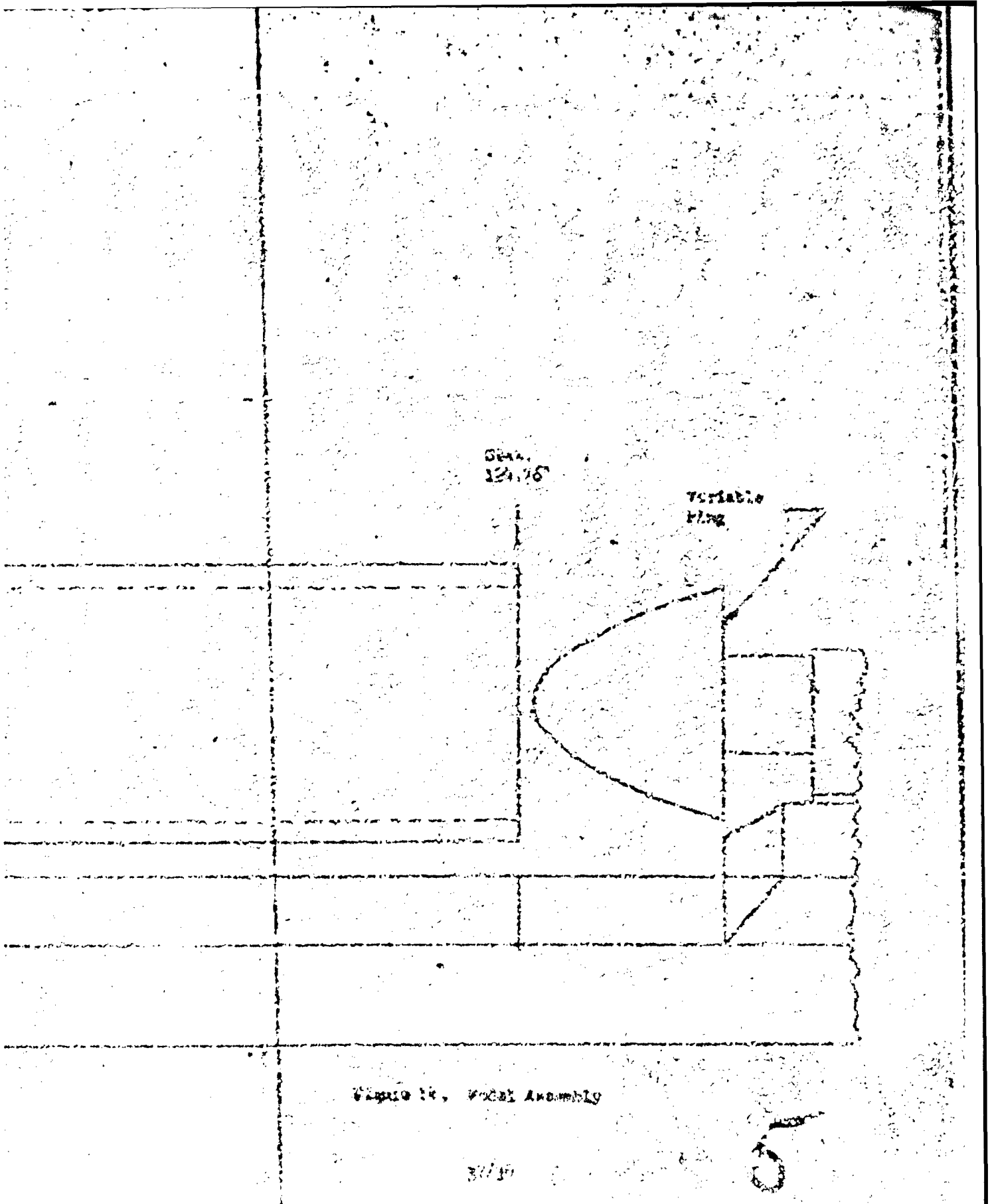

Figure 14. Pedal Assembly

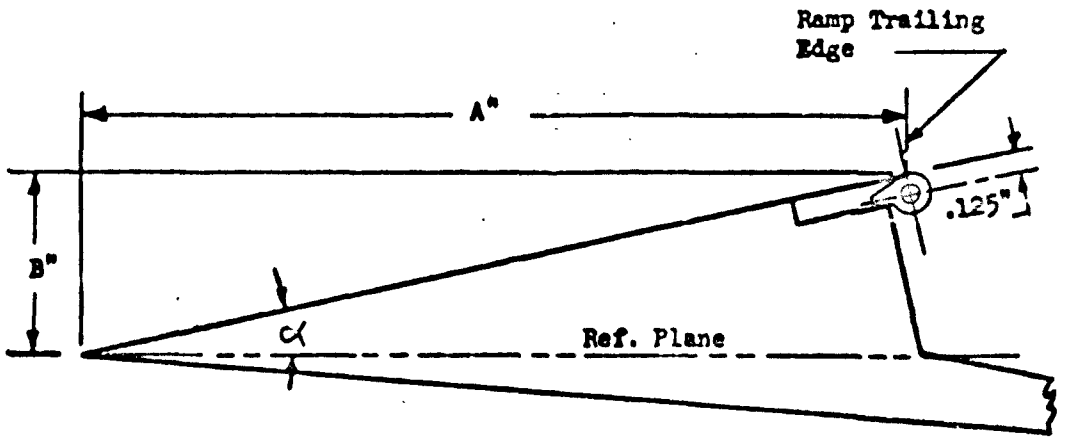

Ramp	A	B	α
R1	4.959	0.434	5°
R2	4.930	0.605	7°
R3	4.853	1.032	12°

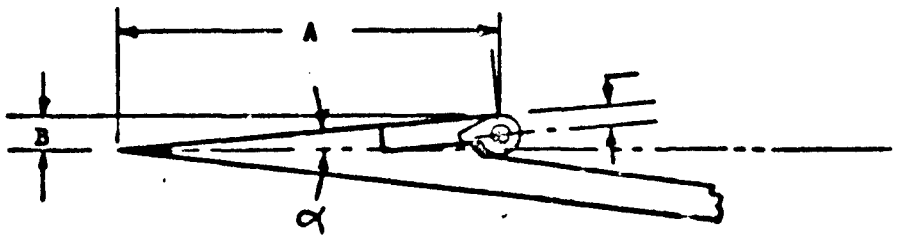

Ramp	A	B	α
R4	2.255	0.197	5°

Figure 16. Ramps R1 Thru R4

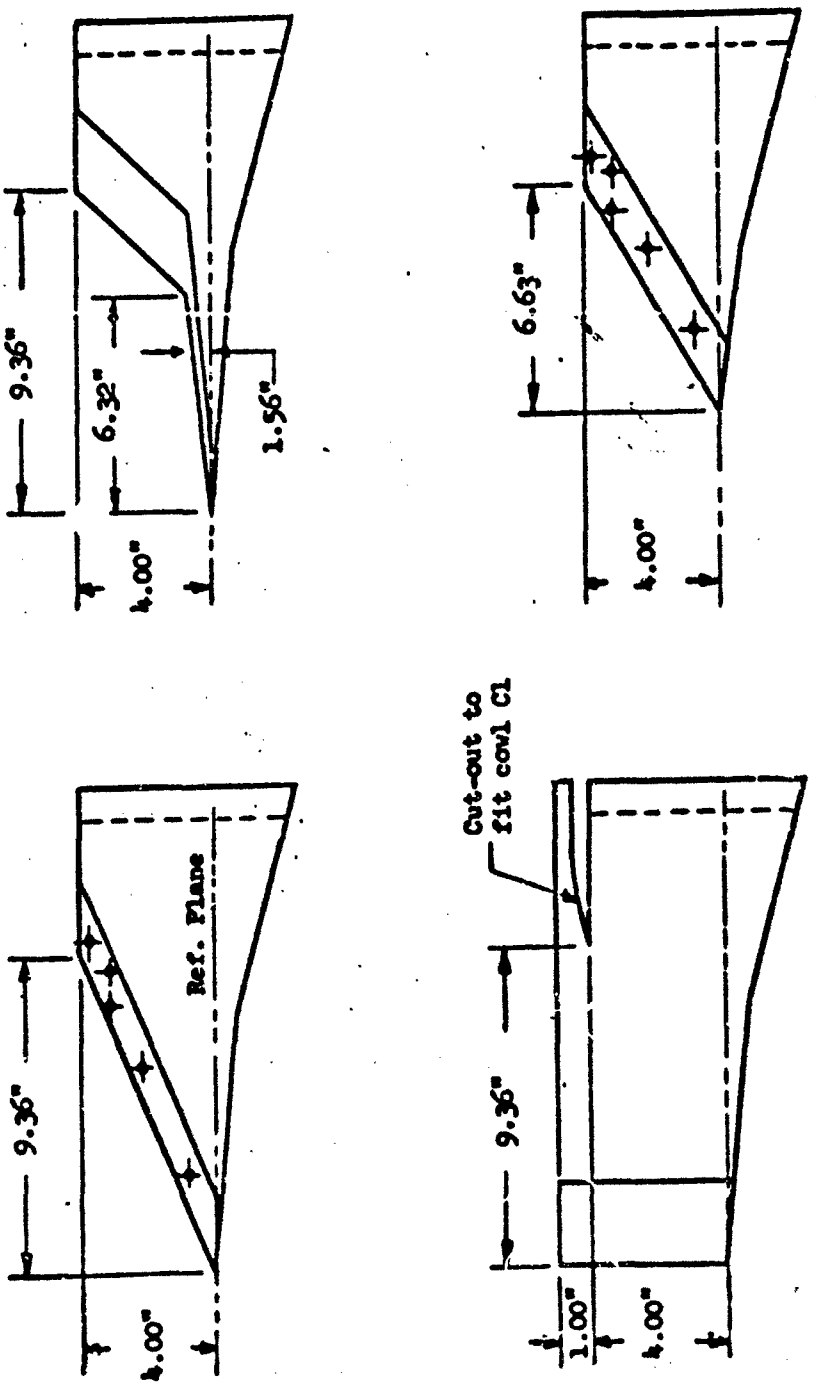

Figure 17. Side Plates SP1 Thru SP4

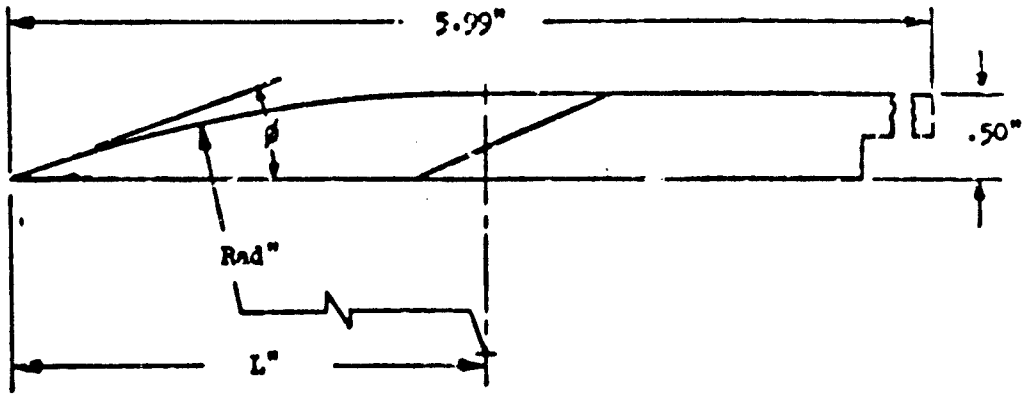

Cowl	L	Rad"	ϕ
C1	5.71	32.89	10°
C5	3.79	24.66	15°

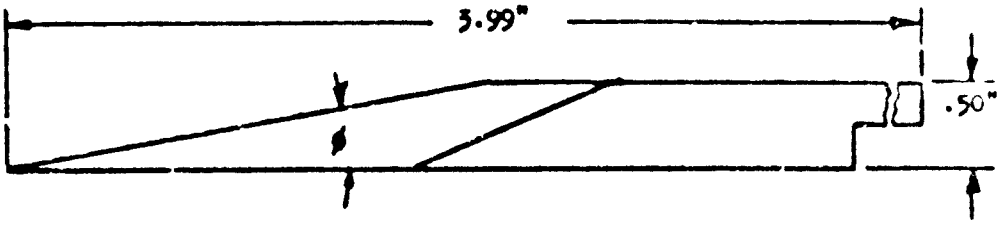

Cowl	ϕ
C2	60
C3	10°
C4	15°

Figure 18. Cowls C1 Thru C5

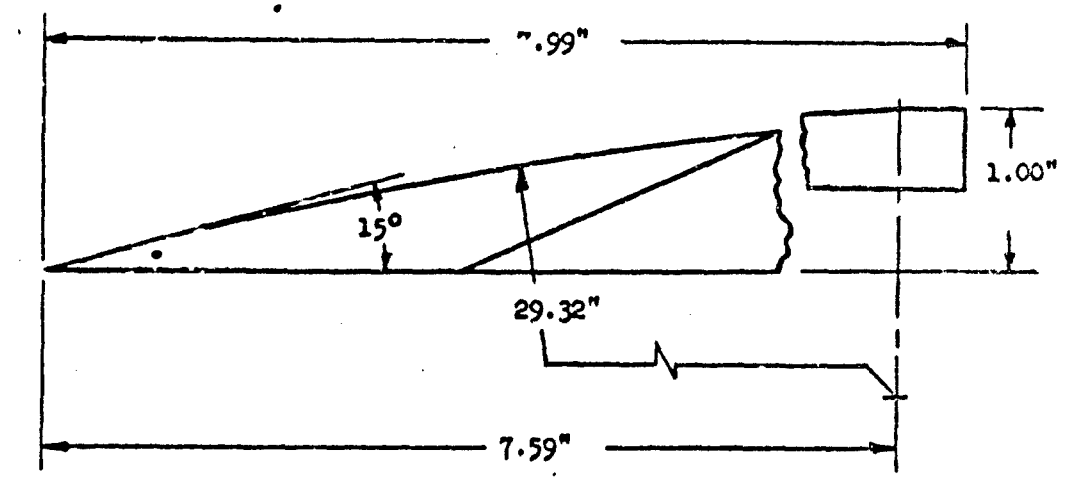

Cowl C6

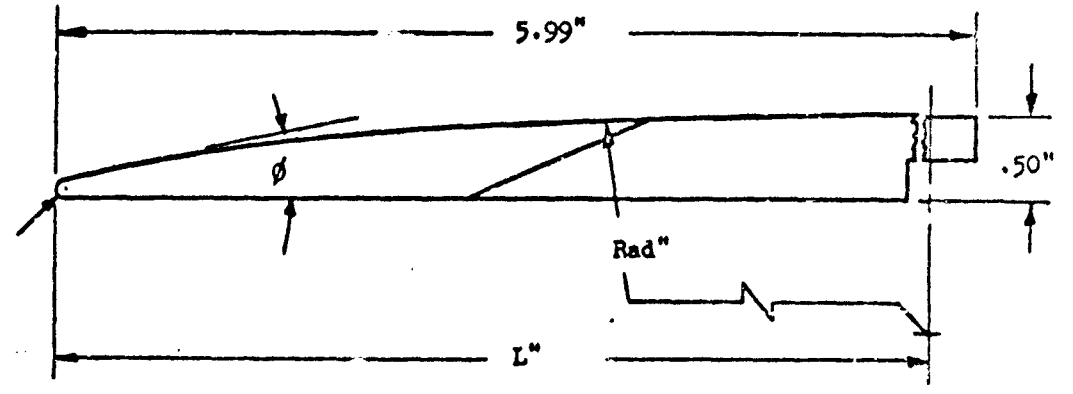

Cowl	L	Rad"	ø	τ
C7	5.71	32.89	10°	.040
C8	5.71	32.89	10°	.100

Figure 19. Cowls C6, C7, C8

Note: Basic Cowl Shape - C1

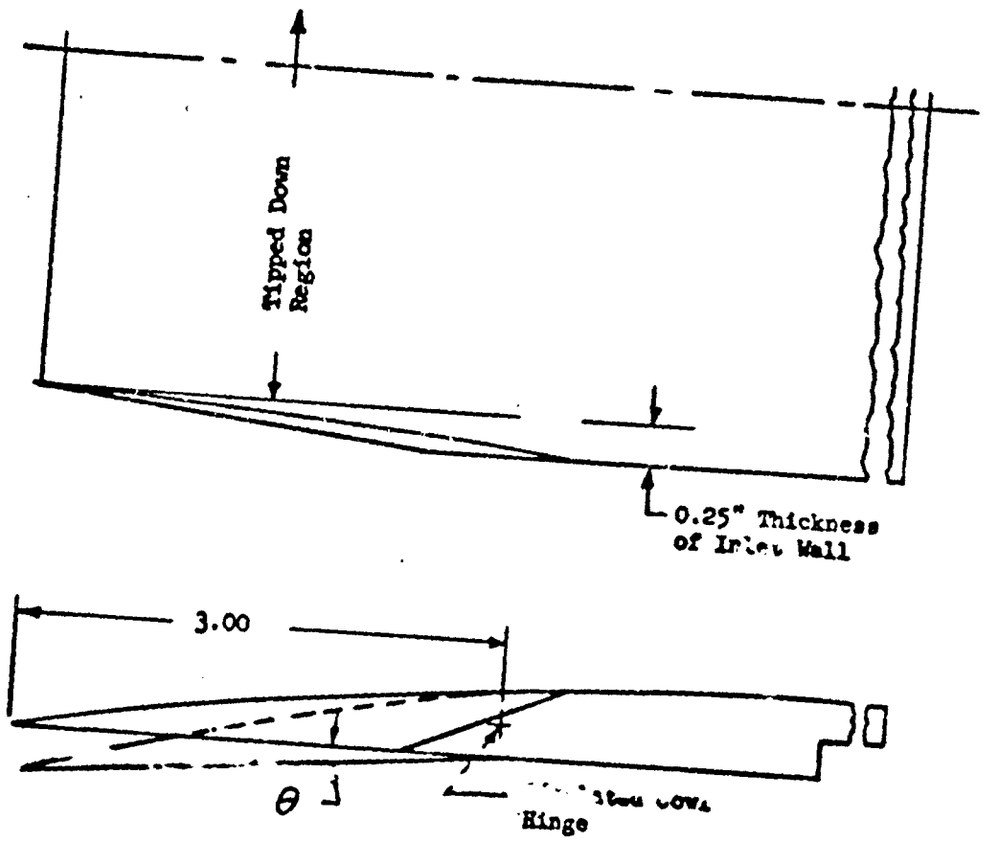

Cowl	θ
C9	5°
C10	10°

Figure 20. Cowls C9, C10

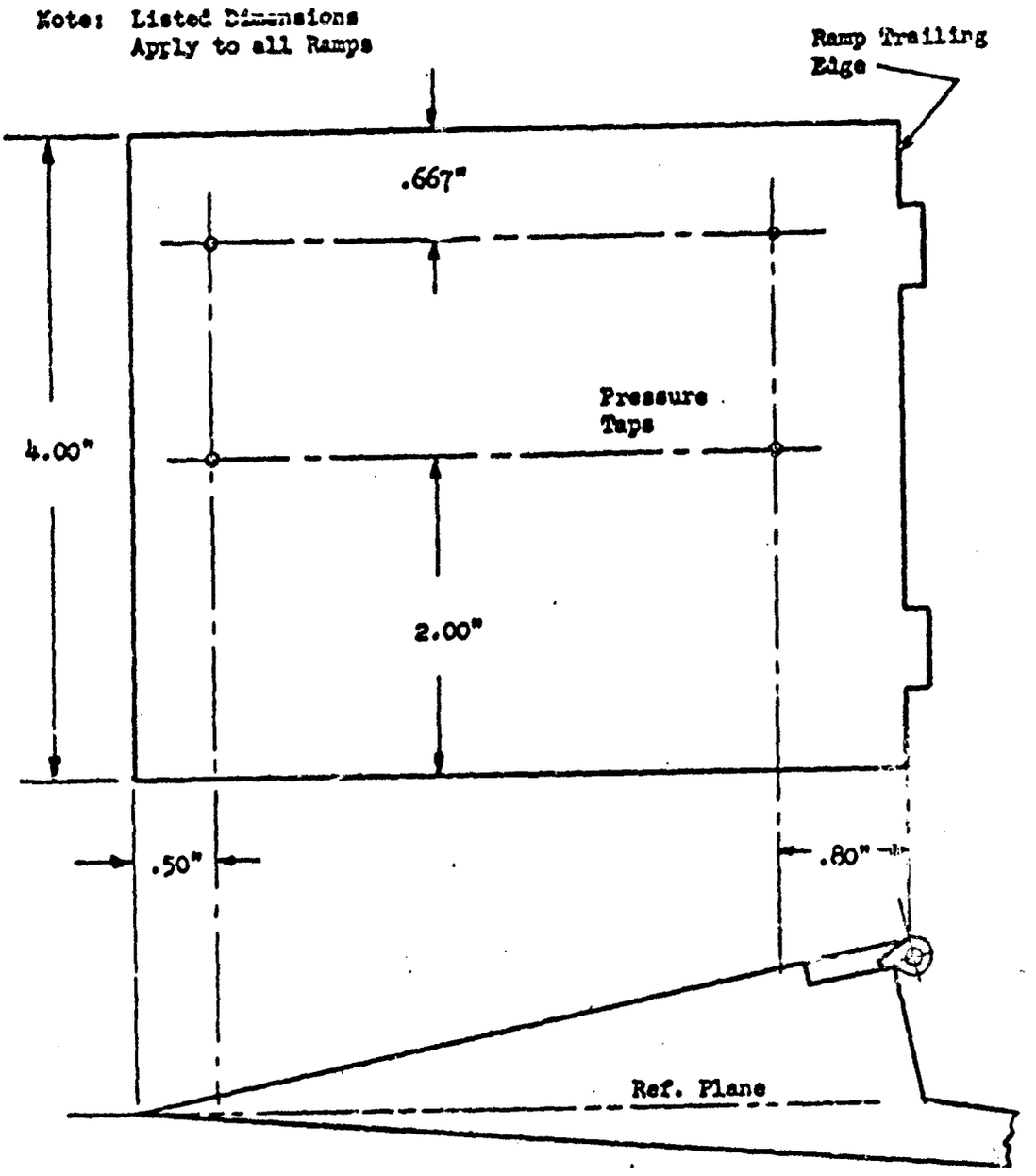

Figure 21. Ramp Pressures

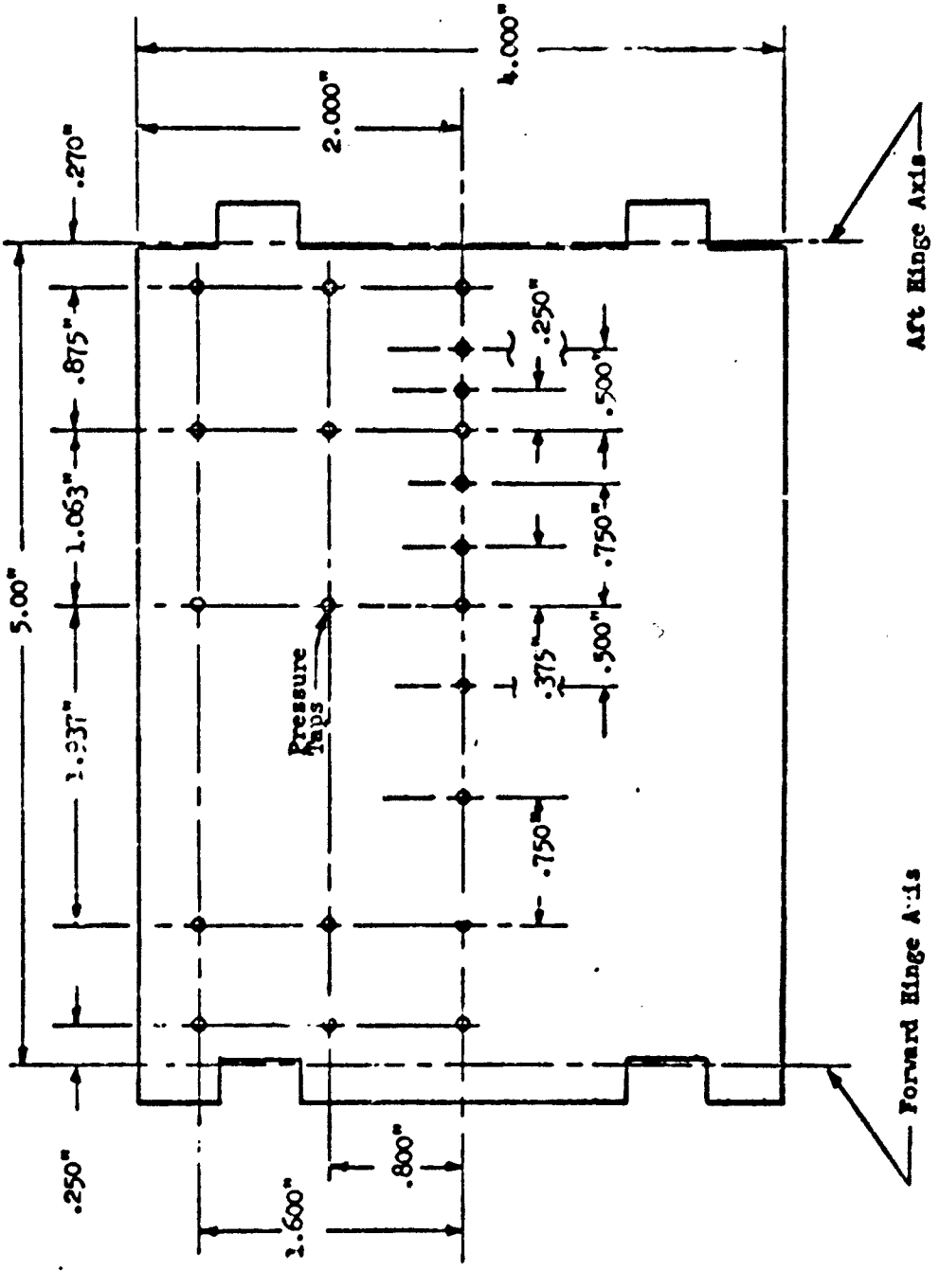

Figure 22. External Moveable Ramp Pressures

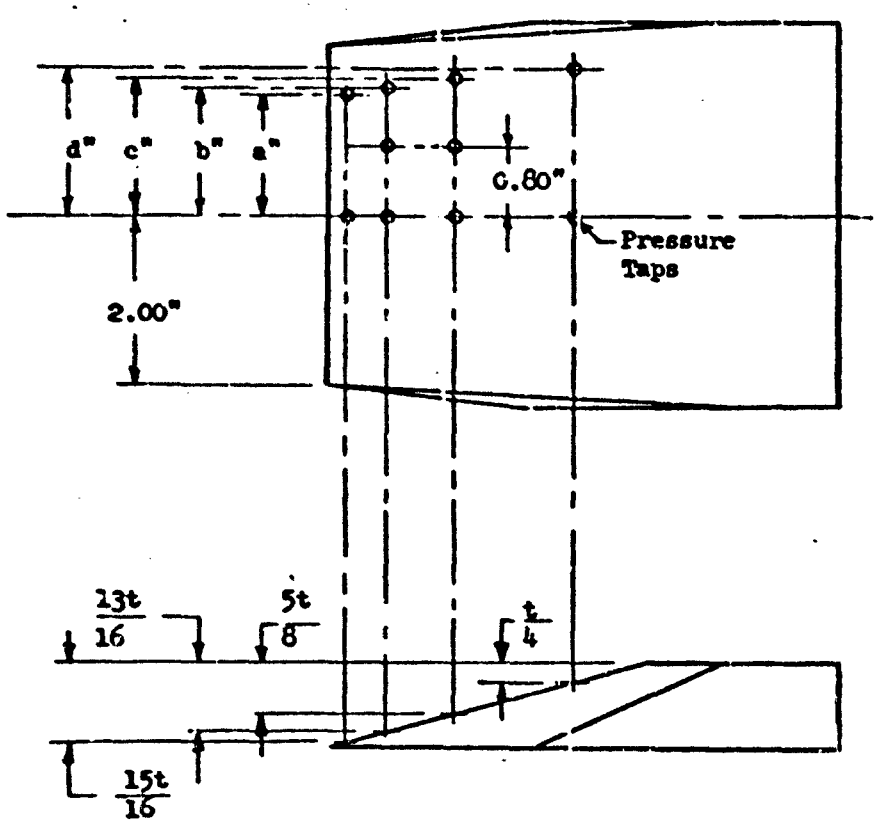

Figure 23. Cowl Pressures

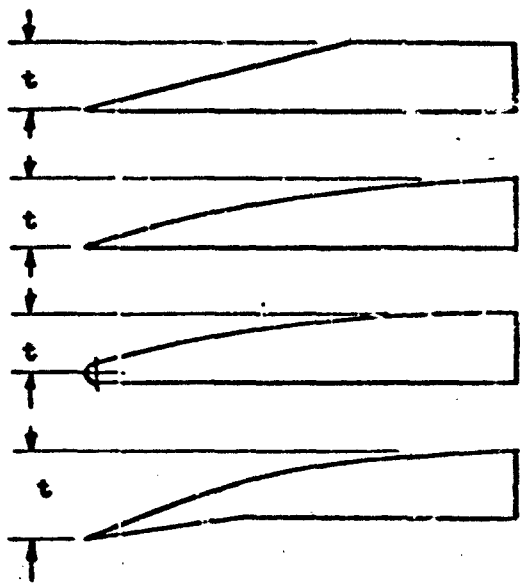

Cowl	a	b	c	d
C1	1.61	1.62	1.64	1.70
C2	1.61	1.64	1.68	1.73
C3	1.61	1.62	1.64	1.68
C4	1.61	1.61	1.63	1.66
C5	1.60	1.62	1.63	1.67
C6	1.61	1.62	1.65	1.73
C7	1.60	1.62	1.64	1.69
C8	1.60	1.61	1.62	1.67
C9	1.60	1.60	1.60	1.60
C10	1.60	1.60	1.60	1.60

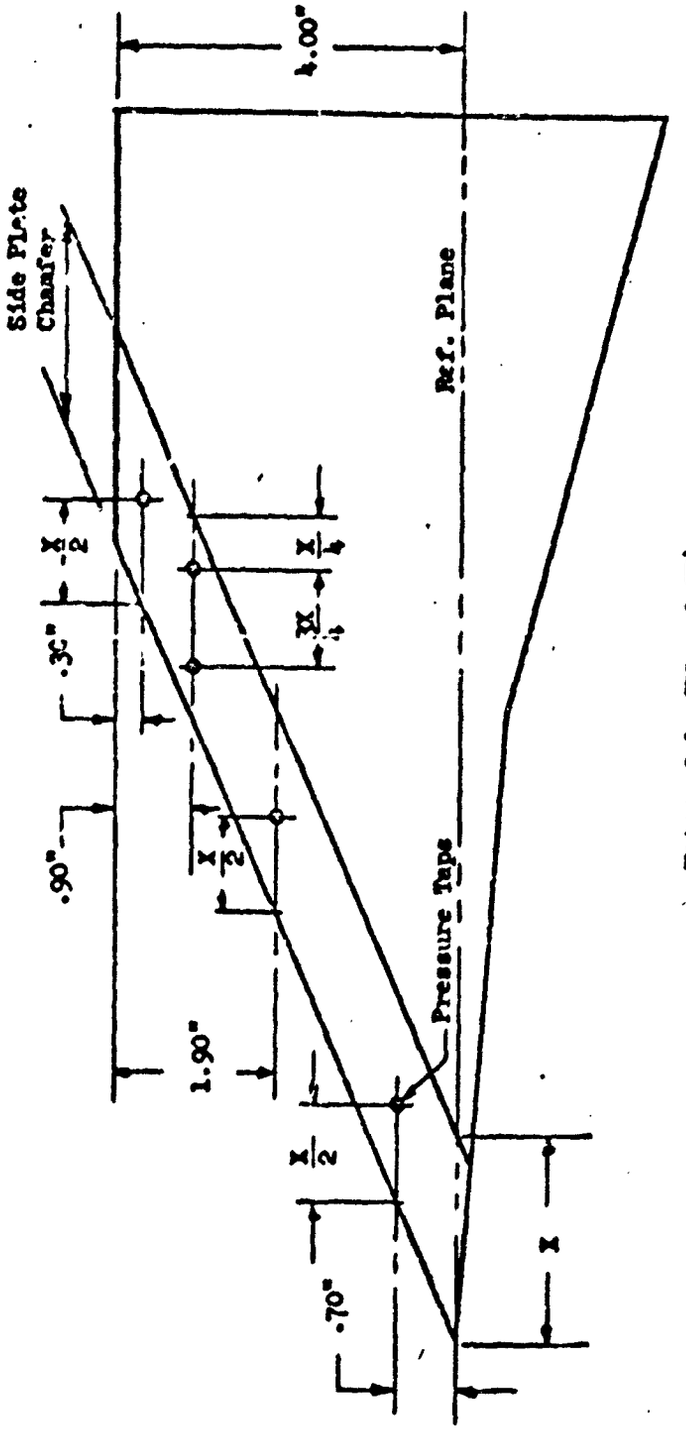

Note: Only SP1 and SP4 Instrumented

Figure 24. Side Plate Pressures

APPENDIX II

THEORETICAL ADDITIVE DRAG COMPUTATION

1. General. Contract AF 33(615)-2496 required that, prior to testing, mathematical models of theoretical additive drag be hypothesized and that those drags be computed for the contractually required test configurations. A Fortran IV machine program was written for this purpose. This appendix documents the mathematical models and the machine program. In the following pages, the mathematical spillage models are discussed first, followed by the program documentation.

2. Mathematical Model - Subsonic. A free body diagram of the subsonic additive drag situation is given in figure 25. Assuming all flow to enter the inlet in the α direction, the theoretical additive drag is

$$(D_{ADD})_{THEORY} = A_{LIP}\cos\alpha\left[\gamma M_{LIP}^2 P_{LIP} + (P_{LIP} - P_o)\right] + D_R - \gamma A_o M_o^2 P_o$$

Eq. (27)

Then, to determine the theoretical additive drag the following assumptions are made:

Assumption 1) Subsonic flow behaves one-dimensionally (including the assumption that all of the flow entering the inlet is in the α direction);
Assumption 2) Perfect gas ($\gamma = 1.4$);

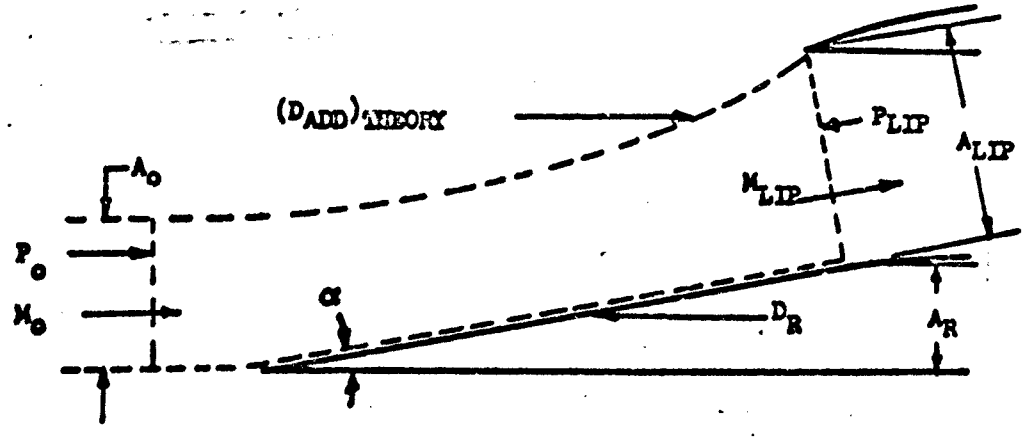

Figure 25. Subsonic Theoretical Additive Drag Momentum Balance

Assumption 3) No subsonic spillage occurs over the side plates;
Assumption 4) All flow processes are isentropic (except thru shock waves);
Assumption 5) $P_R = (P_o + P_{LIP})/2$

The first four assumptions are general and apply to all mathematical models. The fifth assumption applies only to the subsonic case. Assumption 5) enables the calculation of ramp drag,

$$D_R = A_R(P_R - P_o)$$

3. Mathematical Model - Transonic (Detached Initial Shock). The transonic mathematical model of theoretical additive drag is substantially the same as the subsonic model. Assumptions 1) thru 4) apply. Assumption 5) does not. Instead, the average ramp pressure is defined by:

Assumption 6) $P_R = (P_{NS} + P_{LIP})/2$

The average ramp pressure is the arithmatic average of pressure behind a detached normal shock (P_{NS}) and pressure at the lip (P_{LIP}). Again, $(D_{ADD})_{THEORY}$ can be found from equation (15).

4. Mathematical Model - Supersonic (Attached Initial Shock). The supersonic mathematical model and the computer program handle a one external shock wave (one ramp) case only. Model and program can be extended to multiple ramp situations, but contractual computations for which the program was specifically designed were restricted to one ramp cases.

A prime requirement of the models was a simplicity which allows reasonably rapid hand computations of theoretical additive drag. Yet, the mathematical model should produce drag curve shapes similar to measured values if K_{ADD} is to have physical significance. Though this was felt difficult to achieve for the supersonic case, it was successful as is illustrated by figures 45 thru 50.

In the supersonic model, three spillages were considered: supersonic spillage over the cowl, subsonic spillage over the cowl, and supersonic spillage around the inlet side plates. All three spillages are defined below.

On an actual inlet, the terminal shock wave travels fore and aft as a function of subcritical spillage. However, for the mathematical model, Assumption 7) fixes the terminal shock position as illustrated in figure 26.

Assumption 7) The terminal shock wave is defined as a normal shock which has a fixed location an infinitesimal distance forward of the cowl.

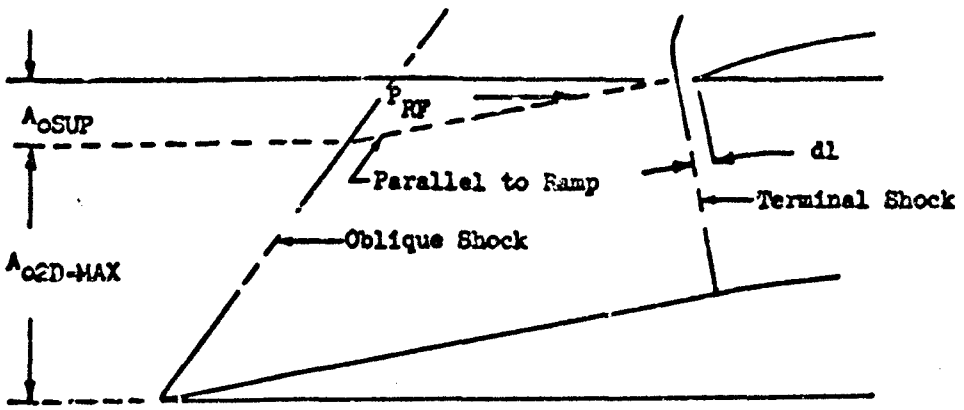

Figure 26. Supersonic Spillage

This assumption leads directly to Assumptions 8) and 9):

Assumption 8) The drag of the air spilled supersonically over the cowl is a fixed value at all mass flow ratios

$$D_{ADD-SUP} = A_{oSUP}(P_{RF} - P_o)$$

where P_{RF} is the pressure behind a two-dimensional oblique shock wave.

Assumption 9) All air spilled subsonically is spilled over the cowl in distance dl. Thus, if side plates are such that side spillage occurs, all side spillage must take place in the supersonic flow region forward of the terminal shock wave.

The mathematical model considers side spillage around inlets that do not have extended side plates. Figure 27 illustrates the area through which side spillage was considered to occur for the mathematical model of an inlet

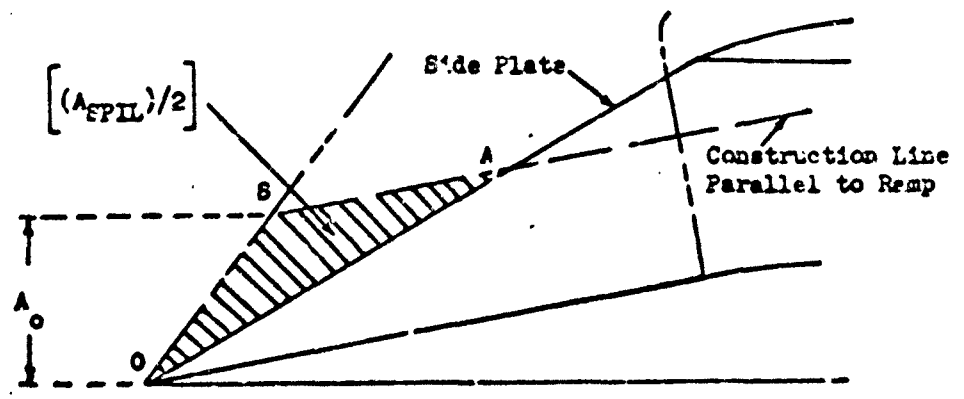

Figure 27. Side Spillage Area

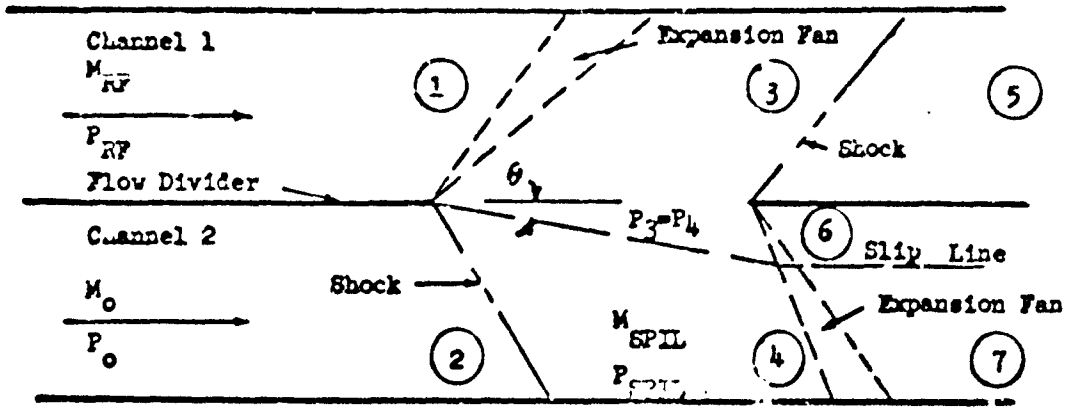

Figure 28. Side Spillage Conditions

having triangular side plates. The inlet shown has freestream tube area A_o entering at the lip. The area 2 OSA = A_{oSPIL} is taken as the total side spillage area for the two sides. To determine the drag of side spillage, the spillage pressure P_{SPIL} must be determined.

Figure 28 illustrates a flow situation similar to side spillage. Two channels of flow are shown. Initially they are divided. Downstream the divider is eliminated for a short distance. Channel #1 conditions are initially similar to conditions on the first ramp of an inlet, P_{FR}, M_{FR}. On an inlet they are obtained by ramp turning from the freestream. Channel #2 represents freestream conditions. As the flow passes the opening in the divider, Channel #1 flow expands into Channel #2. This expansion forms an aerodynamic wedge which creates an oblique shock wave in Channel #2, raising its pressure. The slip line angle is such that pressures in regions 3 and 4 are equal. For the small wedge turning angles, α, of conventional inlets, θ is very closely given by

$$\theta \approx \alpha/2$$

Thus,

Assumption 10) M_{SPIL} and P_{SPIL} are obtained by calculating them to be the conditions after turning thru the wedge half angle from the freestream.

The side spill flow is found from the continuity equation to be

$$A_{oSPIL} = A_{SPIL} \frac{P_{SPIL}}{P_o} \frac{M_{SPIL}}{M_o} \sin\left(\frac{\alpha}{2}\right) \left[\frac{1 + \frac{\gamma-1}{2} M_{SPIL}^2}{1 + \frac{\gamma-1}{2} M_o^2}\right]^{1/2}$$

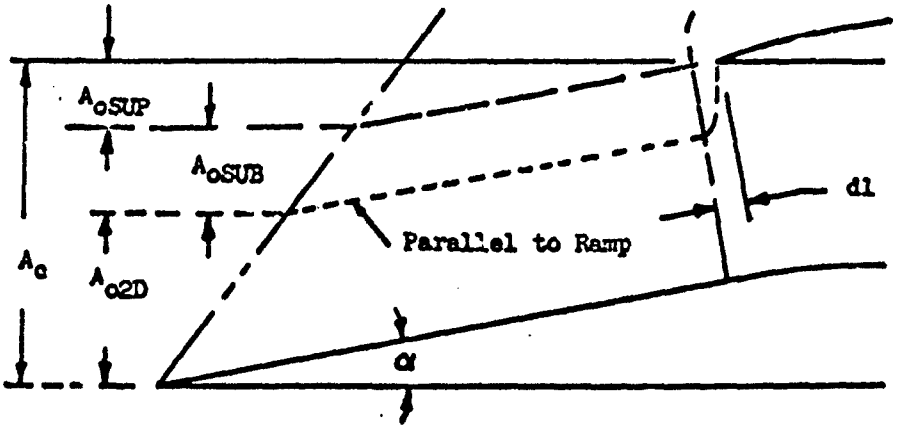

Figure 29. Flow Field Forward of Terminal Shock (No Side Spillage)

and the side spillage drag is

$$D_{ADD-SPIL} = A_{oSPIL}(P_{SPIL} - P_o)$$

In addition to supersonic spillage over the cowl and around the side plates, the mathematical model considers subsonic spillage over the cowl from behind the terminal shock. For the case of an inlet having extended side plates such that no side spillage can occur, figure 29 illustrates the mathematical model flow conditions in the supersonic region forward of the terminal shock wave. Here, flow A_o enters the inlet. Flow A_{oSUP} is spilled supersonically over the cowl, and flow A_{oSUB} is spilled subsonically over the cowl in distance dl. Figure 30 is a blow-up of the cowl lip region illustrating

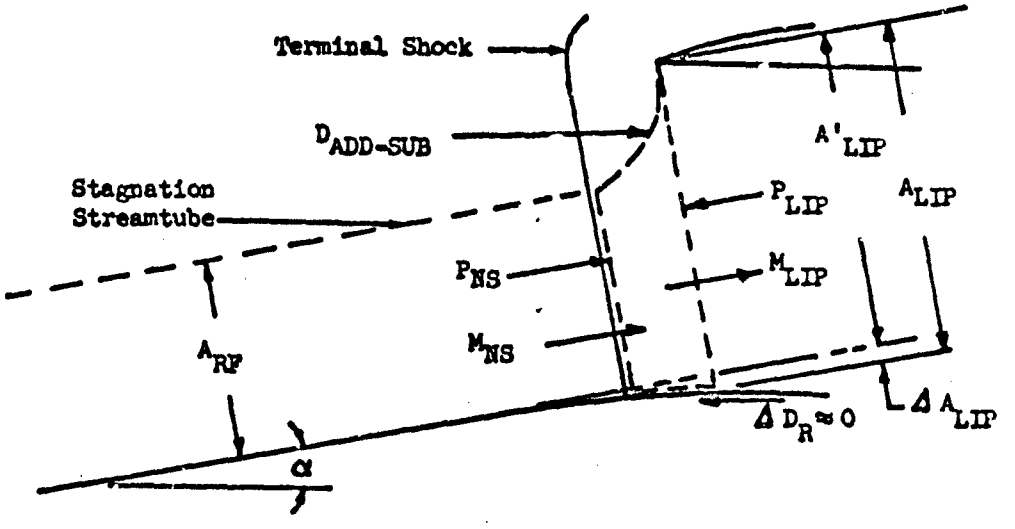

Figure 30. Subsonic Spillage

subsonic spillage behind the terminal shock. The free body force-momentum diagram for obtaining subsonic spillage drag, $D_{ADD-SUB}$, is also shown.

For a few inlet configurations the ramp may "break away" significantly from a straight line ahead of the cowl lip plane, thus producing an expansion of the ramp flow by ΔA_{LIP} (see figure 30). On the wind tunnel model the "break away" was minor. It has been neglected in the mathematical model for simplicity of hand computations.

Assumption 11) The external ramp is defined as a flat surface at angle α up to the cowl lip plane.

Assumptions 10) and 11), respectively, imply and define the supersonic flow conditions on the ramp as being fixed. Assumption 10) implies that P_{RF} and M_{RF} do not change with side spillage, and Assumption 11) eliminates effects of minor ramp curvatures. Assumption 12), below, clearly states this invariance between oblique shock wave and terminal shock wave.

Assumption 12) For inlets with side spillage or minor ramp curvatures, the Mach number and the pressure along the ramp are assumed to be constant and equal to the conditions behind the oblique ramp shock wave.

The subsonic spillage drag by a force-momentum balance is

$$D_{ADD-SUB} = \gamma \cos\alpha \left(P_{LIP}A'_{LIP}M^2_{LIP} - P_{NS}A_{NS}M^2_{NS}\right)$$

$$+ \cos\alpha \left[A'_{LIP}\left(P_{LIP} - P_o\right) - A_{NS}\left(P_{NS} - P_o\right)\right]$$

Figure 31 shows the complete flow field with supersonic spillage, subsonic spillage and side spillage. As the flow travels up the ramp behind the oblique shock some of the air is spilled over the sides, and the stagnation streamtube expands to A_{RF}, although Assumption 12) neglects the effect of this expansion on P_{RF} and M_{RF}. Thus, the mathematical model ramp flow conditions are those of a two-dimensional inlet (no side spillage) with a freestream tube area equal to A_{oEFF} where

$$A_{oEFF} = A_o + A_{oSPIL}$$

and

$$A_{RF} = A_{oEFF}\left(A_{PF}/A^*\right)/\left(H_{RF}/H_o\right)\left(A_o/A^*\right)$$

The total theoretical additive drag for the supersonic case is, then, the sum of the three spillage drags

$$\left(D_{ADD}\right)_{THEORY} = D_{ADD-SUP} + D_{ADD-SUB} + D_{ADD-SPIL}$$

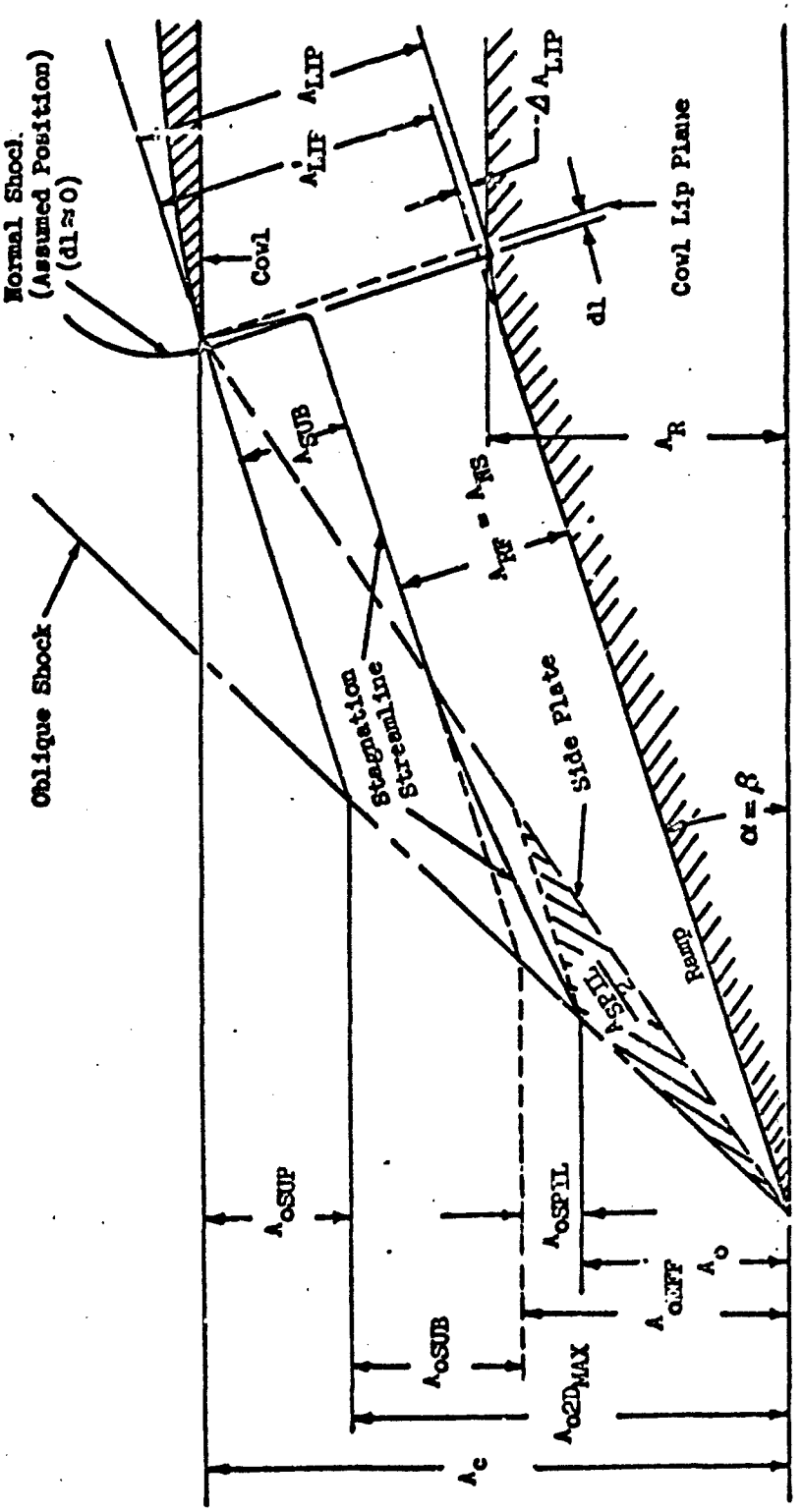

Figure 31. Inlet Supersonic Flow Field and Nomenclature

where, in summary,

$$D_{ADD-SUP} = A_{oSUP}(P_{RF} - P_o)$$

$$D_{ADD-SUB} = \gamma \cos\alpha \ (P_{LIP} A'_{LIP} M^2_{LIP} - P_{SS} A_{SS} M^2_{SS}) + \cos\alpha \left[A'_{LIP} (P_{LIP} - P_o) - A_{SS} (P_{SS} - P_o)\right]$$

$$D_{ADD-SPIL} = A_{oSPIL} (P_{SPIL} - P_o)$$

5. Machine Program. The main program of the rectangular inlet additive drag program solves the $(D_{ADD})_{THEORY}$ equations just described. Table I is a listing of program subroutines. A complete set of flow diagrams and a program listing are included in figures 32 and 33. The supersonic branch includes an iteration process that calculates the maximum mass flow ratio which the inlet can ingest, assuming no internal choking. This routine is entered if the sum of the input mass flow and the side spillage is greater than $A_{c2D-MAX}$. A sample of the output for this case and other output cases are included in figures 34 thru 38. Figure 39 shows the print out key, and table II is a listing of print out definitions.

Two major subroutines included in the program are discussed below. Flow diagrams and program listings for these are included in figures 40, 41, 42, and 43.

The Ideal Deflection (IDEF) subroutine calculates the flow conditions behind attached oblique shock waves using equations from reference 14. If an oblique shock solution is not possible, the main program calculates flow conditions behind a normal shock using equations from the same reference.

The Side Spillage (SPIL) subroutine calculates the freestream tube area of the air that spills supersonically around inlet side plates. It is limited to inlets having only one oblique shock, as is the main program, and to the side plate shapes used in this test. The side spillage area is found by the use of congruent triangles and the known inlet geometry as shown in figure 44. Use is made of the plane geometry theorem:

> For two congruent triangles, the ratio of their areas is equal to the square of the ratio of a representative dimension.

Now A_o is a representative dimension of the triangle OSA, and $A_{c2D-MAX}$ is the corresponding dimension of OEC. Similarly, $(A_{c2D-MAX} - A_o)$ is a representative dimension of ACB, and $A_{c2D-MAX}$ is the corresponding representative dimension of OCB,

$$OSA = A_{MAX-ST} (A_o/A_{c2D-MAX})^2$$

$$ABC = A_{IM}\left[\left(A_{o2D\text{-}MAX} - A_o\right)/ A_{o2D\text{-}MAX}\right]^2$$

$$A_{SPIL} = 2\left[A_{MAX\text{-}ST}\left(A_o/A_{o2D\text{-}MAX}\right)^2 + A_{CUT} - A_{IM}\left(1 - A_o/A_{o2D\text{-}MAX}\right)^2\right]$$

The continuity equation can now be used to convert the stream area of the spilled air to a freestream tube area.

$$A_{oSPIL} = A_{SPIL}(P_{SPIL}/P_o)\,(M_{SPIL}/M_o)\sin(\alpha/2)\left[\frac{1 + \frac{\gamma-1}{2} M_{SPIL}^2}{1 + \frac{\gamma-1}{2} M_o^2}\right]^{1/2}$$

Although any amount of "cut back" area can be used, A_{oSPIL} should not be calculated for mass flows less than A_{oMIN} (see figure 44). To use the program for extended or "two-dimensional" side plates, a large negative number must be put in for A_{CUT}/A_o and zero for A_{IM}/A_o.

Table I

Machine Program Subroutines

Subroutine	Description
GTIS (Main)	Control Program. Also does the majority of the calculations of Additive Drag.
SPIL	Calculates freestream tube area that is spilled supersonically around the side plates.
IDEF	Calculates the conditions behind a two dimensional attached oblique shock.
DECR	Reads in data. If more than one case is being run it is only necessary to have input cards on the inputs that are different than the preceding case. If no new value is given for a particular input it will use the same value that was used in the preceding case
CLEA	Sets the data storage region to zero.
ARCCOS	Calculates the arccosine.
ARCSIN	Calculates the arcsine.
ARCTAN	Calculates the arctangent.
COSSIN	Calculates sine and cosine.
CUBI	Solves basic cubic equation.
CURTOO	Calculates cube root.
SQRT	Calculates square root.

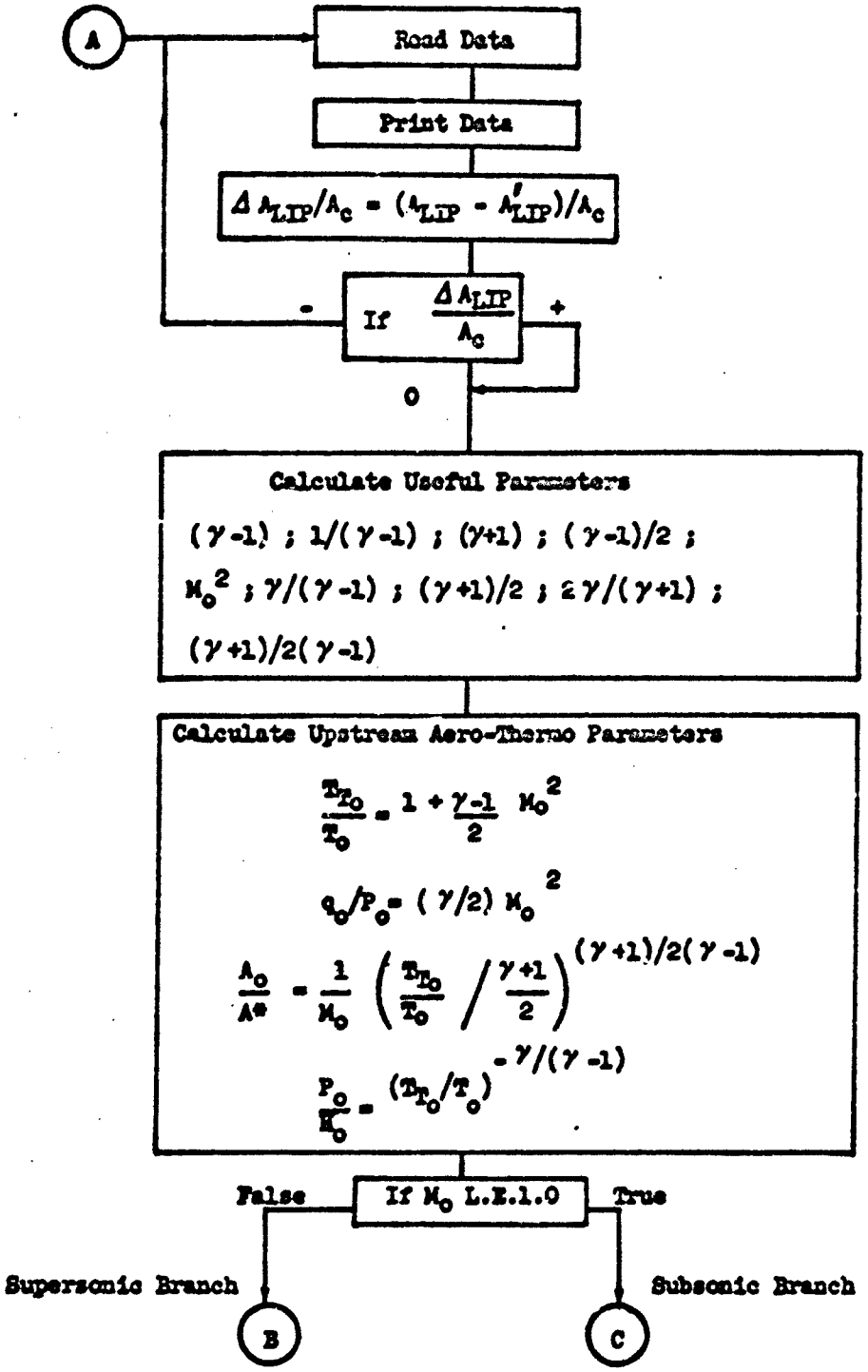

Figure 32. Main Program

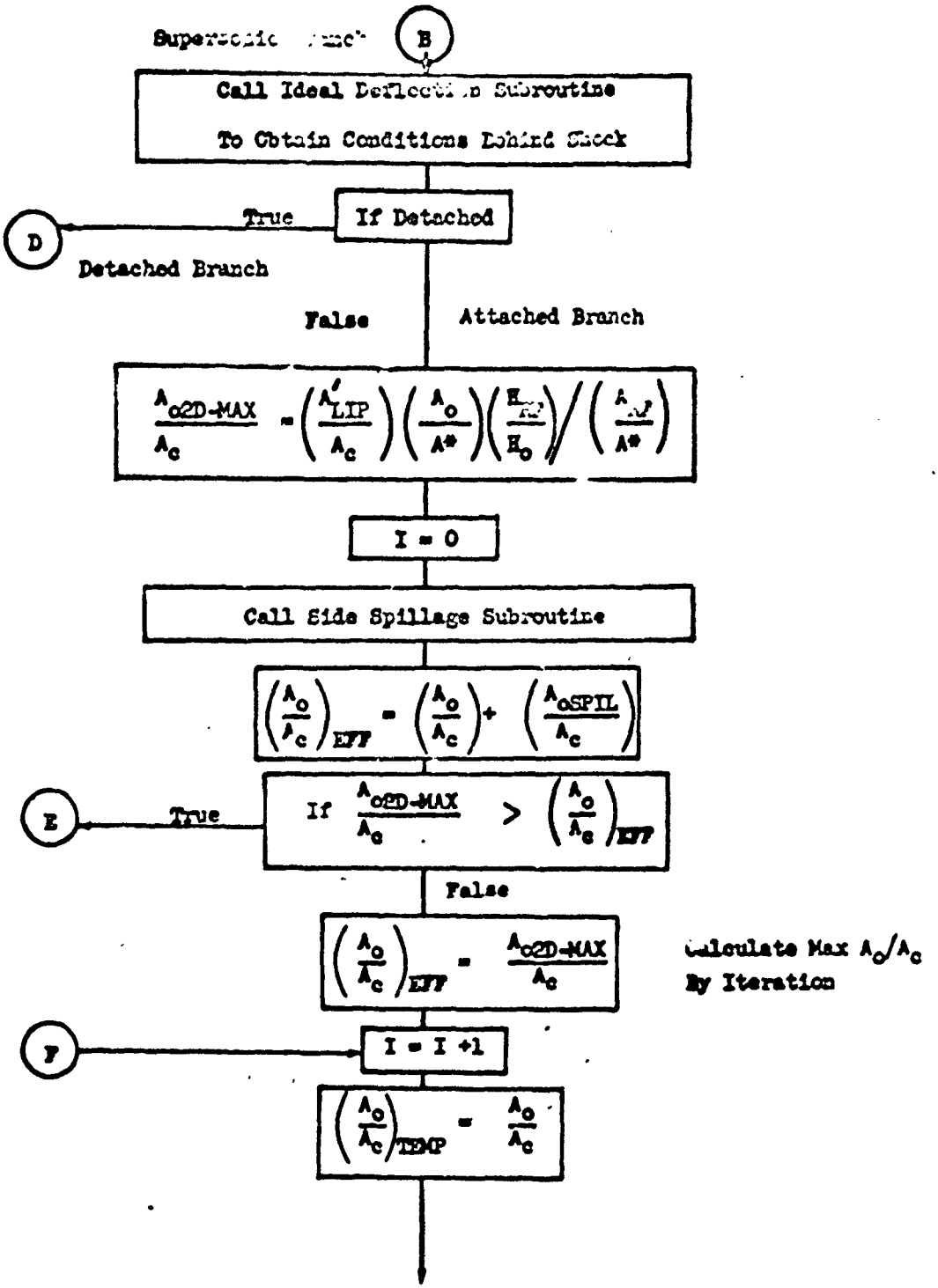

Figure 32. Continued

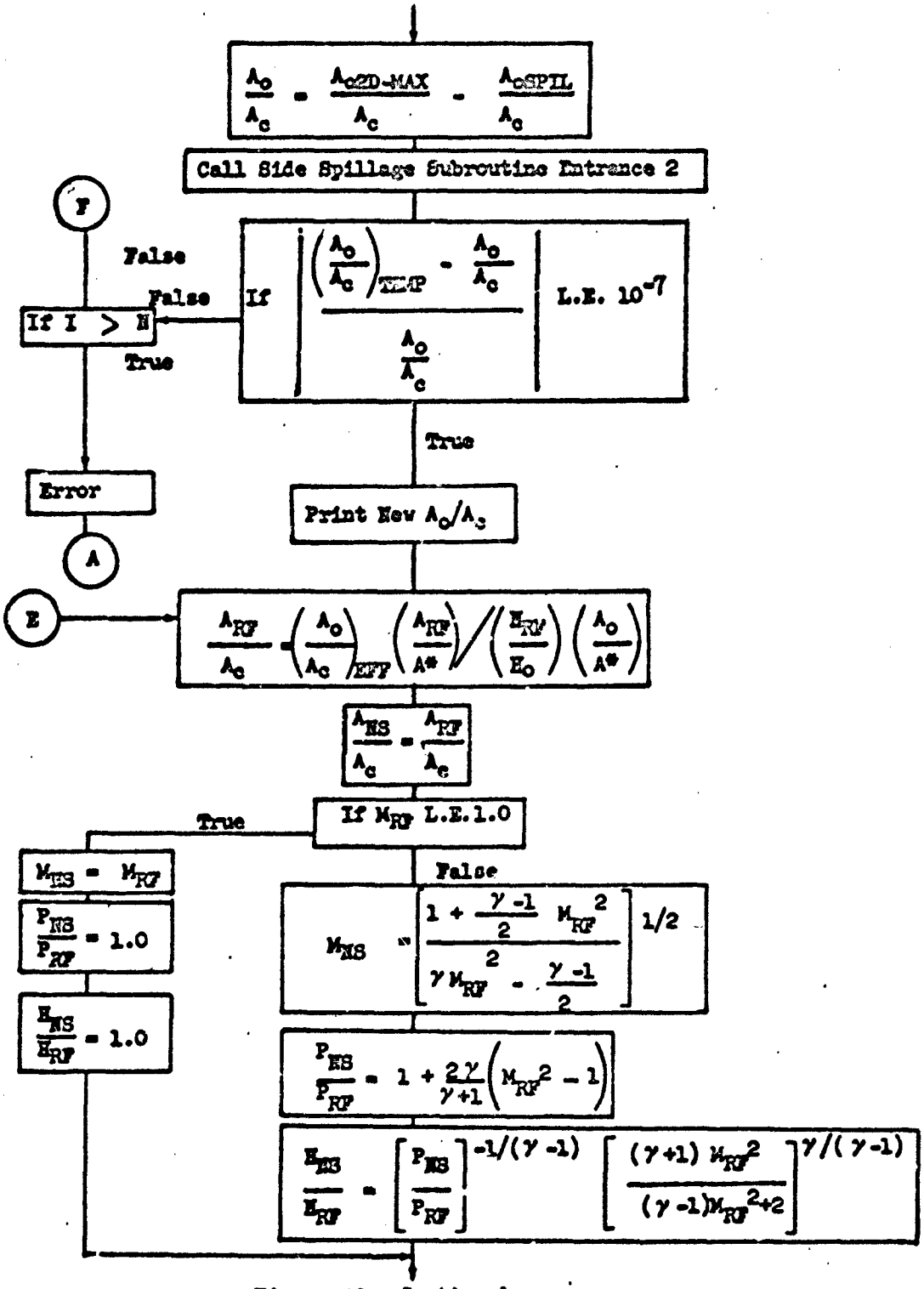

Figure 32. Continued

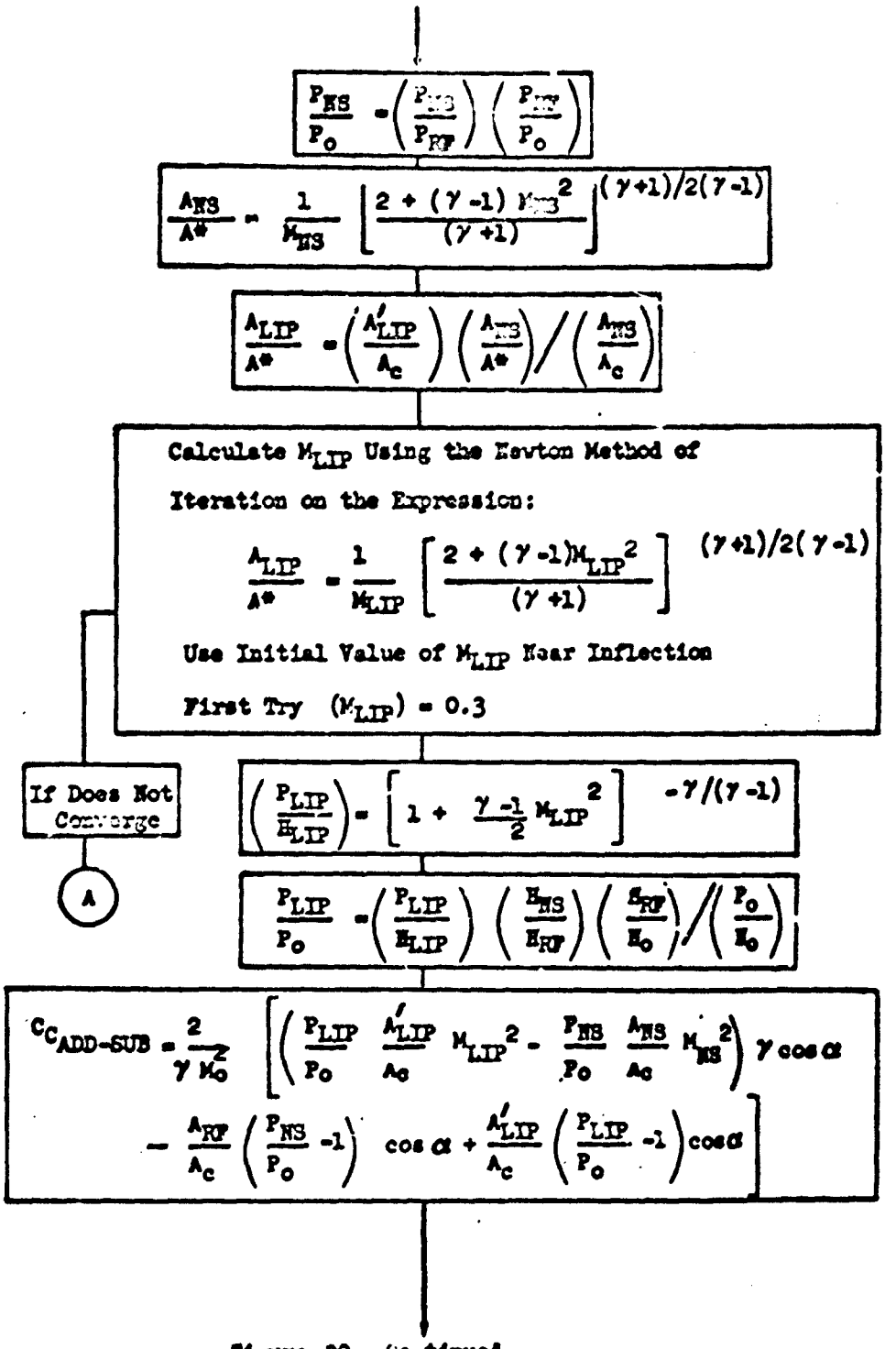

Figure 32. Continued

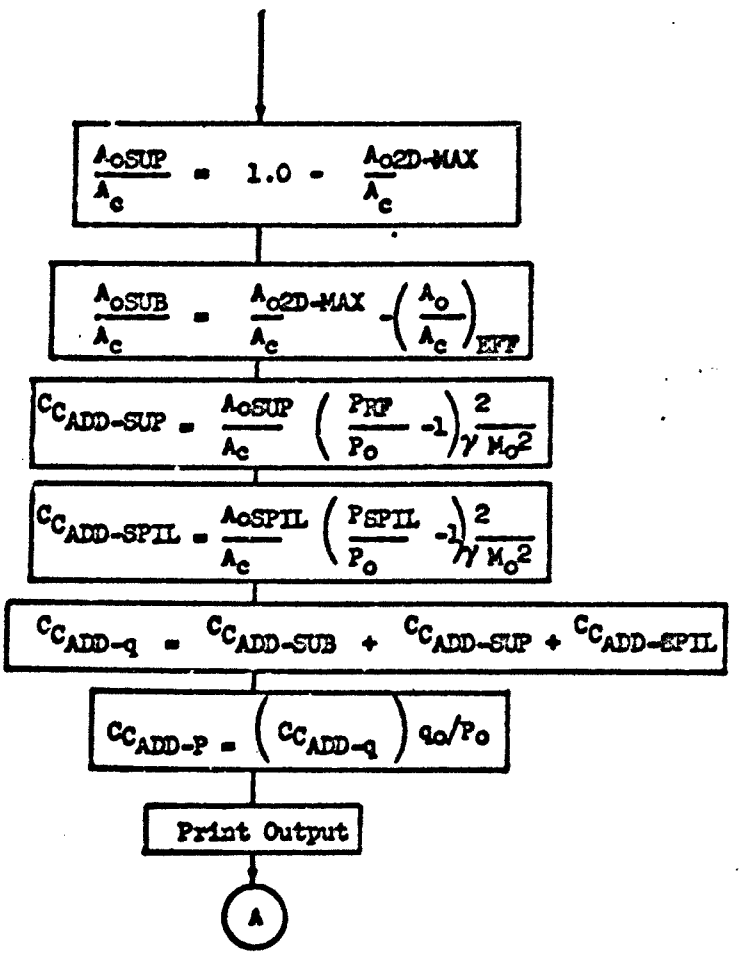

Figure 32 . Continued

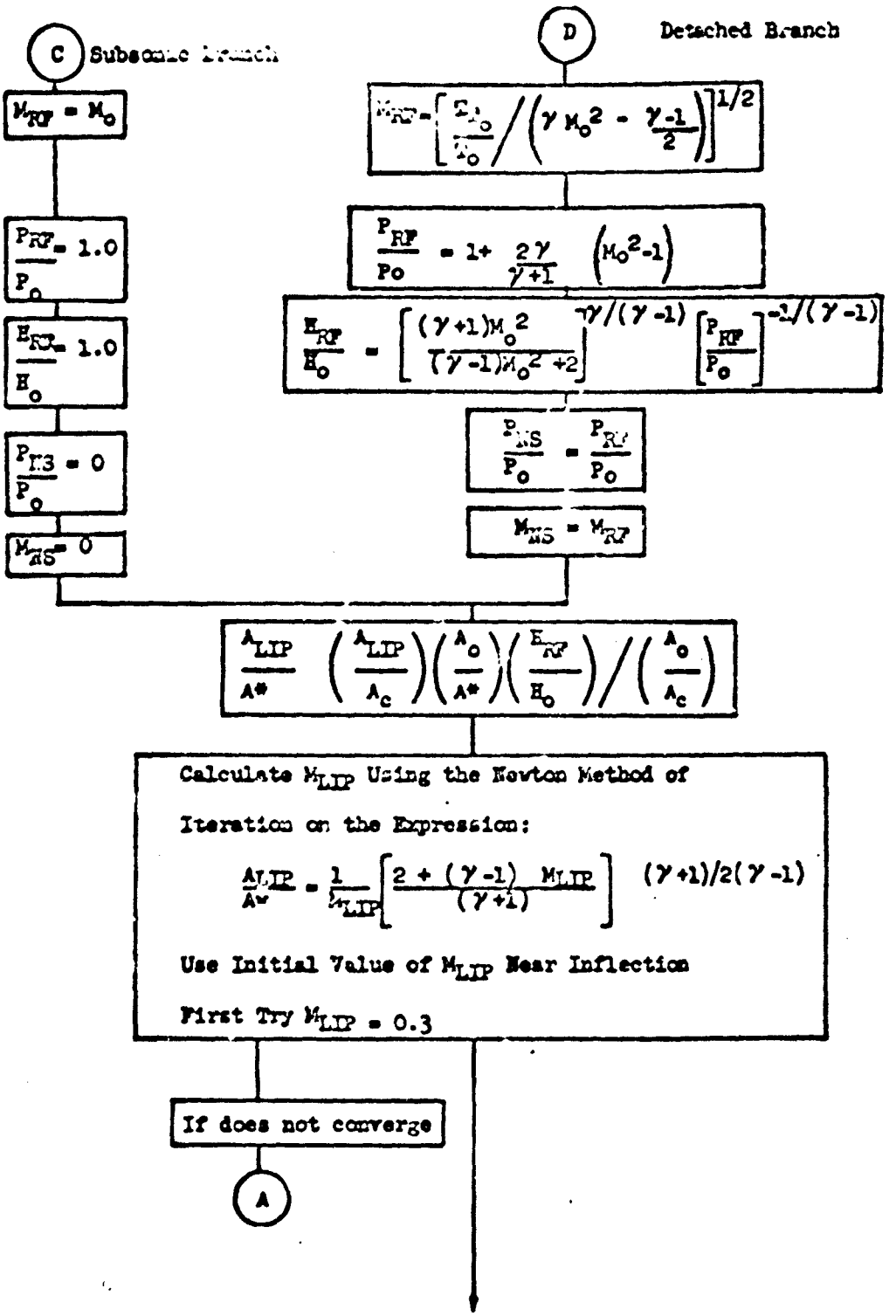

Figure 32. Continued

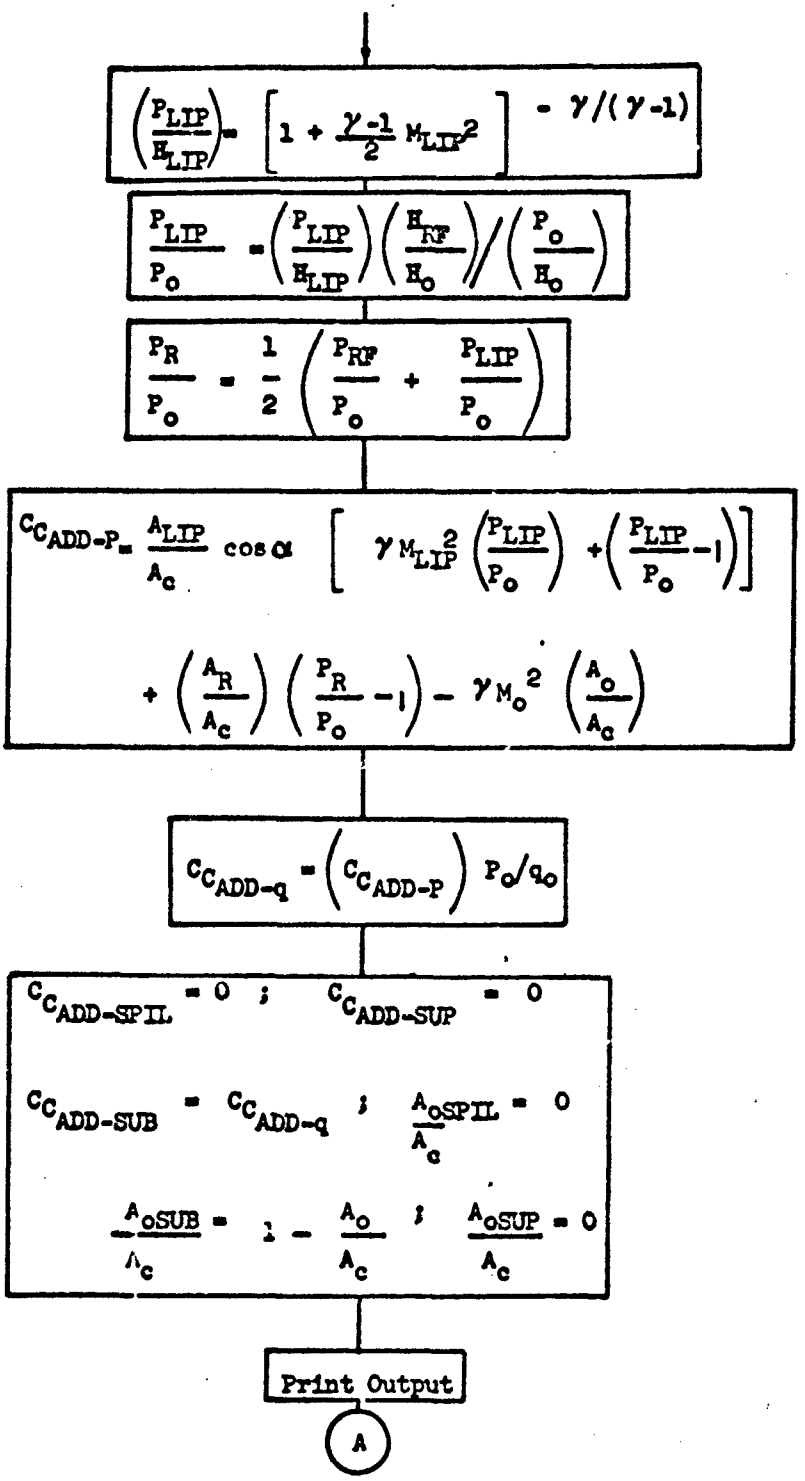

Figure 32. Concluded

GTIS - EFN SOURCE STATEMENT - IFN(S) -

```
      DIMENSION CR(15)                                                          GT ISO040
      COMMON CR                                                                 GT ISO050
      REAL MO,MOSQ,MNSSQ,MRFSQ,MRF,MNS,ML,PLSQ,MFPM                            GT ISO060
C     1 GAM    RATIO SPECIFIC HEATS, ISENTROPIC EXPONENT                        GT ISO110
C     2 W      RAMP WIDTH (SIDE-PLATE SPREAD                          IN.  GT ISO120
C     3 ALFD   RAMP (FLOW DEFLECTION) ANGLE                           DEG  GT ISO130
C     4 ALAC   AREA RATIO (LIP TO CAPTURE)                                    GT ISO140
C     5 APLAC  AREA RATIO (PROJECTED-RAMP LIP TO CAPTURE)                     GT ISO150
C     6 ACUT   TRIANGULAR SIDE PLATE AREA MINUS SIDE PLATE AREA (RATIO)       GT ISO160
C     7 AIM    IMAGINARY SIDE PLATE AREA USED IN CONGRUENT TRIANGLE RATIO      GT ISO170
C     8 X      HORIZONTAL DISTANCE FROM LE TO COWL LIP                 IN.  GT ISO180
C     9 Y      VERTICAL DISTANCE FROM LE TO COWL LIP                   IN.  GT ISO190
C    10 ARAC   RAMP FRONTAL AREA TO INLET LIP STATION                          GT ISO195
C    11 AOAC   UPSTREAM FLOW AREA RATIO                                        GT ISO210
C    12 MO     UPSTREAM MACH NO.                                               GT ISO220
C       ALF    RAMP ANGLE                                              RAD  GT ISO310
C       AOHAC  SUPERSONIC (HIGH) AREA RATIO (UPSTREAM TO CAPTURE)              GT ISO320
C       AOLAC  SUBSONIC (LOW) AREA RATIO                                       GT ISO325
C       CDADH  SUPERSONIC (HIGH) COEF OF ADDITIVE DRAG                         GT ISO330
C       CDADL  SUBSONIC (LOW) COEF OF ADDITIVE DRAG                            GT ISO340
C       CDADP  COEF OF ADDITIVE DRAG BASED ON P(O)                             GT ISO350
C       CDADQ  COEF OF ADDITIVE DRAG BASED ON Q(O)                             GT ISO360
C       CDADSP SPILL COEF OF ADDITIV DRAG                                      GT ISO370
C       DALAC  LIP AREA RATIO INCREMENT                                        GT ISO380
C       DM     ITERATION INCREMENT OF LIP MACH NO.                             GT ISO390
C       ER     ERROR INDICATOR                                                 GT ISO400
C       FGAM   2*GAMMA/(GAMMA+1)                                               GT ISO410
C       FM     ITERATION FUNCTION                                              GT ISO415
C       FT     T(LIP)/T(O)                                                     GT ISO420
C       GP02GM (GAMMA+1)/2/(GAMMA-1), AREA FUNCTION EXPONENT                   GT ISO440
C       MFPM   -DERIVATIVE OF ITERATION FUNCTION                               GT ISO443
C       PLOPO  LIP TO UPSTREAM PRESSURE RATIO                                  GT ISO445
C       POPL   LIP INVERSE RAM PRESSURE RATIO                                  GT ISO450
C       POPO   UPSTREAM INVERSE RAM PRESSURE RATIO                             GT ISO460
C       QUPO   UPSTREAM DYNAMIC PRESSURE RATIO                                 GT ISO470
C       SNBTSQ SINE(DEFLECTED FLOW SHOCK ANGLE)**2                             GT ISO480
```

Figure 33. Main Program Listing

GTIS - EFN SOURCE STATEMENT - IFN(S) -

```
C      TTOTO  RAM TEMPERATURE RATIO                                          GT ISO490
       EQUIVALENCE (GAM,CR(1)),(W,CR(2)),(ALFD,CR(3)),(ALAC,CR(4)),(APLAC   GT ISO510
      1,CR(5)),(ACUT,CR(6)), (AIM,CR(7)),(X,CR(8)),(Y,CR(9)),(ADAC,CR(11)   GT ISO511
      2),(MO,CR(12)),(ARAC,CR(10)),(EN,CR(13))                              GT ISO512
CLEAR COMMON REGION                                                         GT ISO520
       CALL CLEAR (CR,15)                                                   GT ISO530
C READ DATA INTO COMMON REGION                                              GT ISO580    2
   10 CALL DECRD (CR)                                                       GT ISO590
C PRINT INPUT DATA                                                          GT ISO600    4
       WRITE(6,30)(CR(I),I=1,13)                                            GT ISO610    5
   30 FORMAT(1H1,P5E19.7/(1HC5E19.7))                                       GT ISO620
CALC LIP AREA INCREMENT                                                     GT ISO630
       DALAC=ALAC-APLAC                                                     GT ISO640
CHECK, NEXT CASE IF -                                                       GT ISO650
       IF(DALAC)10,40,40                                                    GT ISO660
CALC PRIMARY USEFUL PARAMETERS                                              GT ISO670
   40 ER=.0                                                                 GT ISO680
       N=EN                                                                 GT ISO685
       GM1=GAM-1.                                                           GT ISO690
       RGM1=1./GM1                                                          GT ISO695
       GP1=GAM+1.                                                           GT ISO700
       GM1O2=.5*GM1                                                         GT ISO710
       MOSQ=MO**2                                                           GT ISO720
       ALF=ALFD/57.2957795                                                  GT ISO725
       GOGM1=GAM/GM1                                                        GT ISO730
       GP1O2=.5*GP1                                                         GT ISO740
       FGAM=GAM/GP1O2                                                       GT ISO745
       GP02GM=GP1O2/GM1                                                     GT ISO750
CALC UPSTREAM AERO-THERMO PARAMETERS                                        GT ISO760
       TTOTO=1.+GM1O2*MOSQ                                                  GT ISO765
       QOPO=.5*GAM*MOSQ                                                     GT ISO767
       AOAS=(TTOTO/GP1O2)**GP02GM/MC                                        GT ISO770   15
       POMO=TTOTO**(-GOGM1)                                                 GT ISO790   16
       IF(MO.LE.1.)GOTO80                                                   GT ISO795
C *IDDEF* S/R FOR DEFLECTION FLOW PARAMETERS                                GT ISO800
       CALL IDDEF (MOSQ,GAM,ALF,SNBTSQ,HRFHC,MRFSQ,MRF,PRFPO,ARFAS,ER)      GT ISO810
C IF DETACHED                                                               GT ISO870   20
```

Figure 33. Continued

GTIS - EFN SOURCE STATEMENT - IFA(S) -

```
      IF(ER)50,50,90                                                    GT ISO830
   50 AO2DAC=APLAC*AOAS/ARFAS*HRFHC                                     GT ISO840
      I=0                                                               GT ISO841
      CALL SPILL (AOAC,MO,MOSQ,AO2DAC,X,Y,SNBTSQ,ACUT,AIM,GAM,TTOTO,AOACGT ISO850
     1SP,ALF,W,PSPPO)                                                   GT ISO851    25
      IF(ER.GT.0.)GOTO90                                                GT ISO855
   55 AOACEF=AOAC+AOACSP                                                GT ISO860
      IF(AO2DAC.GT.AOACEF)GOTO 57                                       GT ISO861
      AOACEF=AO2DAC                                                     GT ISO862
   51 I=I+1                                                             GT ISO863
      ATEMP=AOAC                                                        GT ISO864
      AOAC=AO2DAC - AOACSP                                              GT ISO865
      CALL SPILL2(AOAC,MO,MOSQ,AO2DAC,X,Y,SNBTSQ,ACUT,AIM,GAM,TTOTO,AOACGT ISO866
     1SP,ALF,W,PSPPO)                                                   GT ISO867    36
      IF(ER.GT.0.)GOTO90                                                GT ISO868
      DELT=ATEMP-AOAC                                                   GT ISO869
      IF(ABS(DELT/AOAC).LE.1.E-7)GOTO54                                 GT ISO870
      IF(I.GT.N)GOTO52                                                  GT ISO871
      GOTO51                                                            GT ISO872
   52 WRITE(6,53)                                                       GT ISO873    42
   53 FORMAT(1HO 4X, 20HDIVERGING AT MAX MFR)                           GT ISO874
      GOTO10                                                            GT ISO875
   54 WRITE(6,56) AOAC                                                  GT ISO876    50
   56 FORMAT(1HO 4X, 24HMFR TOO LARGE SO USED MFR=, 1E14.7)             GT ISO877
   57 ARFAC=AOACEF/HRFHO*ARFAS/ACAS                                     GT ISO878
      ANSAC=ARFAC                                                       GT ISO880
      IF(MRF.LE.1.) GO TO 58                                            GT ISO885
      MNSSQ=(1.+GM1G2*MRFSQ)/(GAM*MRFSQ-GM1G2)                          GT ISO890
      MNS=SQRT(MNSSQ)                                                   GT ISO900    55
      PNSPRF=1.+FGAM*(MRFSQ-1.)                                         GT ISO920
      MNSMRF=(GP1/(GM1+2./MRFSQ))**GOGM1/PNSPRF**RGM1                   GT ISO930    56    57
      GO TO 59                                                          GT ISO931
   58 MNS=MRF                                                           GT ISO932
      PNSPRF=1.                                                         GT ISO933
      MNSMRF=1.                                                         GT ISO934
      MNSSQ=MNS**2                                                      GT ISO935
   59 PNSPO=PNSPRF*PRFPO                                                GT ISO940
```

Figure 33. Continued

```
      ANSAS=((2.*GM1*MNSSQ)/GP1)**GPO2GM/MNS                          GTIS0950    61
      ALAS=APLAC*ANSAS/ANSAC                                          GTIS0960
C CALC M(LIP) BY ITERATION. START WITH AN M(LIP) NEAR INFLECTION TO INSURE GTIS0964
C CONVERGENCE. NEWTON METHOD  DELTA M(LIP)=-F(M(LIP))/F(PRIME)(M(LIP))  GTIS0965
      ML=.3                                                           GTIS0970
      I=0                                                             GTIS0975
   60 MLSQ=ML**2                                                      GTIS0980
      F1=(2.+GM1*MLSQ)/GP1                                            GTIS0990
      F2=F1**GPO2GM                                                   GTIS1000    63
      I=I+1                                                           GTIS1005
      FM=ALAS-F2/ML                                                   GTIS1010
      MFPM=F2*(1./F1-1./MLSQ)                                         GTIS1020
      DM=FM/MFPM                                                      GTIS1030
      ML=ML+DM                                                        GTIS1040
      IF(ABS(DM/ML).LE.1.E-7)GOTO66                                   GTIS1050
      IF(I.LT.N)GOTO60                                                GTIS1055
      GOTO10                                                          GTIS1056
   66 MLSQ=ML**2                                                      GTIS1060
C CALC DRAG COEFFICIENTS                                              GTIS1065
      POHL=(1.+GM102*MLSQ)**(-GOGM1)                                  GTIS1070    73
      PLOPO=POHL*PNSHRF/POHO*HRFHO                                    GTIS1080
      CDADL=COS(ALF)*((PLOPO*APLAC*MLSQ-PNSPO*ANSAC*MNSSQ)*GAM-ARFAC*(PNGTIS1090
     1SPO-1.)+APLAC*(PLOPO-1.))/QOPO                                  GTIS1100    74
      AOHAC=1.-A02DAC                                                 GTIS1110
      AOLAC=A02DAC-AOACEF                                             GTIS1115
      CDADH=AOHAC*(PRFPO-1.)/QOPO                                     GTIS1120
      CDADSP=AOACSP*(PSPPO-1.)/QOPO                                   GTIS1130
      CDADO=CDADL+CDADH+CDADSP                                        GTIS1140
      CDADP=CDADO*QOPO                                                GTIS1150
C PRINT REQUIRED OUTPUT                                               GTIS1155
   67 WRITE(6,70)CDADP,CDADO,CDADL,CDADH,CDADSP,PLOPO,AOACSP,AOLAC ,AOHAGTIS1160
     1C,HRF,PRFPO,HRFHO,PNS,PNSPO,ML                                  GTIS1170    75
   70 FORMAT(1H0,1P5E20.7)                                            GTIS1180
C BACK FOR NEXT CASE. WILL EXIT IF FINISHED                           GTIS1185
      GOTO10                                                          GTIS1190
C SUBSONIC BRANCH                                                     GTIS1195
   80 MRF=MO                                                          GTIS1200
```

Figure 33. Continued

```
      GTIS      - EFN   SOURCE STATEMENT  -  IFN(S)  -
      PRFPO=1.                                                          GTIS1210
      MRFMO=1.                                                          GTIS1220
      PNSPO=0.                                                          GTIS1221
      MNS=0.                                                            GTIS1222
      GOTO100                                                           GTIS1230
C DETACHED INITIAL SHOCK BRANCH                                         GTIS1235
   90 MRFSQ=TTOTO/(GAM*MOSQ-GM102)                                      GTIS1240
      MRF=SQRT(MRFSQ)                                                   GTIS1250    80
      PRFPO=1.+FGAM*(MOSQ-1.)                                           GTIS1260
      MRFMO=(GP1/(GM1+2./MOSQ))**GOGM1/PRFPO**RGM                       GTIS1270    81    82
      PNSPO=PRFPO                                                       GTIS1271
      MNS=MRF                                                           GTIS1272
  100 ALAS=ALAC*AOAS/AOAC*MRFMO                                         GTIS1280
      ML=.3                                                             GTIS1290
      I=0                                                               GTIS1295
  110 MLSQ=ML**2                                                        GTIS1300
      F1=(2.+GM1*MLSQ)/GP1                                              GTIS1310
      F2=F1**GPOGM                                                      GTIS1320    85
      I=I+1                                                             GTIS1325
      FM=ALAS-F2/ML                                                     GTIS1330
      MFPM=-F2*(1./F1-1./MLSQ)                                          GTIS1340
      DM=FM/MFPM                                                        GTIS1350
      ML=ML+DM                                                          GTIS1360
      IF(ABS(DM/ML).LE.1.E-7)GOTO120                                    GTIS1370
      IF(I.LT.M)GOTO110                                                 GTIS1375
      GOTO10                                                            GTIS1376
  120 MLSQ=ML**2                                                        GTIS1380
      POML=(1.+GM102*MLSQ)**(-GOGM1)                                    GTIS1390    95
      PLOPO=POML*MRFMO/POMO                                             GTIS1400
      PROPO=.5*(PRFPO+PLOPO)                                            GTIS1410
      CDADP= COS(ALF)*ALAC*(GAM*PLOPO*MLSQ+PLOPO-1.)+ARAC*(PROPO-1.)-GAMGTIS1420
     1*AOAC*MOSQ                                                        GTIS1430    98
      CDADQ=CDADP/QOPO                                                  GTIS1440
      CDADSP=0.                                                         GTIS1441
      CDADM=0.                                                          GTIS1442
      CDADL=CDADQ                                                       GTIS1443
      AOACSP=0.                                                         GTIS1444
```

Figure 33 Continued

```
09/10/36

GTIS    - EFN   SOURCE STATEMENT - IFN(S) -
                                              GT IS1445
                                              GT I91446
                                              GT I91450
                                              GT IS1460
   GTIS
AOLAC=1.-ACAC
AOHAC=0.
COT067
END
```

Figure 33. Concluded

1.4000000E 00	4.0000000E 00	5.0000000E 00	7.9625000E-01	7.9425000E-01
0.0000000E-39	0.0000000E-39	9.3600000E 00	4.0000000E 00	2.0680000E-01
8.5000000E-01	6.9200000E-01	2.5000000E 01		
-1.1255243E-02	-3.3577232E-02	-3.3577232E-02	0.0000000E-39	0.0000000E-39
8.8822914E-01	0.0000000E-39	1.5000000E-01	0.0000000E-39	6.9200000E-01
1.0000000E 00	1.0000000E 00	0.0000000E-39	0.0000000E-39	8.1928713E-01

Figure 34. Standard Print Out Format

1.4000000E 00	4.0000000E 00	5.0000000E 00	7.9625000E-01	7.9425000E-01
0.0000000E-39	0.0000000E-39	9.3600000E 00	4.0000000E 00	2.0680000E-01
9.0000000E-01	6.9200000E-01	2.5000000E 01		

NOTE: Input mass flow ratio too large, choking at cowl lip plane

Figure 35. Subsonic Case

```
 1.4000000E 00    4.0000000E 00    5.0000000E 00    7.9625000E-01    7.9425000E-01
 0.0000000E-39    0.0000000E-39    9.3600000E 00    4.0000000E 00    2.0680000E-01
 8.0000000E-01    1.0930000E 00    2.5000000E 01
DETACHED
  3.5035804E-02    4.1896113E-02    4.1896113E-02    0.0000000E-39    0.0000000E-39
  1.1682613E 00    0.0000000E-39    2.0000000E-01    0.0000000E-39    9.1726417E-01
  1.2270905E 00    9.5912674E-01    9.1726417E-01    1.2270905E 00    9.6122157E-01
```

Figure 36. Transonic (Detached Shock) Case


```
 1.4000000E 00    4.0000000E 00    5.0000000E 00    7.9625000E-01    7.9425000E-01
 0.0000000E-39    0.0000000E-39    9.3600000E 00    4.0000000E 00    2.0680000E-01
 9.0000000E-01    1.0930000E 00    2.5000000E 01
DETACHED
```

NOTE: Input mass flow ratio too large, choking at cowl lip plane

Figure 37. Transonic (Detached Shock) Case

```
 1.4000000E 00      4.0000000E 00      5.0000000E 00      7.9625000E-01      7.9425000E-01
 9.0000000E-39      0.0000000E-39      9.3600000E 00      4.0000000E 00      2.0680000E-01
 8.0000000E-01      1.2930000E 00      2.5000000E 01
MFR TOO LARGE SO USED MFR= 0.7803931E 00
  5.8808803E-02      5.0251294E-02      8.5619566E-08      4.3465917E-02      6.7852926E-03
  1.4697074E 00      5.8154777E-02      0.0000000E-39      1.6145214E-01      1.0798022E 00
  1.3150650E 00      9.9790943E-01      9.2787485E-01      1.5697076E 00      9.2787499E-01
```

NOTE: Input mass flow ratio too large, program computes data using maximum possible mass flow ratio.

Figure 38. Supersonic Case

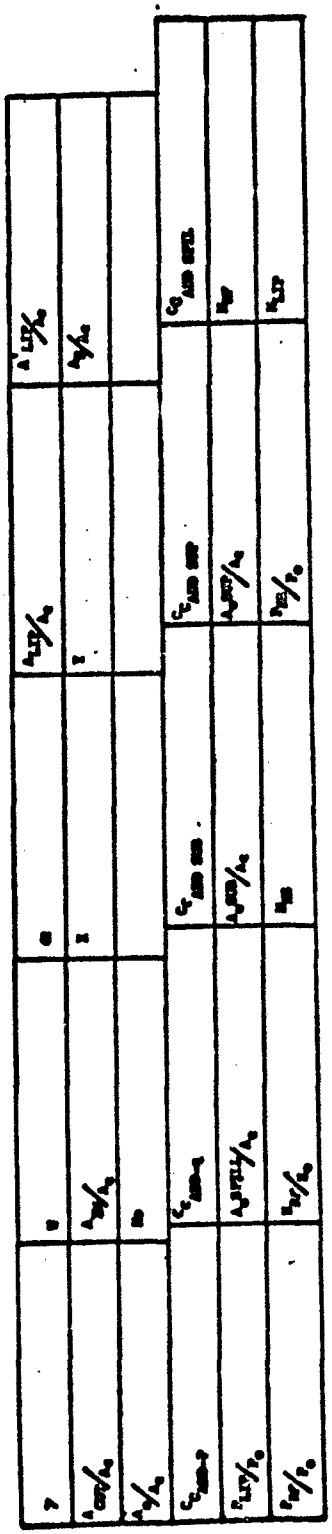

Figure 39. Print Out Key

Table II

Print Out Definitions

Symbol	Definitions
A_{CUT}/A_c	Side plate are ratio minus triangular side plate area ratio.
A_{IM}/A_c	An imaginary area used in side spillage calculation as the known part of a congruent triangle area ratio.
A_{LIP}/A_c	Inlet lip station area ratio measured from cowl leading edge to ramp surface measured perpendicular to the flat part of the second ramp.
A_{LIP}/A_c	Inlet lip station area ratio measured from cowl leading edge to a straight line extension of the forward part of the second ramp measured perpendicular to the forward part of the second ramp.
A_R/A_c	Ramp frontal area ratio measured from first ramp leading edge to inlet lip station defined in A_{LIP}/A_c $(1 - A_{LIP} \cos\beta/A_c)$
A_{oSPIL}/A_c	Mass flow ratio spilled supersonicly around the side.
A_{oSUB}/A_c	Mass flow ratio spilled subsonically over the cowl.
A_{oSUP}/A_c	Mass flow ratio spilled supersonicly over the cowl.
A_o/A_c	Mass flow ratio entering the inlet.
$C_{C_{ADD-P}}$	Additive drag coefficient, (D/P_oA_c).
$C_{C_{ADD-q}}$	Additive drag coefficient, (D/q_oA_c).
$C_{C_{ADD-SPIL}}$	Portion of additive drag due to supersonic spillage of the air around the sides, (D/q_oA_c).
$C_{C_{ADD-SUB}}$	Portion of additive drag due to subsonic spillage of the air over the cowl, (D/q_oA_c).
$C_{C_{ADD-SUP}}$	Portion of additive drag due to supersonic spillage of the air over the cowl, (D/q_oA_c).
H_{RF}/H_o	Total pressure ratio on the ramp.

Table II Continued

Symbol	Definitions
M_{LIP}	Mach number at the inlet lip station.
M_{NS}	Mach number behind the normal shock.
M_{RP}	Initial Mach number on the ramp, (for supersonic M_{RP} is assumed constant over the total ramp).
M_o	Freestream Mach number.
P_{LIP}/P_o	Static pressure ratio at lip station.
P_{NS}/P_o	Static pressure ratio behind the normal shock.
P_{RP}/P_o	Initial static pressure ratio on the ramp.
W	Inlet width
X	Horizontal distance from the first ramp leading edge to the cowl leading edge (in inches).
Y	Vertical distance from the first ramp leading edge to the cowl leading edge (in inches).
α	First ramp angle - from freestream.
γ	Specific heat ratio.

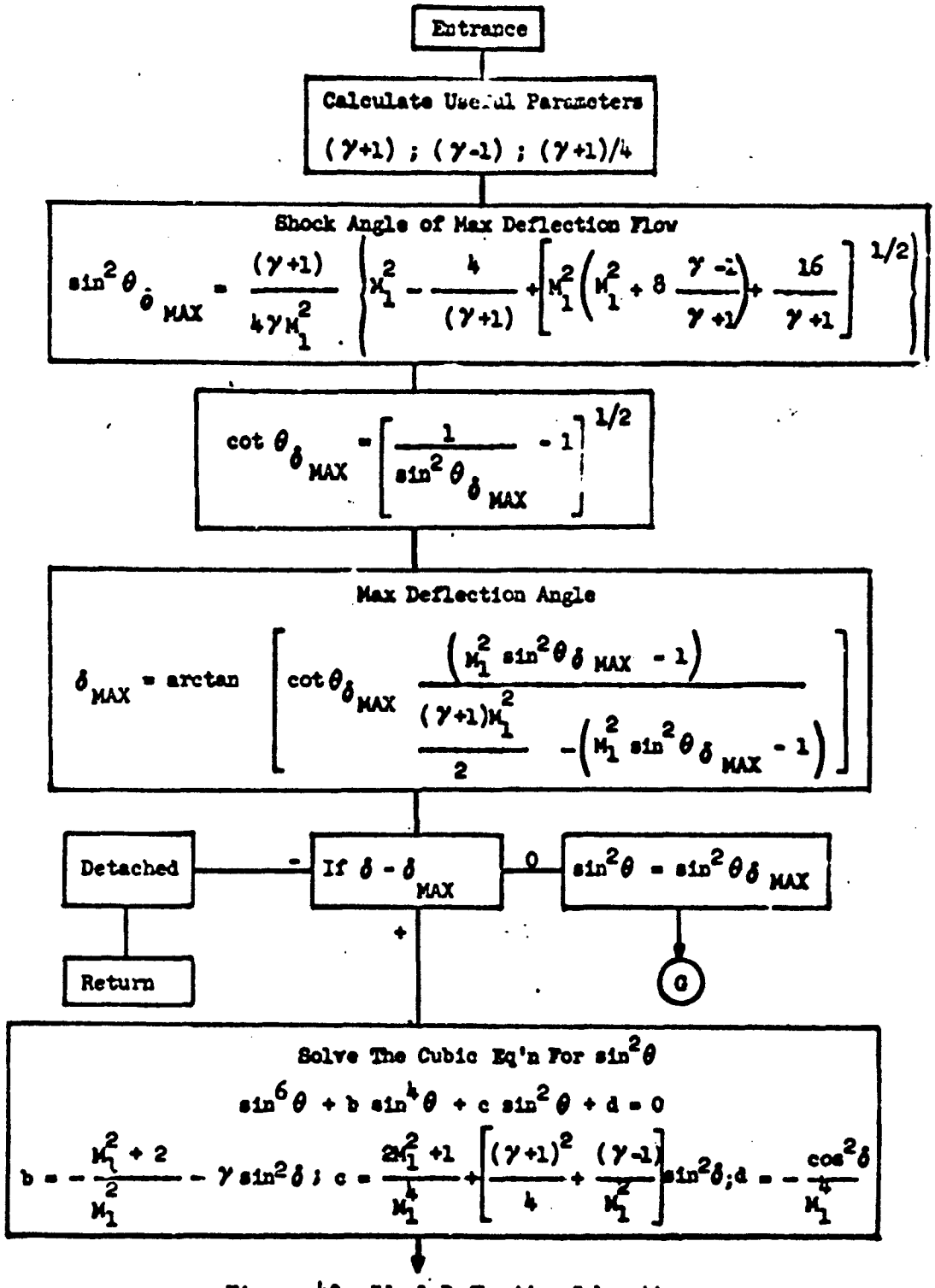

Figure 40 Ideal Deflection Subroutine

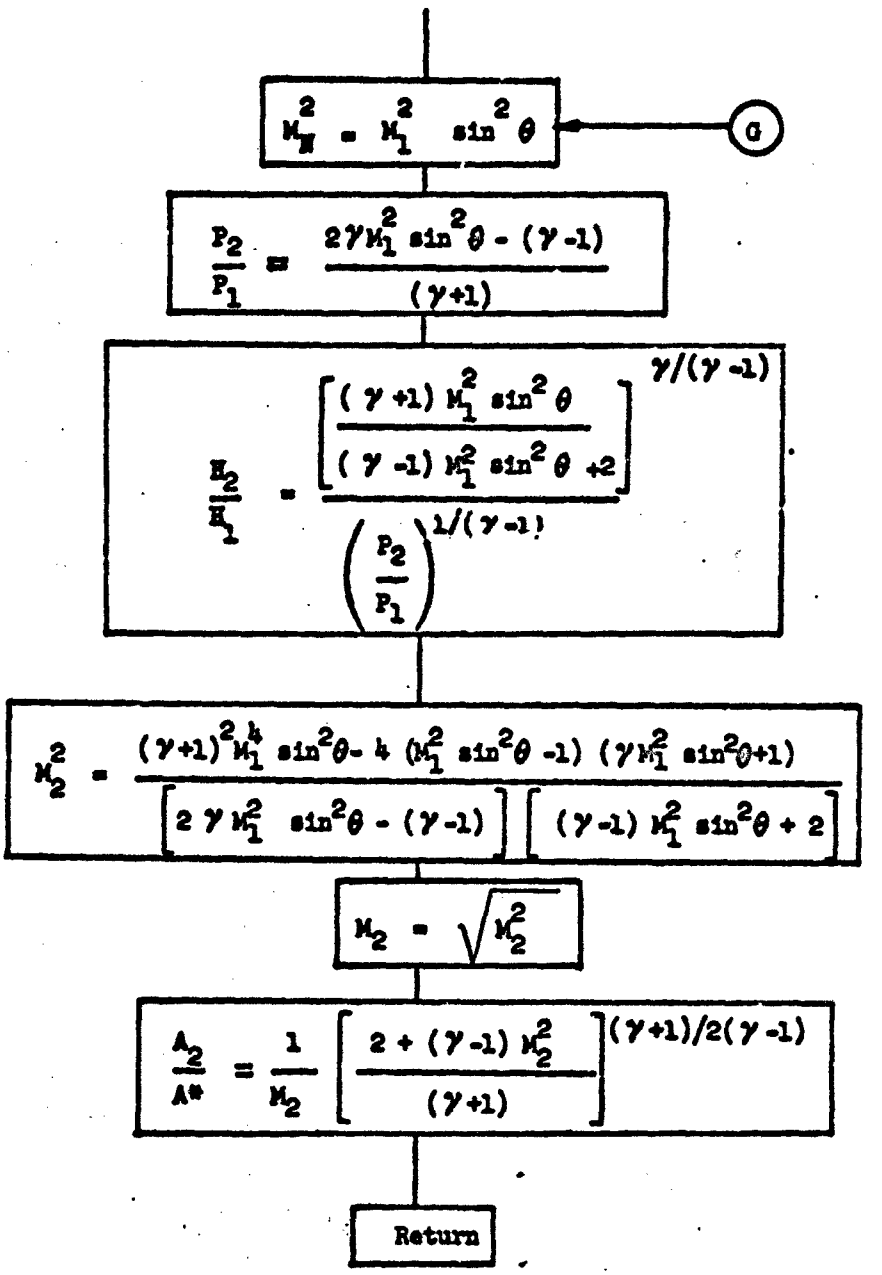

Figure 40. Concluded

IDEF - EFN SOURCE STATEMENT - IFN(S) -

```
      SUBROUTINE ICDEF (M1SQ,GAM,DEL,SNTHSC,H2OH1,M2SQ,M2,P2OP1,A2OAS,ER  IDER0030
     1)                                                                   IDER0031
C REFERENCE.. NACA REPORT NO. 1135 OF 1953                                IDER0035
C     A2OAS  DOWNSTREAM AREA RATIO                                        IDER0038
C     B,C,D  COEF'S OF X**3+B*X**2+C*X+D=0 (X=SNTHSQ)   EQ.(150)          IDER0040
C     CTTDM  COTANGENT(SHOCK ANGLE OF MAXIMUM DEFLECTION FLOW)            IDER0050
C     DEL    FLOW DEFLECTION ANGLE                              RAD      IDER0060
C     DELM   MAXIMUM ATTACHED-SHOCK FLOW-DEFLECTION ANGLE       RAD      IDER0070
C     ER     INDICATOR (DETACHED SHOCK IF OVER 0)                         IDER0080
C     GAM    RATIO OF SPECIFIC HEATS                                      IDER0090
C     H2OH1  RATIO OF STAGNATION PRESSURES ACROSS SHOCK                   IDER0100
C     MNSQ   (NORMAL COMPONENT OF MACH NO.)**2 AND AN INTERMEDIATE FUNC.  IDER0110
C     M1SQ   (UPSTREAM MACH NO.)**2                                       IDER0120
C     M2     DOWNSTREAM MACH NO.                                          IDER0125
C     M2SQ   (DOWNSTREAM MACH NO.)**2                                     IDER0130
C     M14TH  (UPSTREAM MACH NO.)**4                                       IDER0140
C     NR     NO. ROOTS OF CUBIC EQUATION                                  IDER0143
C     P2OP1  RATIO PRESSURES ACROSS SHOCK                                 IDER0145
C     R1,R2,R3 ROOTS OF CUBIC EQUATION                                    IDER0146
C     SNTDMS SINE(SHOCK ANGLE OF MAXIMUM DEFLECTION FLOW)**2              IDER0150
C     SNTHSQ SINE(SHOCK ANGLE)**2                                         IDER0160
      REAL M1SQ,M2SQ,M14TH,MNSQ,M2                                        IDER0170
CALC FUNCTIONS TO BE USED                                                 IDER0180
      GP1=GAM+1.                                                          IDER0190
      GM1=GAM-1.                                                          IDER0200
      GP104=.25*GP1                                                       IDER0210
CALC MAXIMUM FLOW DEFLECTION ANGLE                                        IDER0220
      SNTDMS=GP104/GAM*(M1SQ-4./GP1+SQRT(M1SQ*(M1SQ+2.*GM1/GP104)+4./GP1  IDER0230
     1041))/M1SQ                                                          IDER0240    2
      CTTDM=SQRT(1./SNTDMS-1.)                                            IDER0250    3
      MNSQ=M1SQ*SNTDMS-1.                                                 IDER0260
      DELM=ARCTAN(CTTDM*MNSQ/(.5*GP1*M1SQ-MNSQ))                          IDER0270
CHECK DEFLECTION VS MAXIMUM ALLOWABLE                                     IDER0300    4
      IF(DEL-DELM)50,40,20                                                IDER0310
C PRINT 'DETACHED' SET INDICATOR AND RETURN                               IDER0320
   20 WRITE(6,30)                                                         IDER0330    6
```

Figure 41. Ideal Deflection Subroutine Listing

```
   30 FORMAT(9HDETACHED)                                                    IDEF0340
      ER=1.                                                                 IDEF0350
      GOTO150                                                               IDEF0360
C JUST ATTACHED, SET SHOCK ANGLE = ANGLE OF MAXIMUM DEFLECTION              IDEF0370
   40 SNTHSQ=SNTCMS                                                         IDEF0380
      GOTO140                                                               IDEF0390
C ATTACHED, CALC SHOCK ANGLE                                                IDEF0400
   50 SNDSQ=SIN(DEL)**2                                                     IDEF0410    11
      M14TH=M1SQ**2                                                         IDEF0420
C COEFFICIENTS OF CUBIC IN SINE(THETA)**2, EQ.(150)                         IDEF0430
      B=-(1.+2./M1SQ+GAM*SNDSQ)                                             IDEF0440
      C=(2.*M1SQ+1.)/M14TH+(.25*GP1**2+GM1/M1SQ)*SNDSQ                      IDEF0450
      D=(SNDSQ-1.)/M14TH                                                    IDEF0460
C CUBIC S/R GIVES ROOTS                                                     IDEF0480
      CALL CUBIC (B,C,D,R1,R2,R3,NR)                                        IDEF0490    12
      EN=NR                                                                 IDEF0500
C CHECK NO. ROOTS, 1=DETACHED, 2=JUST ATTACHED, 3= NORMAL ATTACHMENT        IDEF0520
      IF(NR-2)20,40,60                                                      IDEF0530
C CORRECT ROOT IS MIDDLE ROOT                                               IDEF0540
   60 IF(R2-R3)100,40,70                                                    IDEF0550
   70 IF(R2-R1)130,40,80                                                    IDEF0560
   80 IF(R1-R3)110,40,90                                                    IDEF0570
   90 SNTHSQ=R1                                                             IDEF0580
      GOTO140                                                               IDEF0590
  100 IF(R1-R3)120,40,110                                                   IDEF0600
  110 SNTHSQ=R3                                                             IDEF0610
      GOTO140                                                               IDEF0620
  120 IF(R2-R1)90,40,130                                                    IDEF0630
  130 SNTHSQ=R2                                                             IDEF0640
C CALC NEEDED PARAMETERS                                                    IDEF0650
  140 MNSQ=M1SQ*SNTHSQ                                                      IDEF0660
C F'S ASSIST SOLUTION                                                       IDEF0670
      F1=GAM*MNSQ                                                           IDEF0680
      F2=2.*F1-GM1                                                          IDEF0690
      F3=F1*MNSQ                                                            IDEF0700
      F4=F1-MNSQ+2.                                                         IDEF0710
      P20P1=F2/GP1                                                          IDEF0715
```

Figure 41. Continued

```
                                                                    09/18/36
      IDEF      - EFN   SOURCE STATEMENT  -  IFN(S)  -

      M2OM1=(F3/F4)**(GAM/GM1)/P2OP1**(1./GM1)                      IDEF0720    31    32
      M2SQ=(GP1*M1SQ*F3-4.*(MNSQ-1.)*(F1+1.))/F2/F4                 IDEF0730
      M2=SQRT(M2SQ)                                                 IDEF0733    33
      A2OAS=((2.+GM1*M2SQ)/GP1)**(.5*GP1/GM1)/M2                    IDEF0736
COMPLETION                                                          IDEF0740    34
  150 RETURN                                                        IDEF0760
      END                                                           IDEF0770
```

Figure 41. Concluded

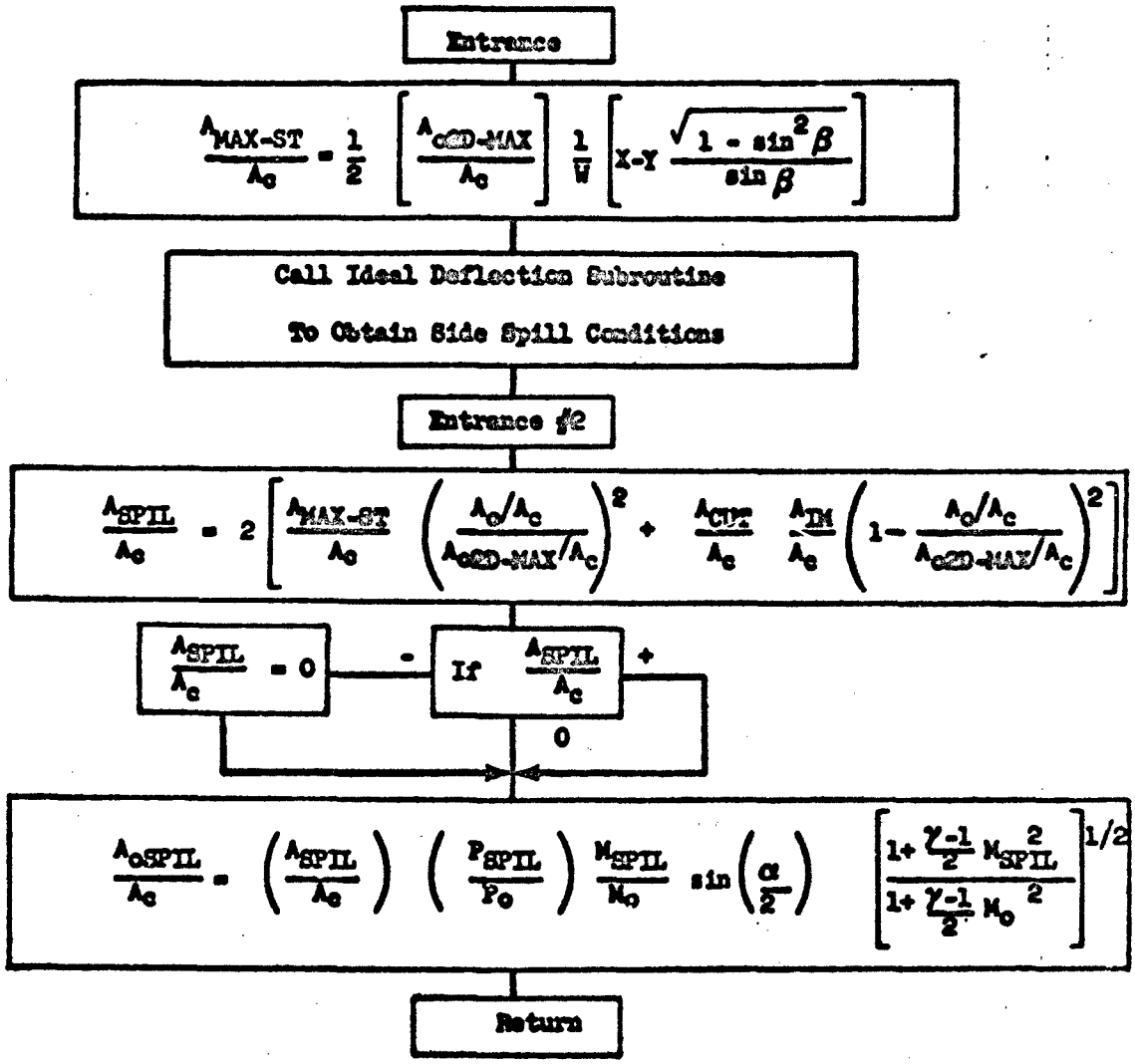

Figure 42. Side Spillage Subroutine

```
                                                                                09/10/36
      SPIL      - EFN   SOURCE STATEMENT -  IFN(S)  -

      SUBROUTINE SPILL (AOAC,MC,MOSO,AO2DAC,X,Y,SNBTSQ,ACUT,AIM,GAM,TTOTSPIL0030
     1O,AOACSP,ALF,W,PSPPO)                                                SPIL0031
      REAL MO,MOSO,MSP,MSPSO                                               SPIL0040
      ASPACM=.5*AJ2DAC/W*(X-Y*SQRT(1./SNBTSQ-1.))                          SPIL0200    2
      ALF02=.5*ALF                                                        SPIL0210
      CALL IDDEF (MOSO,GAM,ALF02,SNBSQ2,MSPHO,MSPSO,MSP,PSPPO,ASPAS,ER) SPIL0220
C ER MAY INDICATE TROUBLE IN IDDEF S/R, START NEXT CASE                   SPIL0221    3
      IF(ER.GT.0.0) GO TO 20                                              SPIL0222
      GO TO 10                                                            SPIL0223
      ENTRY   SPILL2   (AOAC,MC,MOSO,AO2DAC,X,Y,SNBTSQ,ACUT,AIM,GAM,TTOTSPIL0230
     1C,AOACSP,ALF,W,PSPPO)                                               SPIL0231
   10 ASPAC=2.*(ASPACM*(AOAC/AO2DAC)**2+ACUT-AIM*(1.-(AOAC/AO2DAC))**2) SPIL0235
      IF(ASPAC)1,2,2                                                      SPIL0236
    1 ASPAC=.J                                                            SPIL0237
    2 AOACSP=ASPAC*PSPPO/MO*MSP*SIN(ALF02)*SQRT((1.+.5*(GAM-1.)*MSPSQ)/TSPIL0240
     1TOTO)                                                               SPIL0241   14   15
   20 RETURN                                                              SPIL0250
      END                                                                 SPIL0260
```

Figure 43. Side Spillage Subroutine Listing

$A_{SPILL} = 2(OSED)$ $A_{cut} = OCD$ $A_{IM} = OCR$ $A_{MAX-ST} = OSC$

$A_{SPIL} = 2(OSA+OCD-ACB)$

$$A_{SPILL} = 2\left[A_{MAX-ST}\left(\frac{A_o}{A_{c2D-MAX}}\right)^2 + A_{CUT} - A_{IM}\left(1 - \frac{A_o}{A_{c2D-MAX}}\right)^2\right]$$

Assumes $A_o > A_{cMIN}$ (Stagnation Streamline Above Point D)

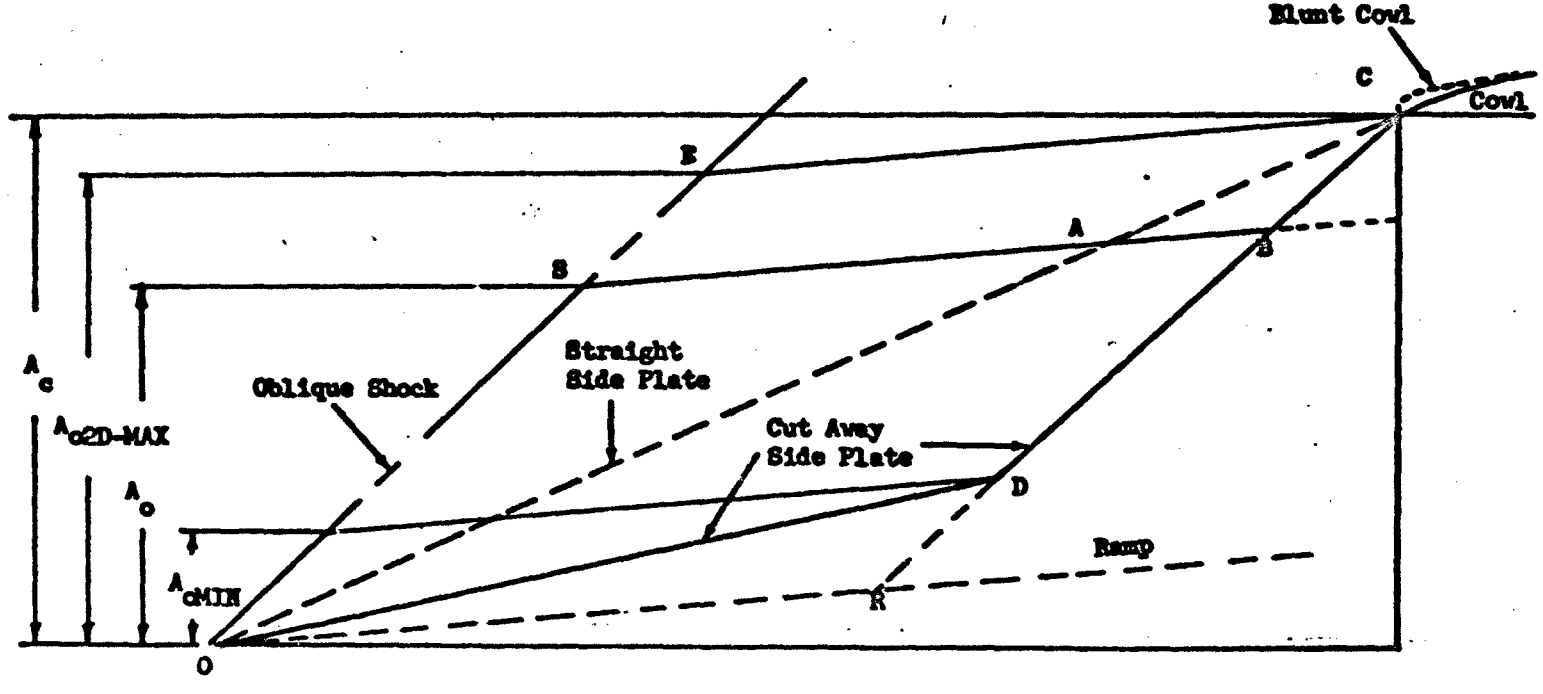

Figure 44. Inlet Nomenclature

APPENDIX III

COMPILATION OF DATA PLOTS

Appendix III is an accumulation of plots of data or factors derived from data, figures 45 thru 115 inclusive.

SYM.	CONFIG.	α°	β°	M_o	(A_o/A_c) ref.
○	R1SP1C1	5°	5°	0.69	0.796
△	C2	"	"	"	"
□	C3	"	"	"	"
◇	C4	"	"	"	"
▽	C5	"	"	"	"
▯	C6	"	"	"	"

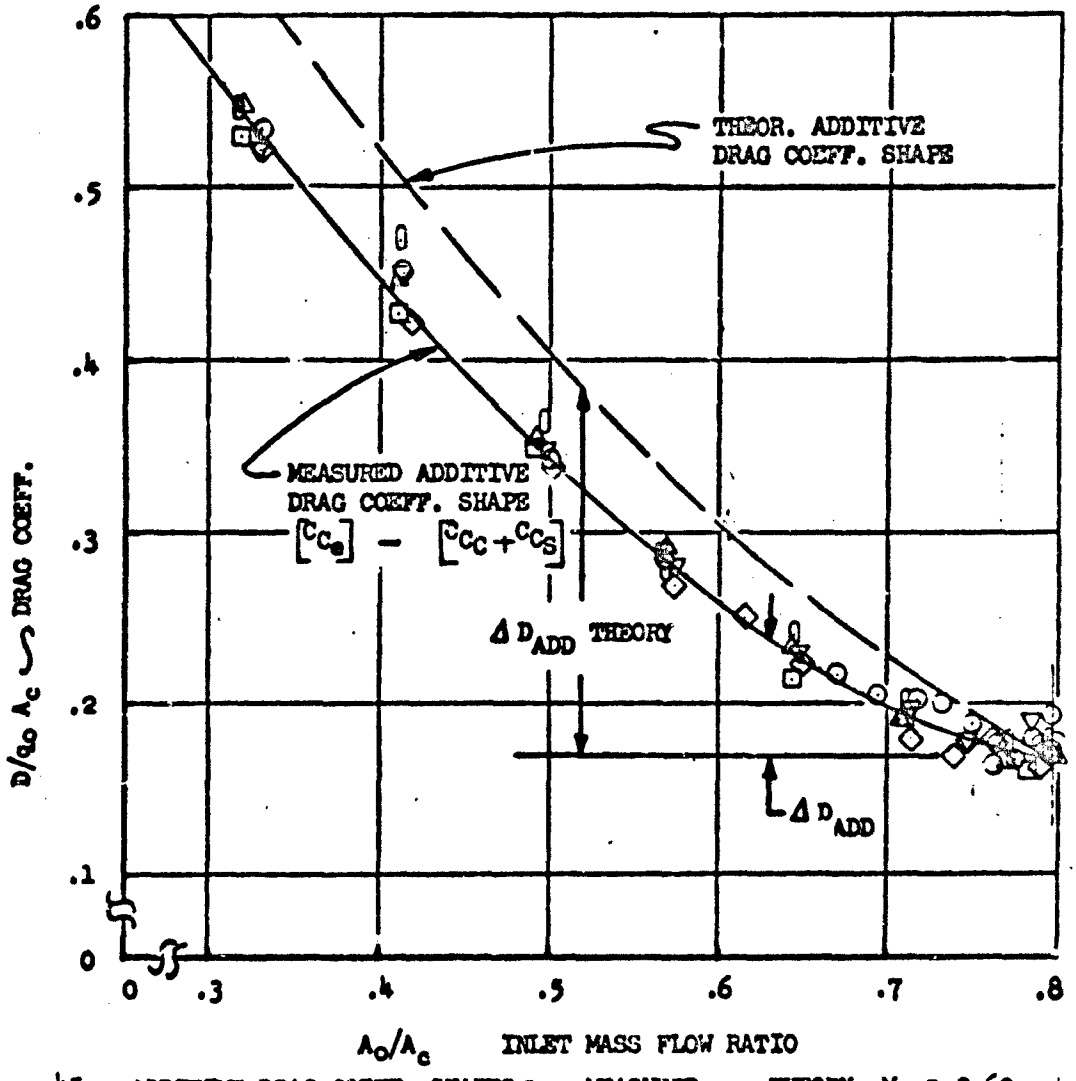

Figure 45. ADDITIVE DRAG COEFF. SHAPES ⤳ MEASURED vs. THEORY, M_o = 0.69

SYM.	CONFIG.	$\alpha°$	$\beta°$	M_o	(A_o/A_c) ref.
○	R1SP1C1	5°	5°	0.84	0.796
△	C2	"	"	"	"
□	C3	"	"	"	"
◇	C4	"	"	"	"
▽	C5	"	"	"	"
▯	C6	"	"	"	"

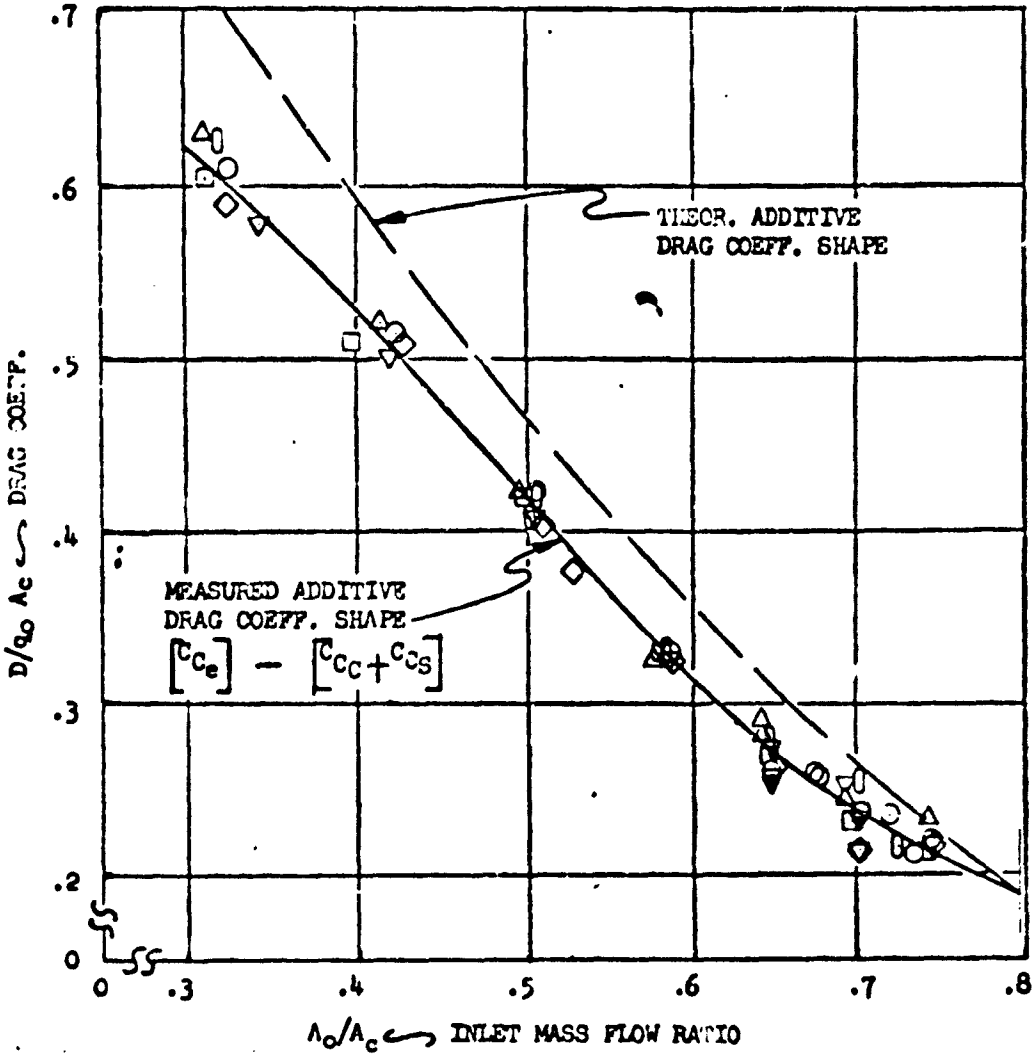

Figure 46. ADDITIVE DRAG COEFF. SHAPES ⤳ MEASURED vs. THEORY, M_o = 0.84

SYM.	CONFIG.	α°	β°	M_o	(A_o/A_c) ref.
○	R1SP1C1	5°	5°	1.09	0.796
△	C2	"	"	"	"
□	C3	"	"	"	"
◇	C4	"	"	"	"
▽	C5	"	"	"	"
⬯	C6	"	"	"	"

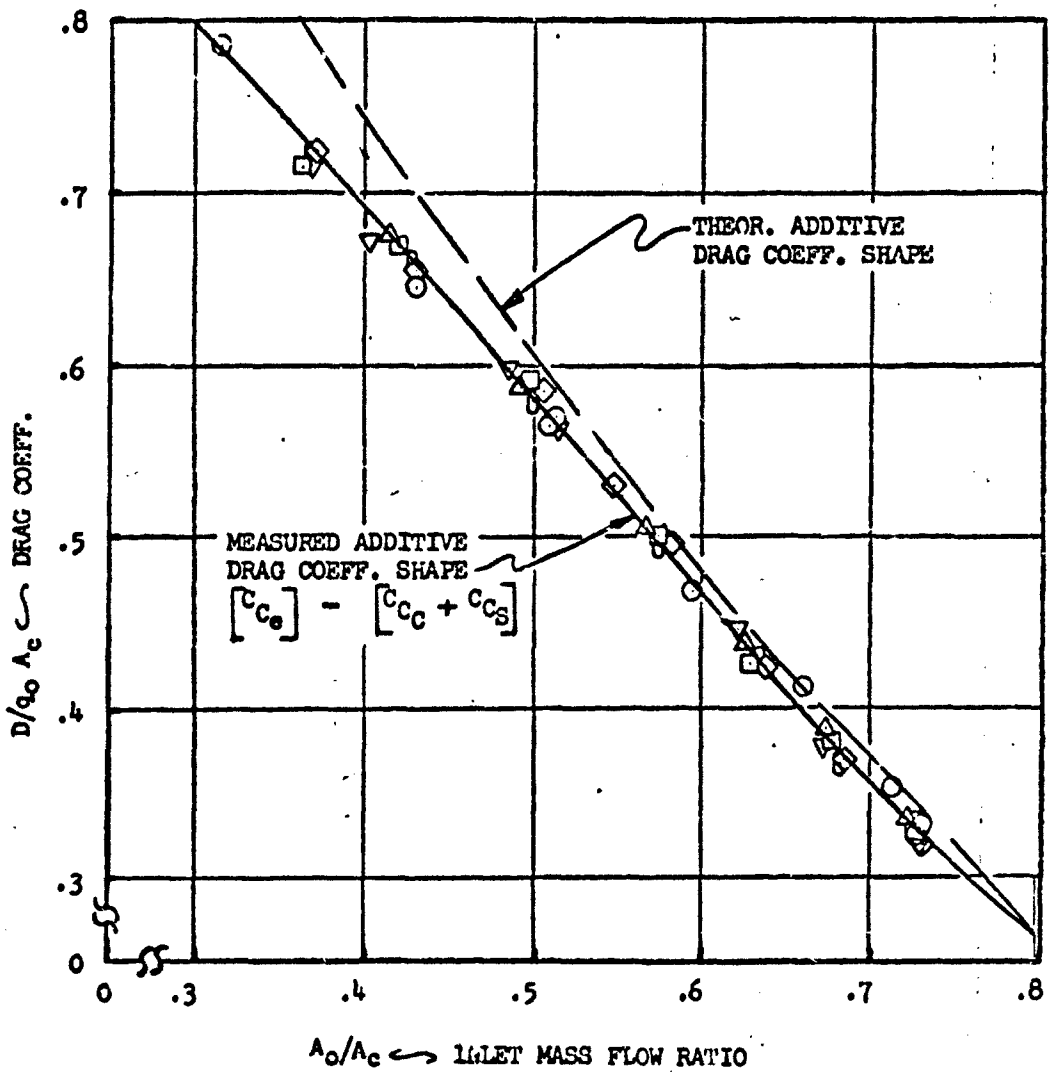

Figure 47. ADDITIVE DRAG COEFF. SHAPES ⤳ MEASURED *vs.* THEORY, $M_o = 1.09$

SYM.	CONFIG.	$\alpha°$	$\beta°$	M_o	(A_o/A_c) ref.
○	R1SP1C1	5°	5°	1.29	0.780
△	C2	"	"	"	"
□	C3	"	"	"	"
◇	C4	"	"	"	"
▽	C5	"	"	"	"
⬯	C6	"	"	"	"

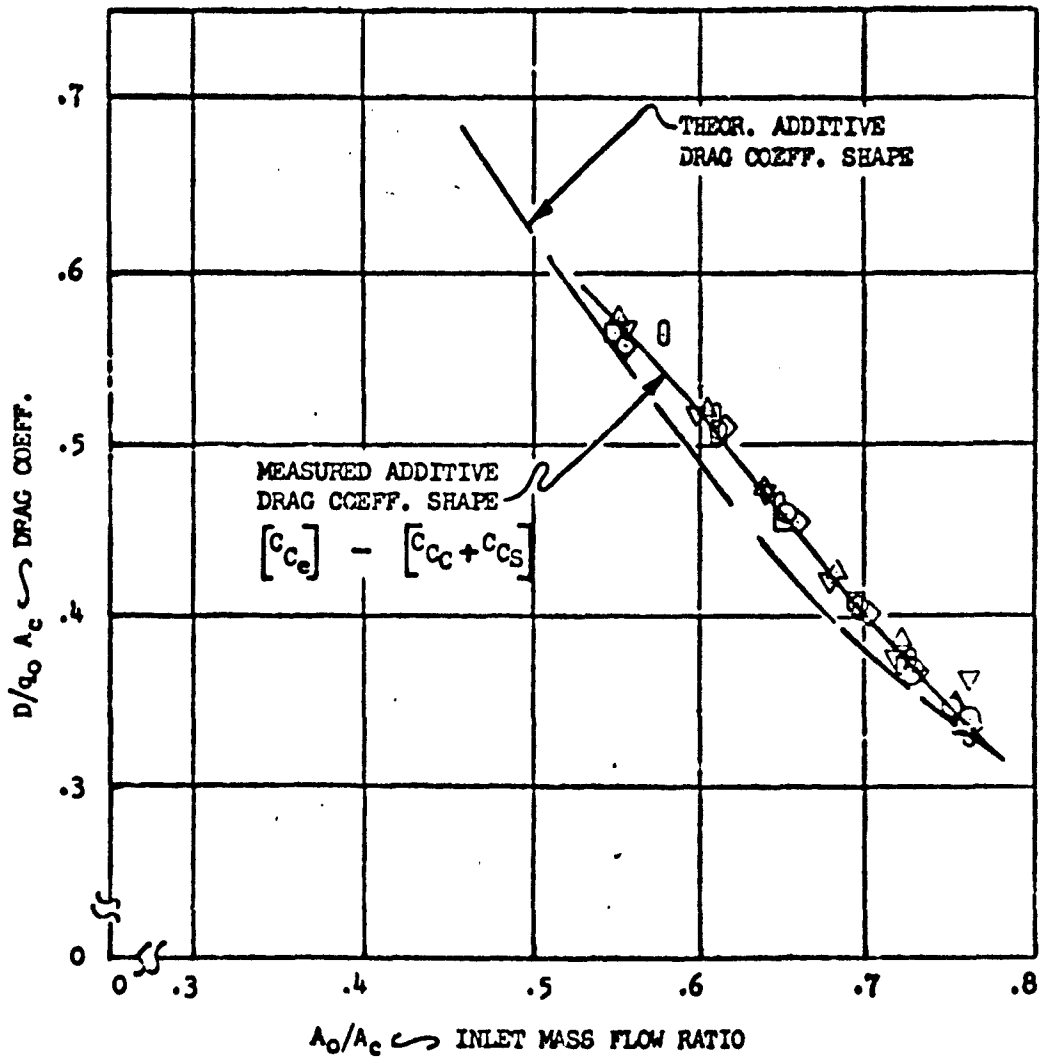

Figure 48. ADDITIVE DRAG COEFF. SHAPES ⤳ MEASURED vs. THEORY, M_o = 1.29

SYM.	CONFIG.	$\alpha°$	$\beta°$	M_o	(A_o/A_c) ref.
○	R1SP1C1	5°	5°	1.39	0.799
△	C2	"	"	"	"
□	C3	"	"	"	"
◇	C4	"	"	"	"
▽	C5	"	"	"	"
▯	C6	"	"	"	"

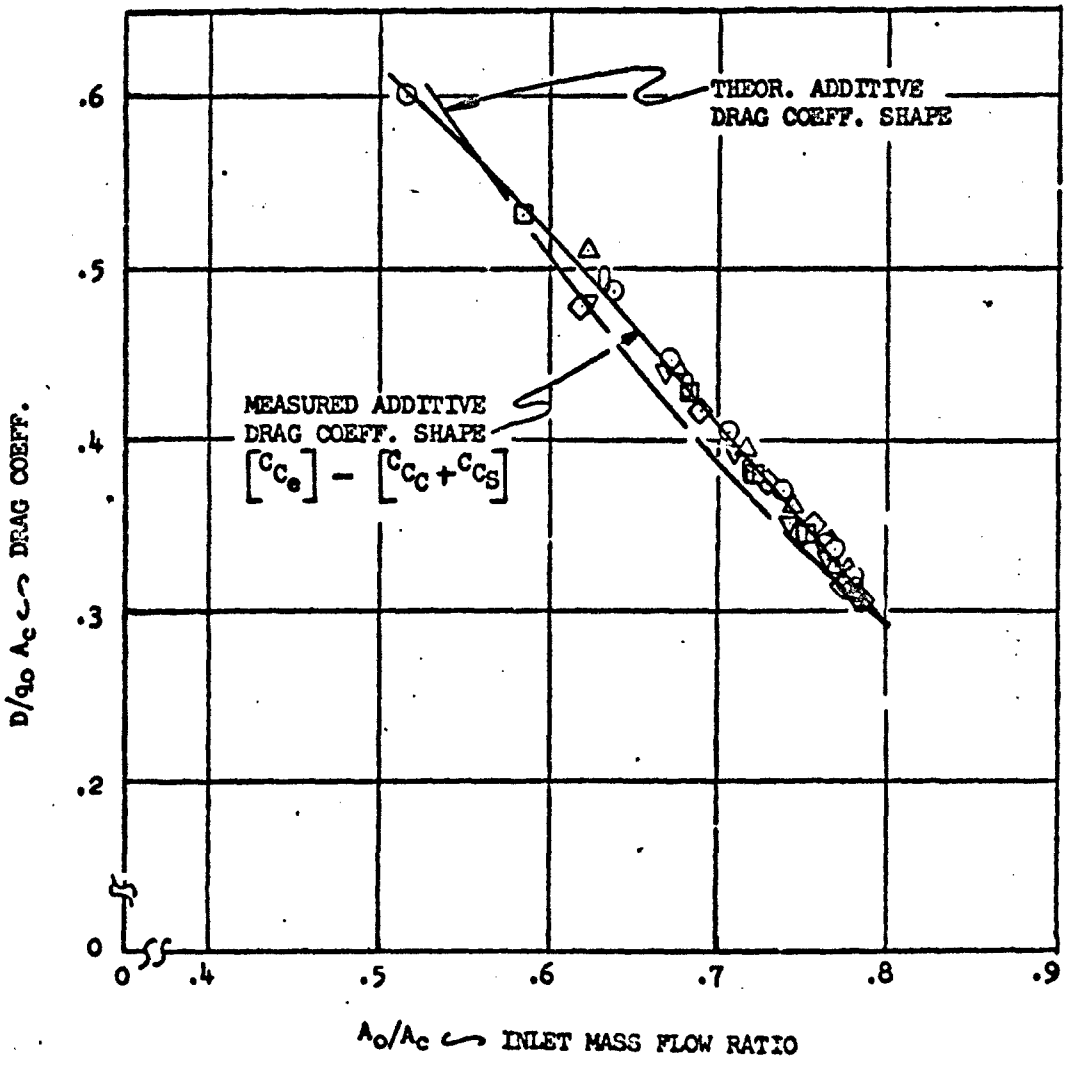

Figure 49. ADDITIVE DRAG COEFF. SHAPES ⤻ MEASURED vs. THEORY, M_o = 1.39

SYM	CONFIG.	α°	β°	M_0	(A_0/A_c) ref.
○	R1SP1C1	5°	5°	1.69	0.841
▽	C5	"	"	"	"

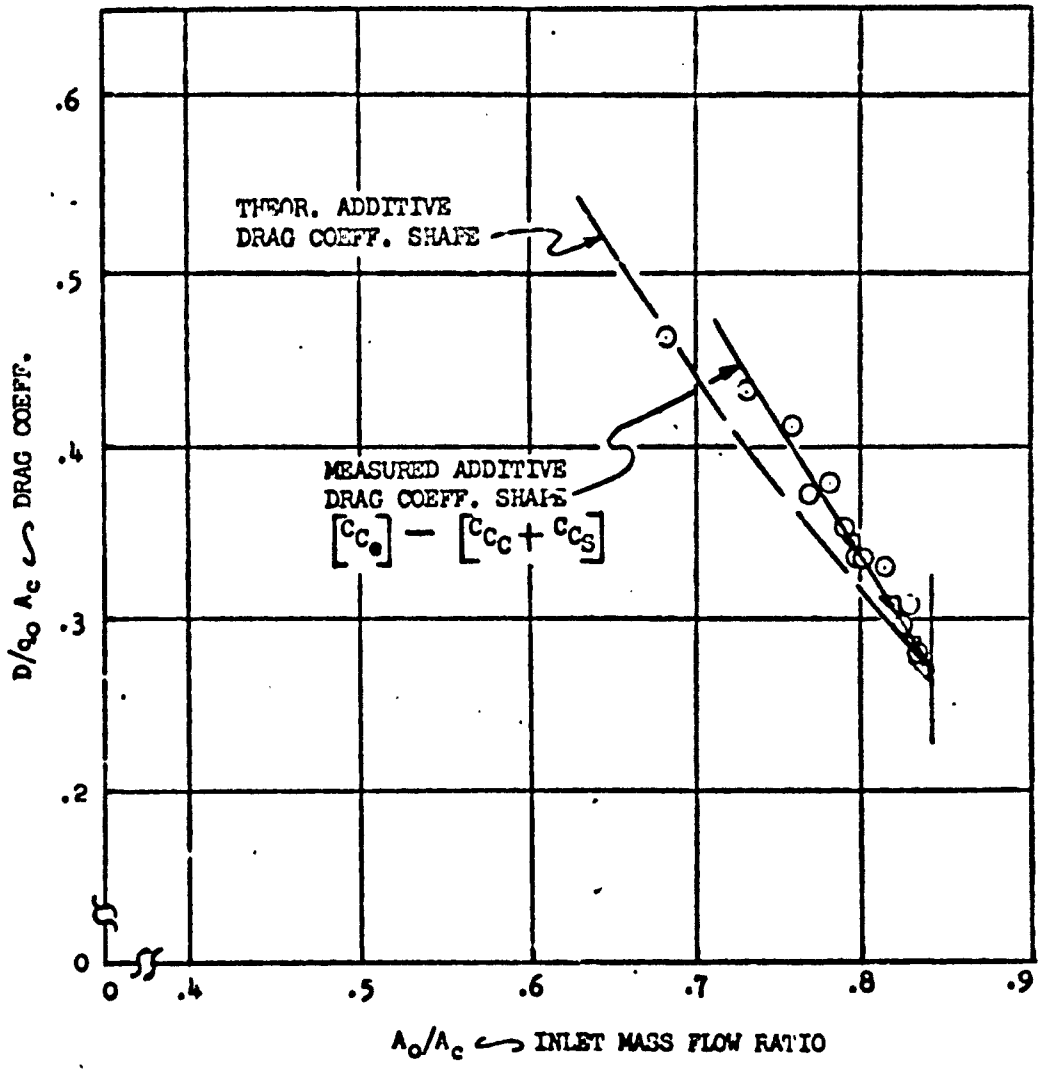

Figure 50. ADDITIVE DRAG COEFF. SHAPES ⤻ MEASURED vs. THEORY, $M_0 = 1.69$

NOTE: EACH DRAG CURVE HAS A DIFFERENT ZERO LEVEL (AS INDICATED) TO SPREAD DATA. BASIC SCALE SHOWN FOR C1 ONLY.

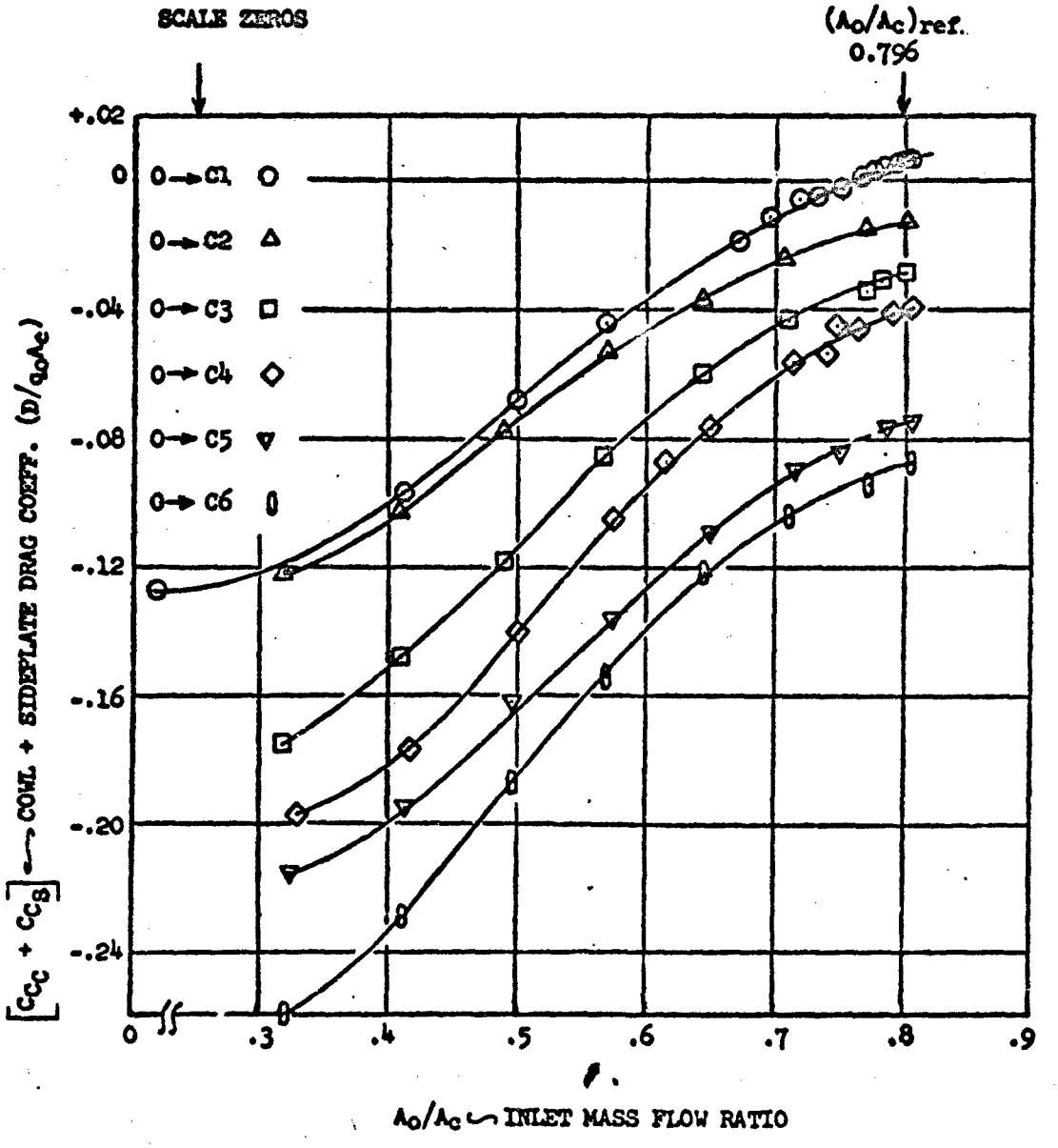

Figure 51. COWL + SIDEPLATE DRAG → RLSP1C1 THRU C6, $\alpha = \beta = 5^\circ$, $M_o = 0.69$

NOTE: EACH DRAG CURVE HAS A DIFFERENT ZERO LEVEL (AS INDICATED) TO SPREAD DATA. BASIC SCALE SHOWN FOR C1 ONLY.

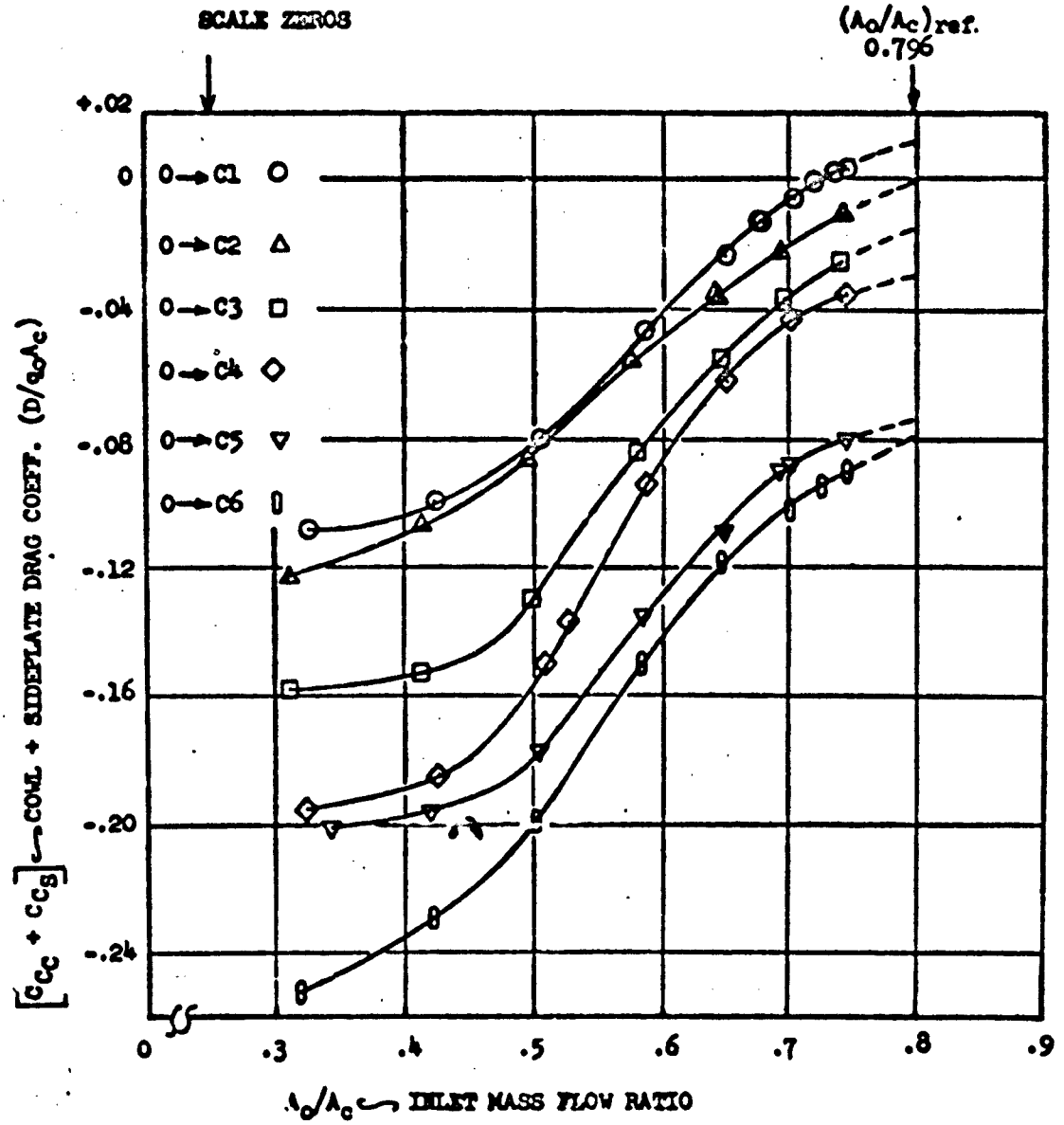

Figure 52. COWL + SIDEPLATE DRAG → RLSP1C1 THRU C6, $\alpha=\beta=5^\circ$, $M_0 = 0.84$

NOTE: EACH DRAG CURVE HAS A DIFFERENT ZERO LEVEL (AS INDICATED) TO SPREAD DATA. BASIC SCALE SHOWN FOR C1 ONLY.

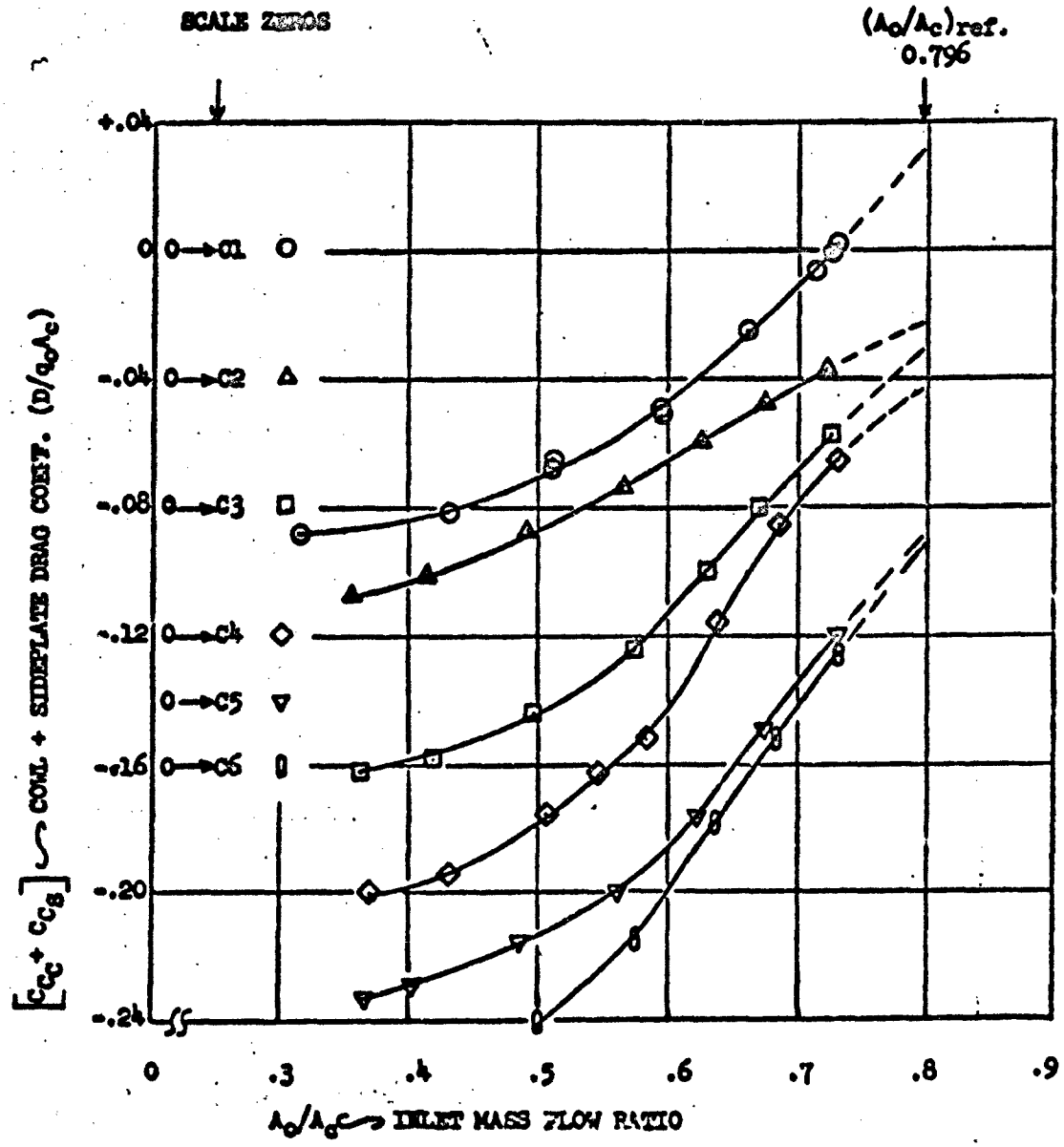

Figure 53. COWL + SIDEPLATE DRAG ⤻ RISPIC1 THRU C6, $\alpha = \beta = 5^\circ$, $M_o = 1.09$

NOTE: EACH DRAG CURVE HAS A DIFFERENT ZERO LEVEL (AS INDICATED) TO SPREAD DATA. BASIC SCALE SHOWN FOR C1 ONLY.

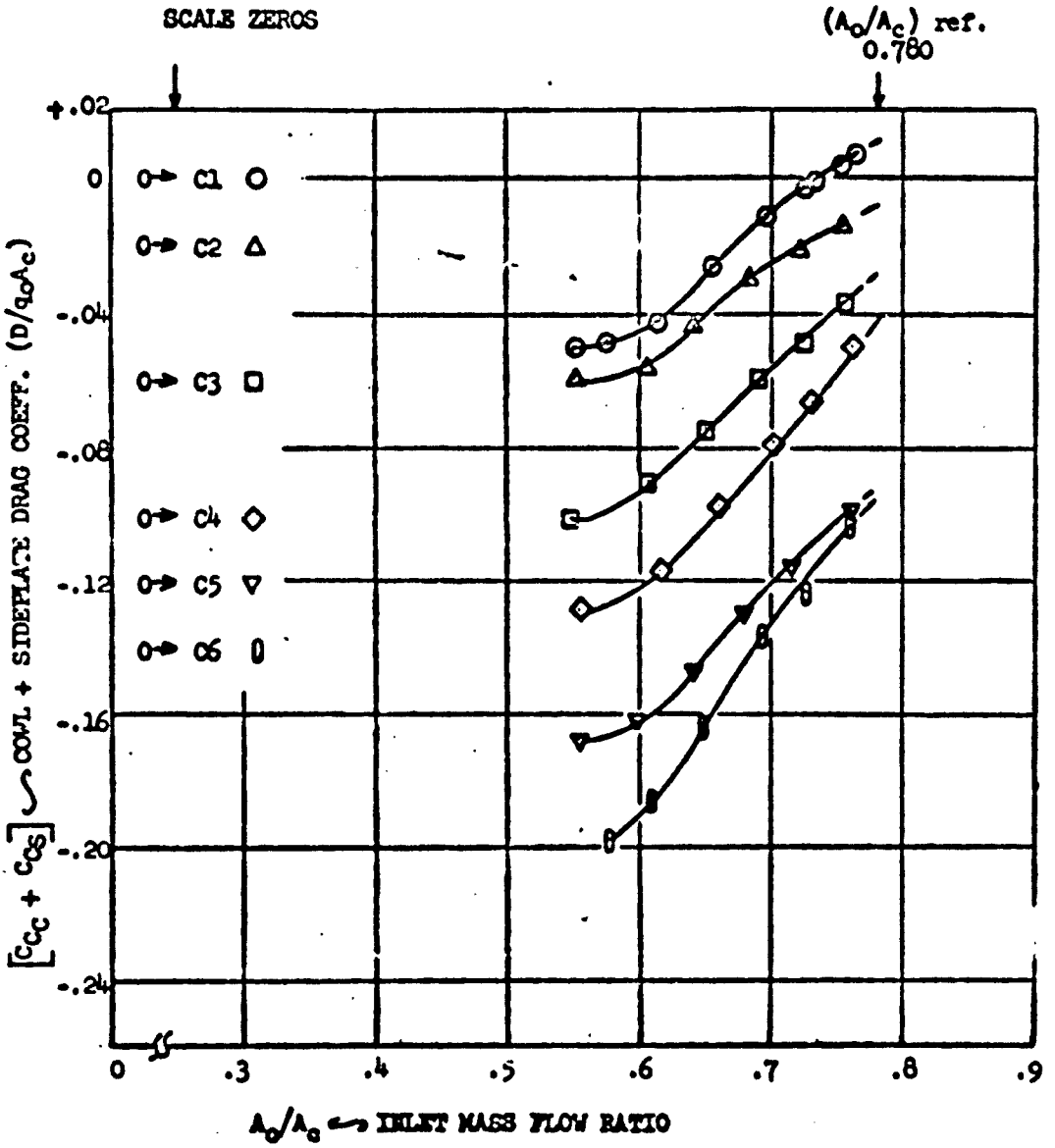

Figure 54. COWL + SIDEPLATE DRAG RUNS C1 THRU C6, $\alpha = \beta = 5°$, $M_o = 1.29$

NOTE: EACH DRAG CURVE HAS A DIFFERENT ZERO LEVEL (AS INDICATED) TO SPREAD DATA. BASIC SCALE SHOWN FOR C1 ONLY.

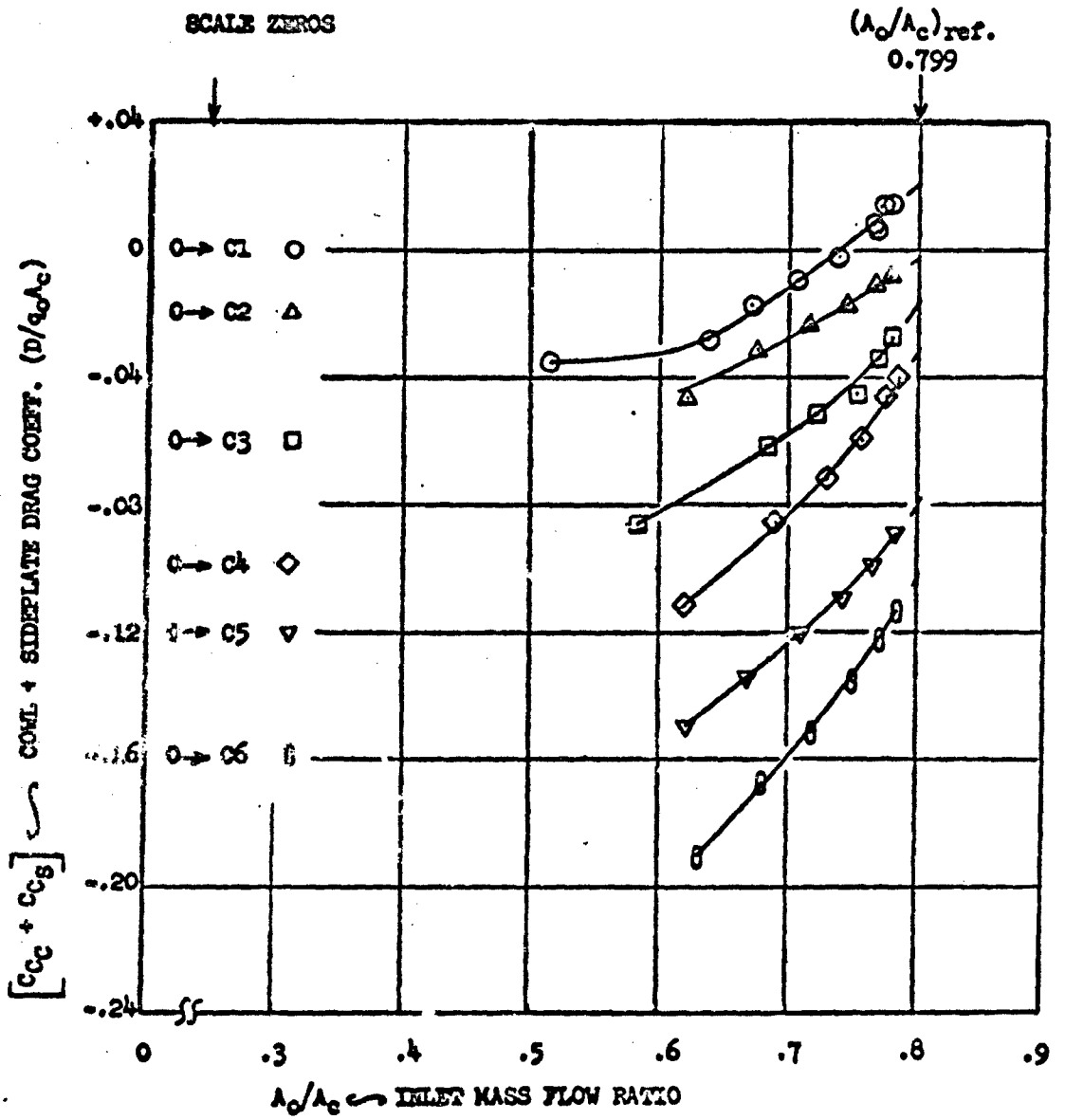

Figure 55. COWL + SIDEPLATE DRAG ⤳ RISE-1C1 TERM C6, $\alpha = \beta = 5°$, $M_o = 1.39$

CONFIG.	α°	β°	M_o	(A_o/A_c) ref.
R1SP1C1	5°	5°	0.69	0.796
C2	"	"	"	"
C3	"	"	"	"
C4	"	"	"	"
C5	"	"	"	"
C6	"	"	"	"

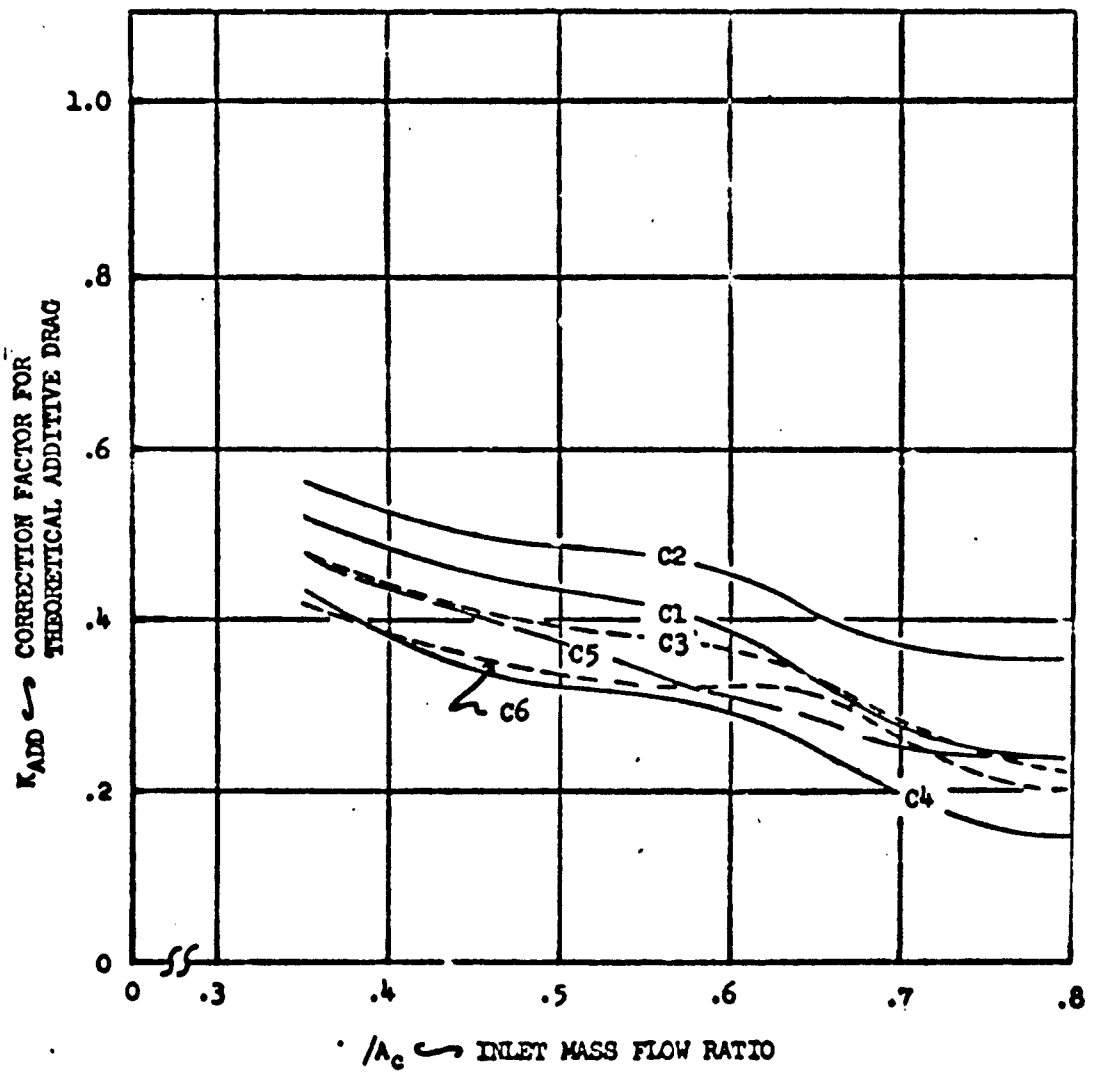

Figure 56. K_{ADD}, R1SP1C1-C6, M_o = 0.69

CONFIG.	$\alpha°$	$\beta°$	M_o	(A_o/A_c) ref.
R1SP1C1	5°	9°	0.69	0.715

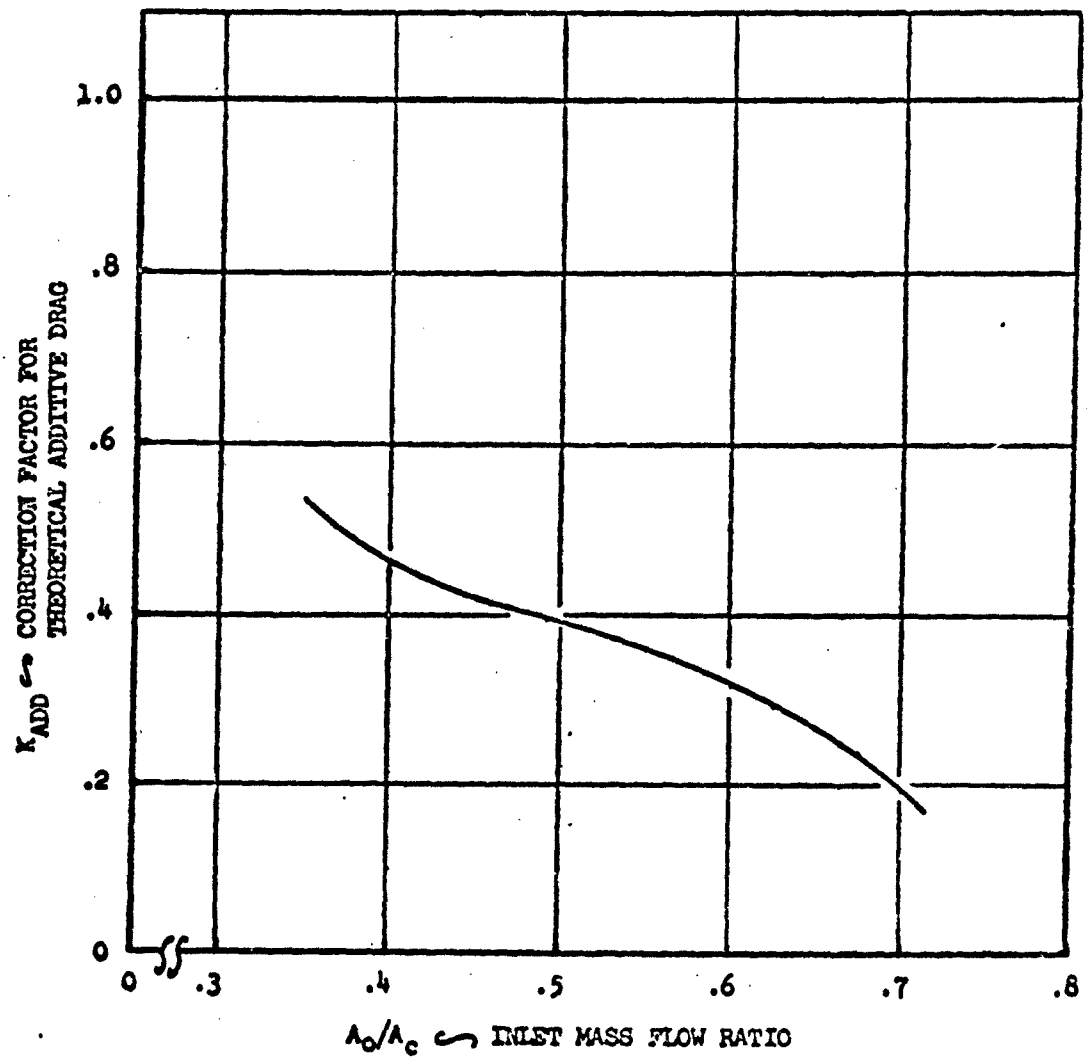

Figure 57. K_{ADD}, R1SP1C1, M_o = 0.69

CONFIG.	α°	β°	M_o	(A_o/A_c) ref.
R1SP1C1	5°	12°	0.69	0.715

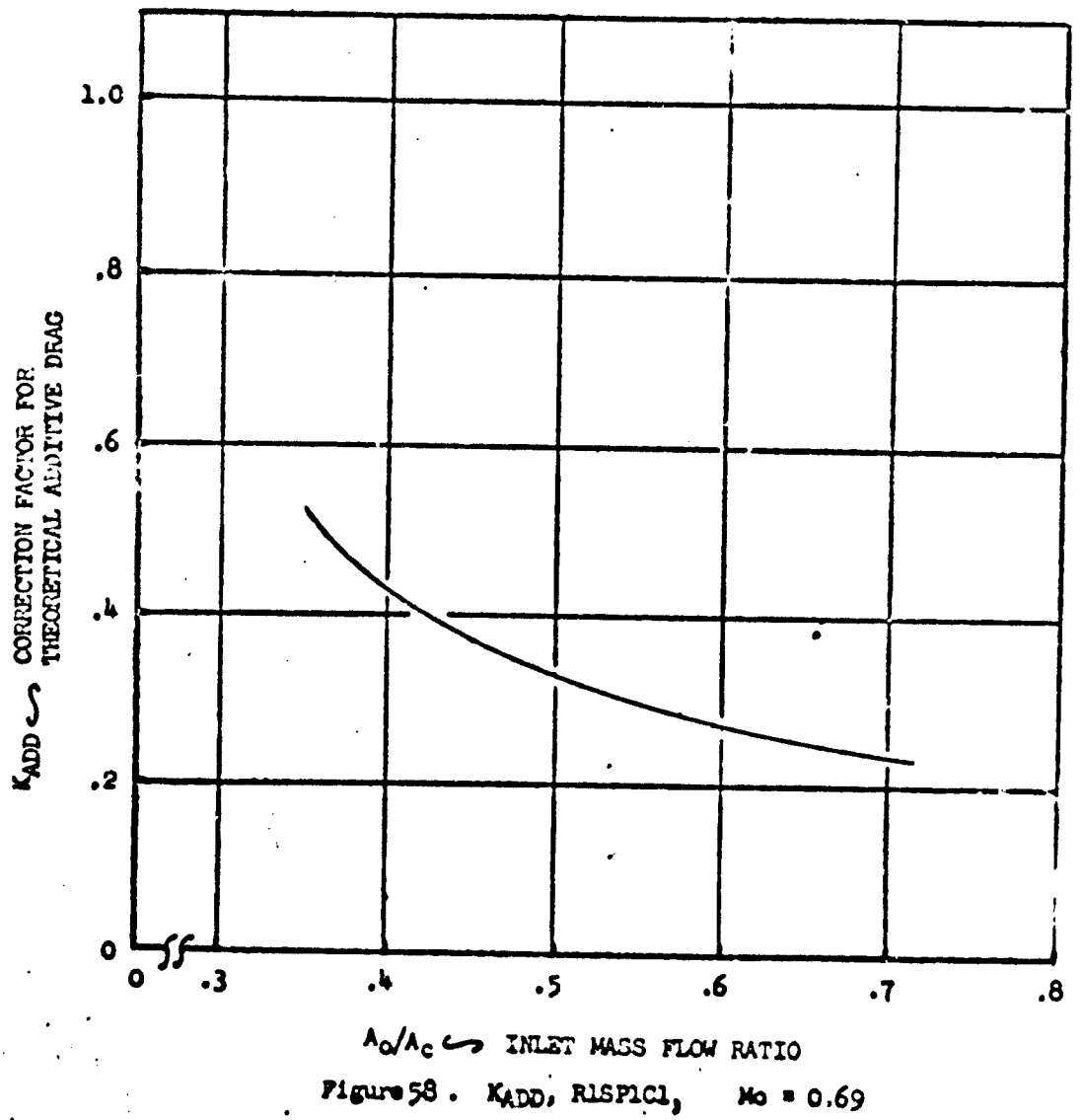

Figure 58. K_{ADD}, R1SP1C1, M_o = 0.69

CONFIG.	α°	β°	M_o	(A_o/A_c) ref.
R1SP2C1	5°	5°	0.69	0.795

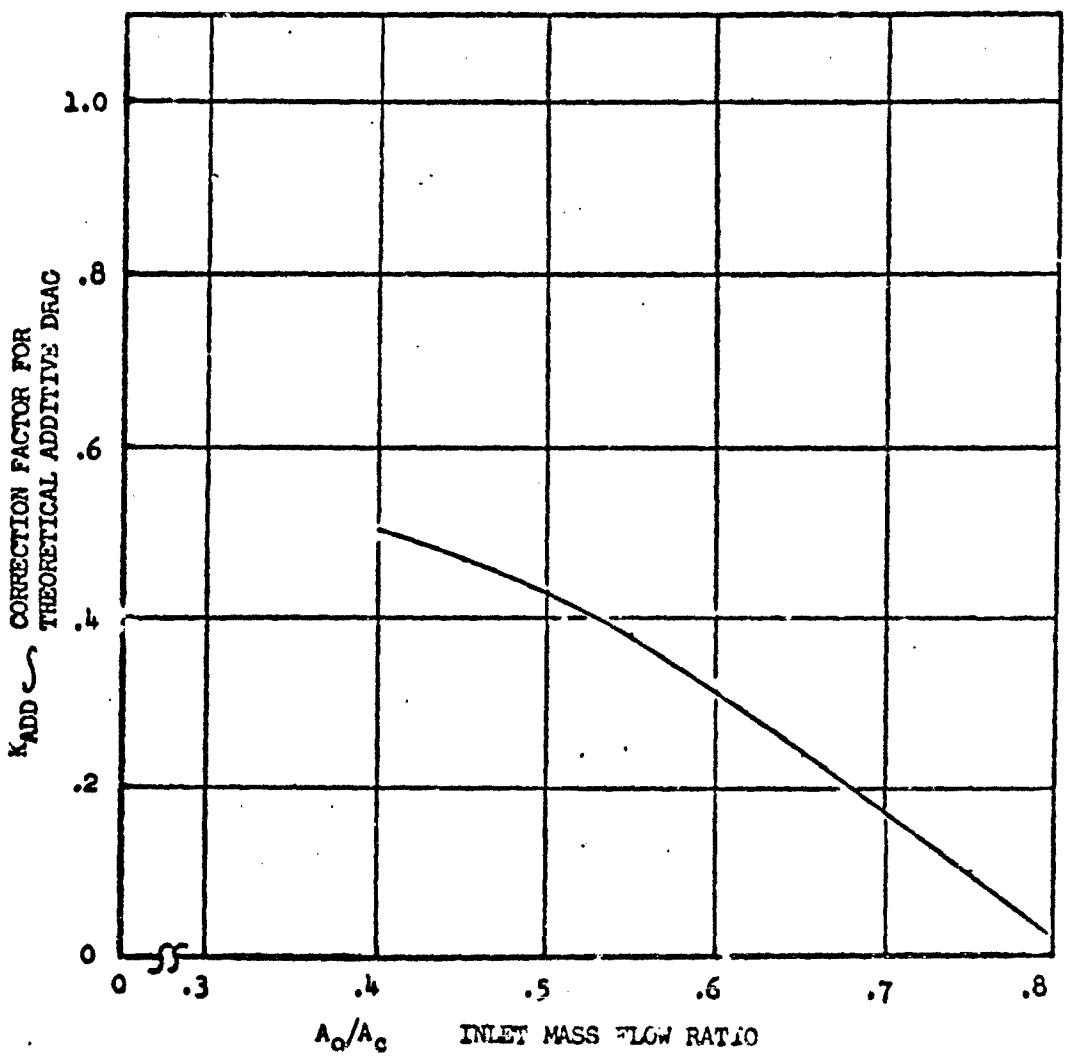

Figure 59. K_{ADD}, R1SP2C1, M_o = 0.69

CONFIG.	$\alpha°$	$\beta°$	M_0	(A_0/A_c) ref.
R1SP3C1	5°	5°	0.71	0.796

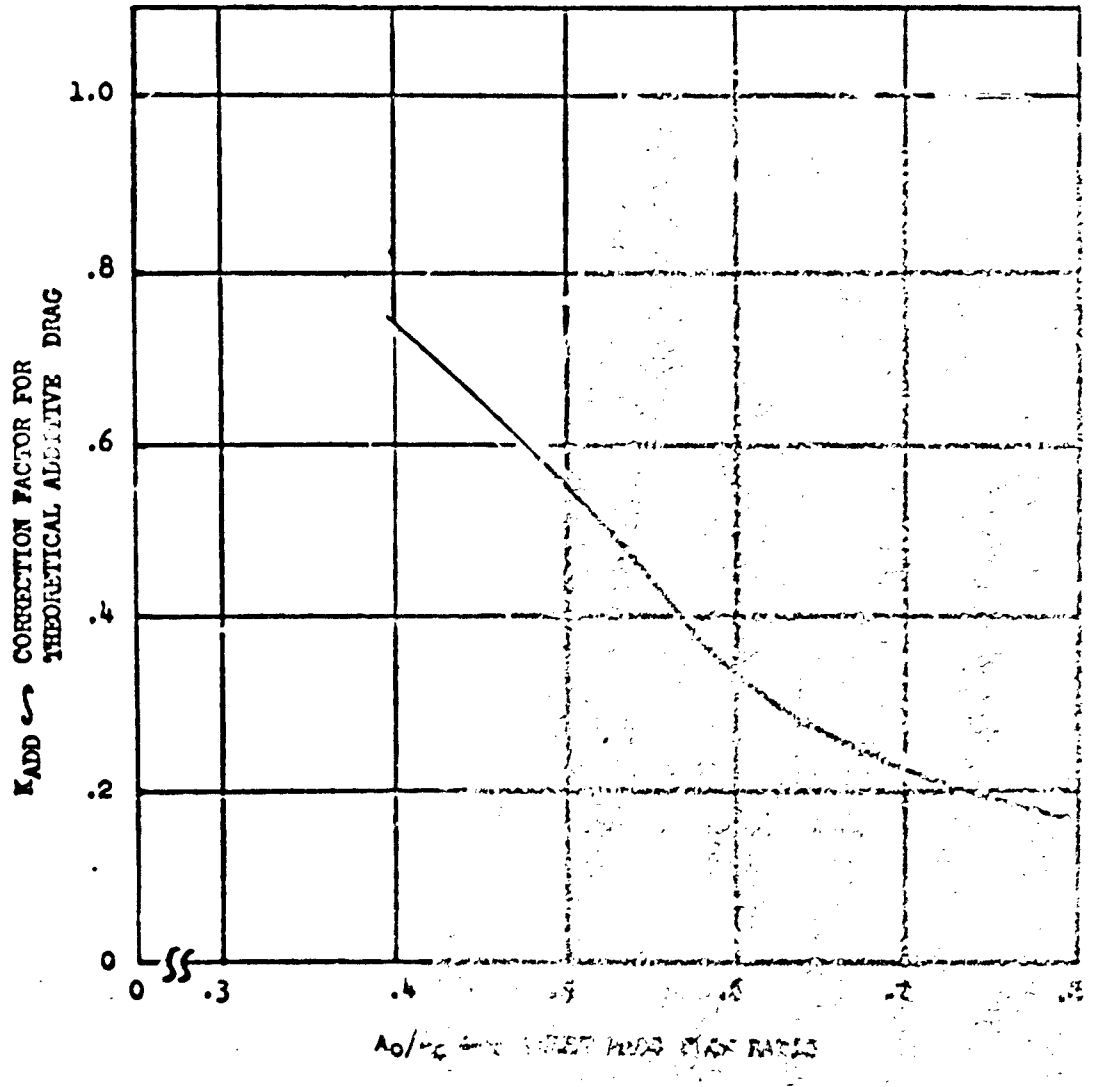

Figure 60. [illegible]

CONFIG.	α°	β°	M_O	(A_O/A_C) ref.
F8SP1C1	T	T	0.71	0.713

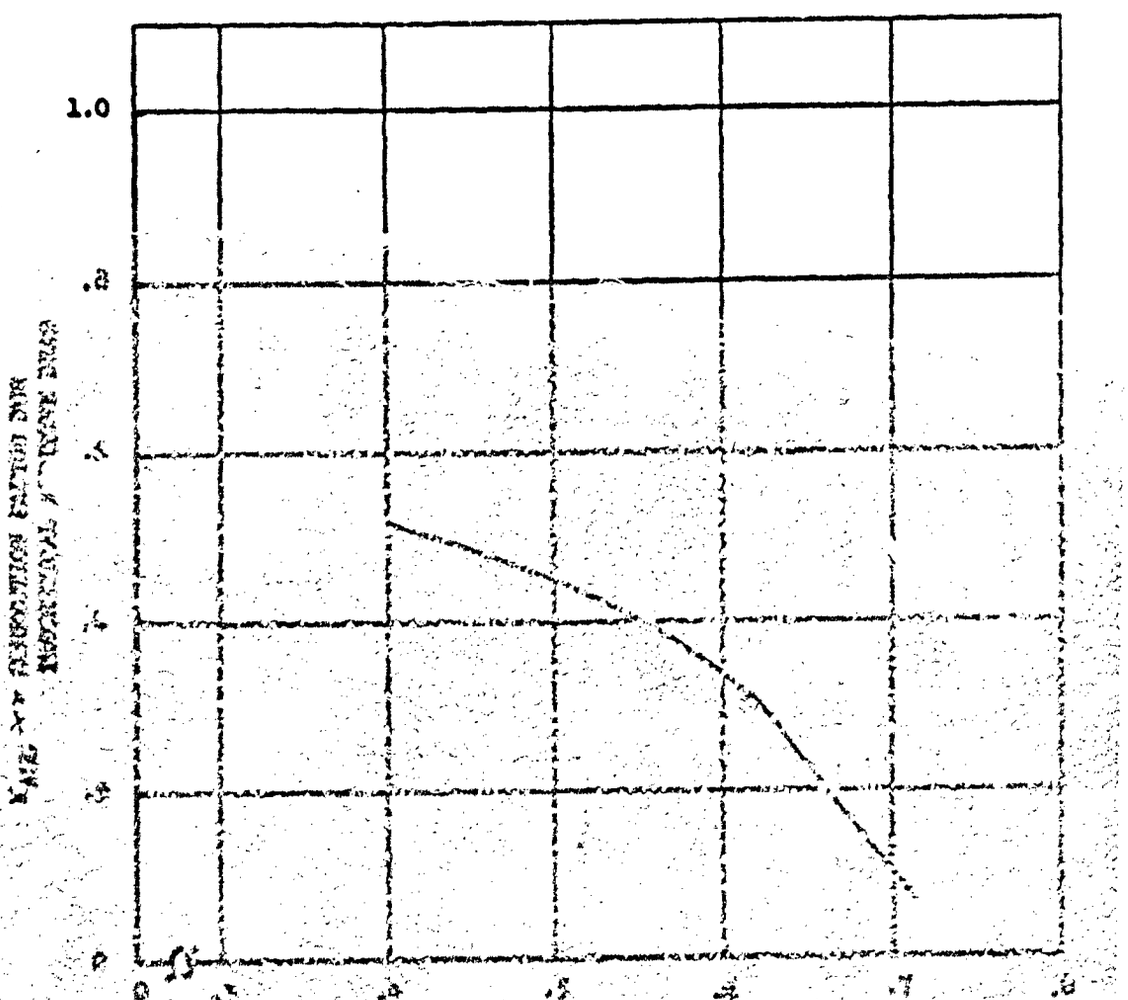

FIGURE 62. K_{AOM} FUNCTION, $M_O = 0.72$

CONFIG.	$\varphi°$	$\beta°$	M_0	(A_0/A_c) ref.
R3SP1C1	12°	12°	0.71	0.50

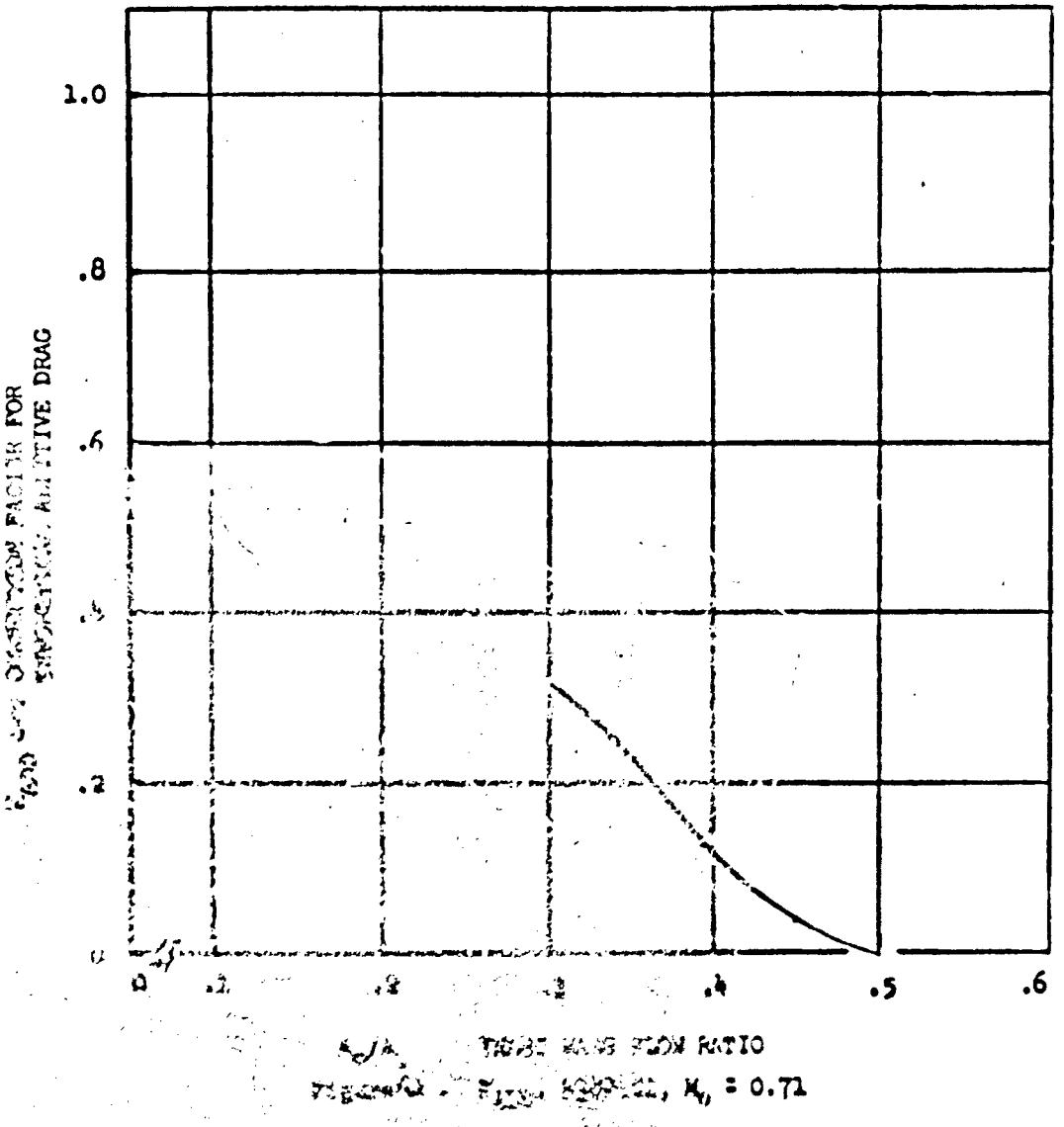

$K_{\Delta p}$ DRAG INTERFERENCE FACTOR FOR SUPERSONIC ADDITIVE DRAG

A_0/A_c TRUE MASS FLOW RATIO

$M_0 = 0.71$

CONFIG.	$\varphi°$	$\beta°$	M_o	$(A_o/A_c)_{ref.}$
R4SP4C1	5°	5°	0.71	0.852
C6	"	"	"	"

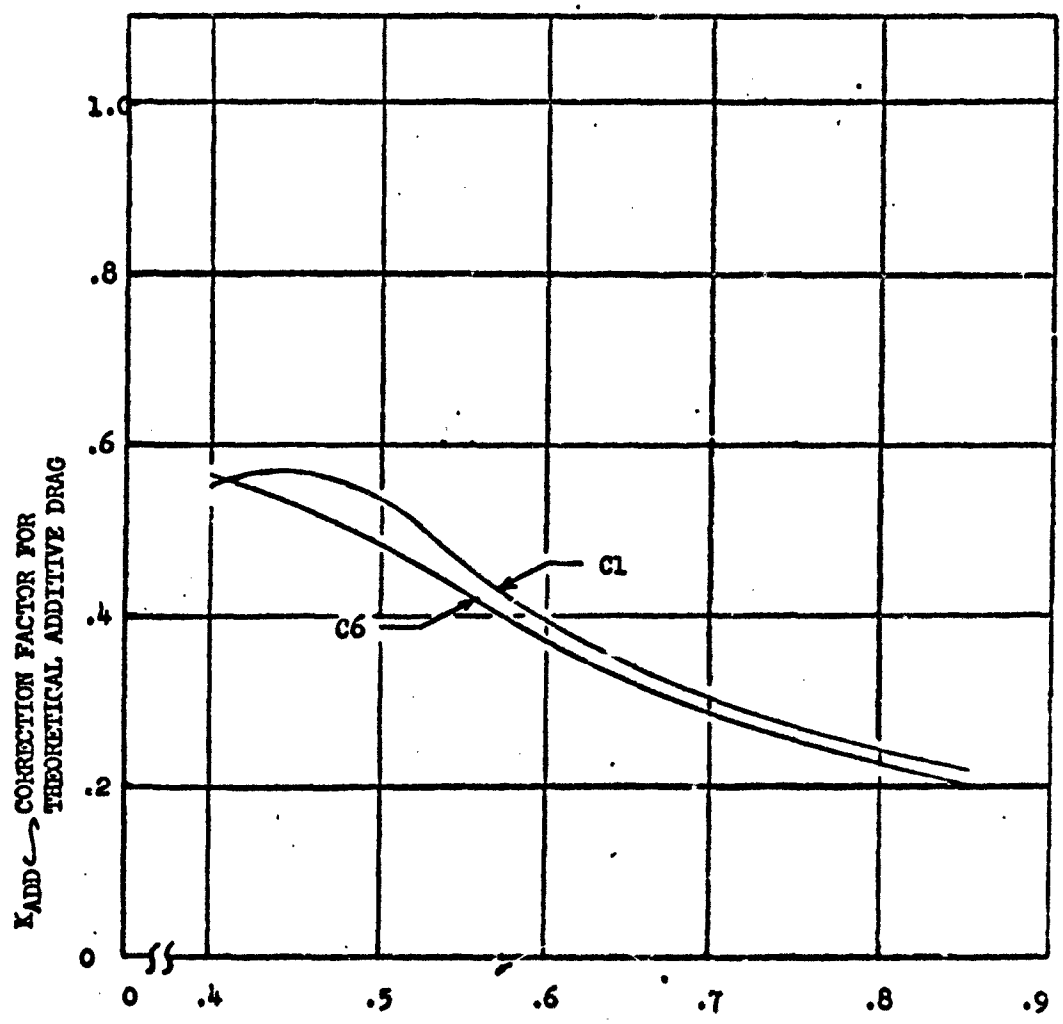

Figure 63. K_{ADD}, R4SP4C1, C6, M_o = 0.71

CONFIG.	$\alpha°$	$\beta°$	M_0	(A_0/A_c) ref.
R1SP1C1	5°	5°	0.84	0.796
C2	"	"	"	"
C3	"	"	"	"
C4	"	"	"	"
C5	"	"	"	"
C6	"	"	"	"

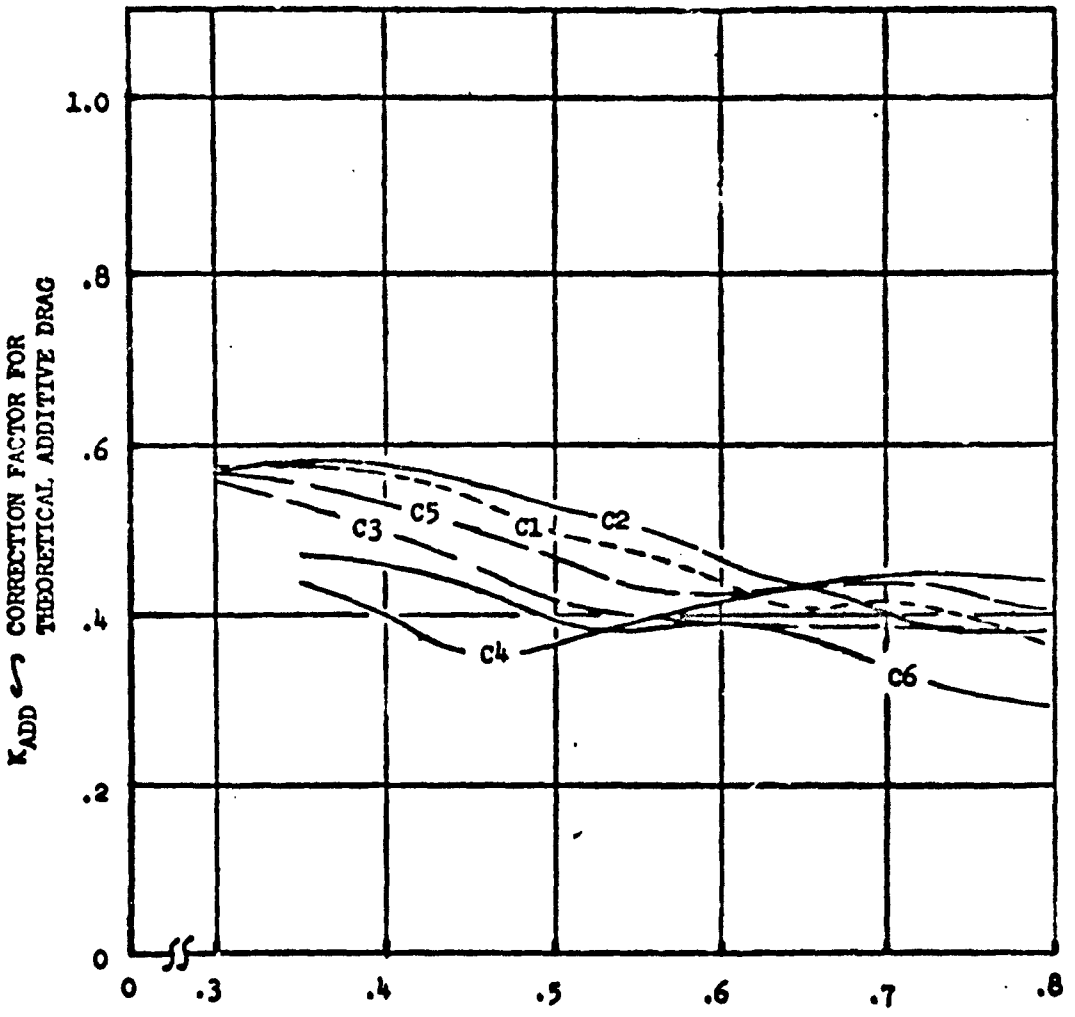

Figure 64. K_{ADD}, R1SP1C1-C6, M_0 = 0.84

CONFIG.	α°	β°	M_o	(A_o/A_c) ref.
R1SP1C1	5°	9°	0.84	0.715

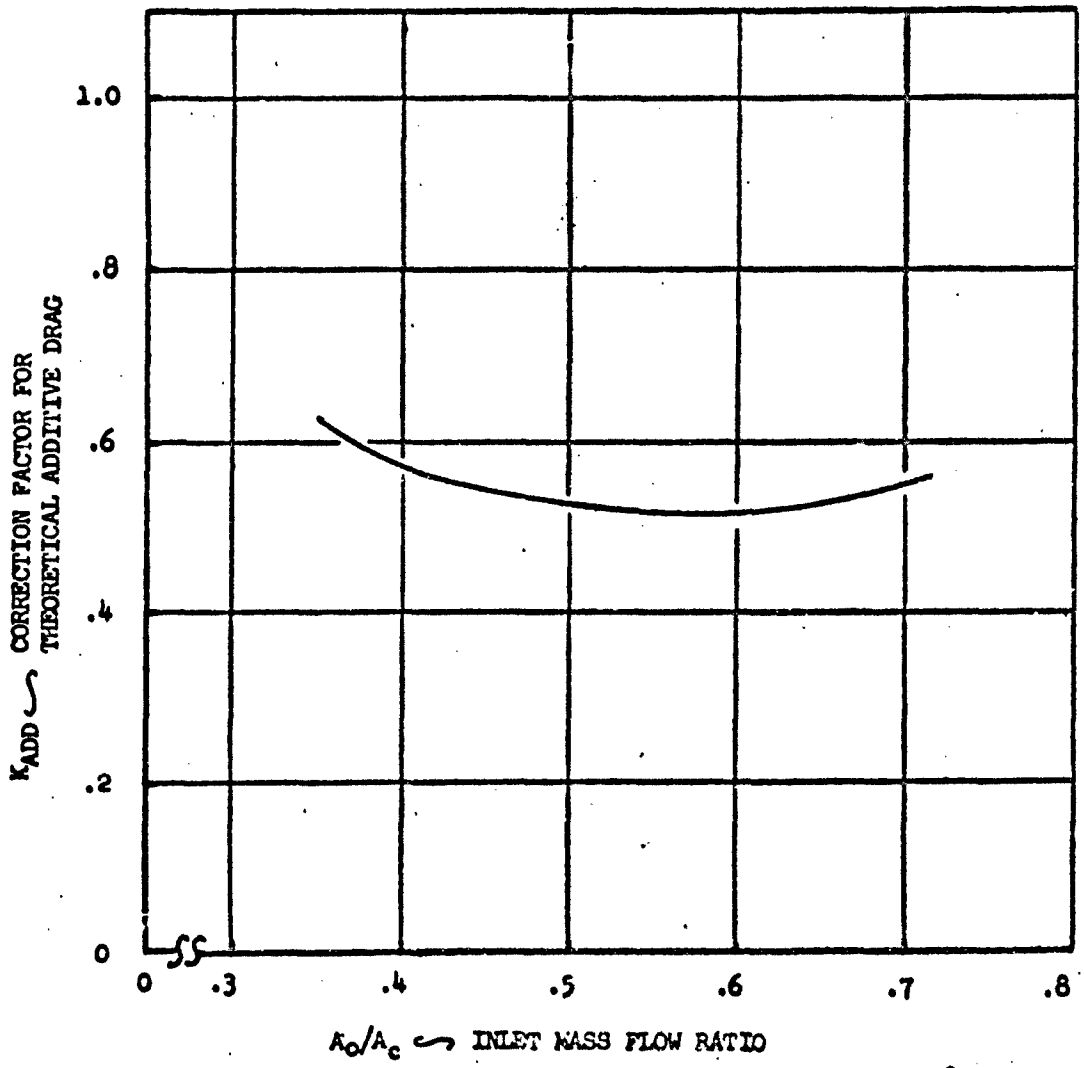

Figure 65. K_{ADD}, R1SP1C1, M_o = 0.84

CONFIG.	α°	β°	K_D	(A_b/A_B) ref.
R1SP1C1	5°	12°	[illegible]	[illegible]

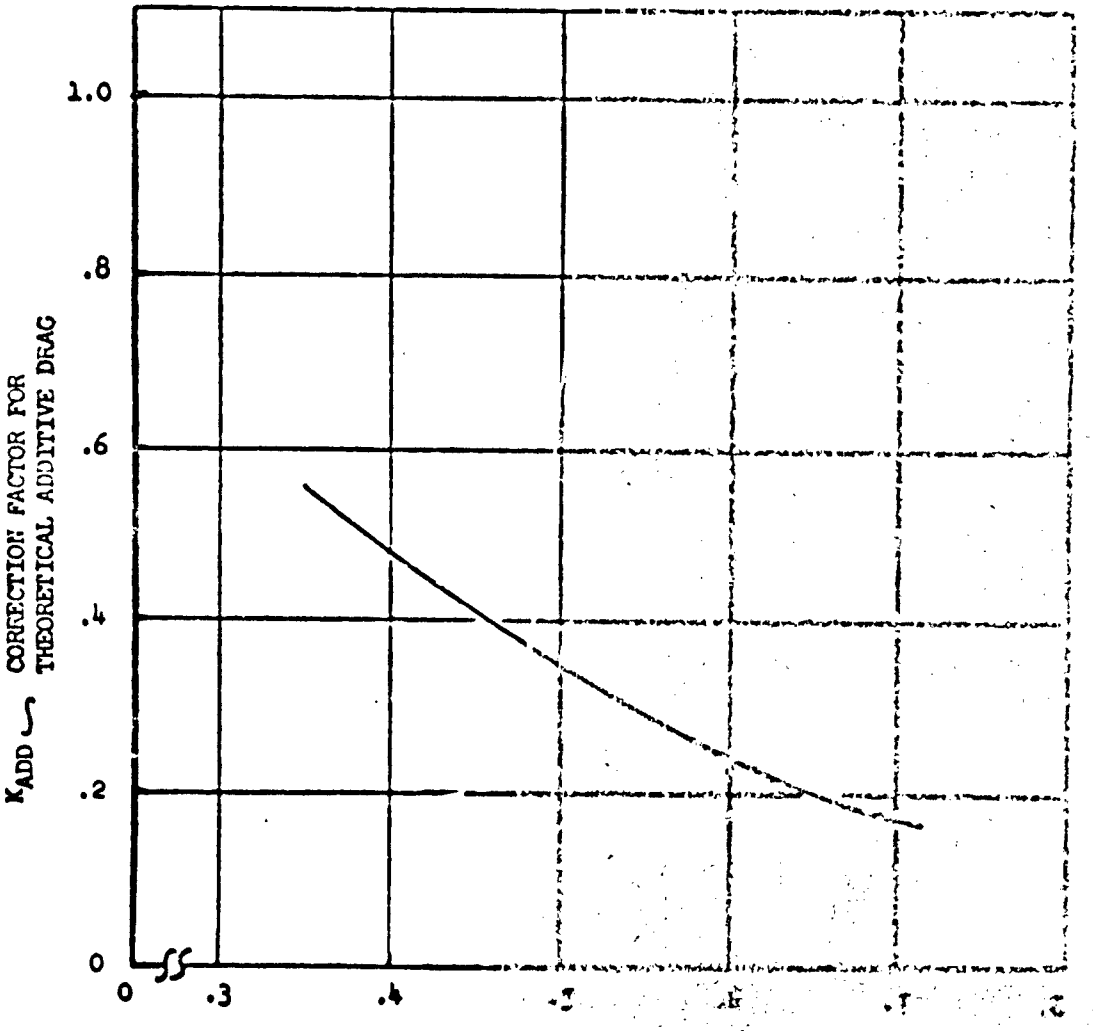

Figure 66. [illegible]

CURVE	α_c°	β°	M_0	(A_0/A_c) calc.
[illegible]	5°	2°	0.8	0.735

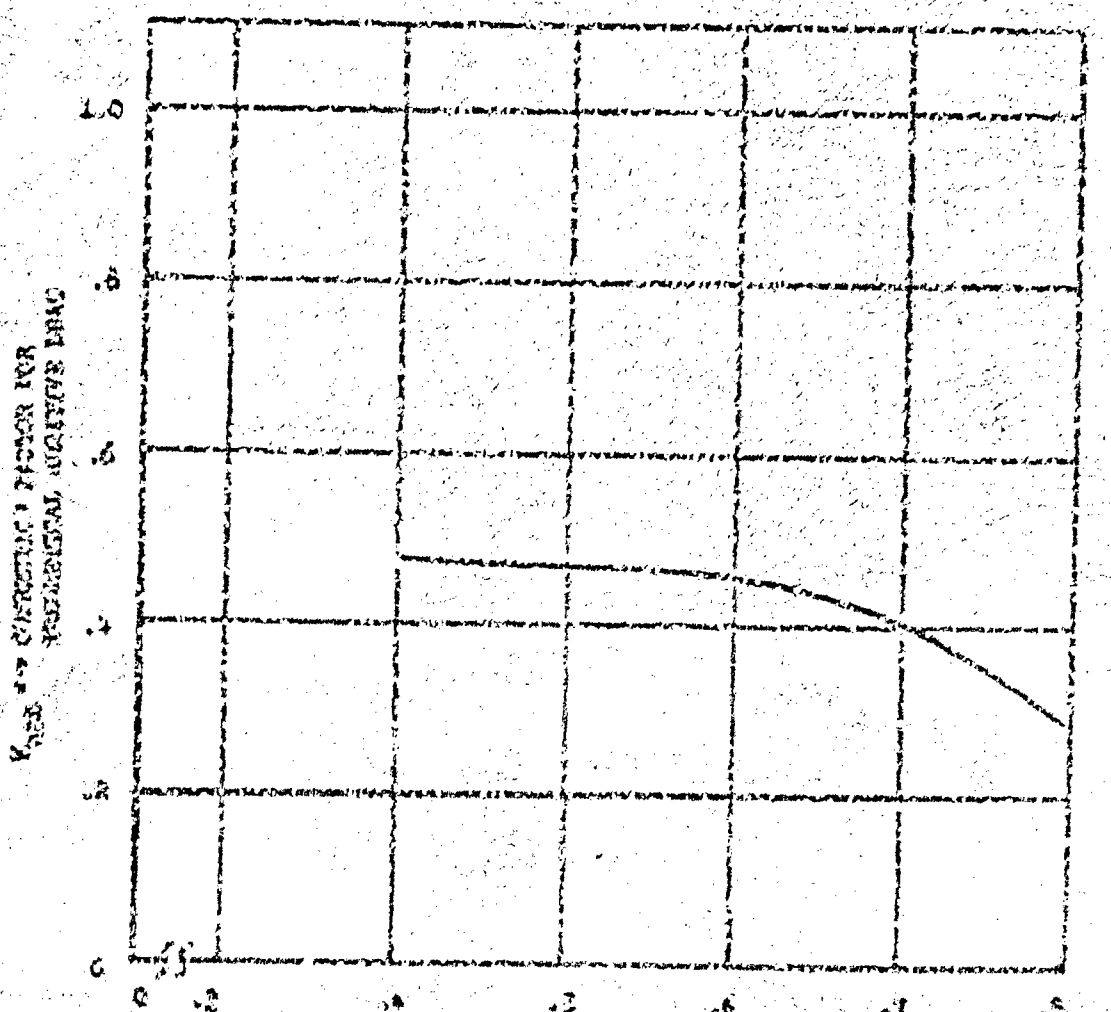

A_0/A_c = EFFECTIVE INLET AREA RATIO

FIGURE C1 - $K_{(A_0)}$ CORRECTION FACTOR, M_0 = 0.8

[illegible]	45°	2°	A_0	(c_0/A_c) ref.
RECTANGULAR	1	5°	0.365	0.736

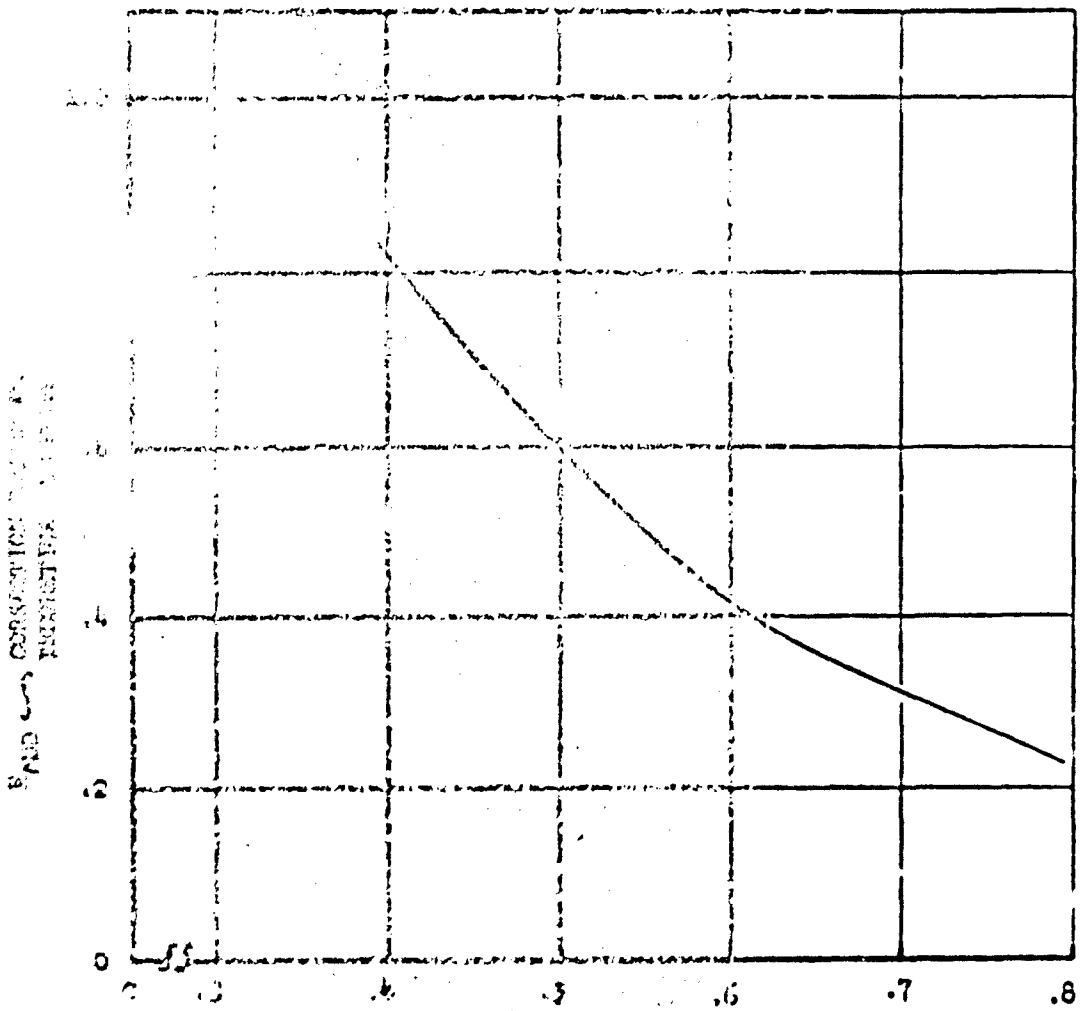

[illegible] FOR RECTANGULAR WING PLAN FORMS

[illegible] A_0 = 0.365

CONFIG.	α°	β°	M_o	(A_o/A_c) ref.
R2SP1C1	7°	7°	0.865	0.713

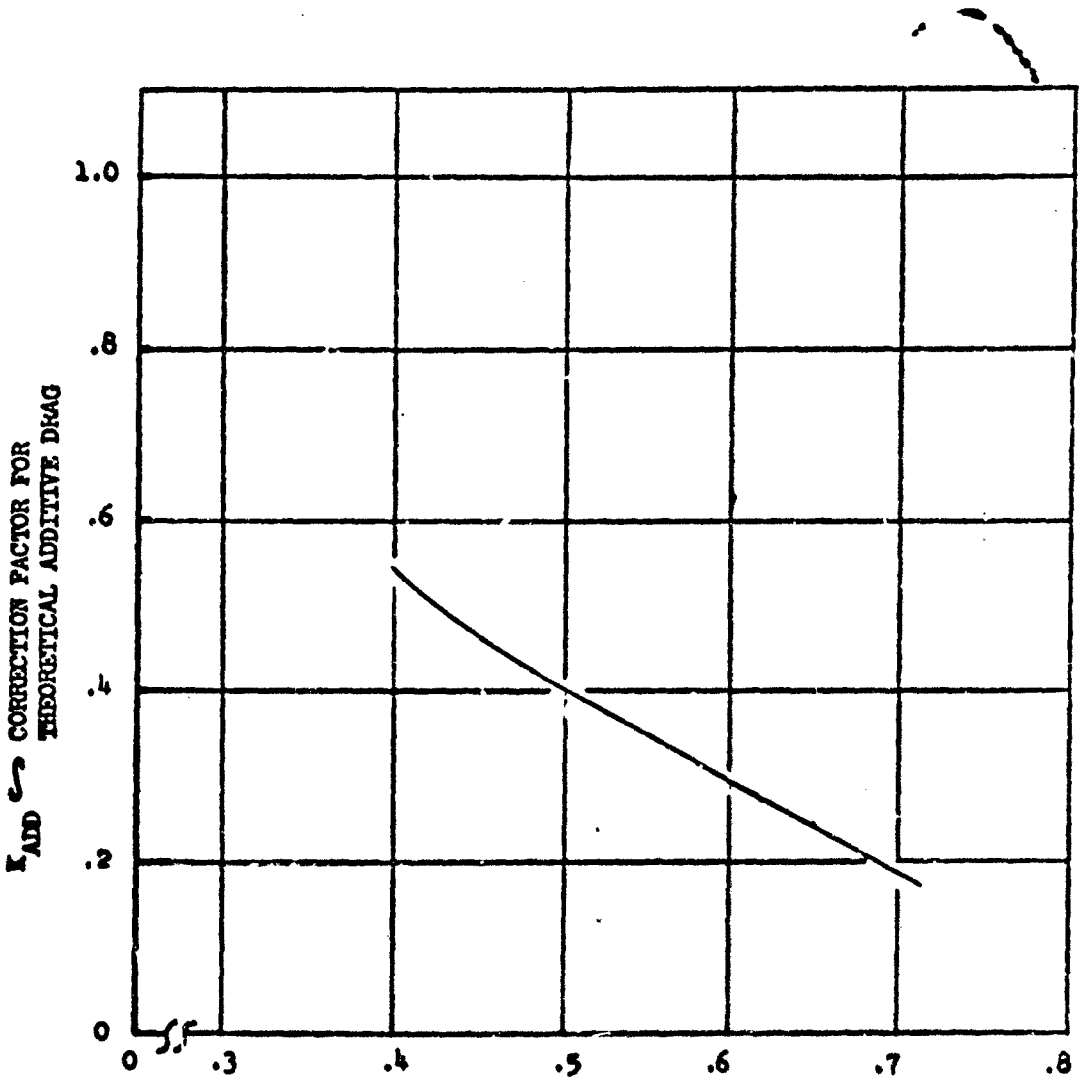

Figure 69. K_{ADD}, R2SP1C1, $M_o = 0.865$

CONFIG.	α°	β°	Mo	(A_0/A_c) ref.
R3SP1C1	12°	1.	0.865	0.50

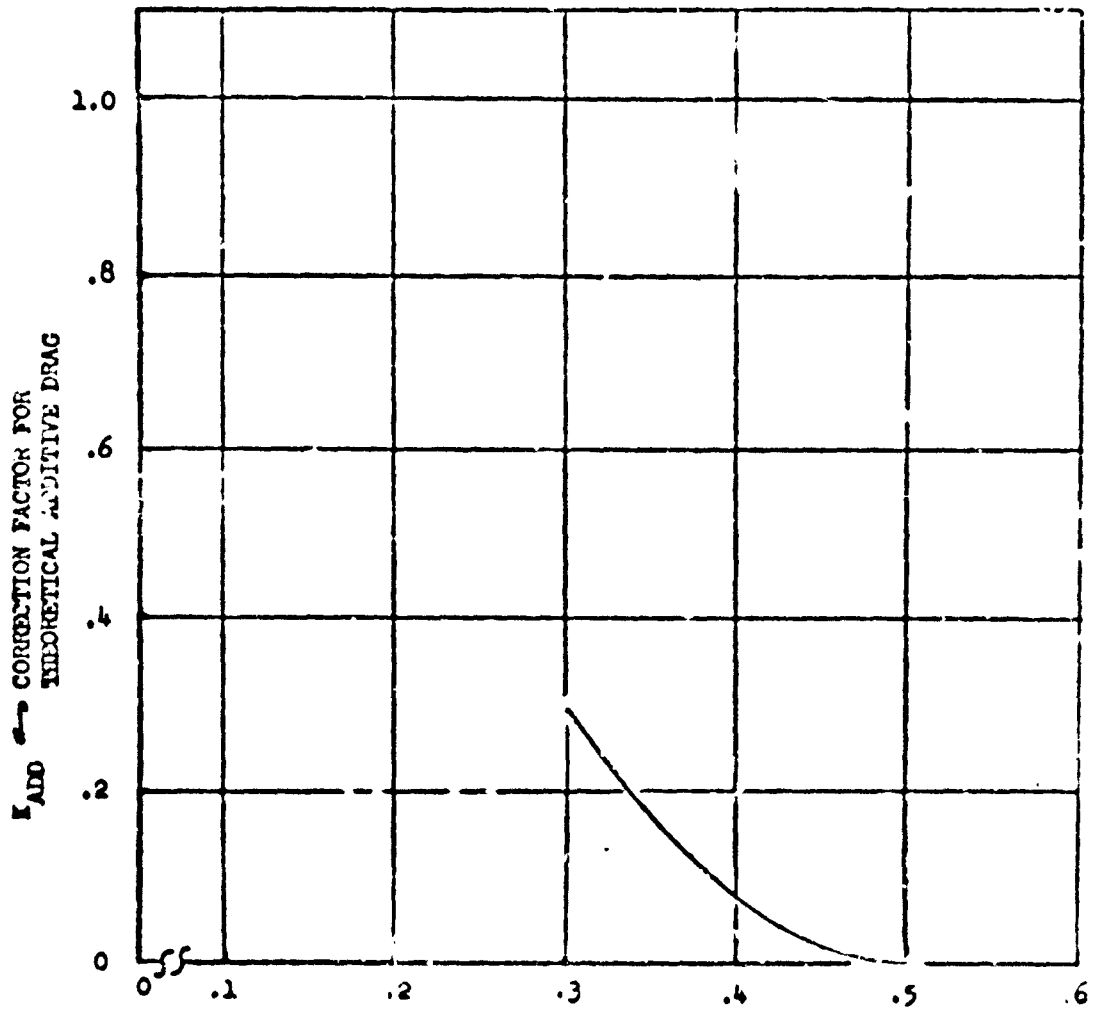

Figure 70. K_{ADD}, R3SP1C1, Mo = 0.865

CONFIG.	α°	β°	M_o	$(A_o/A_c)_{ref.}$
R4SP4C1	5°	5°	0.865	0.852
C6	"	"	"	"

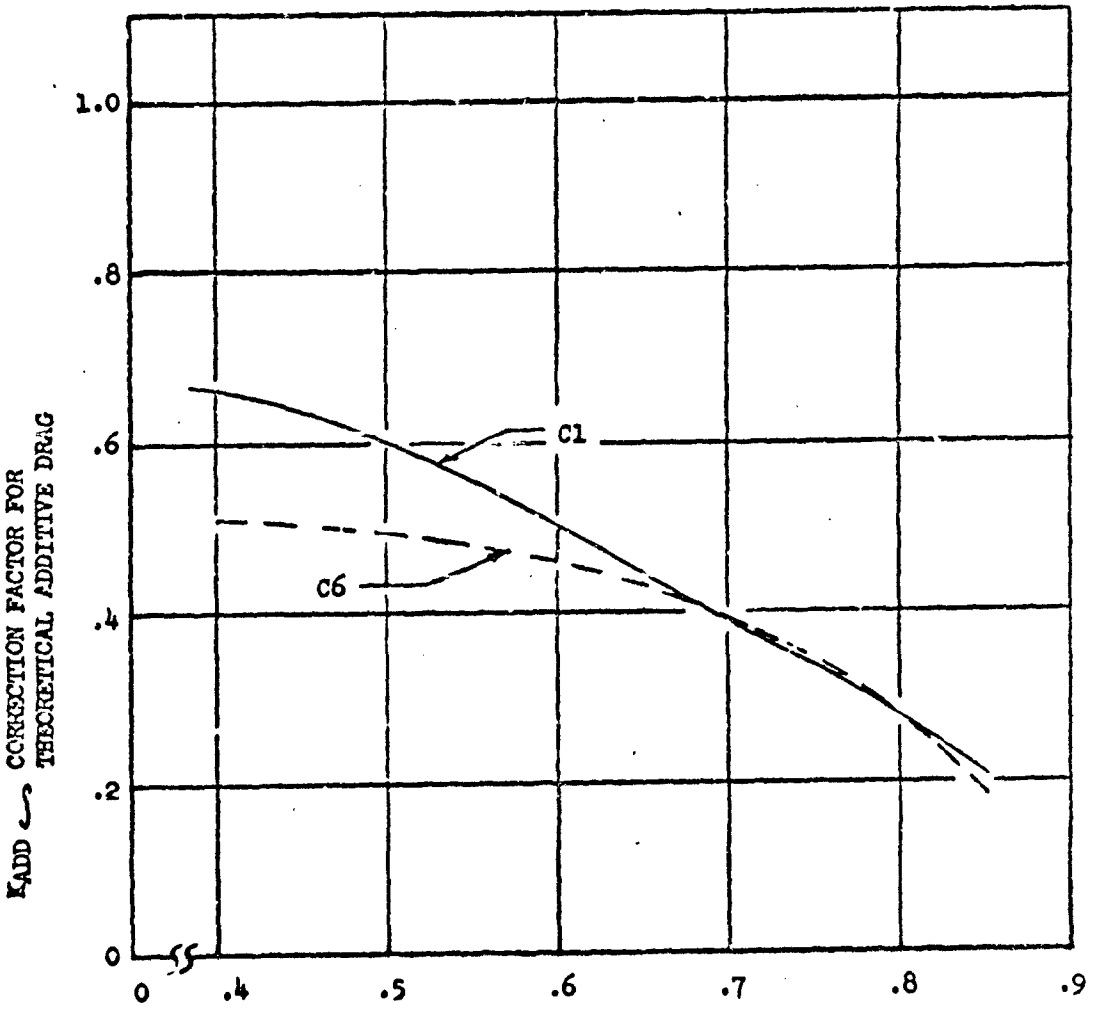

Figure 71. K_{ADD}, R4SP4C1, C6, M_o = 0.865

CONFIG.	$i°$	$\beta°$	M_0	(A_0/A_c) ref.
R4SP406	5°	0°	.865	0.774

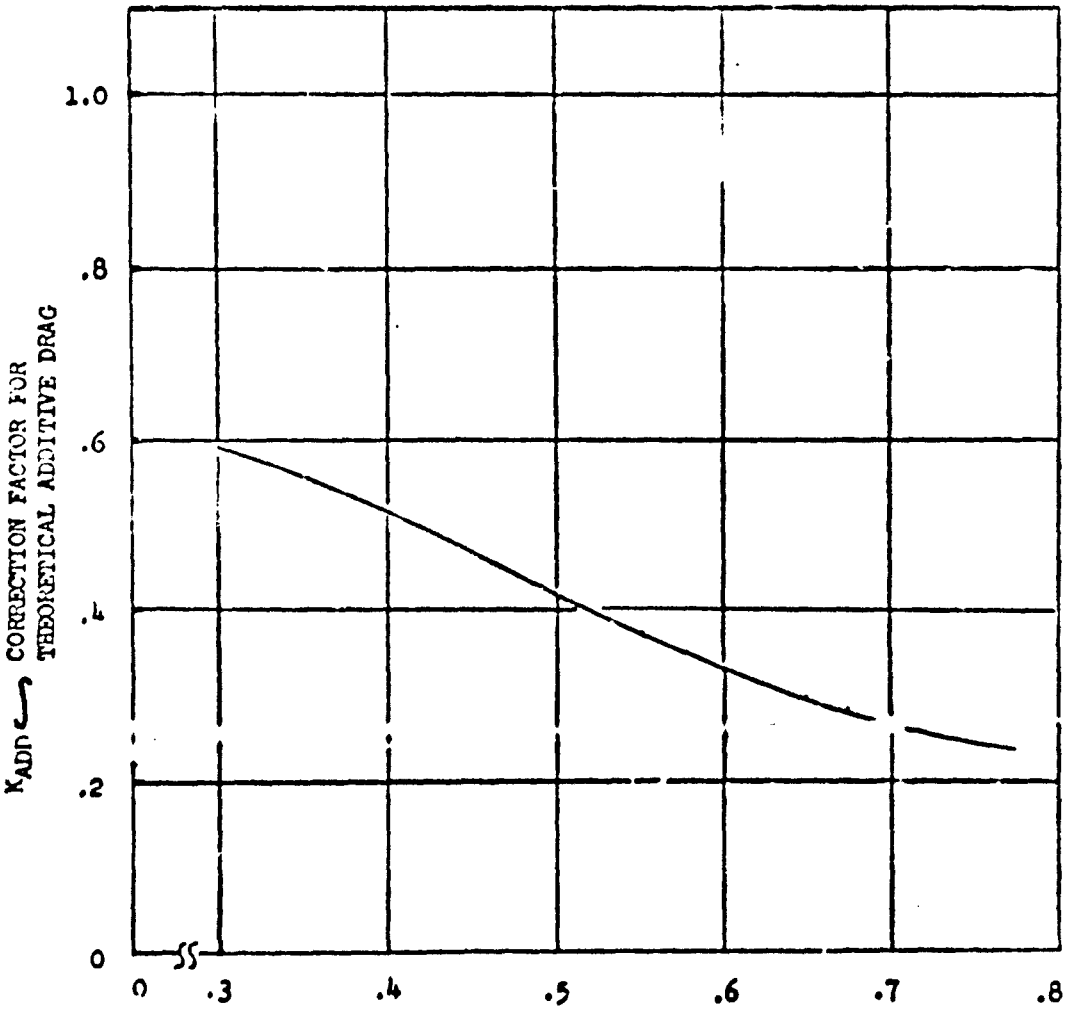

Figure 72. K_{ADD}, R4SP406, M_0 = 0.865

CONFIG.	α°	β°	M_o	$(A_o/A_c)_{ref.}$
R4SP4C1	5°	12°	0.865	0.712
C6	"	"	"	"

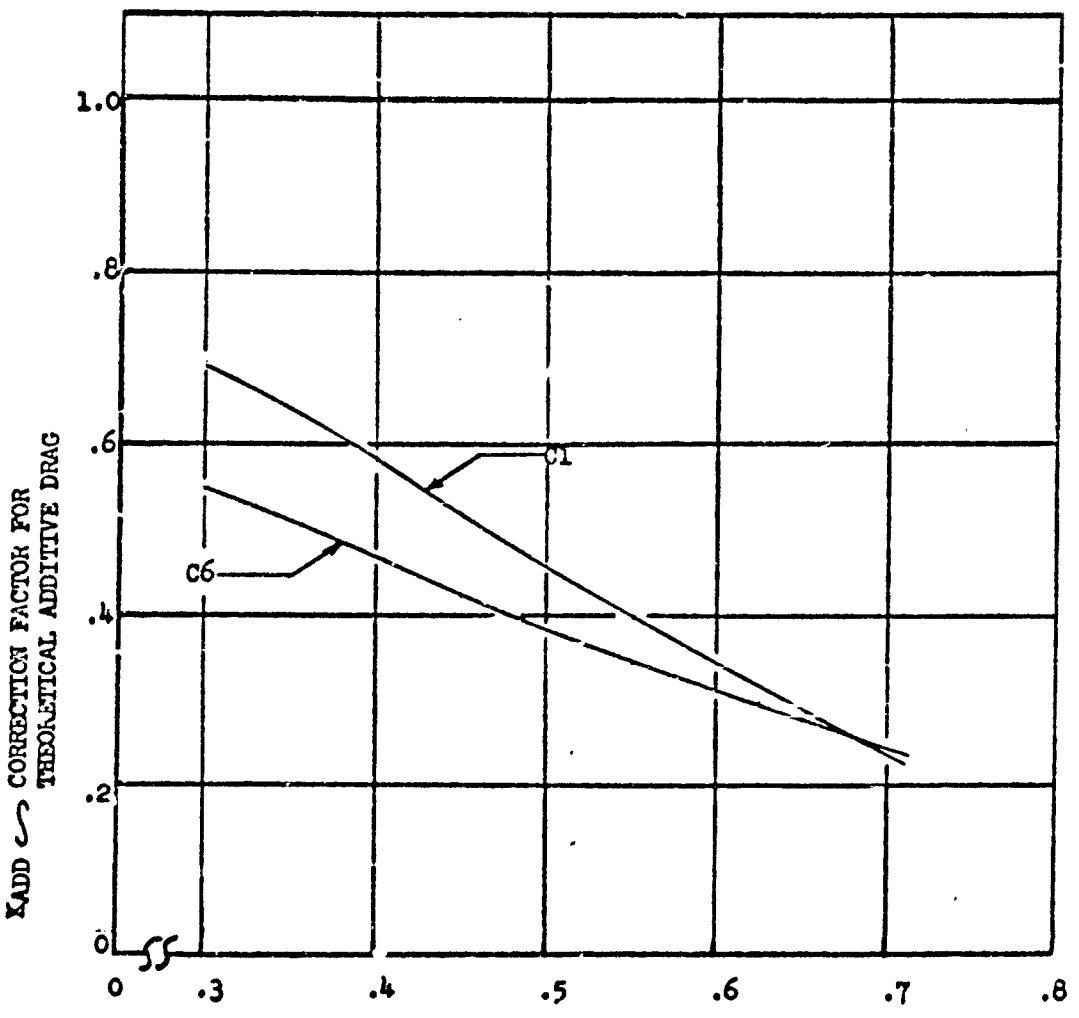

Figure 73. K_{ADD}, R4SP4C1, C6. Mo = 0.865

CONFIG.	α°	β°	M_c	$(A_c/A_c)_{ref.}$
R1SP1C1	0	0	1.09	0.796
C2	"	"	"	"
C3	"	"	"	"
C4	"	"	"	"
C5	"	"	"	"
C6	"	"	"	"

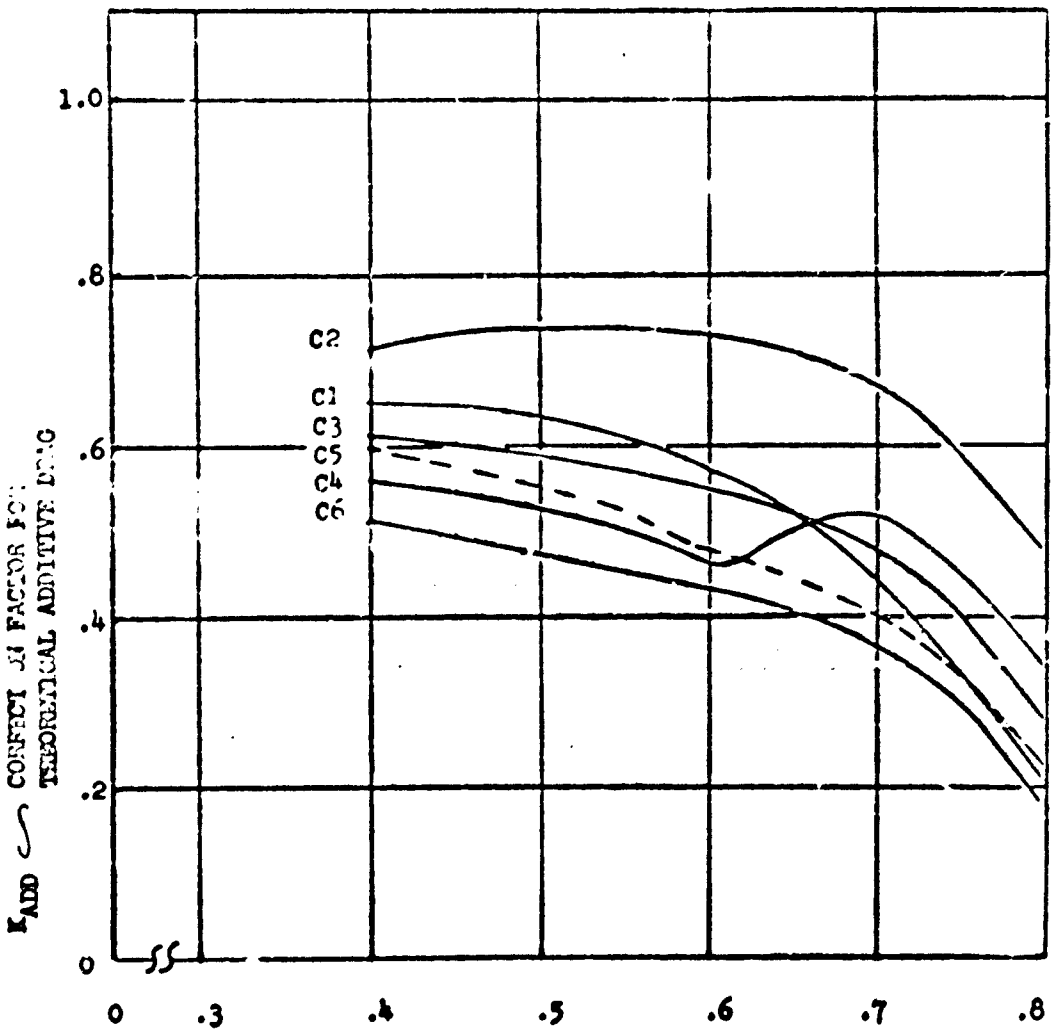

Figure 74. K_{ADD}, R1SP1C1-C6, M_o = 1.09

CONFIG.	α°	β°	M_0	(A_0/A_c) ref.
R1SP1C1	5°	9°	1.09	0.715

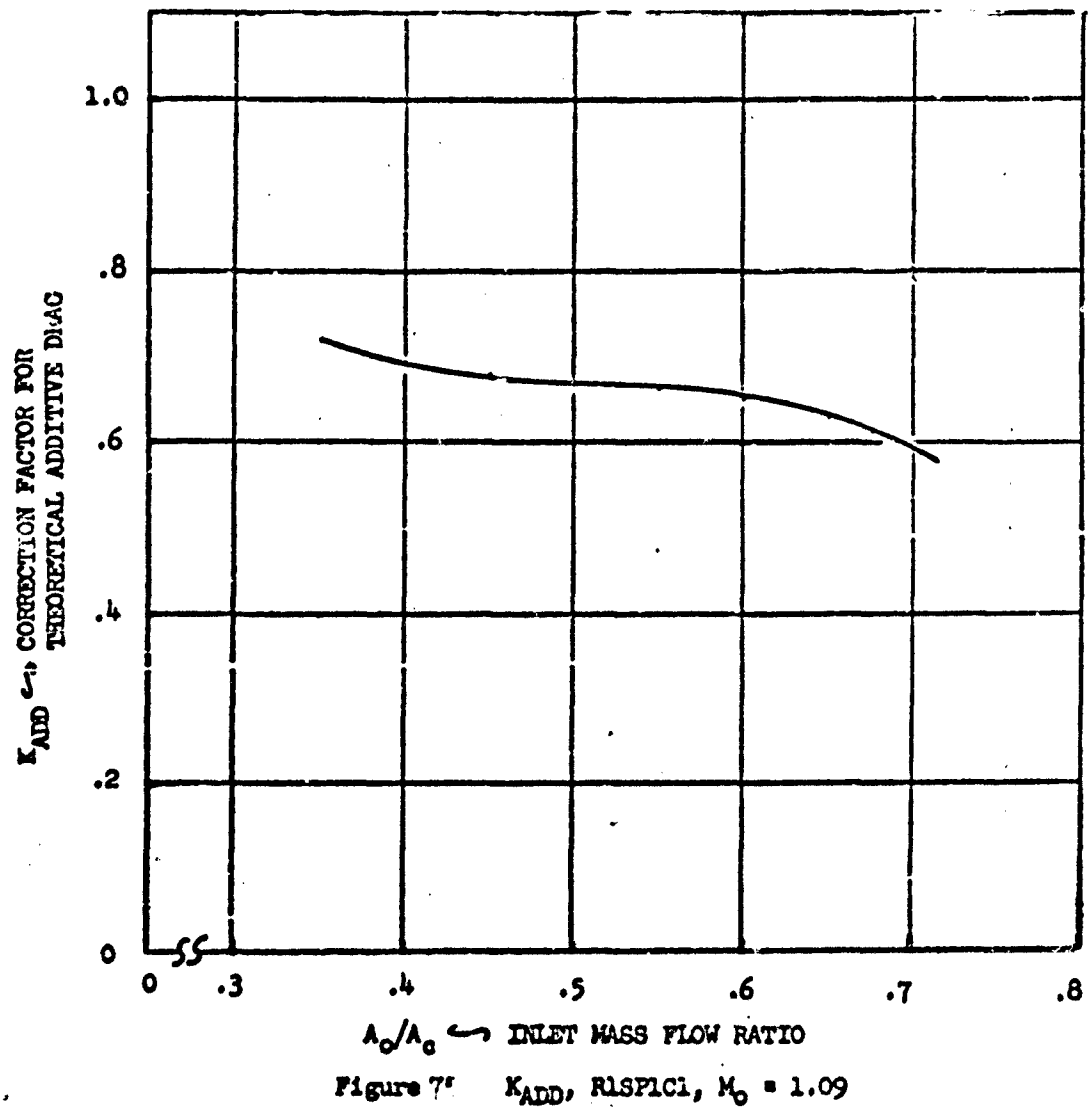

Figure 7. K_{ADD}, R1SP1C1, M_0 = 1.09

	α°	β°	M_0	(A_0/A_c) ref.
R1SP1C1	5°	12°	1.09	0.715

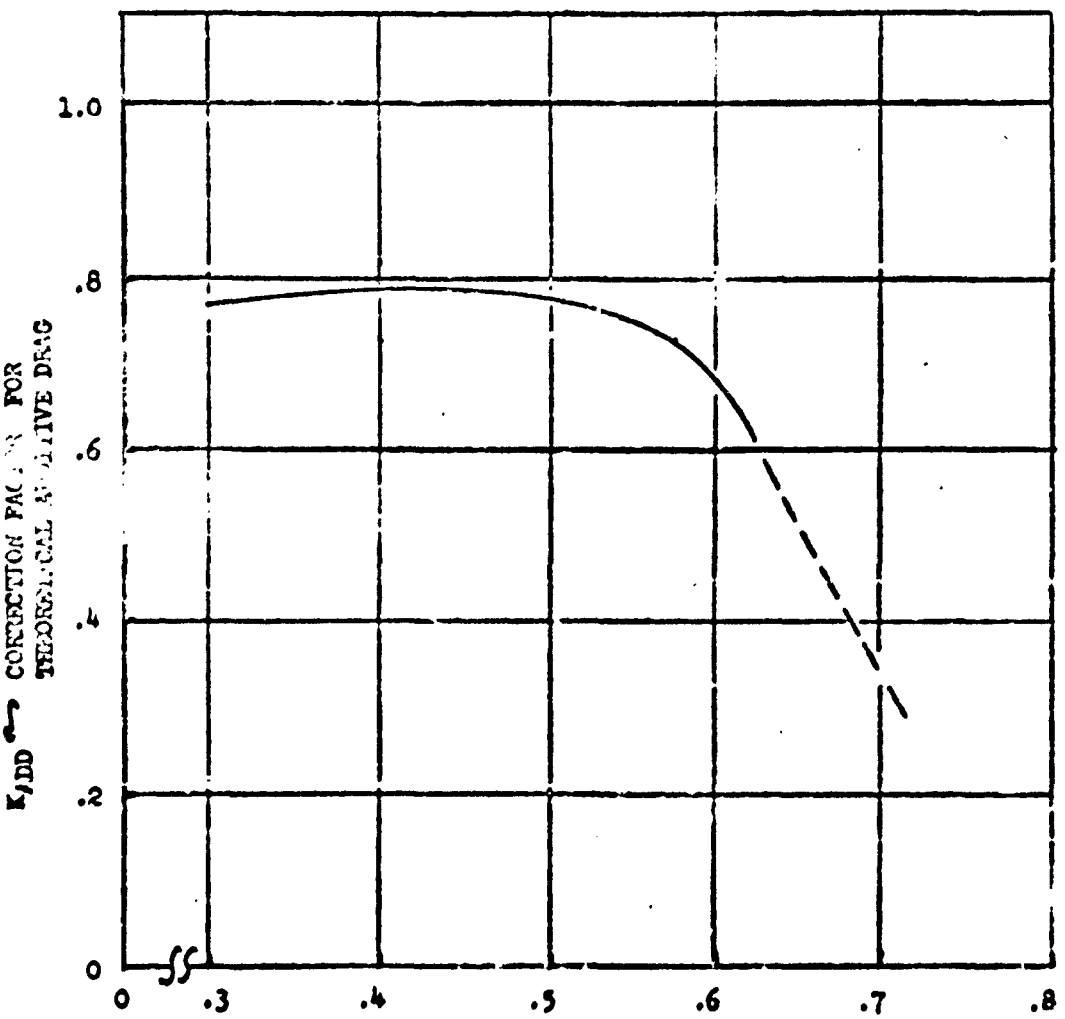

Figure 76. K_{1DD}, R1SP1C1, M_0 = 1.09

CONFIG.	$\alpha°$	$\beta°$	M_o	(A_o/A_c) ref.
R1SP2C1	5°	5°	1.09	0.796

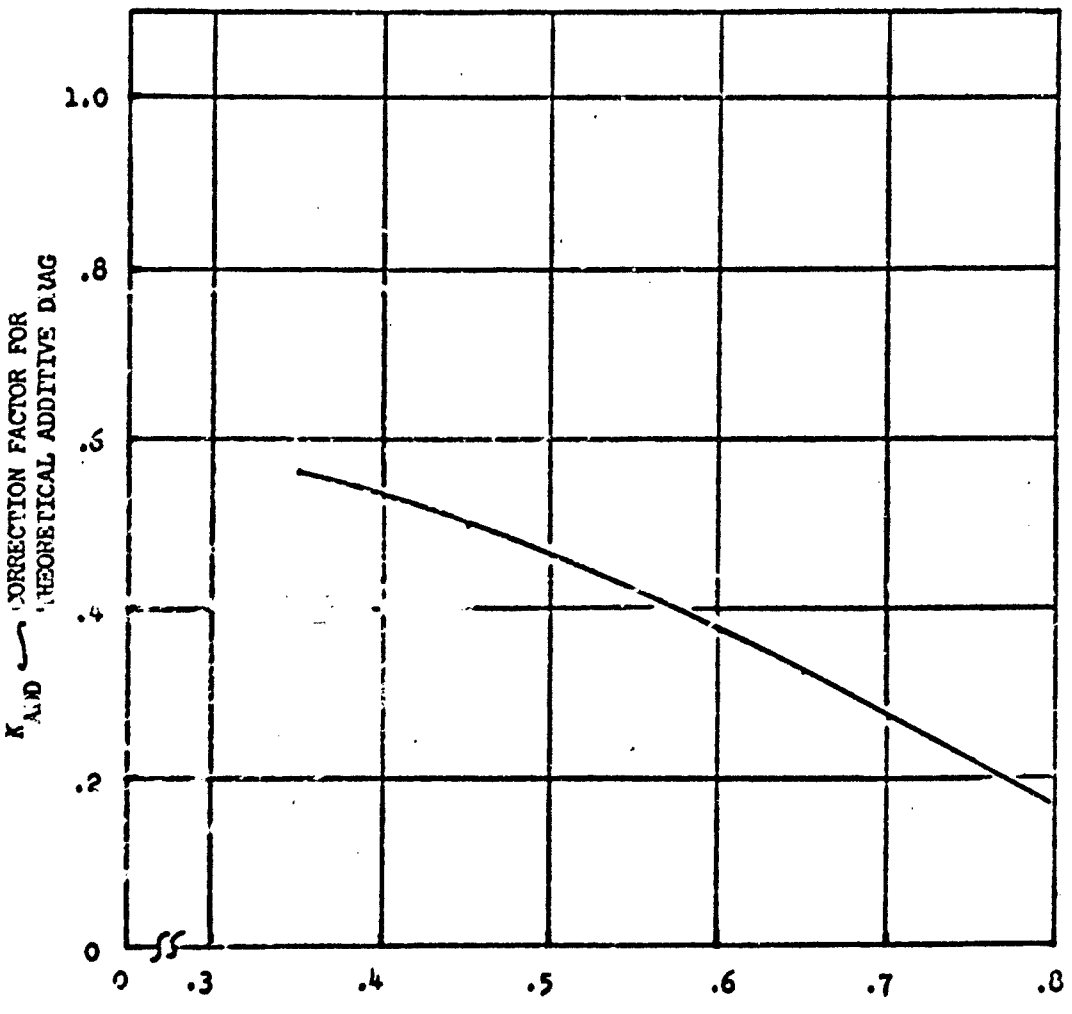

Figure 77. K_{ADD}, R1SP2C1, M_o = 1.09

CONFIG.	γ°	β°	M_0	(A_c/A_c) ref.
R1SP3C1	5°		1.11	0.796

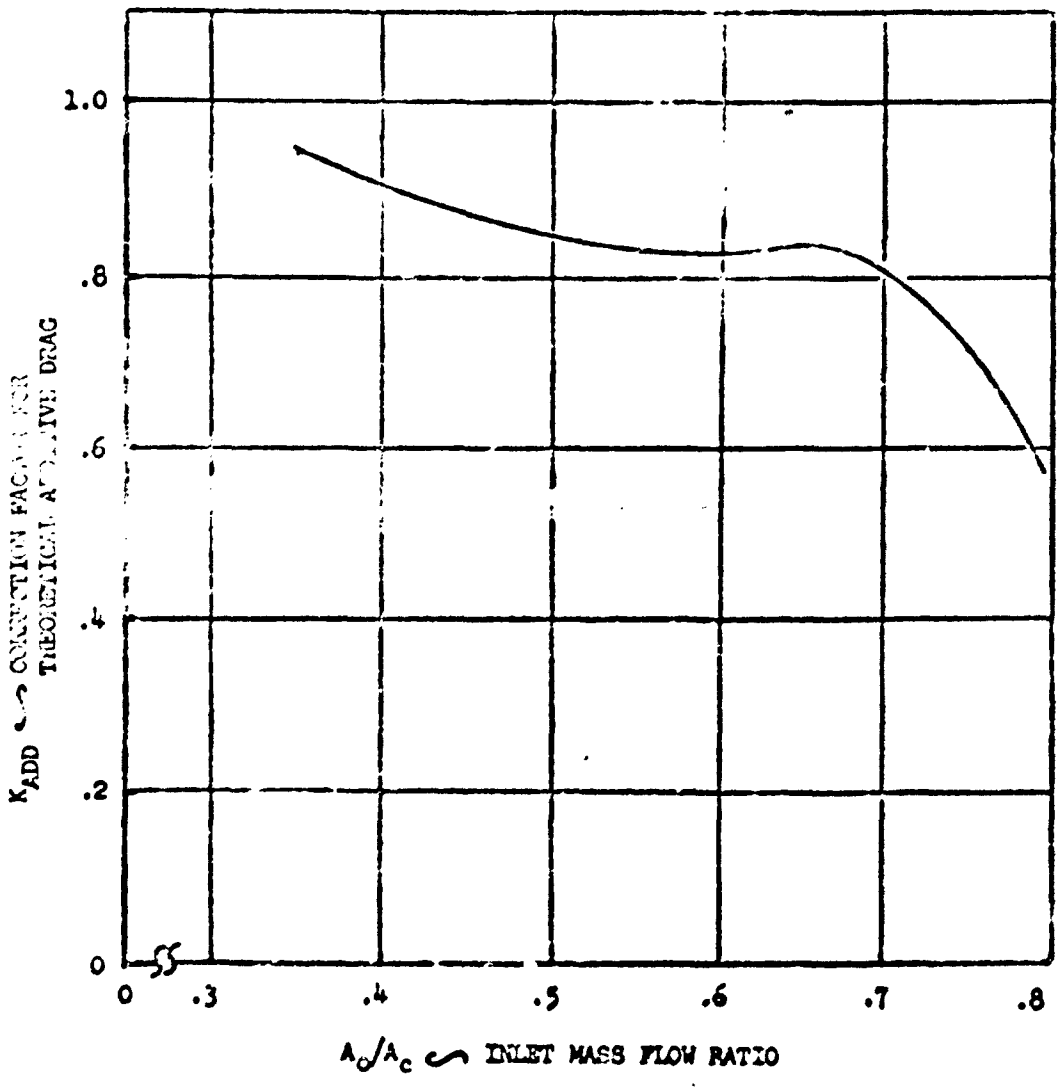

Figure 78. K_{ADD}, R1SP3C1, M_0 = 1.11

CONFIG.	α°	β°	M_0	(A_0/A_c) ref.
R3SP1C1	12°	12°	1.11	0.50

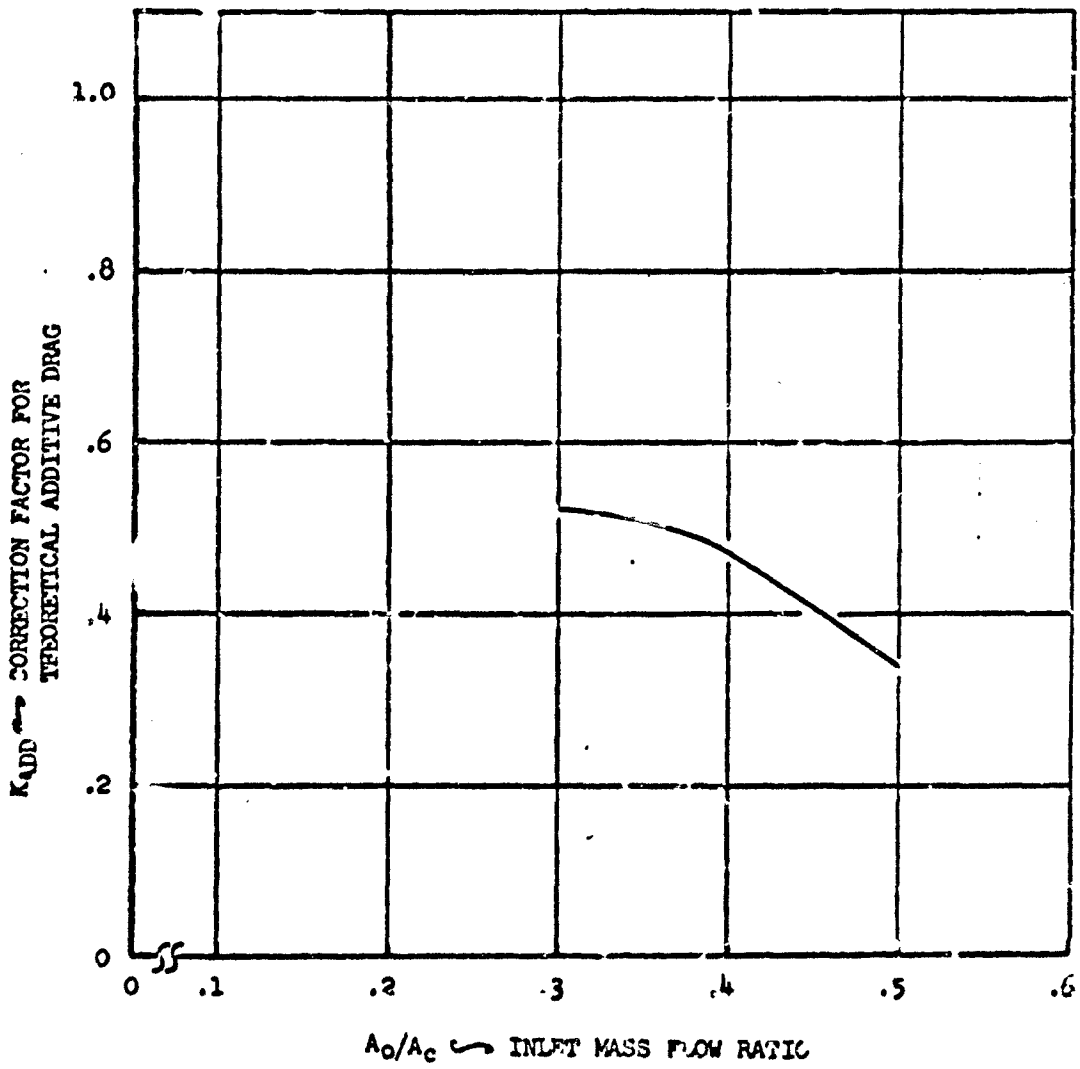

Figure 79. K_{ADD}, R3SP1C1, M_0 = 1.11

CONFIG.	$\alpha°$	$\beta°$	M_o	$(A_o/A_m)_{ref.}$
R4SP4C1	5°	0°	1.11	0.8
C4	"	"	"	"
C6	"	"	"	"

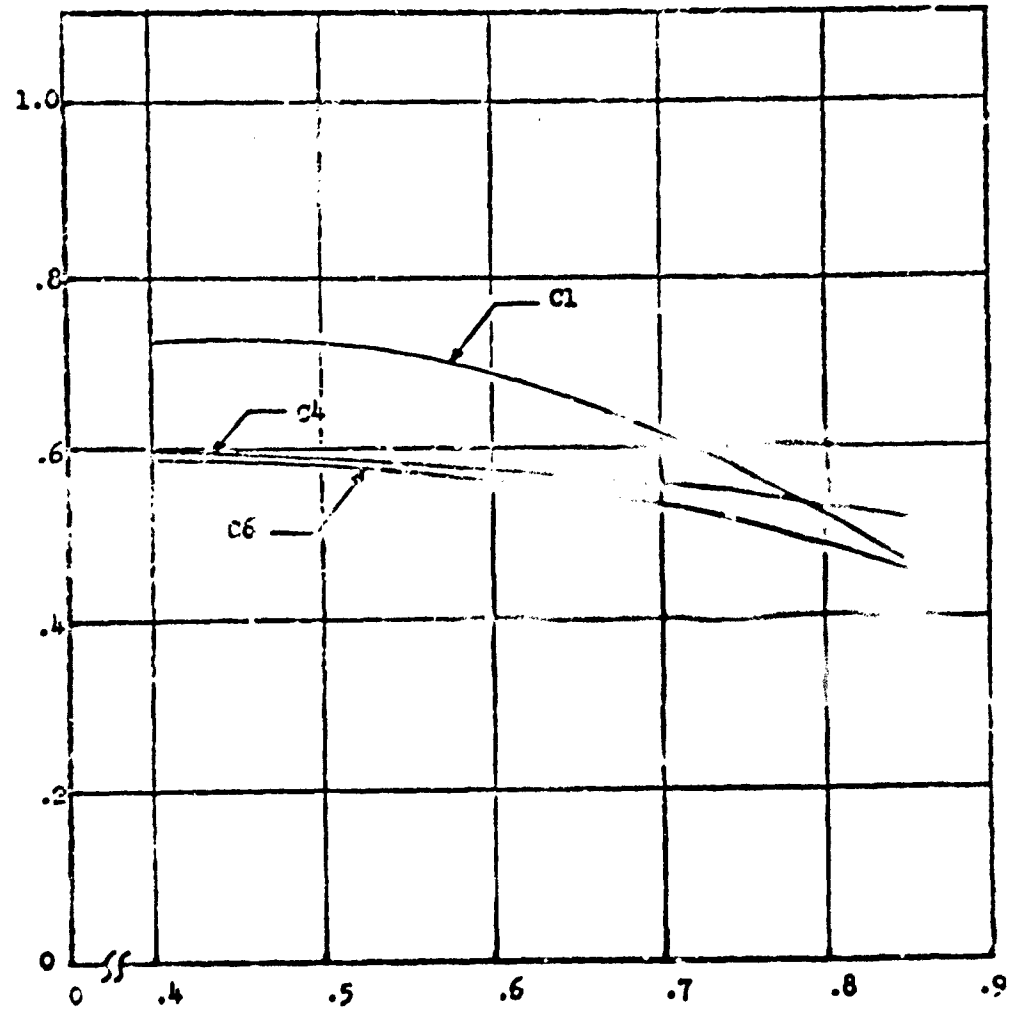

A_o/A_c → INLET MASS FLOW RATIO

Figure 80. KADD, R4SP4C1, C4, C6, M_o = 1.11

CONFIG.	$\alpha°$	$\beta°$	M_o	(A_o/A_c) ref.
R4SP4C6	5°	9°	1.11	.774

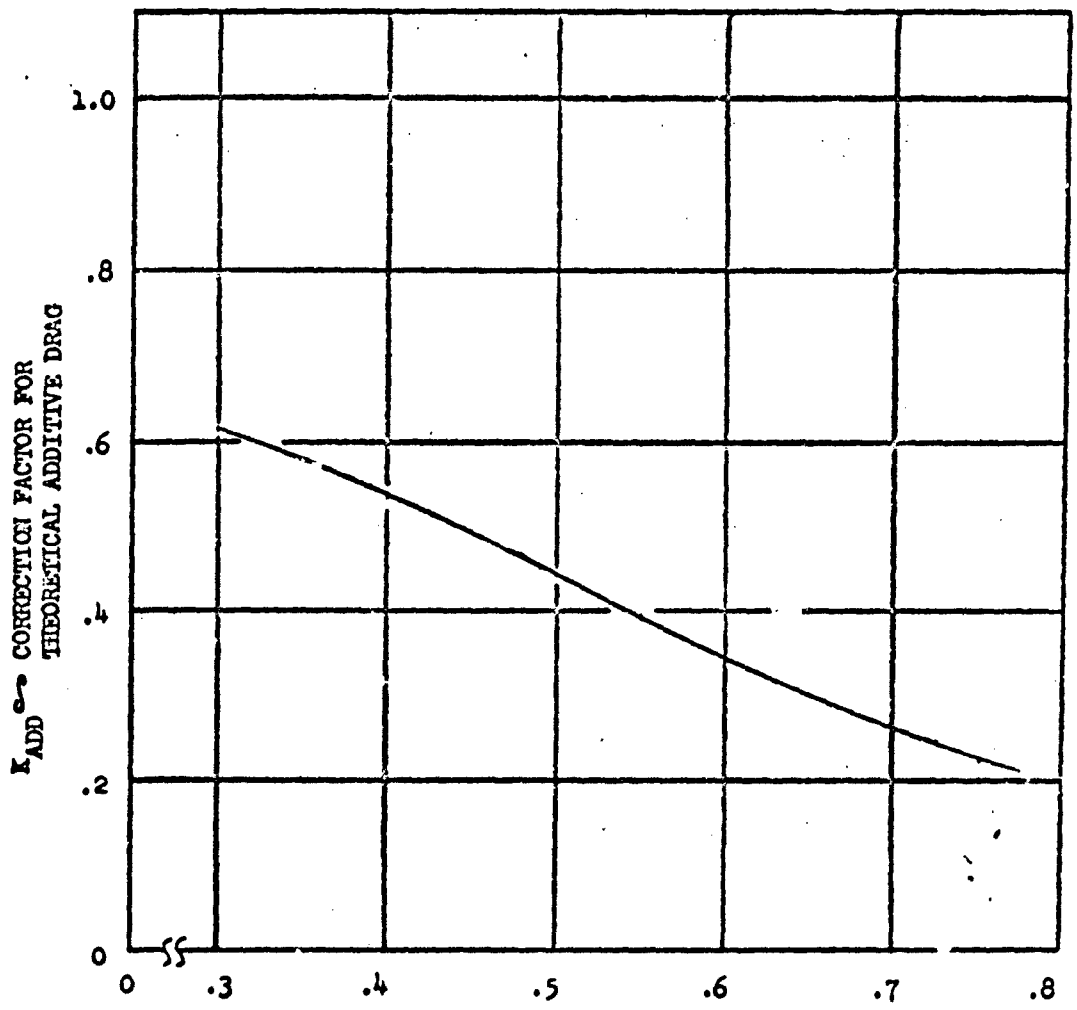

Figure 81 K_{ADD}, R4SP4C6, M_o = 1.11

CONFIG.	$\alpha°$	$\beta°$	M_0	$(A_0/A_c)_{ref.}$
R4SP4C1	3°	12°	1.11	0.712
C6	"	"	"	"

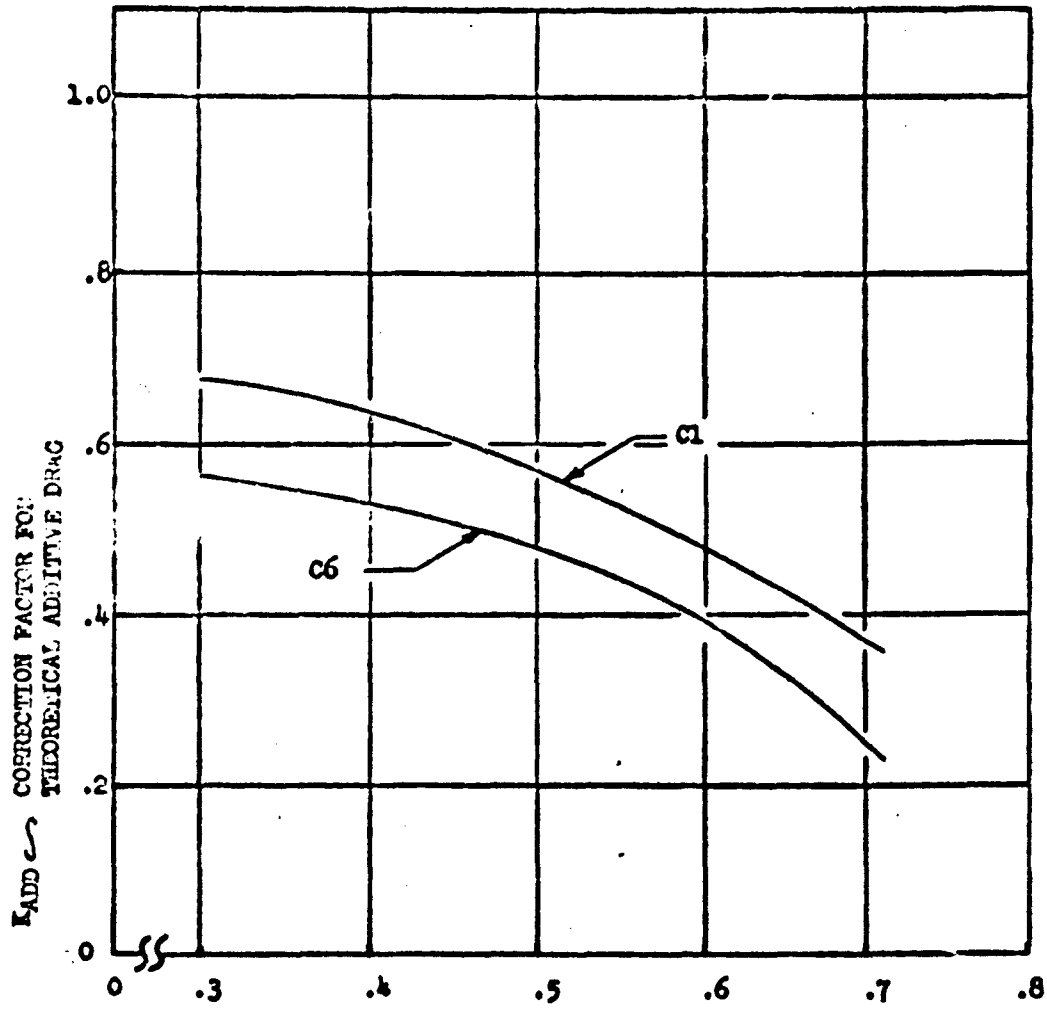

Figure 82. K_{ADL}, R4SP4C1, C4, M_0 = 1.11

CONFIG.	γ°	β°	M_0	$(A_0/A_c)_{ref.}$
R1SP1C1	5°	5°	1.29	0.780
C2	"	"	"	"
C3	"	"	"	"
C4	"	"	"	"
C5	"	"	"	"
C6	"	"	"	"

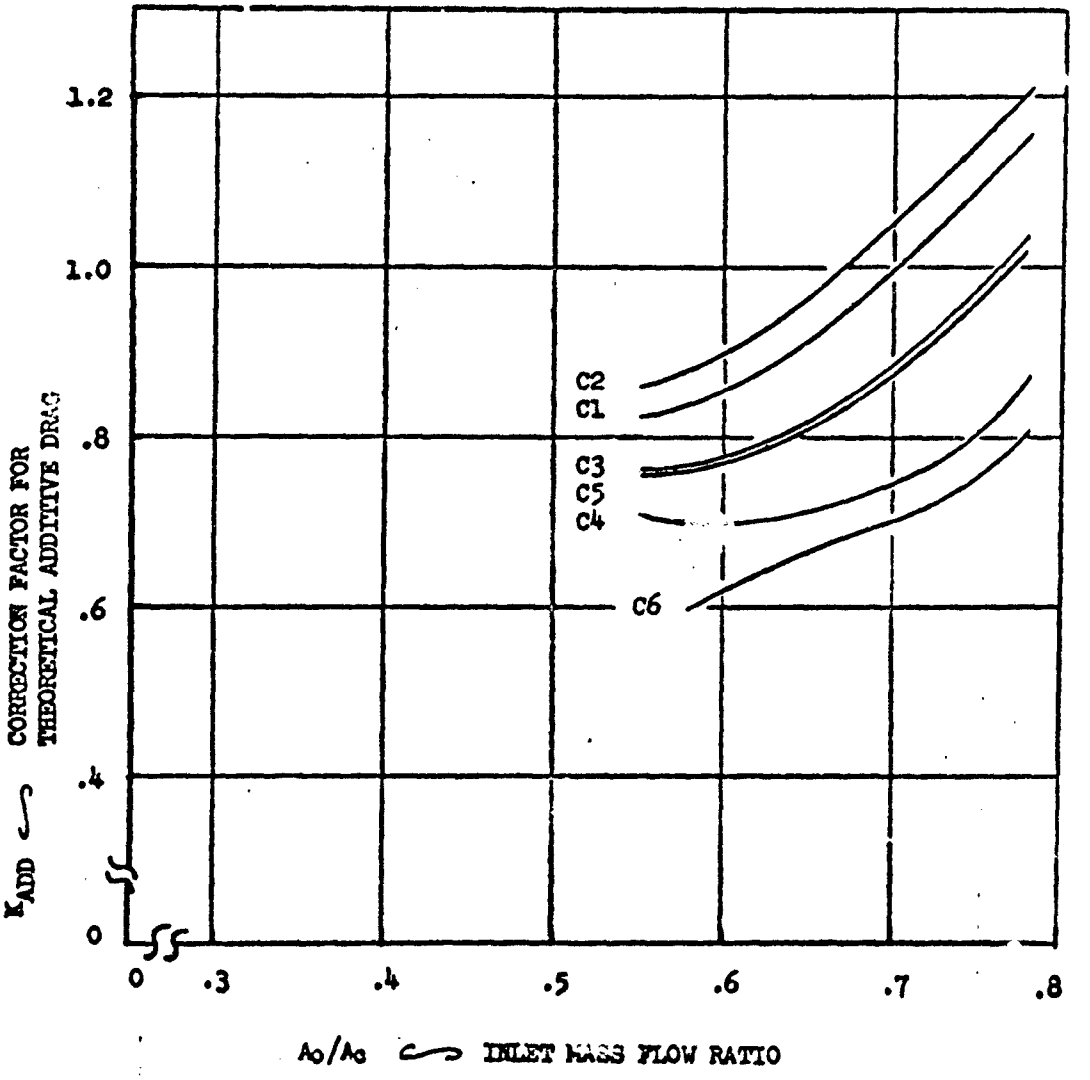

Figure 83. K_{ADD}, R1SP1C1-C6, M_0 = 1.29

CONFIG.	$\alpha°$	$\beta°$	M_0	(A_0/A_c) ref.
R1SP2C1	2°	5°	1.29	0.75

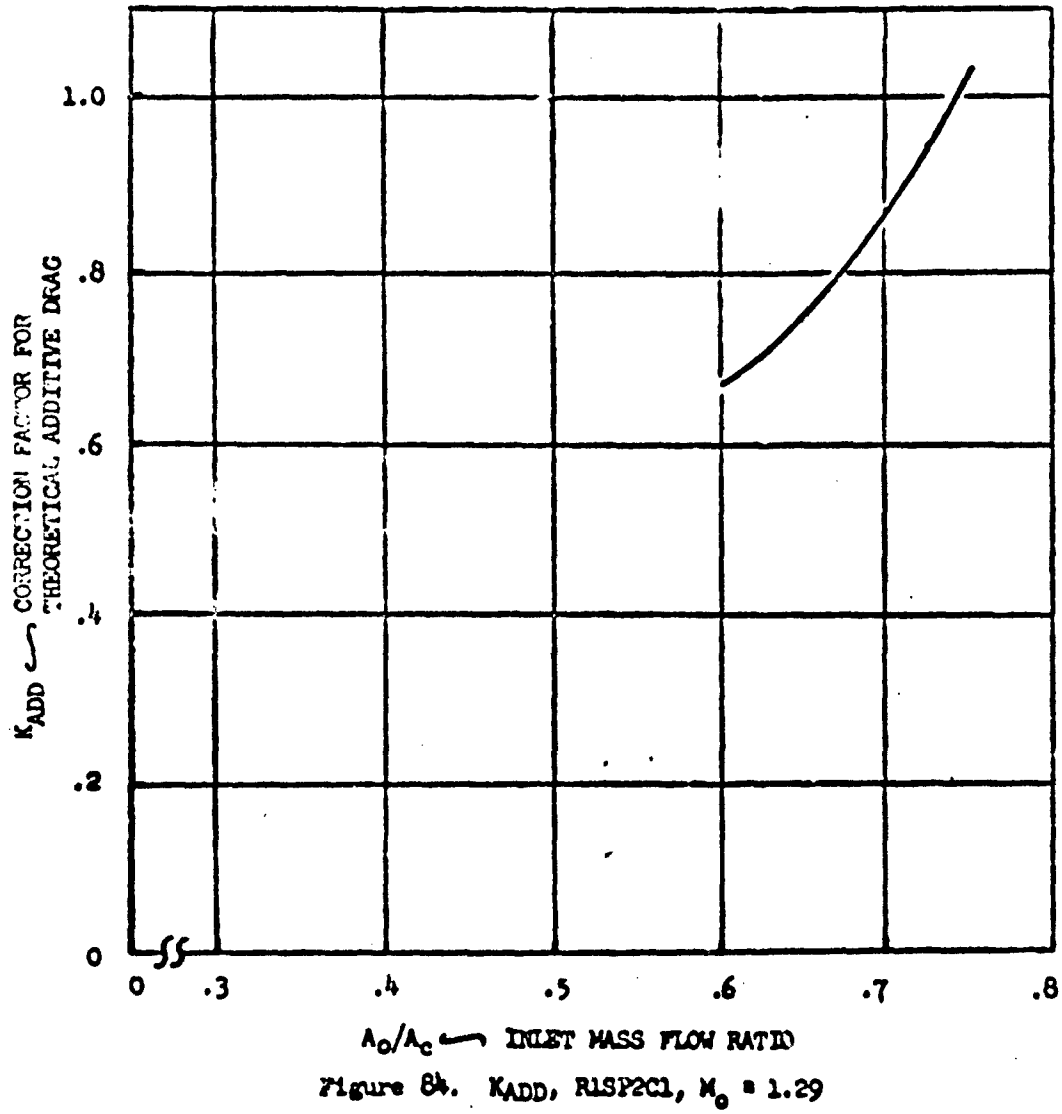

Figure 84. K_{ADD}, R1SP2C1, $M_0 = 1.29$

CONFIG.	α°	β°	M_0	(A_0/A_c) ref.
R1SP3C1	5°	5°	1.31	0.842

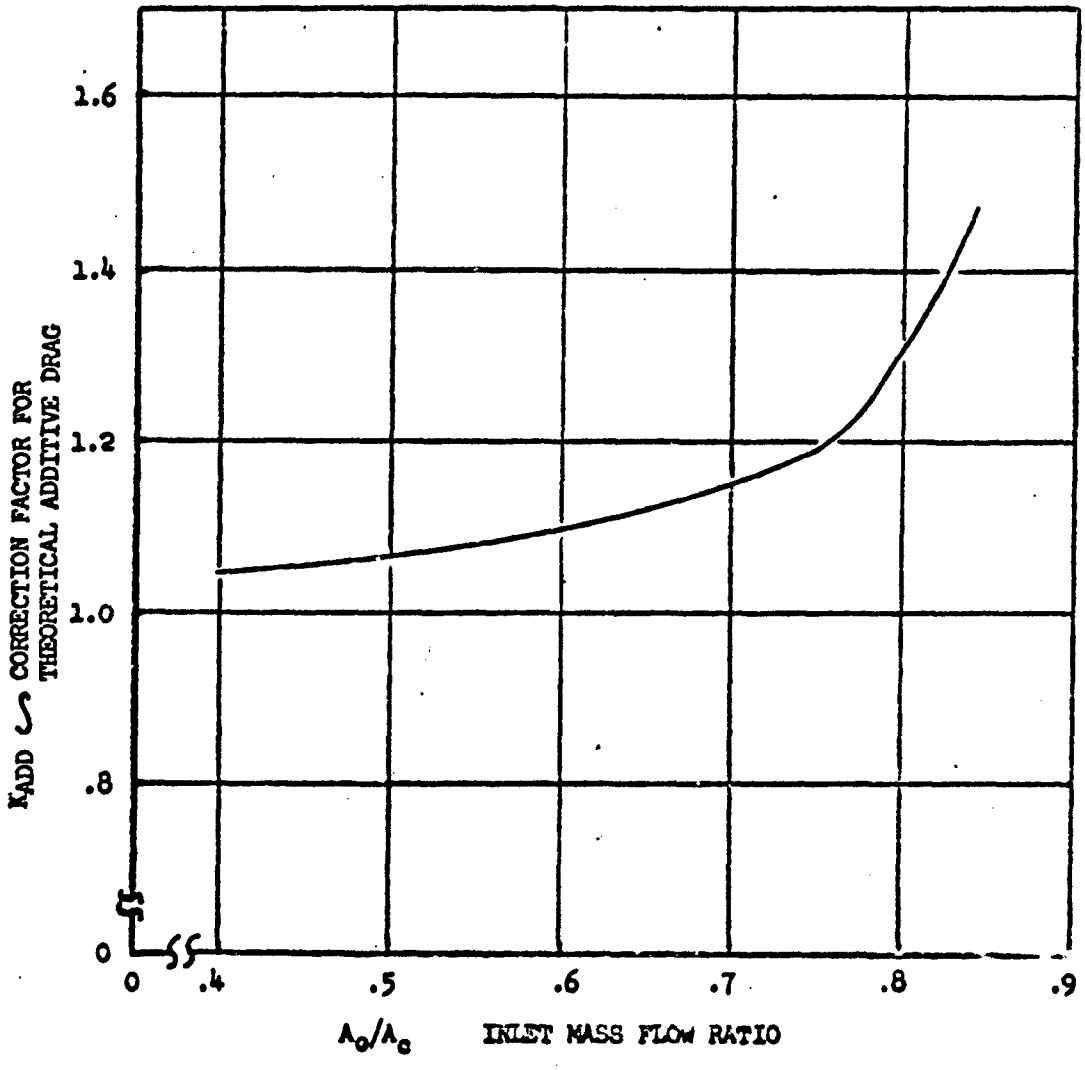

Figure 85. K_{ADD}, R1SP3C1, M_0 = 1.31

CONFIG.	α°	β°	M_o	(A_o/A_c) ref.
R2SP1C1	7°	7°	1.31	0.752

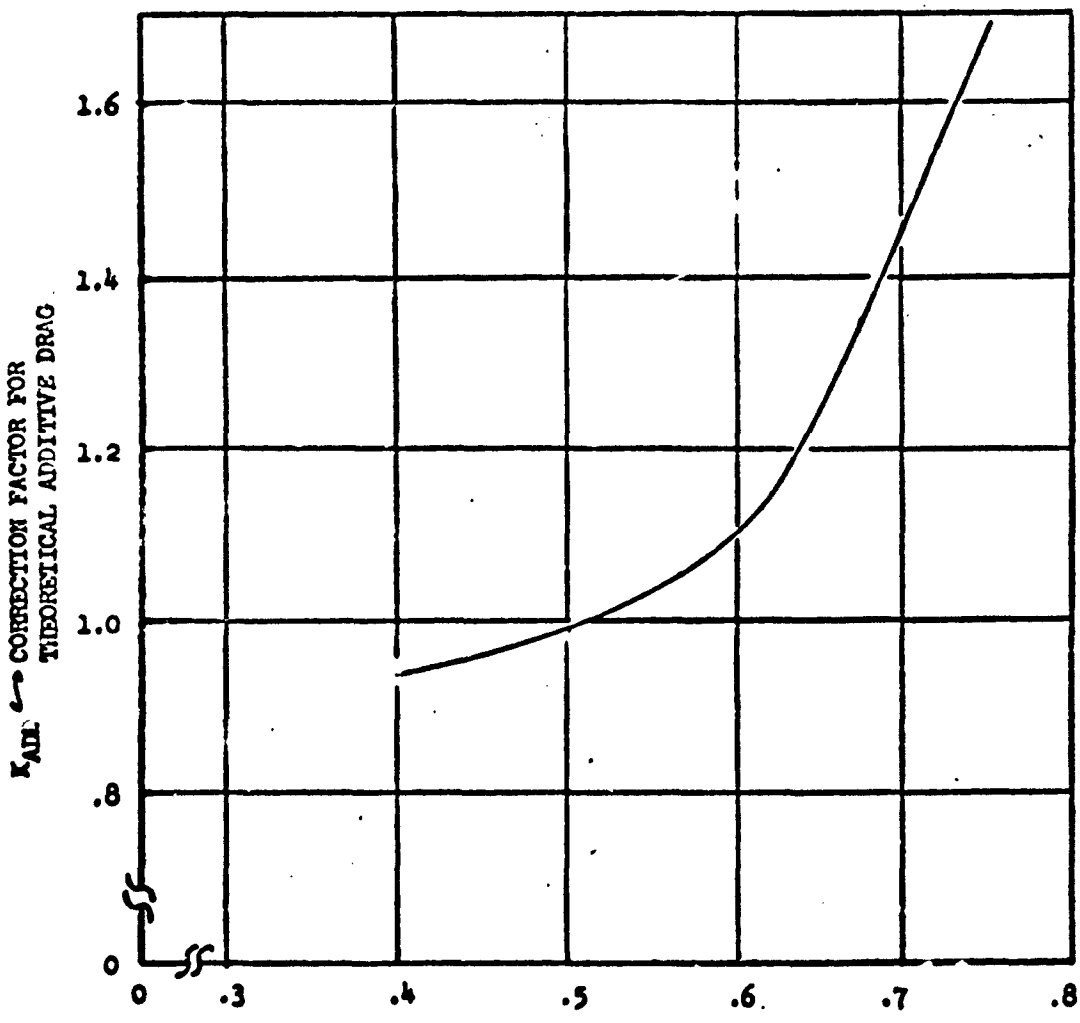

Figure 86. K_{ADD}, R2SP1C1, M_o = 1.31

CONFIG.	$\alpha°$	β	Mo	(A_o/A_c) ref.
R3SP1C1	12°	12°	1.31	0.50

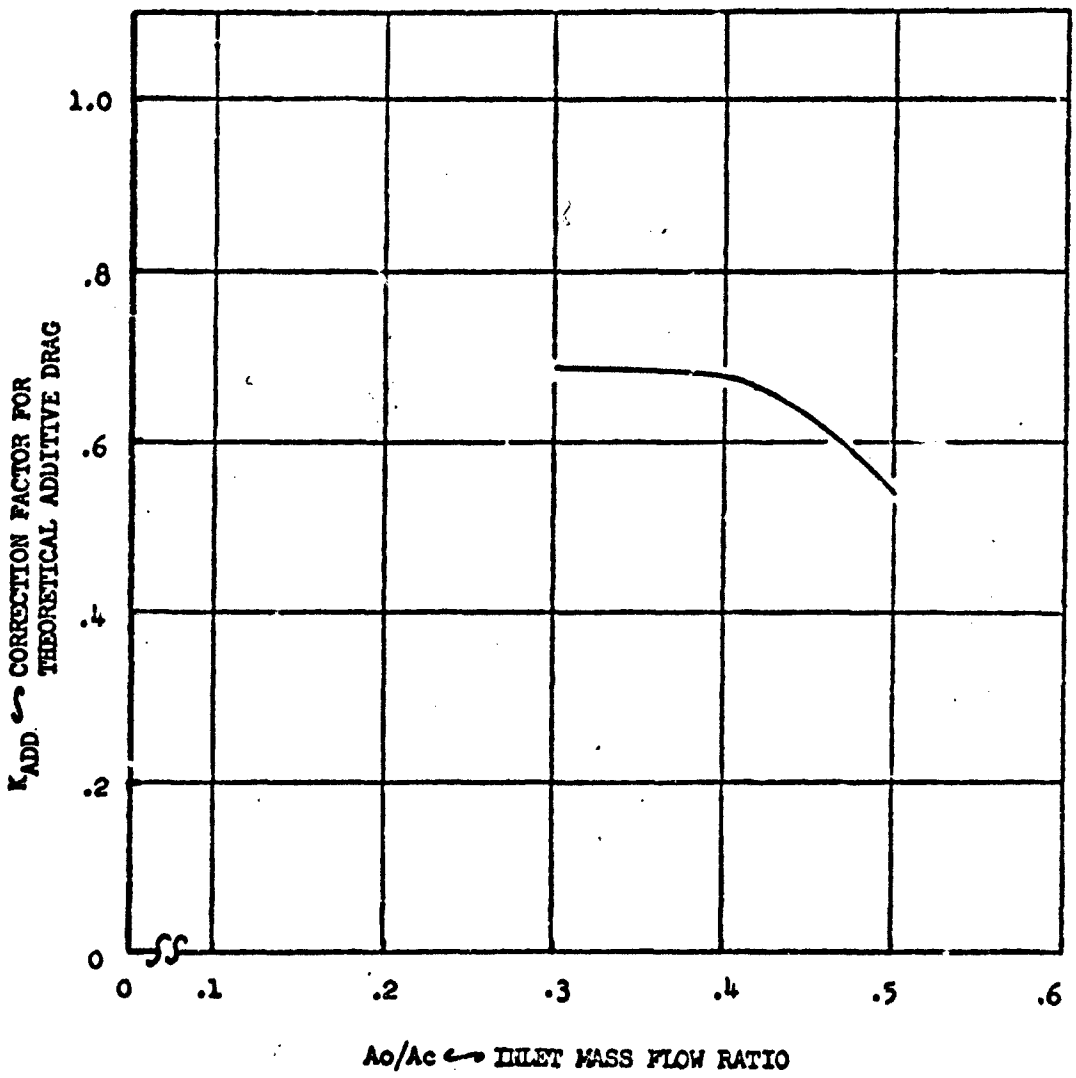

Figure 87. K_{ADD}, R3SP1C1, Mo = 1.31

CONFIG.	α°	β°	M_o	$(A_o/A_c)_{ref.}$
R4SP4C1	5°	5°	1.31	0.864
C4	"	"	"	"
C6	"	"	"	"

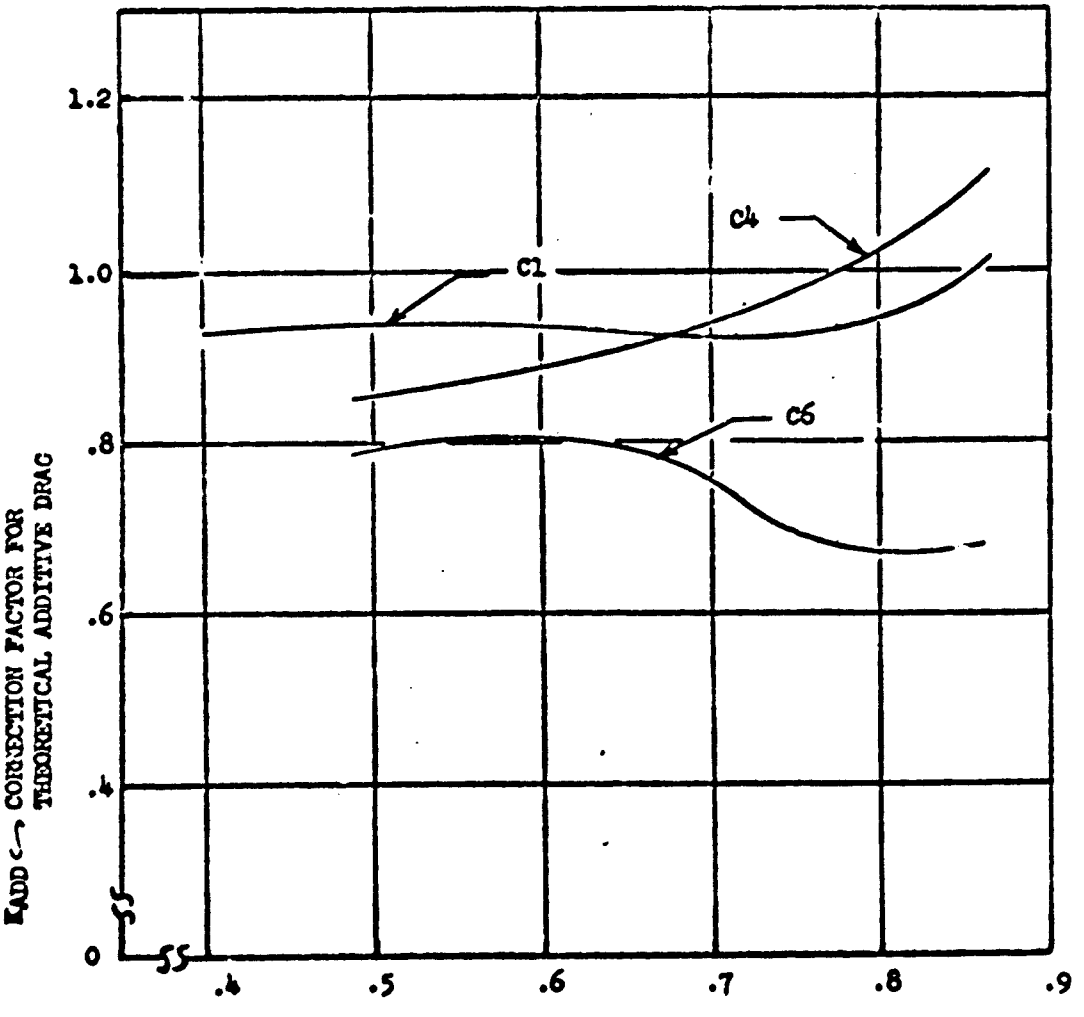

Figure 88. K_{ADD}, R4SP4C1, C4, C6, M_o = 1.31

CONFIG.	α°	β°	M_o	$(A_o/A_c)_{ref.}$
R1SP1C1	5	5	1.39	0.799
C2	"	"	"	"
C3	"	"	"	"
C4	"	"	"	"
C5	"	"	"	"
C6	"	"	"	"

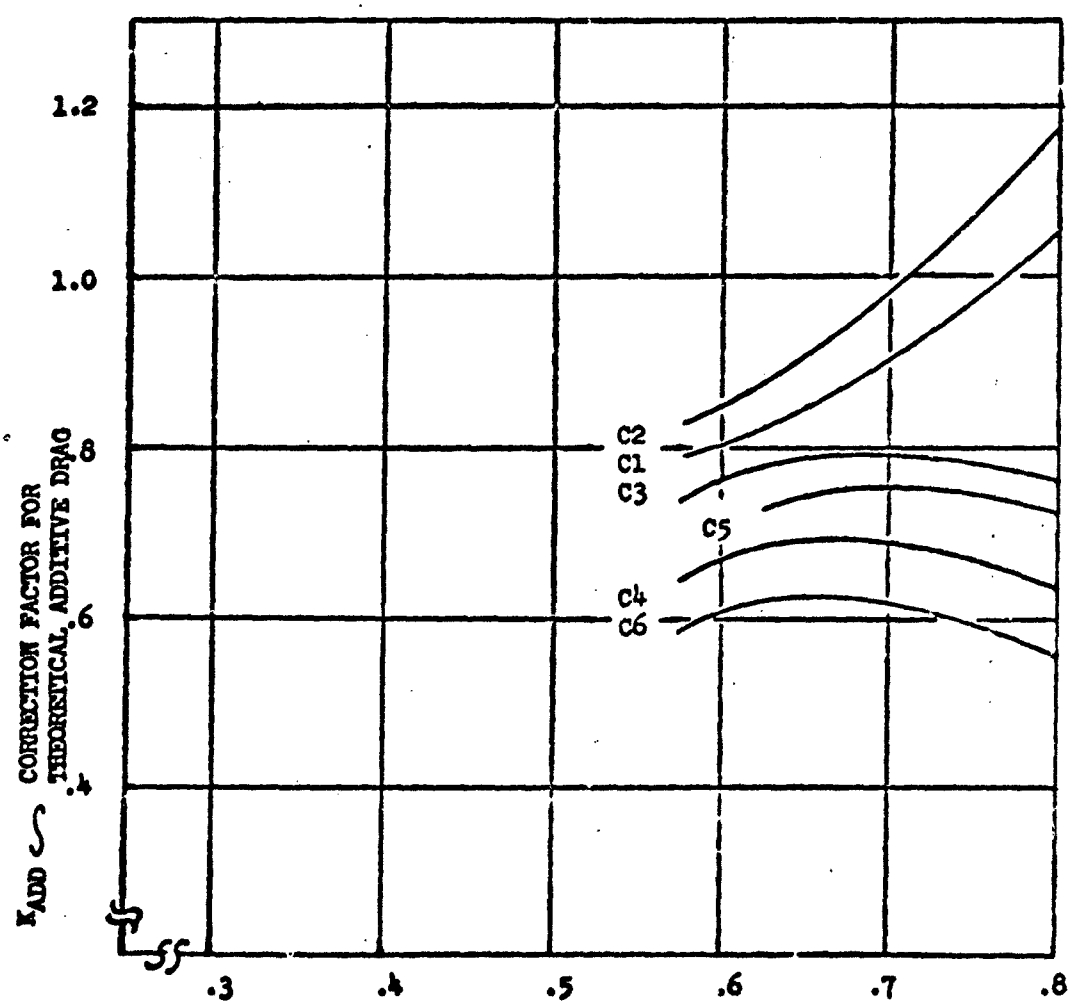

Figure 89. K_{ADD}, R1SP1C1-C6, M_o = 1.39

CONFIG.	α°	β°	M_0	(A_0/A_c) ref.
R1SP2C1	5°	5°	1.39	0.7675

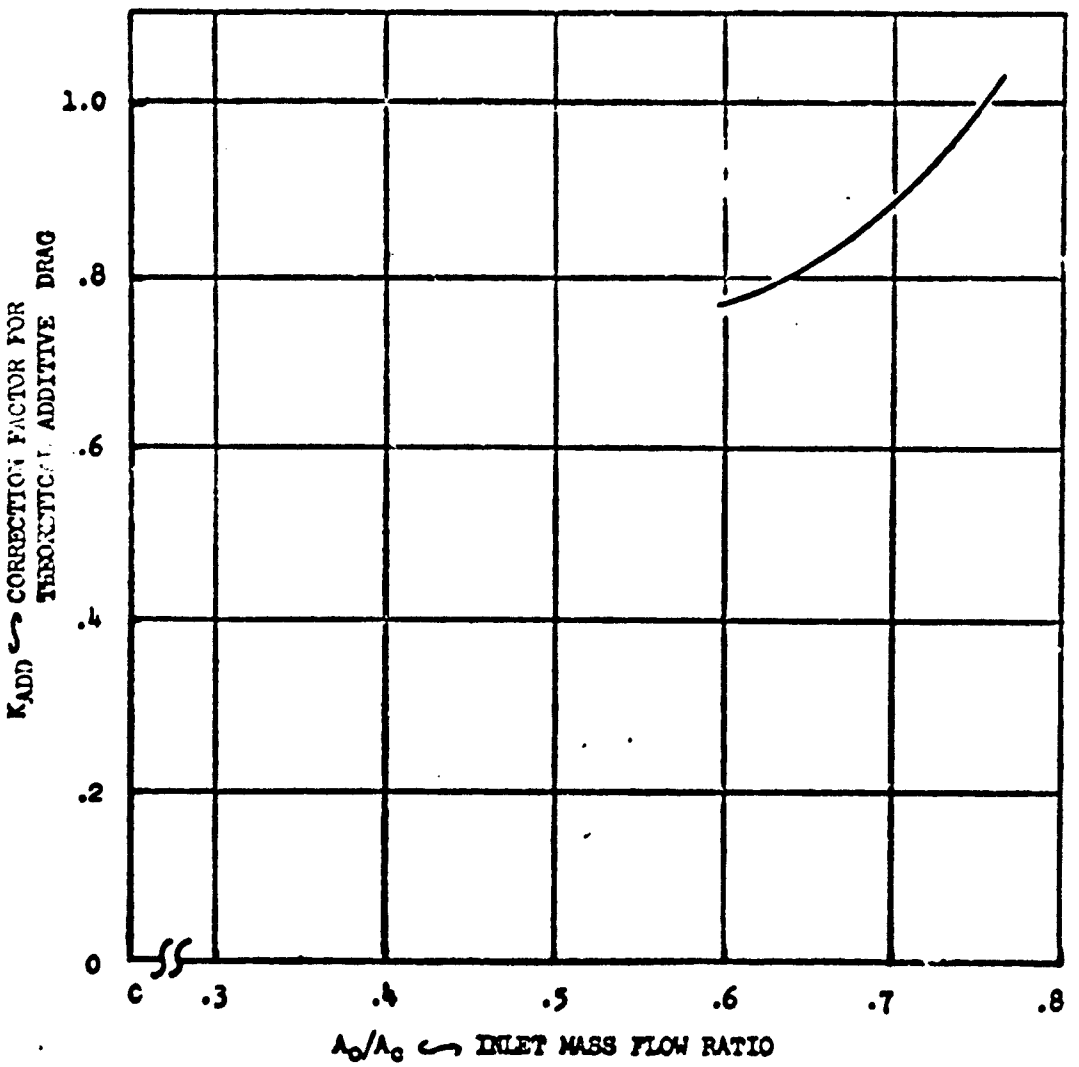

Figure 90. K_{ADD}, R1SP2C1, M_0 = 1.39

CONFIG.	α°	β°	M_0	(A_0/A_c) ref.
R1SP3C1	5°	5°	1.41	0.856

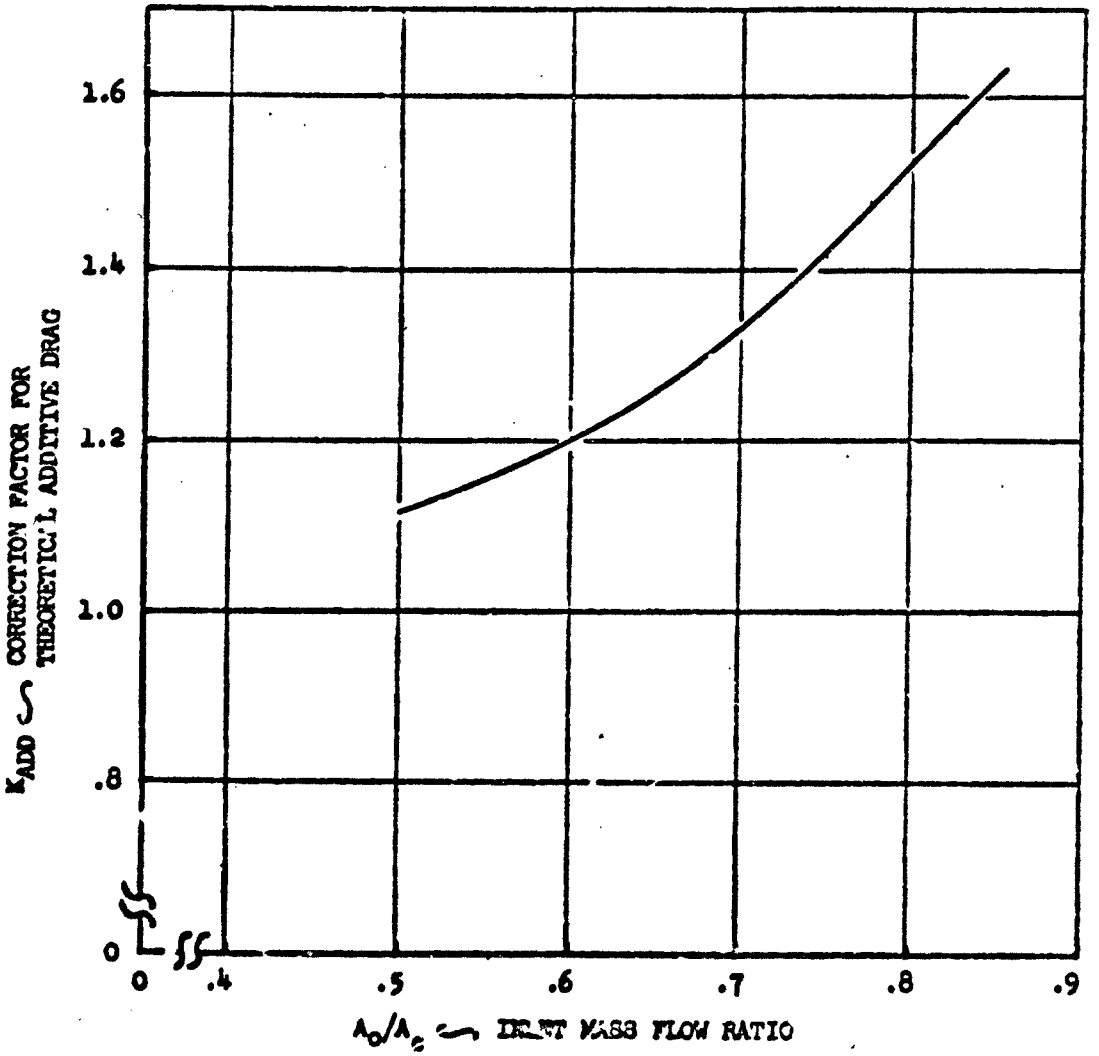

Figure 91. K_{ADD}, R1SP3C1, M_0=1.41

CONFIG.	α'°	β°	Mo	(A_o/A_c) ref.
R3SF1C1	12°	12°	1.41	0.50

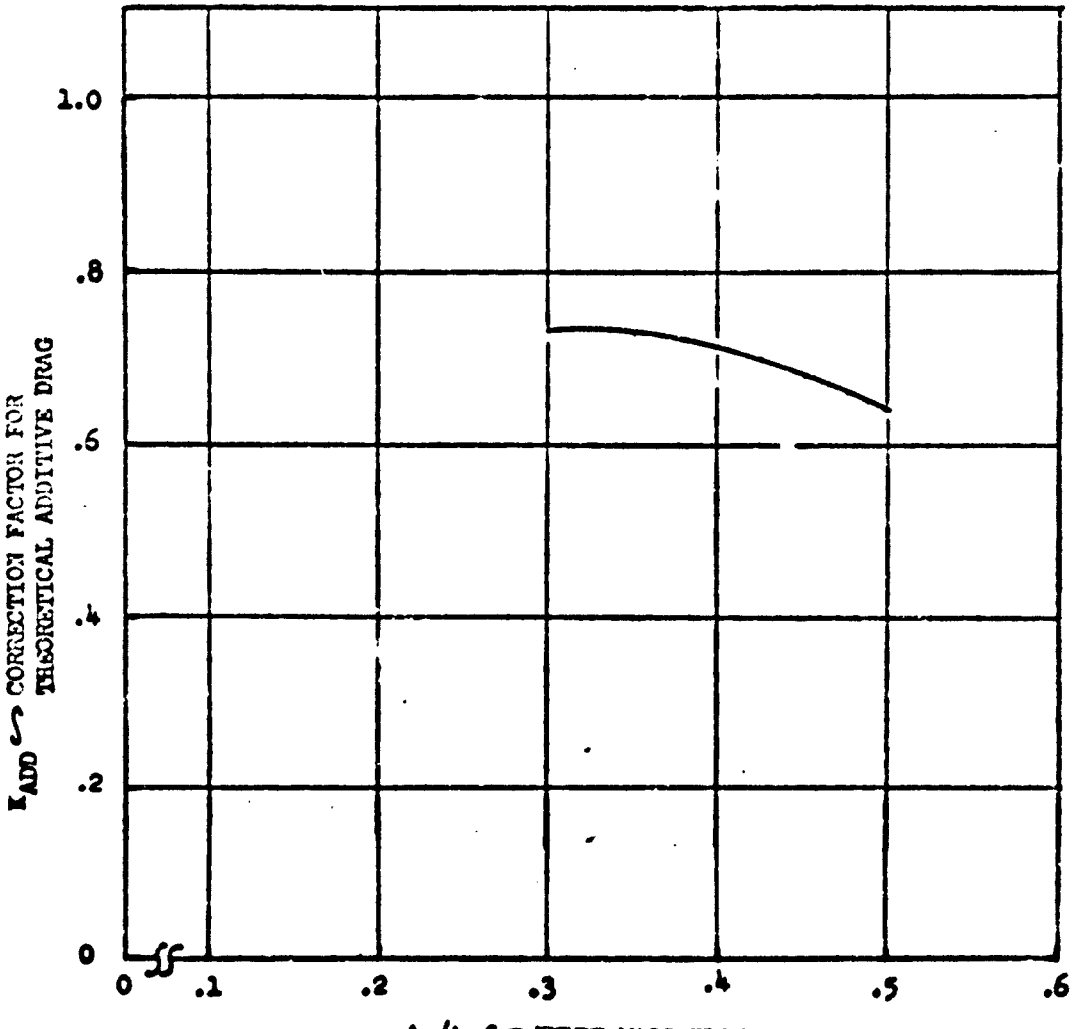

Figure 92. K_{ADD}, R3SF1C1, Mo = 1.41

CONFIG.	α°	β°	M_o	$(A_o/A_c)_{ref.}$
R4SP4C1	5°	5°	1.41	0.885
C4	"	"	"	"
C6	"	"	"	"

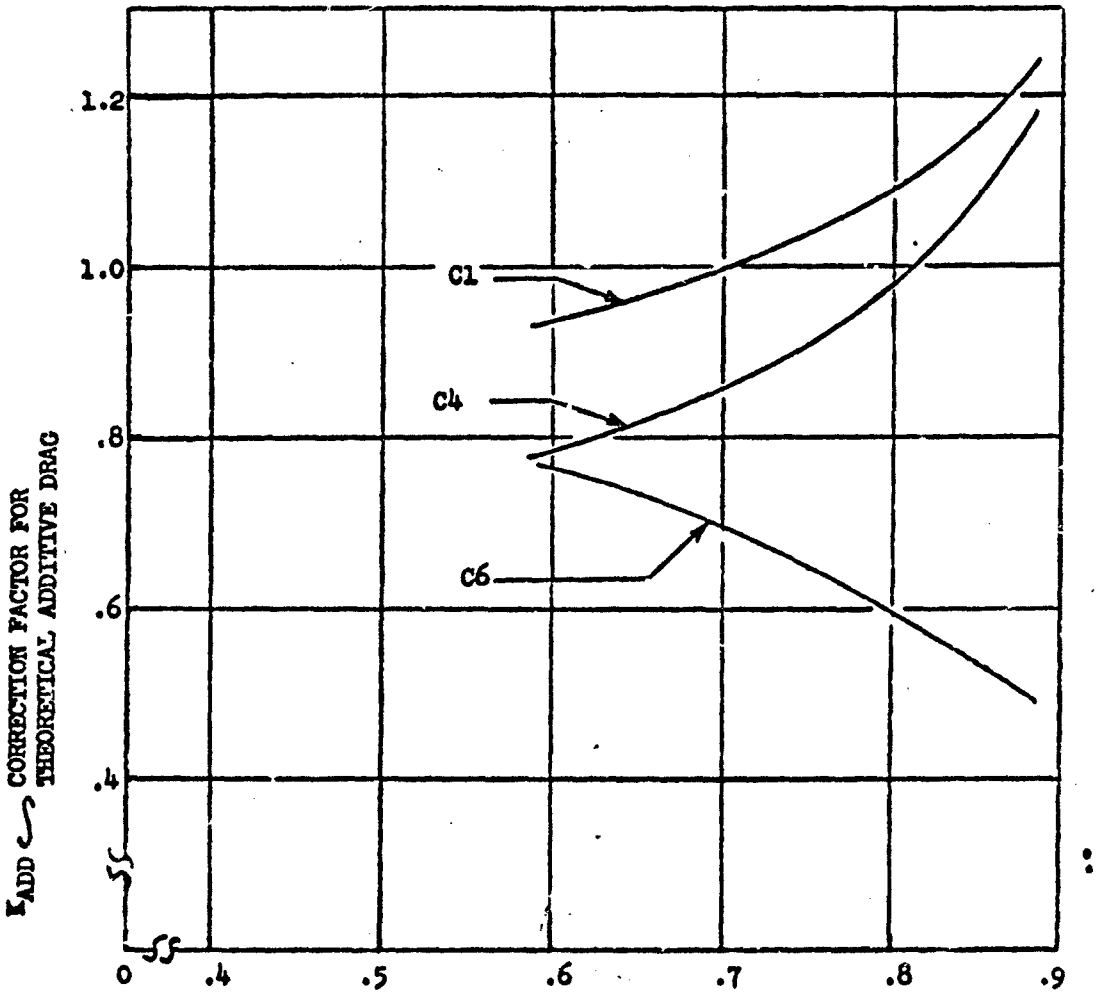

Figure 93. K_{ADD}, R4SP4C1, C4, C6, M_o = 1.41

CONFIG.	α°	β°	M_0	(A_0/A_c) ref.
R1SP1C1	5°	5°	1.69	0.841
C5	"	"	"	"

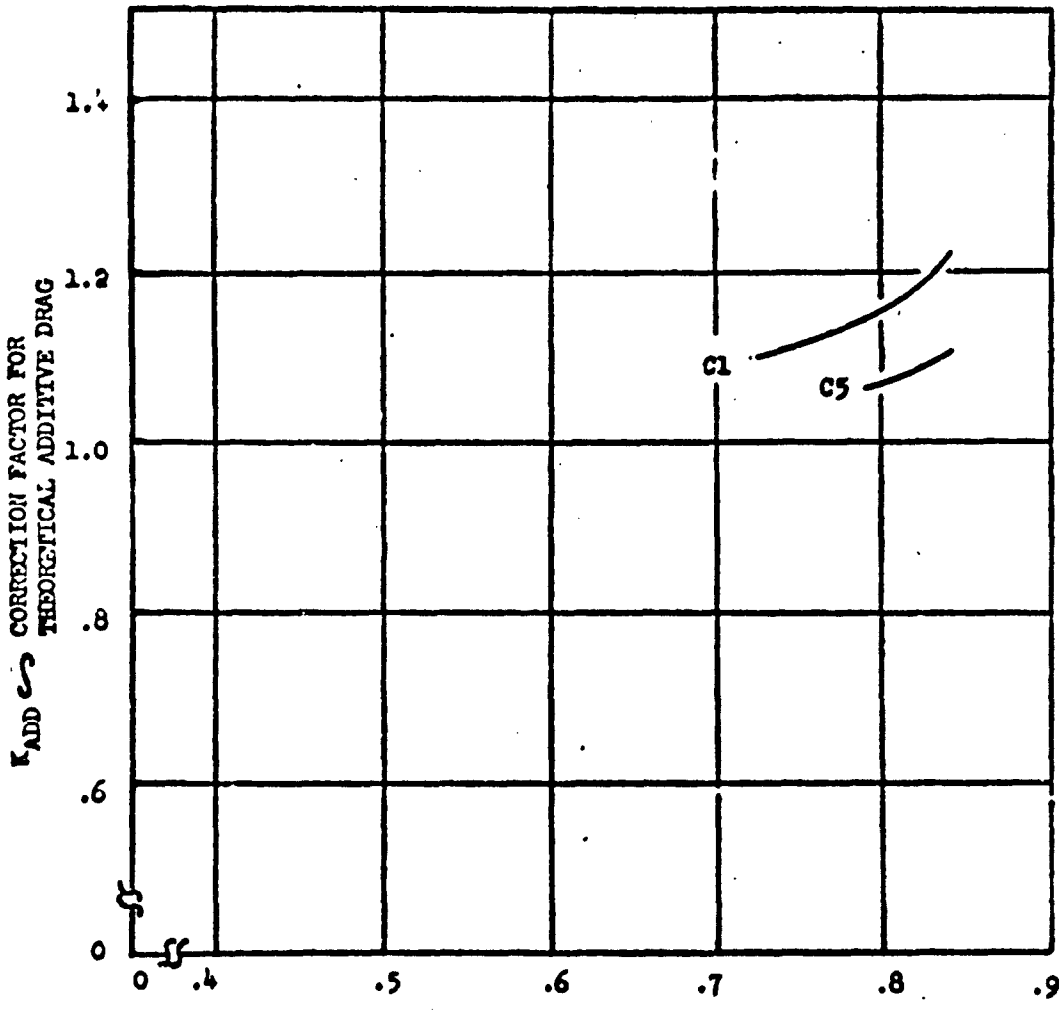

Figure 94. K_{ADD}, R1SP1C1, C5, M_0 = 1.69

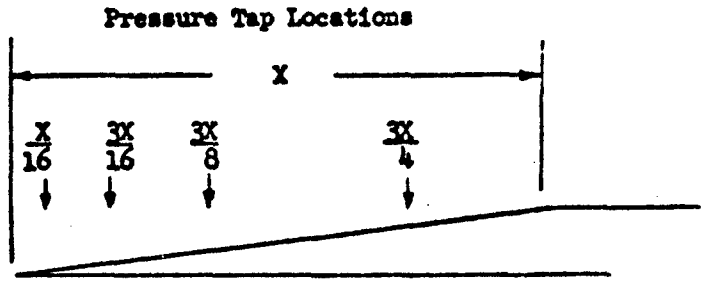

$M_o = 1.09$

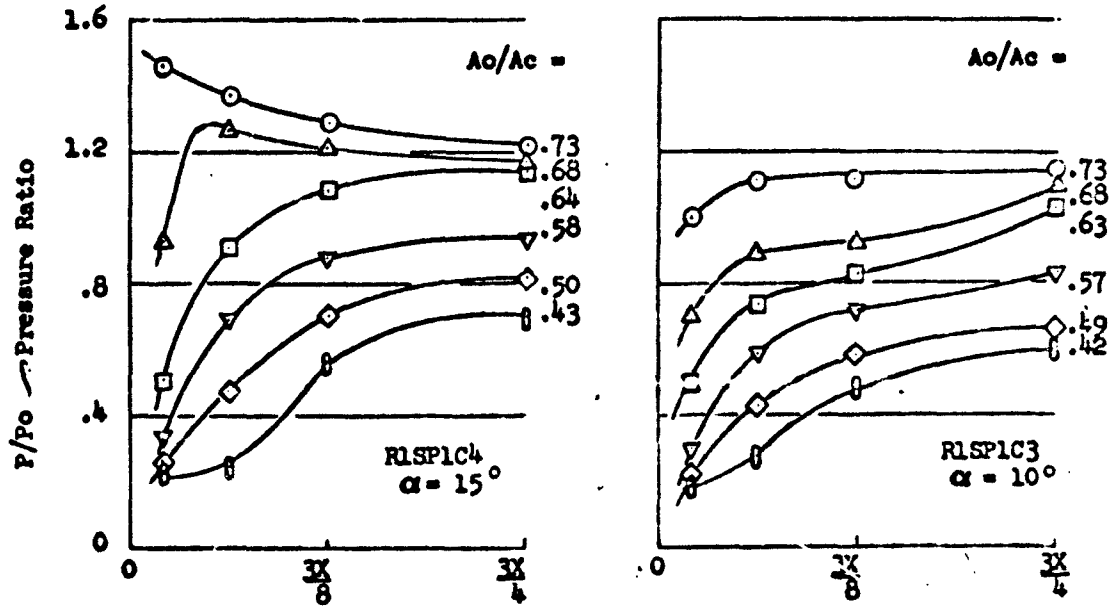

Figure 95. Cowl Centerline Pressure Distributions

CONFIG.	α°	β°	Mo	(A_o/A_c) ref.
R1SP1C1	5°	5°	0.69	0.796
SP2	"	"	0.69	0.796
SP3	"	"	0.71	0.796

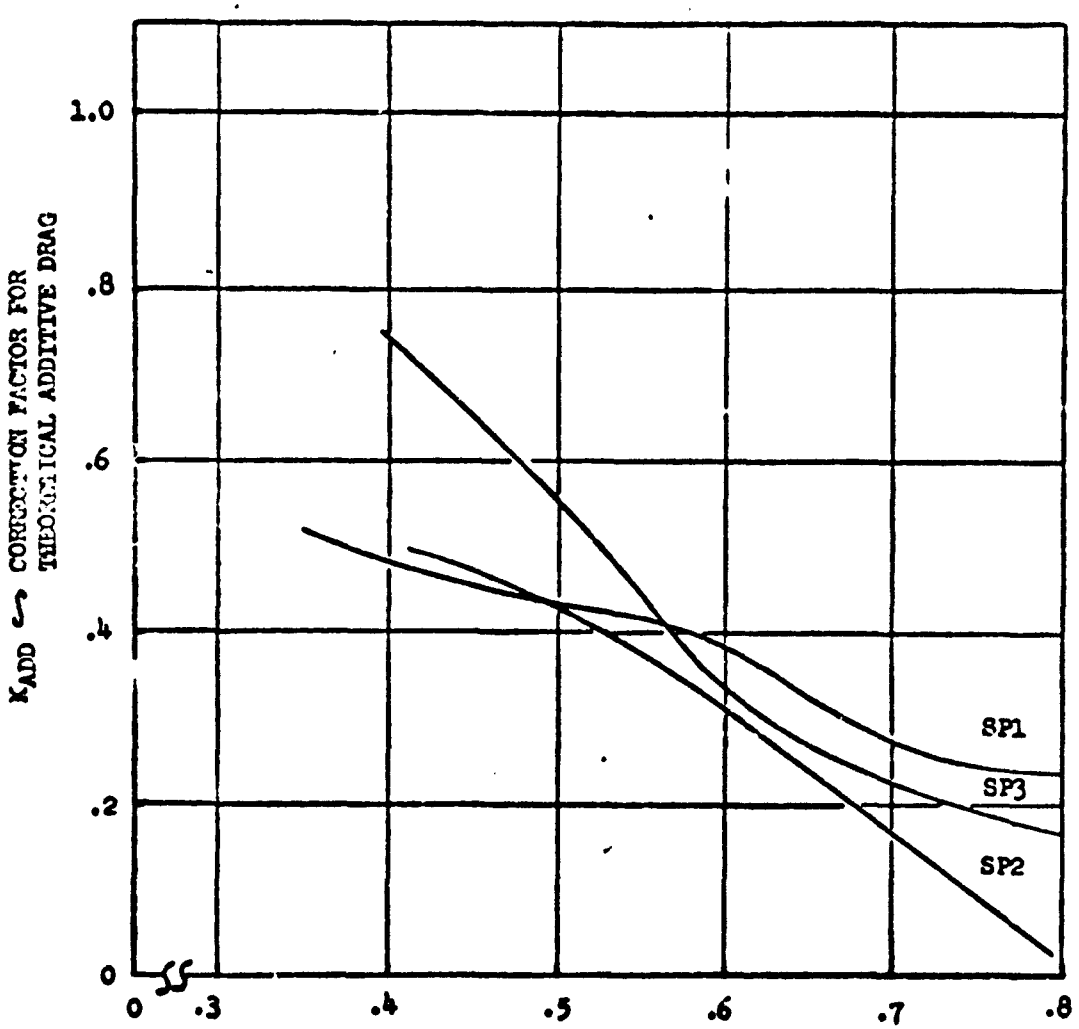

Figure 96. K_{ADD}, SEVERAL SIDE PLATES, Mo = 0.7

CONFIG.	$\alpha°$	$\beta°$	Mo	(Ao/Ac) ref.
R1SP1C1	5°	5°	0.84	0.796
SP2	"	"	0.84	"
SP3	"	"	0.865	"

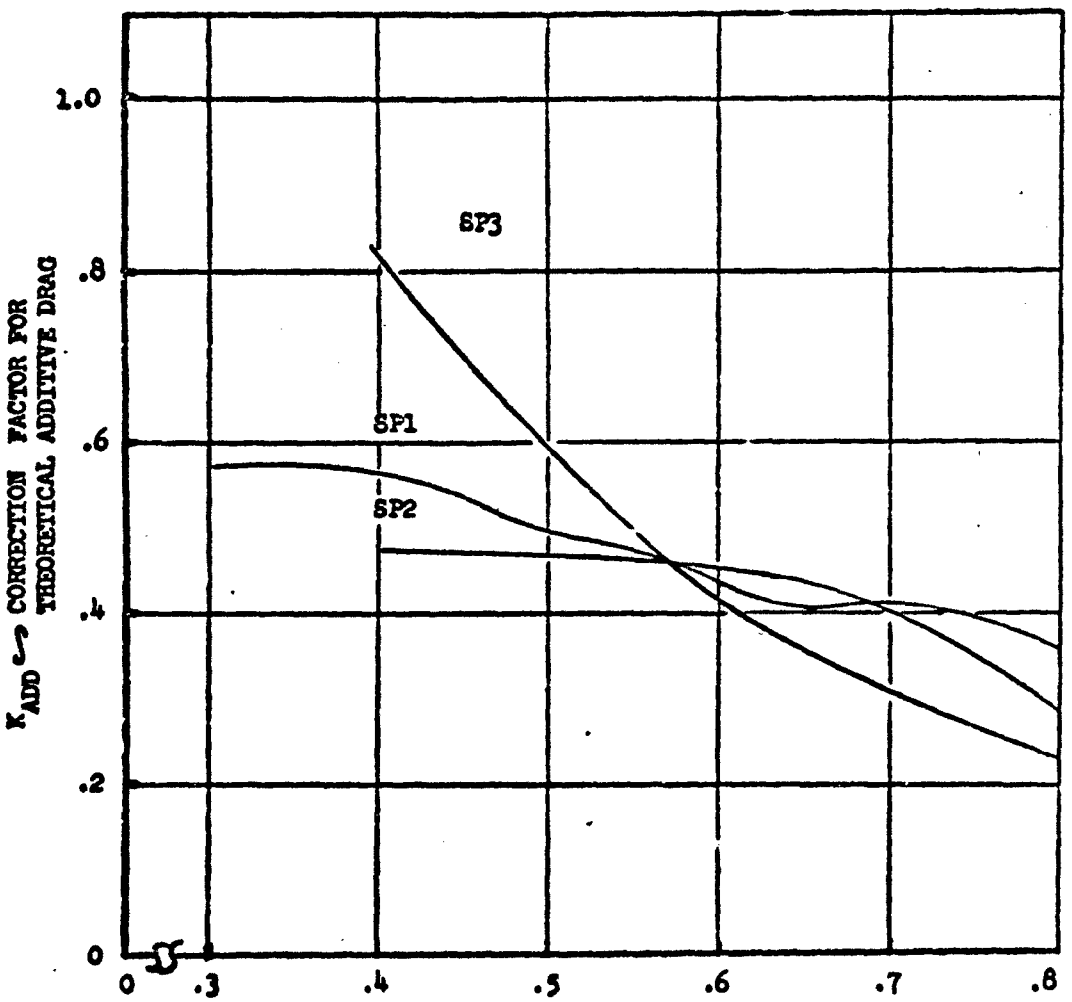

Figure 97. K_{ADD}, SEVERAL SIDE PLATES, M_o = 0.85

CONFIG.	α °	β°	Mo	(A_o/A_c) ref.
R1SP1C2	5°	5°	1.09	0.796
SP2	"	"	1.09	"
SP3	"	"	1.11	"

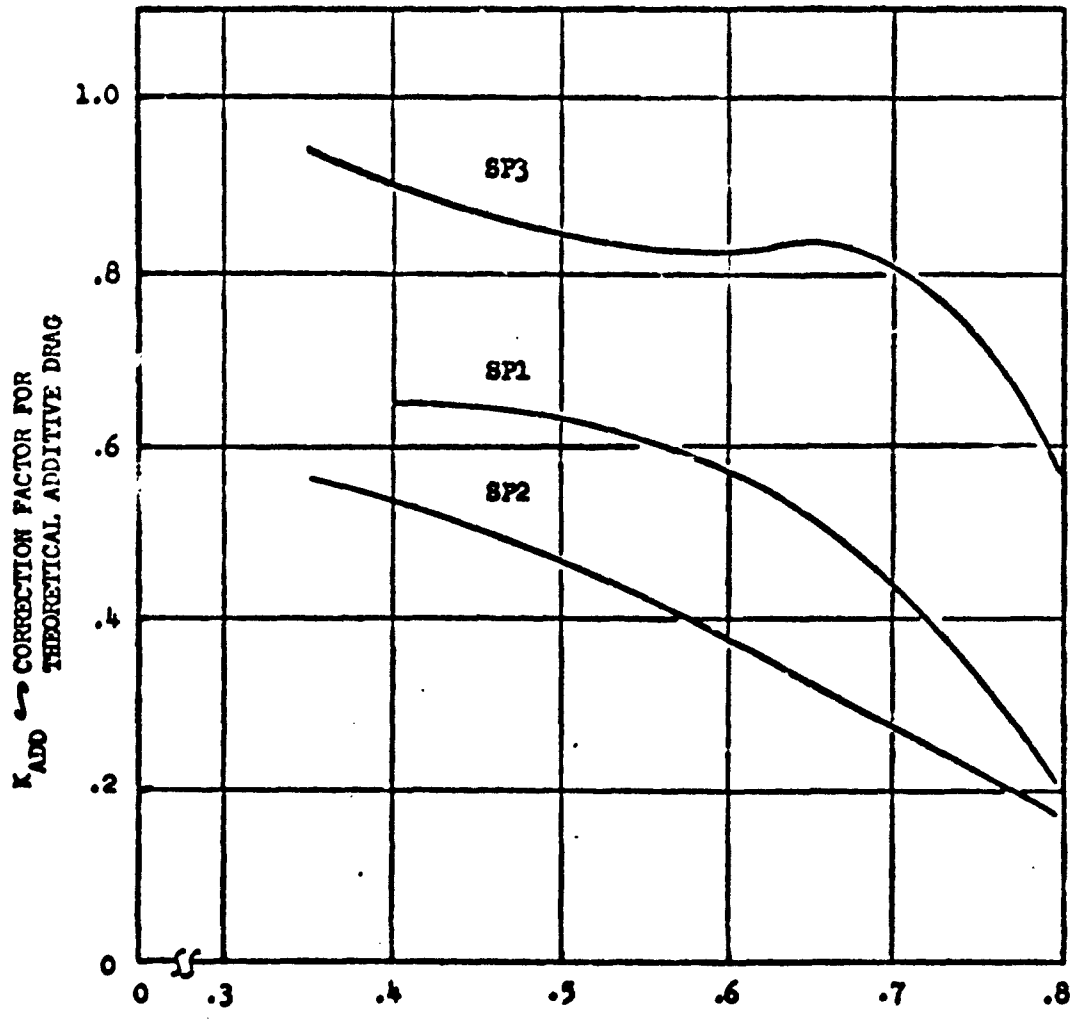

Figure 98. K_{ADD}, SEVERAL SIDE PLATES, Mo = 1.1

CONFIG.	$\alpha°$	$\beta°$	M_0	(Ao/Ac) ref.
R1SP1C1	5°	5°	1.29	0.730
SP2	"	"	1.29	0.75
SP3	"	"	1.31	0.84

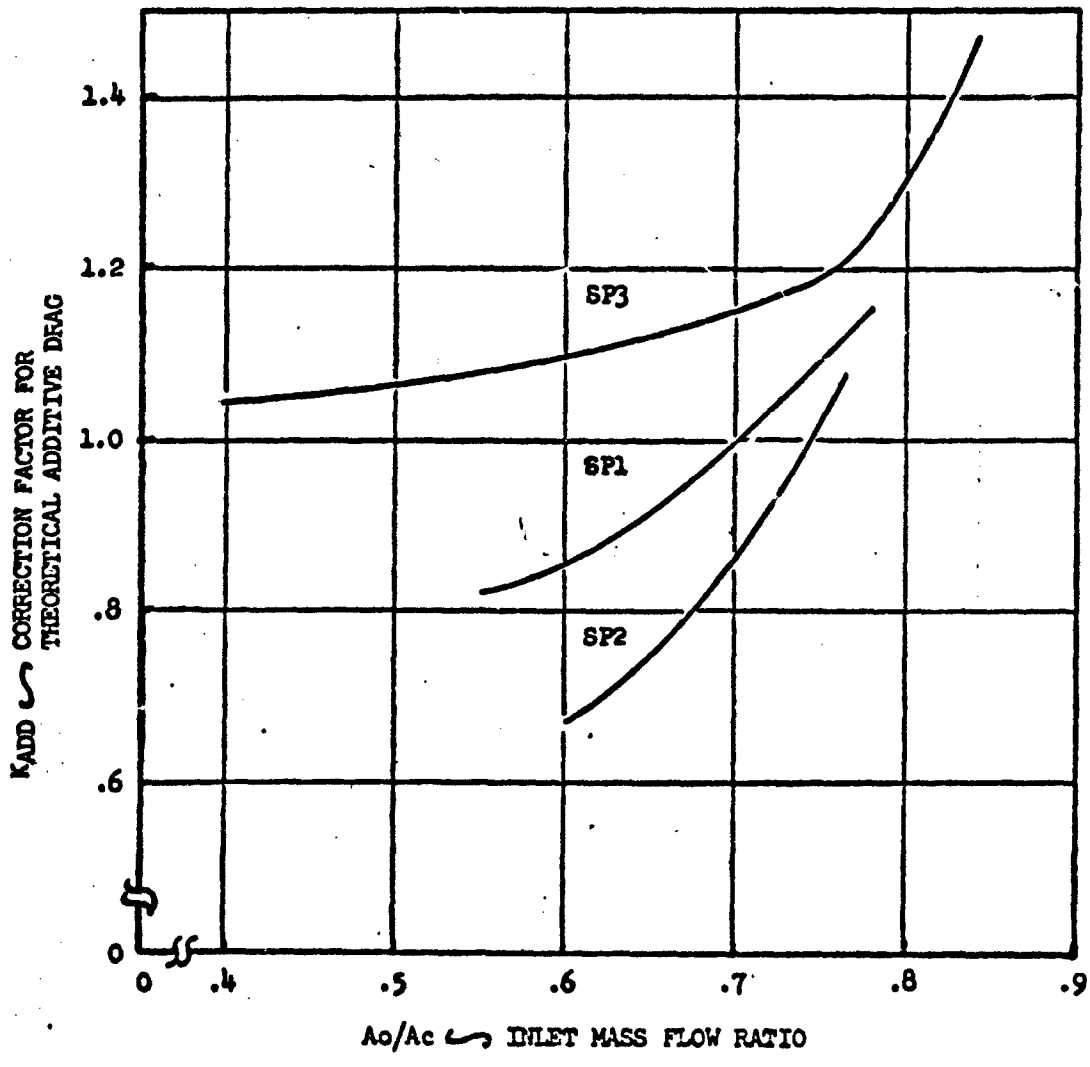

Figure 99. K_{ADD}, SEVERAL SIDE PLATES, $M_0 = 1.3$

CONFIG.	α°	β°	M_o	(A_o/A_c) ref.
R1SP1C1	5°	5°	1.39	0.799
SP2	"	"	1.39	0.767
SP3	"	"	1.41	0.856

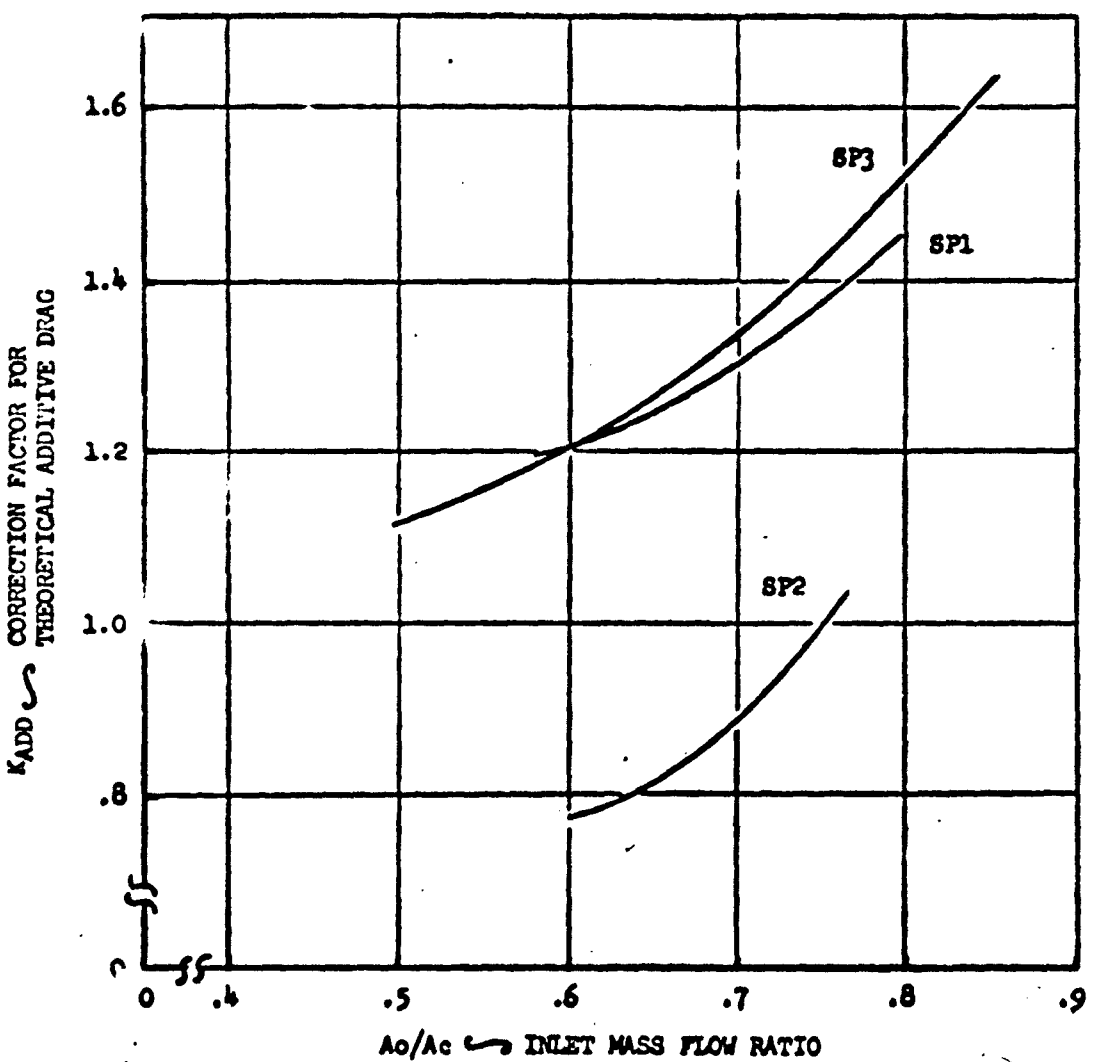

Figure 100. K_{ADD}, SEVERAL SIDE PLATES, M_o = 1.4

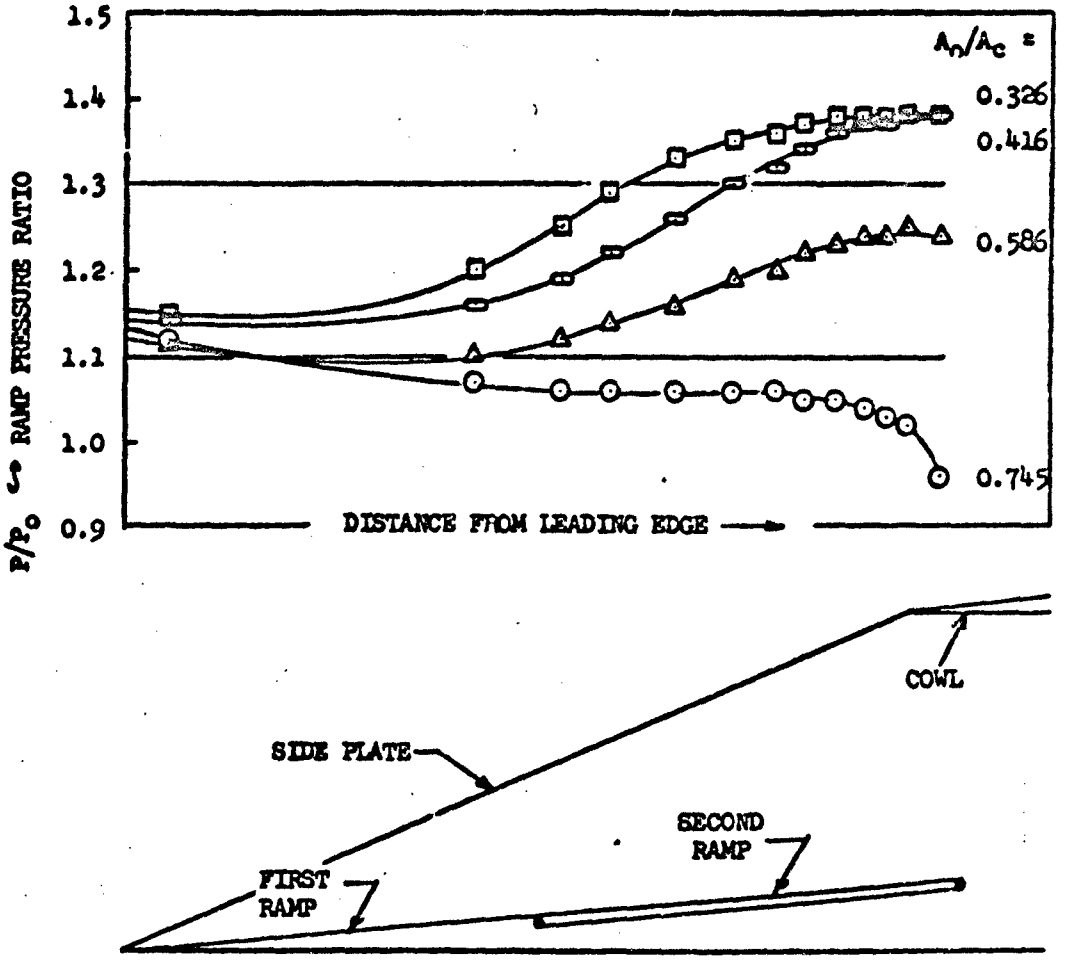

Figure 10L RAMP PRESSURE DISTRIBUTION

RLSP1C1; $\alpha = \beta$ 5°; M_0 = 0.84

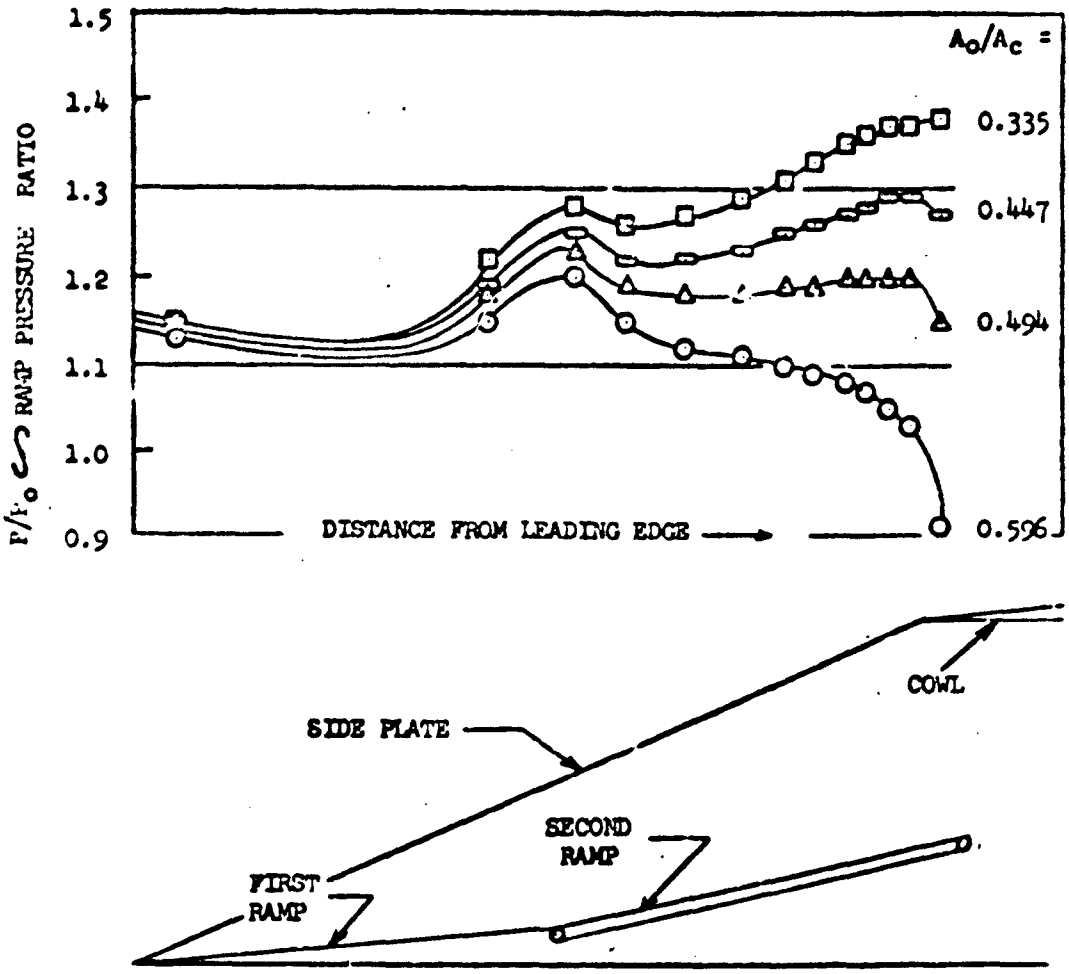

Figure 102. RAMP PRESSURE DISTRIBUTION

MISP1C1; $\alpha = 5^\circ$, $\beta = 12^\circ$; $M_0 = 0.84$

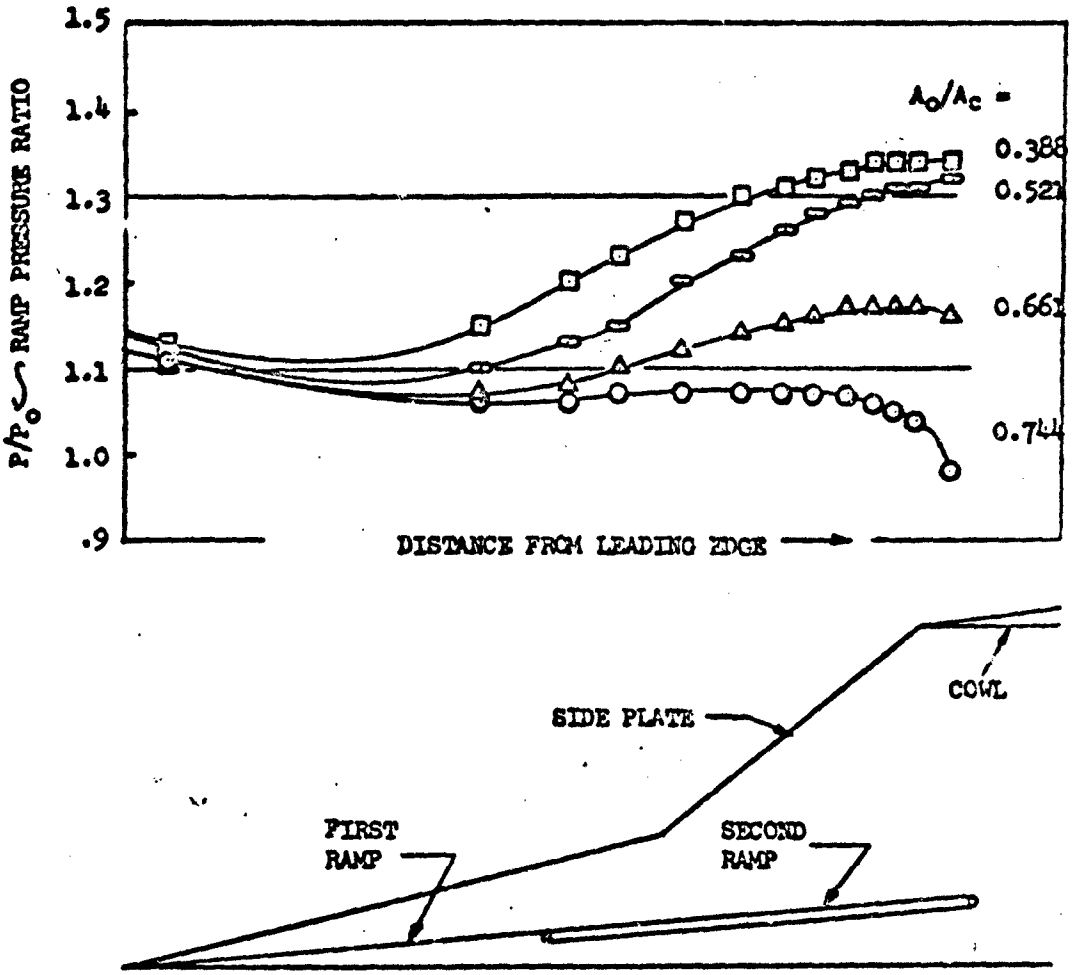

Figure 103. RAMP PRESSURE DISTRIBUTION

RLSP2C1; $\alpha = \beta = 5^\circ$; $M_\infty = 0.34$

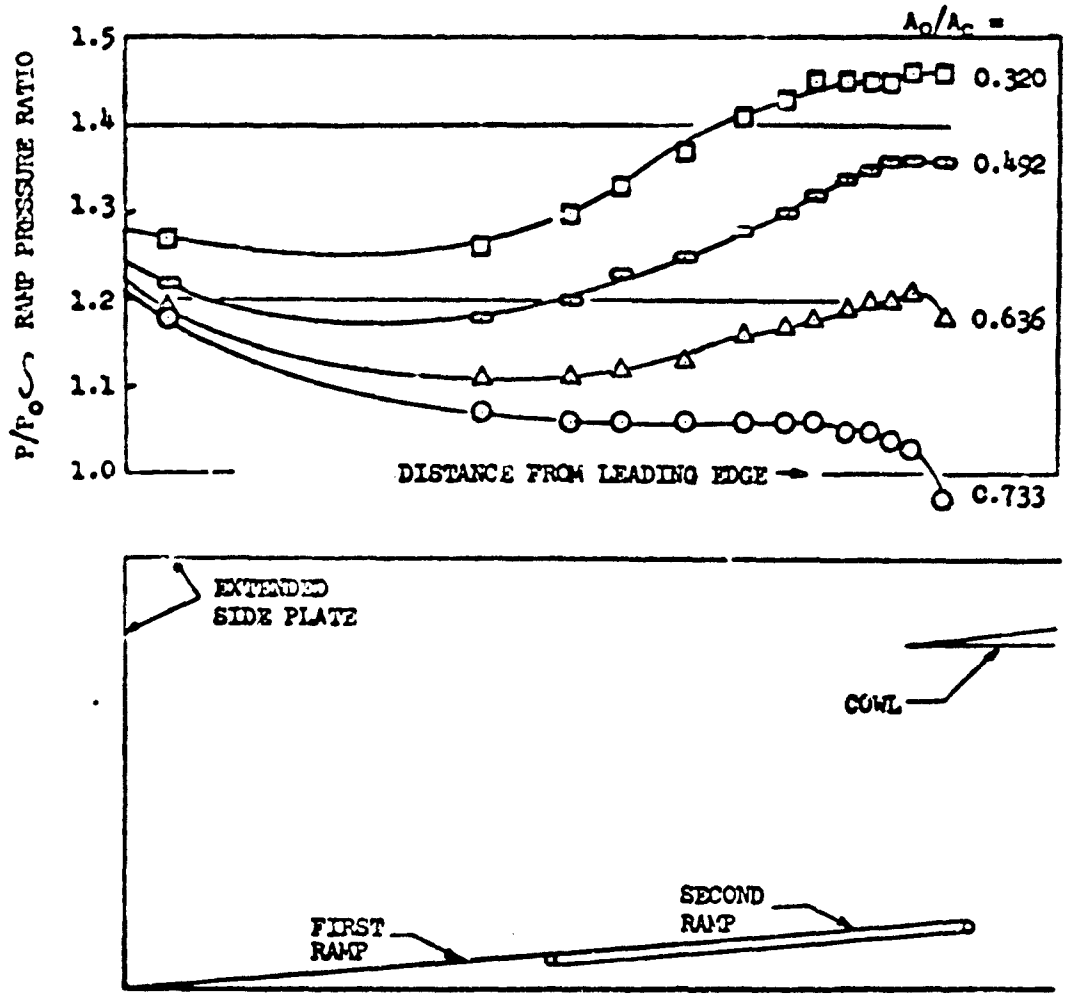

Figure 104. RAMP PRESSURE DISTRIBUTION

R1SP3C1; $\alpha = \beta = 5°$; $M_o = 0.865$

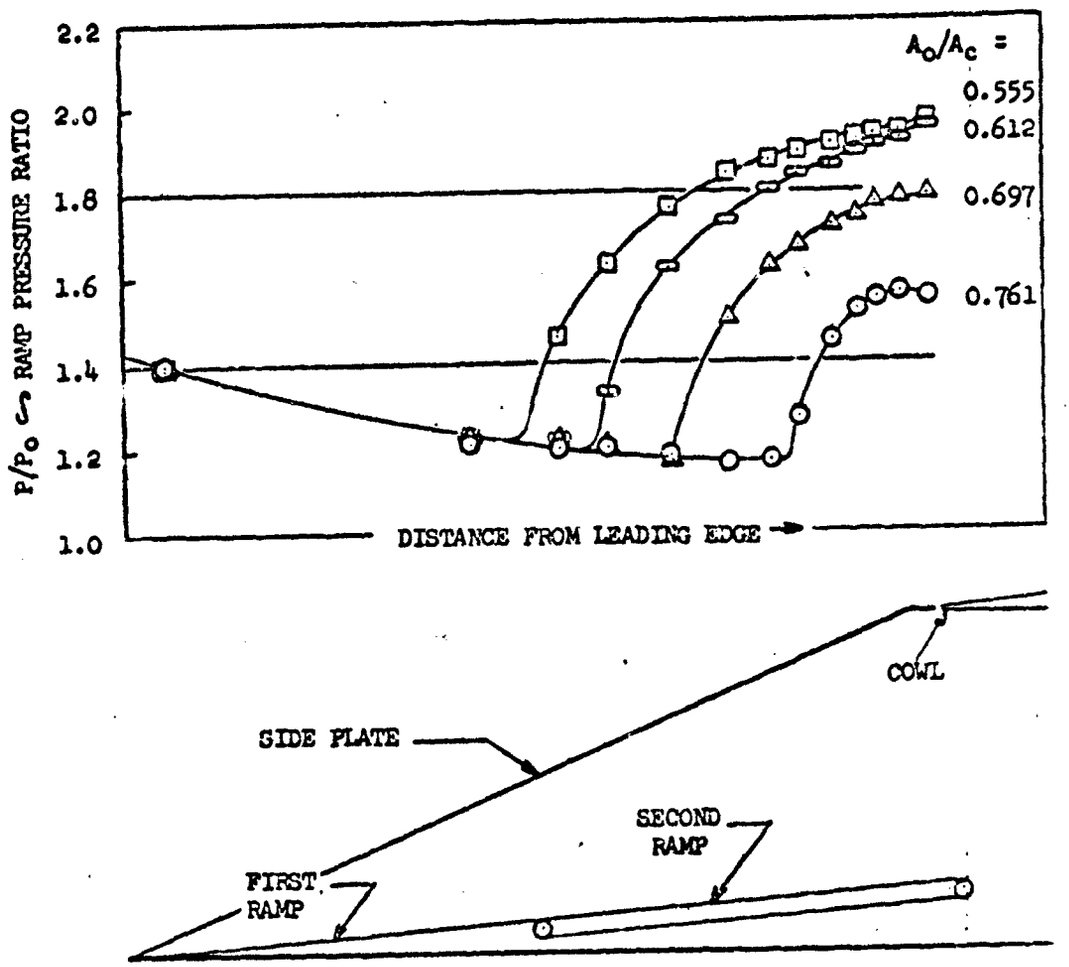

Figure 105. RAMP PRESSURE DISTRIBUTION

R1SP1C1; $\alpha = \beta = 5^{\circ}$; $M_0 = 1.29$

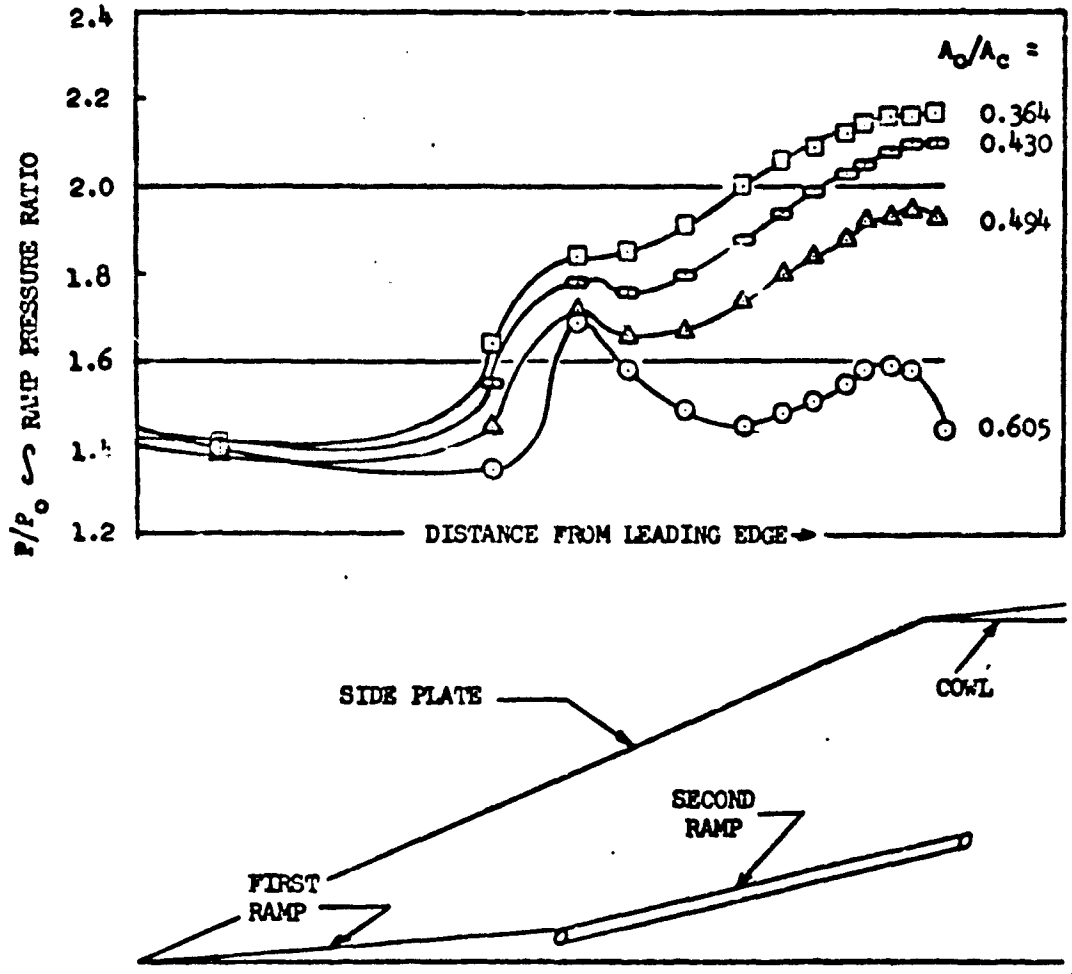

Figure 106. RAMP PRESSURE DISTRIBUTION

RESP1C1; $\alpha = 5^\circ$, $\beta = 12^\circ$; $M_0 = 1.29$

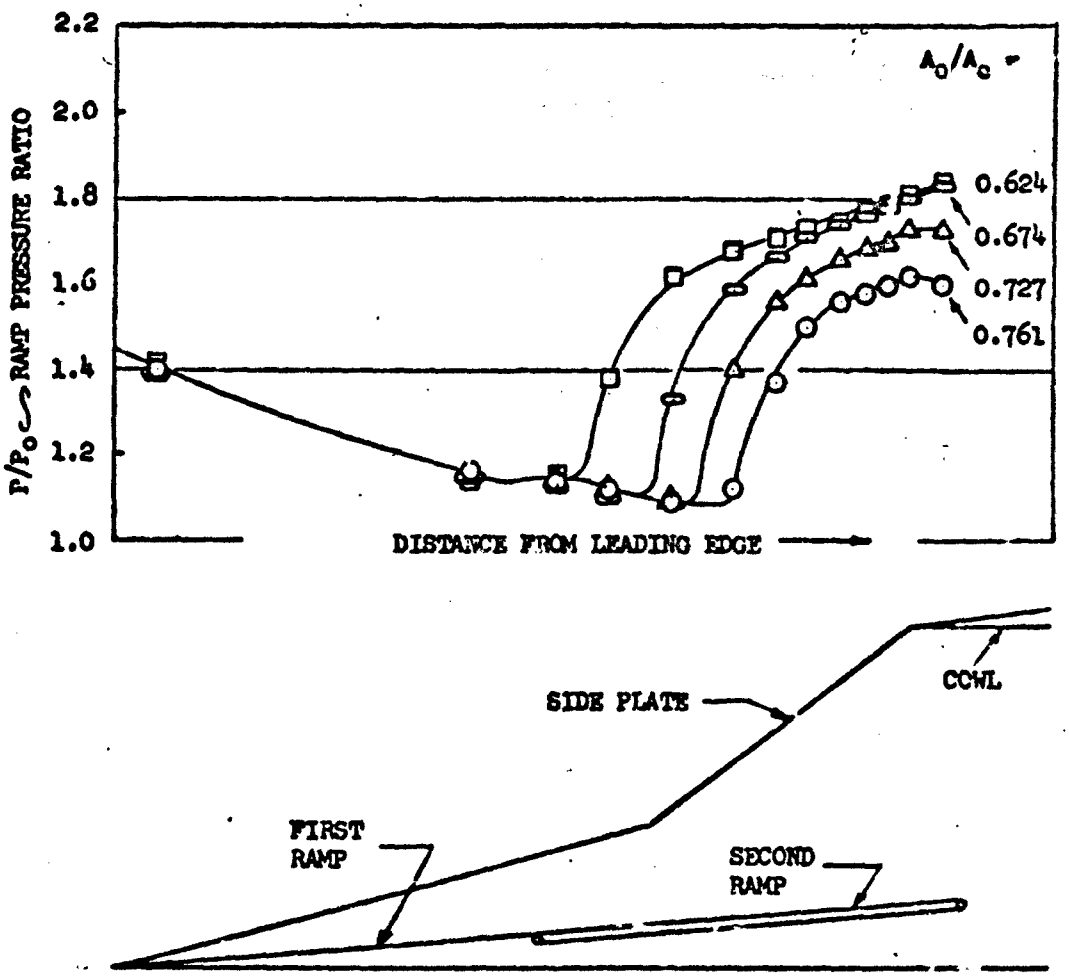

Figure 107 RAMP PRESSURE DISTRIBUTION

R1SP2C1; $\alpha = \beta = 5^{\circ}$; $M_0 = 1.29$

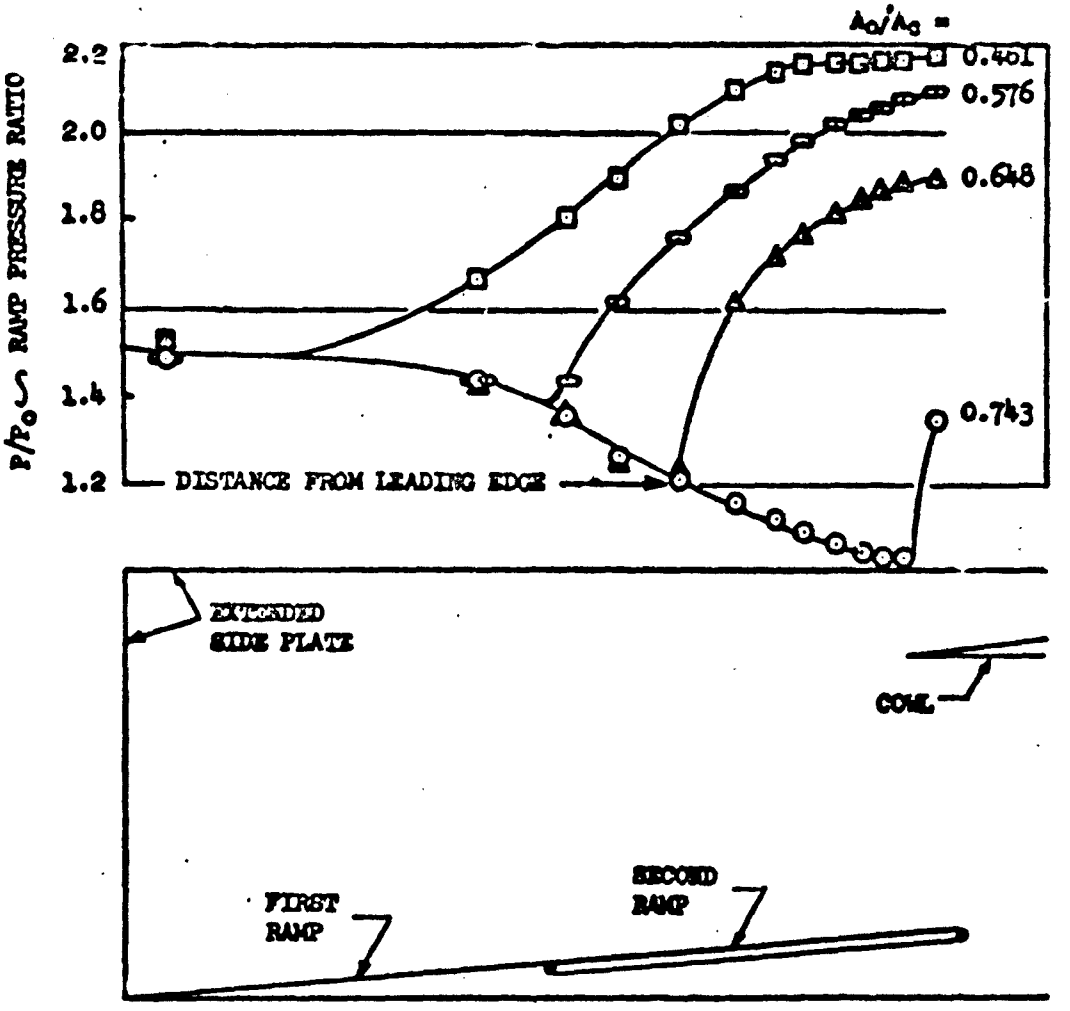

Figure 108 RAMP PRESSURE DISTRIBUTION

RLSP3C1; $\alpha = \beta = 5^\circ$; $M_o = 1.31$

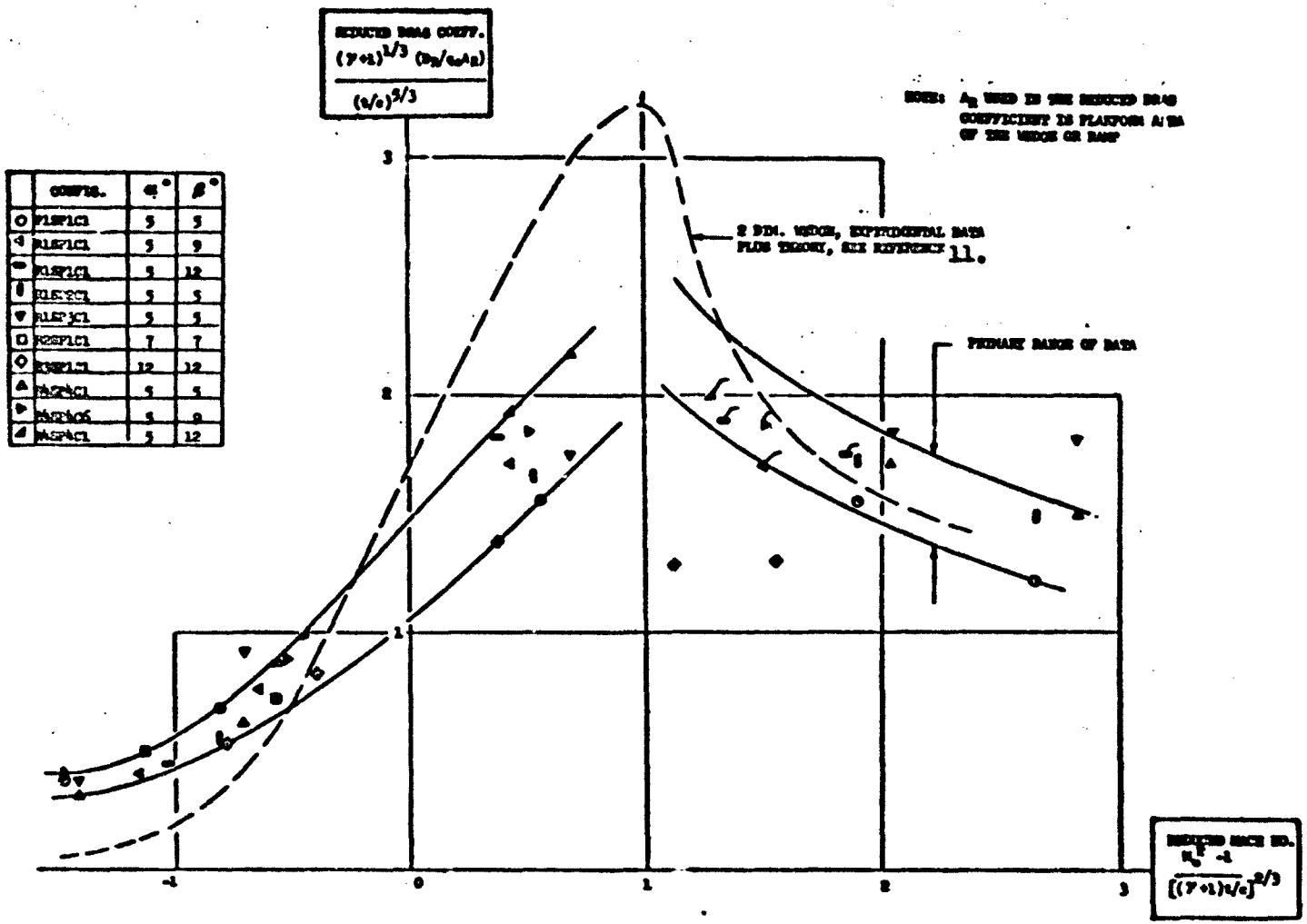

Figure 109. SUGGESTED REFERENCE RAMP DRAG, $(D_R)_{REF}$

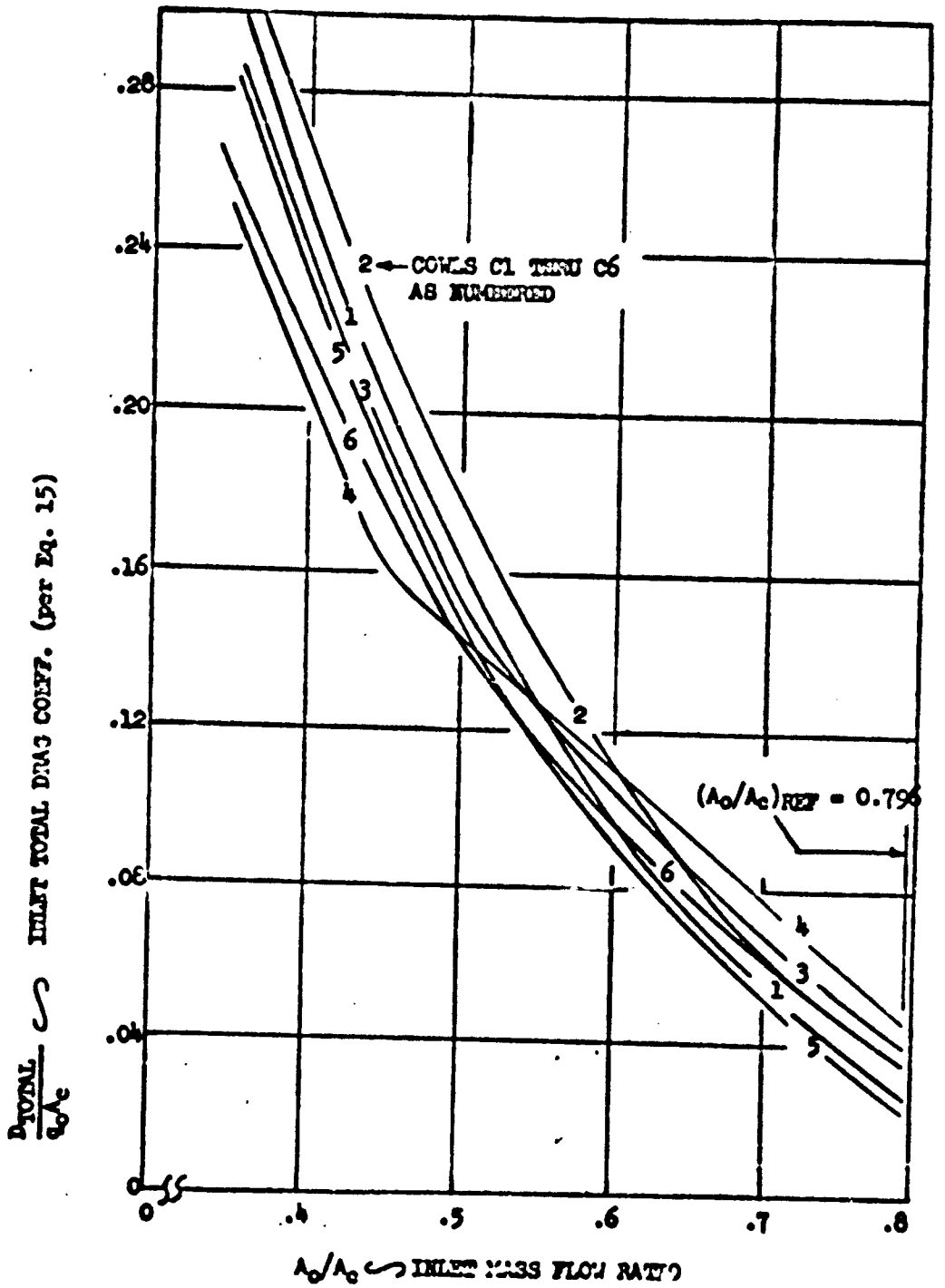

Figure 110. INLET TOTAL DRAG, FLSF1C1 - C6, M_o = 0.84

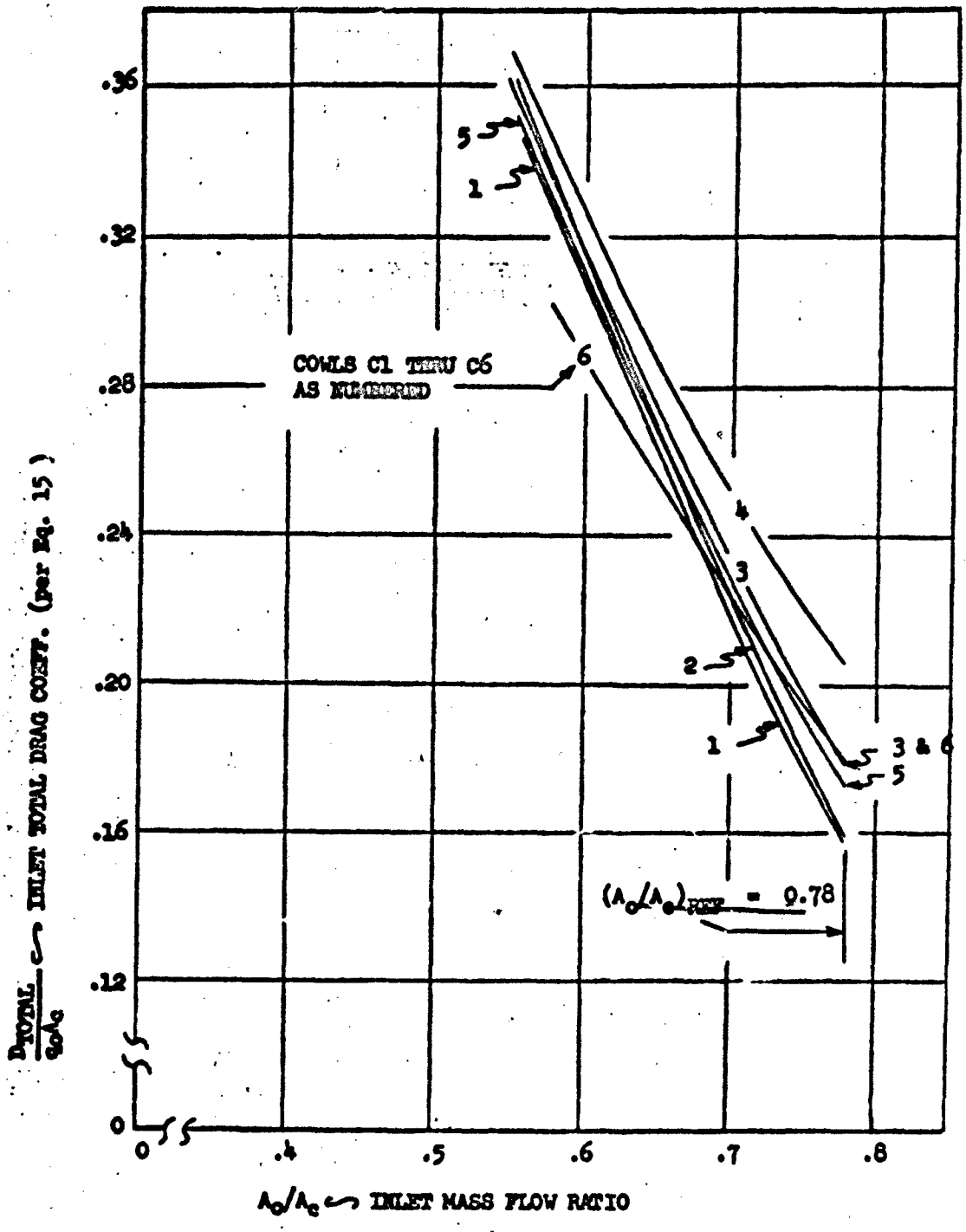

Figure 111. INLET TOTAL DRAG, RISP1C1 - C6, M_o = 1.29

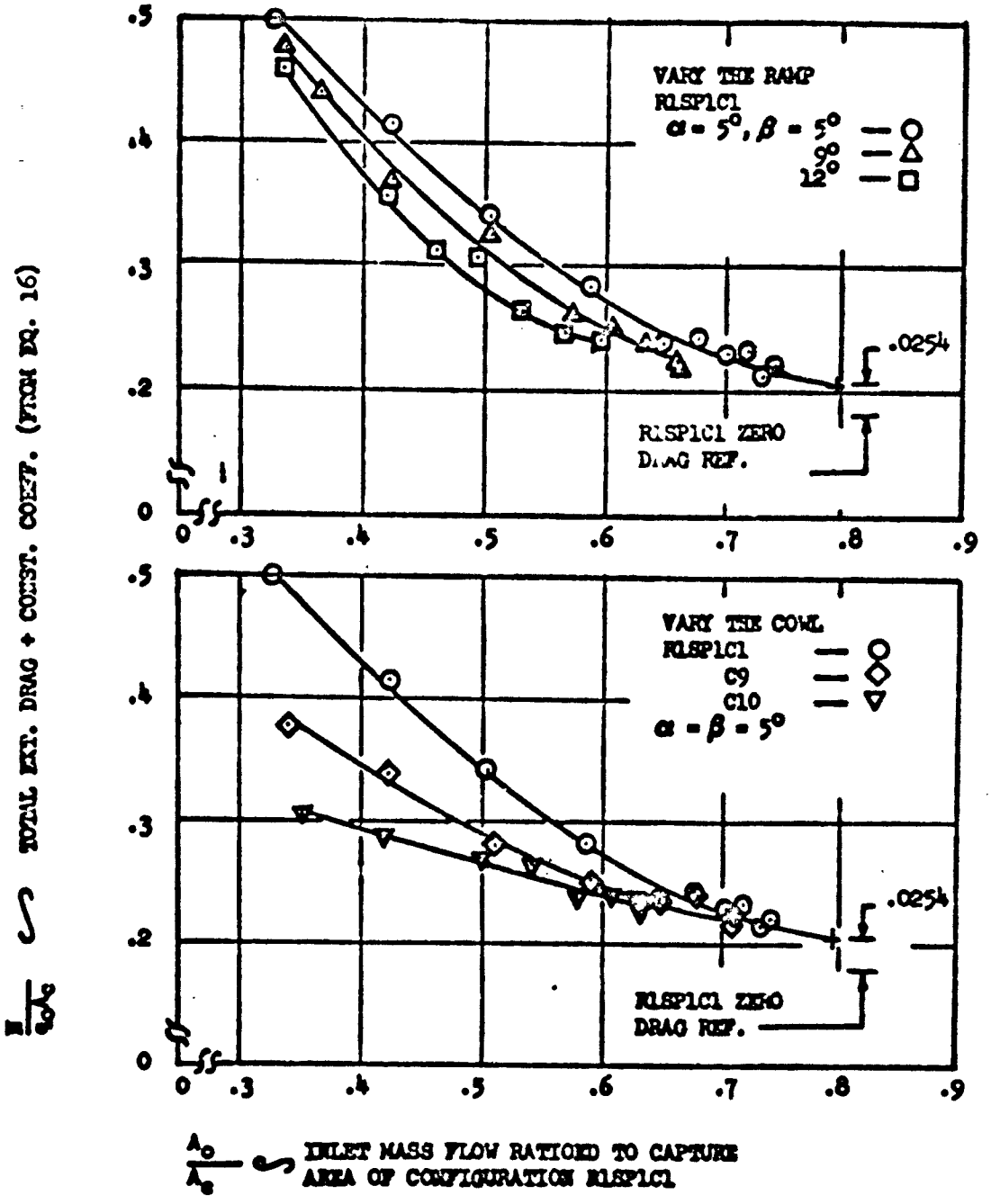

Figure 112. SPILLAGE BY VARYING RAMP AND COWL, $M_0 \approx .85$

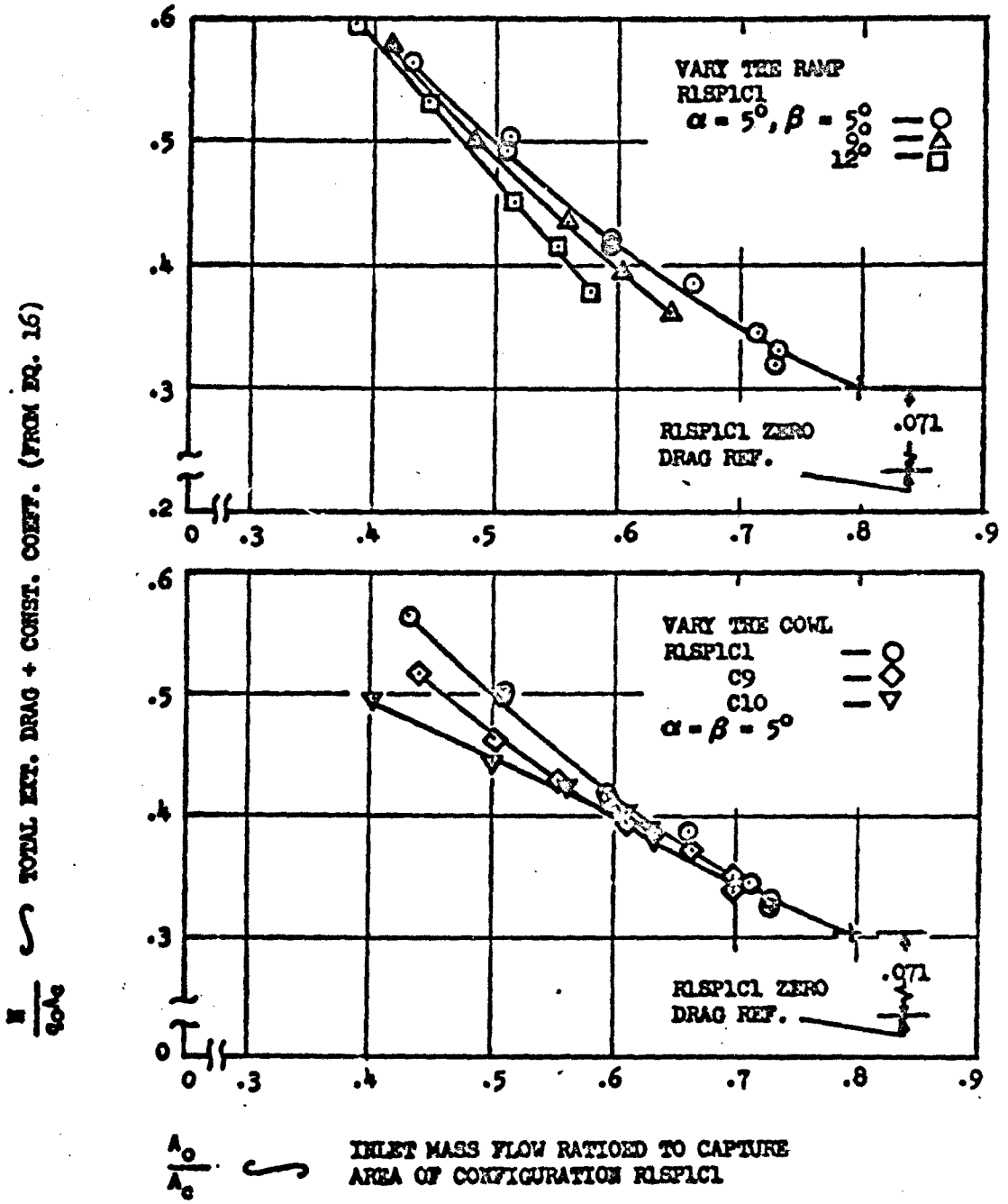

Figure 113. SPILLAGE BY VARYING RAMP AND COWL, $M_0 \approx 1.1$

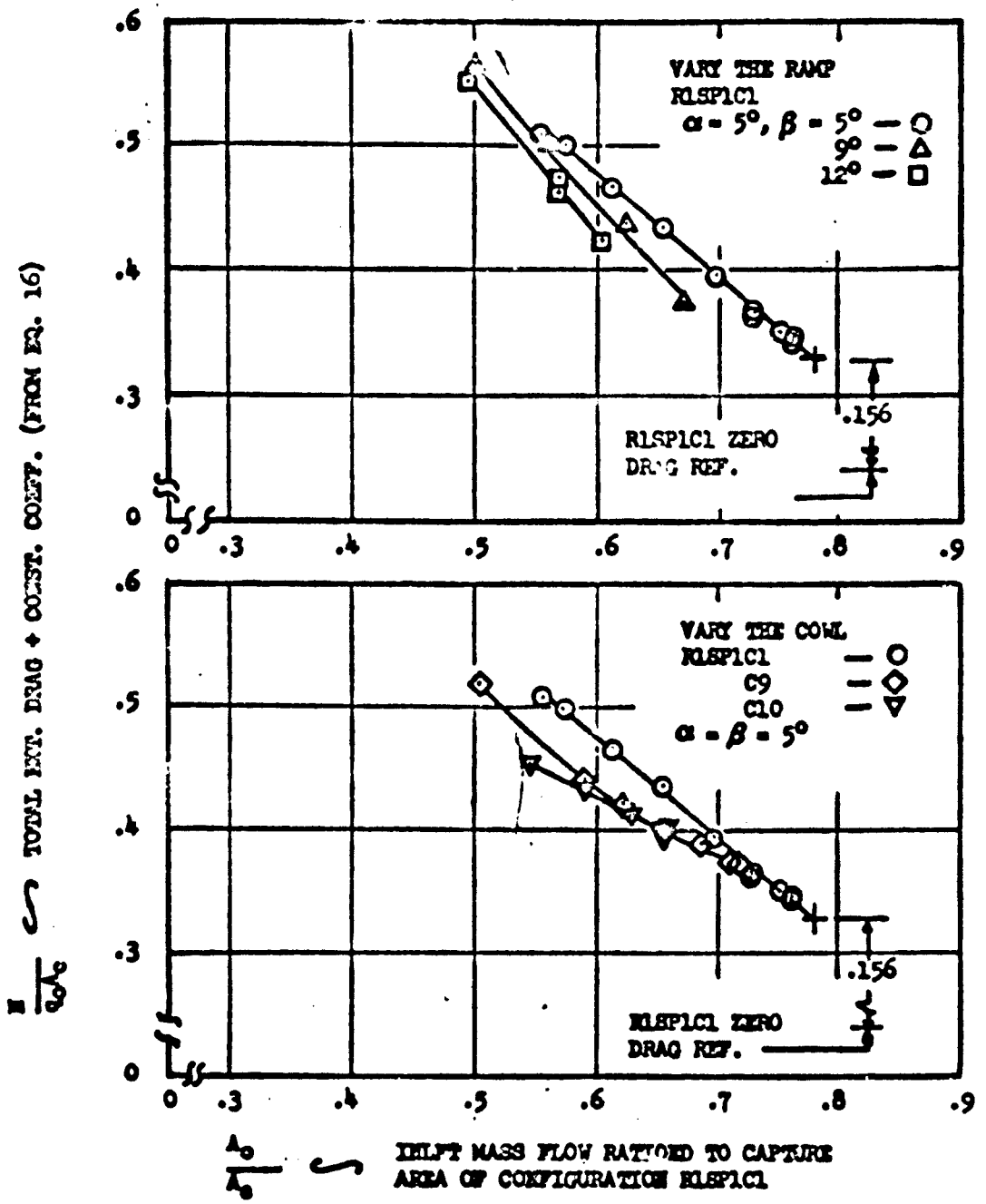

Figure 114. SPILLAGE BY VARYING RAMP AND COWL, $M_0 \approx 1.3$

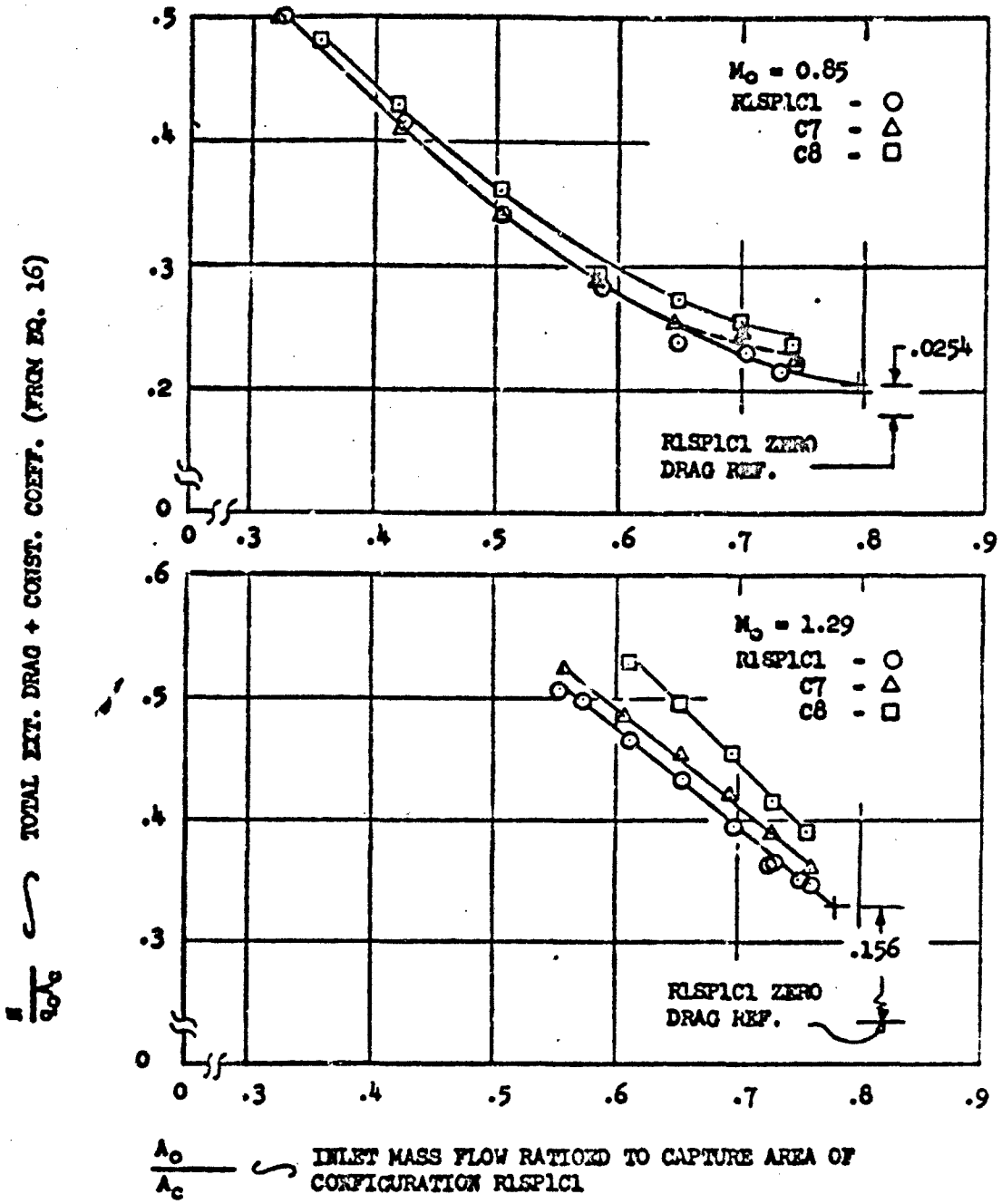

Figure 115. DRAG COMPARISON, SHARP vs. BLUNT COWLS, M_o = 0.85, 1.29

REFERENCES

1. Leroy L. Presley, William P. Peterson, A Comparison of Four Side Mounted Inlets Over a Mach Number Range of 0.60 to 2.2 and Angles to 14°, TM X-107; NASA, Washington; 1960, Unclassified.

2. A. Vernon Gnos, Performance of a Top Inlet with a Vertical Porous Wedge at Mach Numbers of 1.6 to 2.35, Memo 2-2-59A; NASA, Washington; 1959, Unclassified.

3. Wallace F. Davis, Richard Scherrer, Aerodynamic Principles for the Design of Jet Engine Induction Systems, RM A55F16; NACA, Washington; 1956; Unclassified.

4. L. E. Stitt, R. W. Cubbison, R. J. Flaherty, Performance of Several Half-Conical Side Inlets at Supersonic and Subsonic Speeds, RM E55J10a; NACA, Washington; 1956, Unclassified.

5. J. L. Allen, L. G. Piercy, Performance Characteristics of an Under-slung Vertical-Wedge Inlet with Porous Suction at Mach Numbers of 0.63 and 1.5 to 2.0, RM E56B15; NACA, Washington; 1956, Unclassified.

6. L. M. Randall, G. Goldshine, Experimental Investigation of 0.09 Scale Full Span Ducted Model of the F-107a Airplane at Mach Numbers of 0.8, 0.9, 1.1, 1.25, NA-56-335, North American Aviation, Inc., Los Angeles Division; 1956, Unclassified.

7. M. A. Sulkin, Experimental Investigation of a 0.09 Scale Ducted Force Model of the F-107a Airplane at Mach Numbers of 1.6, 1.8, 2.0 and 2.2/Top Inlet Version of the Airplane, NA-56-1166; North American Aviation, Inc., Los Angeles Division; 1956, Unclassified.

8. L. W. Pearson, Theoretical and Experimental Transonic Additive Drag, NA-64-363; North American Aviation, Inc., Los Angeles Division; 1964, Unclassified.

9. Joseph S. Mount, The Effect of Additive Drag Upon Aircraft Performance, NA-64-780, North American Aviation, Inc., Los Angeles Division; 1964, Unclassified. Also available as AIAA Paper No. 64-599; American Institute of Aeronautics and Astronautics, 1290 Avenue of the Americas, New York, New York; 1964, Unclassified. Also available in Volume 2, Number 5, September - October 1965 issue of the Journal of Aircraft.

10. Joseph S. Mount, Additive Drag on Inlet Cowls and Its Effect on Aircraft Propulsion, NA-65-918, North American Aviation, Inc., Los Angeles Division; 1965, Unclassified. Also available in AGARDograph 103, Part I, Aerodynamics of Power Plant Installation, AGARD - 64 Rue de Varenne Paris 7e France; October 1965, Unclassified.

11. Arthur E. Bryson, An Experimental Investigation of Transonic Flow Past Two-Dimensional Wedge and Circular-Arc Sections Using a Mach -Zehnder Interferometer, TN 2560; NACA Washington; 1951, Unclassified.

12. Martine W. Petersen, Gordon C. Tumplin, First Quarterly Progress Report for Experimental Study of Additive Drag of Supersonic Propulsion Systems AF 33(615)-2496, NA-65-523; North American Aviation, Inc., Los Angeles Division; July 1965, Unclassified.

13. Wind Tunnels Group, Pretest Information for Wind Tunnel Tests of an Additive Drag Research Model in the NASA Ames Research Center 6' x 6' Supersonic Wind Tunnel, NA-65-371; North American Aviation, Inc., Los Angeles Division; April 1965, Unclassified.

14. NACA Ames Research Staff, Equations, Tables and Charts for Compressible Flow, Report 1135; NASA, Washington; 1953 Unclassified.

Security Classification

DOCUMENT CONTROL DATA - R&D

(Security classification of title, body of abstract and indexing annotation must be entered when the overall report is classified)

1. ORIGINATING ACTIVITY (Corporate author)
North American Aviation, Inc.
Los Angeles Division

2a. REPORT SECURITY CLASSIFICATION
Unclassified

2b. GROUP

3. REPORT TITLE
Experimental Review of Transonic Spillage Drag of Rectangular Inlets

4. DESCRIPTIVE NOTES (Type of report and inclusive dates)
Final Report; April 1965 - April 1966

5. AUTHOR(S) (Last name, first name, initial)
Petersen, Martine W., Tamplin, Gordon C.

6. REPORT DATE	7a. TOTAL NO. OF PAGES	7b. NO. OF REFS
May 1966	xvi + 162 = 178	14

8a. CONTRACT OR GRANT NO.	9a. ORIGINATOR'S REPORT NUMBER(S)
AF33(615)-2496	NA-66-10
b. PROJECT NO.	
c.	9b. OTHER REPORT NO(S) (Any other numbers that may be assigned this report)
d.	AFAPL-TR-66-30

10. AVAILABILITY/LIMITATION NOTICES This document is subject to special export controls and each transmittal to foreign governments or foreign nationals may be made only with prior approval of, Air Force Propulsion Lab., Components, Branch of Research and Tech., Division of Air Force Systems Command, Wright-Patterson Air Force Base, Ohio

11. SUPPLEMENTARY NOTES

12. SPONSORING MILITARY ACTIVITY
Air Force Aero Propulsion Laboratory
Research and Technology Division
Air Force Systems Command
Wright-Patterson Air Force Base, Ohio

13. ABSTRACT Inlets sized for supersonic aircraft operation are oversized at transonic speeds. Spilling excess air around the inlet creates spillage drag which can seriously penalize the low altitude penetration range of mixed mission aircraft. Spilling, also, creates inlet cowl lip suction forces which can cancel a portion of this drag, but available data on spillage drag and its partial recovery on the cowl lip were not sufficient for necessary design and performance studies. Generalized wind tunnel studies of inlet spillage were required to supply the needed information.

In 1964, NAA/LAD designed and built a "workhorse" model for in-house tests of pitot inlet spillage drag. Under contract AF33(615)-2496, the "workhorse" portion of this model was fitted with rectangular supersonic inlets. Wind tunnel tests were conducted and are reported herein. Testing was done in the NASA Ames Research Center's 6'x6' Supersonic Wind Tunnel, primarily in the 0.7 to 1.4 Mach number range. The model had four interchangeable ramps, four sets of side plates and ten interchangeable cowls.

Low drag flow spillage requires decreasing the inlet flow area by (a) increasing the external ramp angle or (b) rotating the cowl inward. Test data show that ramp spillage creates lower total drag. The minimum spillage drag configuration would use minor deflections of both ramp and cowl. However, the cowl actuation weight penalty must be considered.

Experimental transonic ramp pressure drags were normalized and compared with transonic similarity work on wedge airfoils. These ramp drag data, together with cowl drag and spillage drag correction (KADD) factors developed in this report, are valuable tools for inlet design and performance studies.

DD FORM 1 JAN 64 1473

Security Classification

Security Classification

14 KEY WORDS	LINK A		LINK B		LINK C	
	ROLE	WT	ROLE	WT	ROLE	WT
Additive drag						
Transonic additive drag						
Rectangular inlets						
Wind tunnel test						

INSTRUCTIONS

1. ORIGINATING ACTIVITY: Enter the name and address of the contractor, subcontractor, grantee, Department of Defense activity or other organization *(corporate author)* issuing the report.

2a. REPORT SECURITY CLASSIFICATION: Enter the overall security classification of the report. Indicate whether "Restricted Data" is included. Marking is to be in accordance with appropriate security regulations.

2b. GROUP: Automatic downgrading is specified in DoD Directive 5200.10 and Armed Forces Industrial Manual. Enter the group number. Also, when applicable, show that optional markings have been used for Group 3 and Group 4 as authorized.

3. REPORT TITLE: Enter the complete report title in all capital letters. Titles in all cases should be unclassified. If a meaningful title cannot be selected without classification, show title classification in all capitals in parenthesis immediately following the title.

4. DESCRIPTIVE NOTES: If appropriate, enter the type of report, e.g., interim, progress, summary, annual, or final. Give the inclusive dates when a specific reporting period is covered.

5. AUTHOR(S): Enter the name(s) of author(s) as shown on or in the report. Enter last name, first name, middle initial. If military, show rank and branch of service. The name of the principal author is an absolute minimum requirement.

6. REPORT DATE: Enter the date of the report as day, month, year; or month, year. If more than one date appears on the report, use date of publication.

7a. TOTAL NUMBER OF PAGES: The total page count should follow normal pagination procedures, i.e., enter the number of pages containing information.

7b. NUMBER OF REFERENCES: Enter the total number of references cited in the report.

8a. CONTRACT OR GRANT NUMBER: If appropriate, enter the applicable number of the contract or grant under which the report was written.

8b, 8c, & 8d. PROJECT NUMBER: Enter the appropriate military department identification, such as project number, subproject number, system numbers, task number, etc.

9a. ORIGINATOR'S REPORT NUMBER(S): Enter the official report number by which the document will be identified and controlled by the originating activity. This number must be unique to this report.

9b. OTHER REPORT NUMBER(S): If the report has been assigned any other report numbers *(either by the originator or by the sponsor)*, also enter this number(s).

10. AVAILABILITY/LIMITATION NOTICES: Enter any limitations on further dissemination of the report, other than those imposed by security classification, using standard statements such as:

(1) "Qualified requesters may obtain copies of this report from DDC."

(2) "Foreign announcement and dissemination of this report by DDC is not authorized."

(3) "U. S. Government agencies may obtain copies of this report directly from DDC. Other qualified DDC users shall request through _____."

(4) "U. S. military agencies may obtain copies of this report directly from DDC. Other qualified users shall request through _____."

(5) "All distribution of this report is controlled. Qualified DDC users shall request through _____."

If the report has been furnished to the Office of Technical Services, Department of Commerce, for sale to the public, indicate this fact and enter the price, if known.

11. SUPPLEMENTARY NOTES: Use for additional explanatory notes.

12. SPONSORING MILITARY ACTIVITY: Enter the name of the departmental project office or laboratory sponsoring *(paying for)* the research and development. Include address.

13. ABSTRACT: Enter an abstract giving a brief and factual summary of the document indicative of the report, even though it may also appear elsewhere in the body of the technical report. If additional space is required, a continuation sheet shall be attached.

It is highly desirable that the abstract of classified reports be unclassified. Each paragraph of the abstract shall end with an indication of the military security classification of the information in the paragraph, represented as *(TS), (S), (C), or (U)*.

There is no limitation on the length of the abstract. However, the suggested length is from 150 to 225 words.

14. KEY WORDS: Key words are technically meaningful terms or short phrases that characterize a report and may be used as index entries for cataloging the report. Key words must be selected so that no security classification is required. Identifiers, such as equipment model designation, trade name, military project code name, geographic location, may be used as key words but will be followed by an indication of technical context. The assignment of links, roles, and weights is optional.

GPO 916-887

Security Classification

END

DATE
FILMED

8 — 66